Force-Responsive Polymers, Networks, and Catalysts

by

Zachary Shane Kean

Department of Chemistry
Duke University

Date:_____

Approved:

_____
Stephen L. Craig, Supervisor

_____
Ross A. Widenhoefer

_____
Stefan Zauscher

_____
Benjamin J. Wiley

Dissertation submitted in partial fulfillment of
the requirements for the degree of Doctor
of Philosophy in the Department of
Chemistry in the Graduate School
of Duke University

2014

ABSTRACT

Force-Responsive Polymers, Networks, and Catalysts

by

Zachary Shane Kean

Department of Chemistry
Duke University

Date:_____
Approved:

_____
Stephen L. Craig, Supervisor

_____
Ross A. Widenhoefer

_____
Stefan Zauscher

_____
Benjamin J. Wiley

An abstract of a dissertation submitted in partial fulfillment of the requirements for the degree of Doctor of Philosophy in the Department of Chemistry in the Graduate School of Duke University

2014

Abstract

The acceleration of chemical reactions under mechanical stress has been known since the earliest days of polymer science. Once limited to the simple scission of polymer chains, mechanical force can now be used to produce a wide array of productive chemistry. The development of so-called "covalent mechanochemistry," has allowed chemists to challenge and support classically held models of chemical reactivity, impacting both synthetic chemistry and material science. This work aims to develop molecular tools that respond to stress and explore the mechanisms behind that response. While a wide-range of fields may be impacted, the overall inspiration for the work herein is the development of materials with rich and robust molecular responses to otherwise destructive forces. To this end we focus on: (a) developing new mechanochemically reactive organic molecules (mechanophores) that undergo constructive covalent transformations in linear *polymers* under stress; (b) probing the nature of force transduction across length scales, from bulk (macroscopic) to microscopic stress, in *networks* thus informing material design; (c) constructing systems that reversibly amplify mechanochemical signals via *catalysis*.

Force induced transformations of polymer bound mechanophores have the potential to produce a rich array of stress responsive behavior. One area of interest is the activation of non-scissile mechanophores in which latent reactivity can be unveiled.

Under the appropriate conditions, this new reactivity could lead to constructive bond formation, and potentially a pathway to mechanochemical stress strengthening. In chapter 2, the mechanical activation of a bicyclo[3.2.0]heptane (BCH) mechanophore is demonstrated via selective labeling of bis-enone products. BCH ring-opening, via a formal [2+2] cycloreversion, produces large local elongation (> 4 Å) and products that are reactive to Michael-type additions under mild conditions. Subsequent photocyclization regenerates the initial BCH functionality, providing switchable structure and reactivity along the polymer backbone in response to stress and visible light.

In chapter 3, the mechanochemical [2+2] cycloreversion of cyclobutanes is further explored through the development of bicyclo[4.2.0]octane (BCO) mechanophores. Using carbodiimide polyesterification, BCO units were incorporated into high molecular weight polymers containing up to 700 mechanophores per polymer chain. Under exposure to the otherwise destructive elongational forces of pulsed ultrasound, these mechanophores unravel by ~7 Å per monomer unit to form α,β-unsaturated esters that react constructively via nucleophilic thiol-ene conjugate addition to form sulfide functionalized copolymers and cross-linked polymer networks. The wide variety of possible product stereochemistry provided an opportunity to probe the dynamics of the mechanochemical ring opening. A series of bicyclo[4.2.0]octane derivatives that varied in stereochemistry, substitution, and symmetry were synthesized and activated. Product

stereochemistry was analyzed by ^{1}H NMR, ^{13}C NMR, and gas chromatography, which enabled inquiry into the mechanism of the mechanochemical [2+2] cycloreversion. These results support that the ring opening is not concerted, but proceeds via a 1,4 diradical intermediate. Additionally, insight is provided into the 1,4-diradical dynamics prior to product formation.

We next turn our attention to the molecular level responses of polymer materials under macroscopic stress. Hydrogels and organogels made from polymer networks are widely used in biomedical applications and soft, active devices for which the ability to sustain large deformations is required. The strain at which polymer networks fracture is typically improved through the addition of elements that dissipate energy, often strong, yet reversible interactions. The result is often tougher materials, resulting from both greater nominal strains and moduli. These materials require extra work to achieve a desired level of deformation, however, there is little evidence that large amounts of energy dissipation is required to achieve greater nominal strains. In chapter 4, we show that the addition of mechanically "invisible" supramolecular crosslinks causes substantial increases in the ultimate gel properties without incurring the added energetic costs of dissipation. We then incorporated a chemiluminescent stress-sensor, the bis(adamantyl)dioxetane covalent cross-linker, first developed in the Sijbesma group, which emits light in the event of covalent bond scission. In these experiments we

demonstrate that the occurrence of macroscopic failure (from stress-strain curves) coincides with the molecular level failure of the underlying covalent network.

Finally, in chapter 5, we turn our attention to the development of mechanocatalytic systems. By activating or otherwise altering the activity of a catalyst using force, a single mechanochemical event may be amplified (i.e. by catalyst turnover). Such systems have been previously reported in the form of force-activated polymer bound transition metal complexes. Beyond these on/off systems, we imagine that force may be used to tune catalyst selectivity, via the perturbation of ligand geometry. Here, we report a catalyst that couples a photoswitch to the biaryl backbone of a chiral bis(phosphine) ligand, thus allowing photochemical manipulation of ligand geometry without significantly altering the electronic structure. The changes in catalyst activity and selectivity upon switching can be attributed to intramolecular mechanical forces, laying the foundation for a new class of catalysts whose selectivity can be varied smoothly and *in situ* over a useful range by controlling molecular stress experienced by the catalyst during turnover. Forces on the order of 100 pN are generated, leading to measureable changes in the enantioselectivities of asymmetric Heck arylations and Trost allylic alkylations.

Contents

List of Tables

List of Figures

List of Schemes

1. Introduction*

At the core of many applications of polymeric materials are their mechanical properties, and in particular their ability to withstand an applied load or stress. Mechanical forces are distributed (unequally) amongst the individual polymer molecules within a macroscopic material,[1-4] and molecular responses dictate the material properties. For example, force-induced conformational changes along a polymer backbone might store the deformation energy, where it can eventually be released through entropically driven relaxation of an extended chain segment to a collapsed structure–the underlying basis of rubber elasticity.[5-8] Chemical or topological entanglements serve as anchors for the elastic response, pinning the ends of stress-bearing chain segments and preserving the stored energy.[9,10] Molecular responses, such as the scission of bonds or the slipping of chains through physical entanglement points, therefore regulate whether the deformation energy is stored or lost as viscous heat. These responses are accompanied by irreversible changes in structure at the molecular, mesoscopic, and macroscopic levels.[11-13] In a sense, one can think of the stress-bearing subchains as nanoscale devices for "force management", in that responses at the level of

---

*This chapter adapted from: Kean et al. (2012) *Polymer*, *53*, 1035-1048.

chemical bonds are ultimately tied to the macroscopic mechanical properties and to the failure or survival of the material under acute or chronic loading environments.

It should be considered in this context that there is a dramatic mismatch between the magnitude of the macroscopic and molecular forces that are typical of most applications: the mechanical forces that are typical of daily life (on the order of Newtons or greater) dwarf those between, for example, the atoms in a carbon-carbon bond (order ~10^{-9} N). One consequence of this mismatch is that covalent bonds have been shown to break under certain macroscopic loading environments,[14-16] and in some circumstances bond scission is believed to be an early stage of macroscopic material failure. Not only are macroscopic forces many orders of magnitude greater than atomic forces, they are also directional. They therefore differ from conventional forms of energy input such as heat and light, because specific nuclei can literally be pulled or pushed in a desired direction, for example along a particular reaction coordinate, overriding the reactivity preferences that are dictated by the electronic wave functions. Recently, several studies[17] have demonstrated that macroscopic mechanical forces can be harnessed at the molecular level, creating a new tool for the organic and materials chemist alike.

It has been noted that the opportunities in this area can broadly be divided into two categories.[18] First, there is the opportunity to develop new chemistry in the service of polymer science by designing and synthesizing mechanically active functional groups (mechanophores) and incorporating them into materials, in essence using chemistry to

create new forms of "force management." This approach has the potential to elicit subsequent macroscopic responses, for example stress-sensing or stress-responsive properties. As will be discussed further over the course of this chapter, the fact that mechanical forces are often destructive ties into a specific vision along these lines, in which typically destructive forces are diverted into new *constructive* pathways that might enhance mechanical properties and prolong material lifetime. The second opportunity is the complement of the first – using polymers to transmit macroscopic forces to targeted molecules and drive chemical reactions that are either difficult or impossible to access by traditional methods. In relaying these concepts, focus will be on recent activity in the Craig group, but draw on the many important contributions by others in context; a more general review has been recently published.[17] As is hopefully clear, both completed work and remaining challenges range from the fundamental to the applied. Potential applications include, in the realm of chemistry, new stoichiometric reactions and methods of catalysis, as well as stress-strengthening and self-healing polymers in the realm of materials. In a more general sense, this work aims to better understand and leverage fundamental elements of chemical reactivity in regimes where force alters kinetic and thermodynamic behavior.

1.1 Overview of Contemporary Mechanochemistry

While polymer mechanochemistry has been known for decades,[8,13,19,20] until recently its purview has been largely limited to the homolytic scission[19,21] of main chain

carbon-carbon bonds under high shear flow.[22,23] The earliest forays into more specific bond activation by mechanical force targeted the scission of weak bonds such as metal-ligand coordination bonds[24-26] and covalent peroxide and azo linkages.[27,28] In 2007, following some preliminary success in the Moore group,[28,29] Hickenboth et al. published a landmark paper in which they demonstrated that mechanical force can be utilized to drive constructive and selective chemical reactions. Here, the benzocyclobutene (BCB) moiety was tethered via two ester linkages to poly(ethylene glycol) (PEG) chains and Woodward-Hoffman disallowed cycloreversions were observed when the direction of the applied force opposed the rotation required to follow the allowed pathway.[30] Further examples from the recent literature include the sonochemical and solid state colorimetric ring opening reaction of spiropyran to merocyanine[31-35] and mechanical dissociation of metal complexes,[24,25,36,37] most of which have been recently reviewed by Caruso et al[17] and Groote et al.[38] Mechanically induced retro-Diels-Alder reactions[39,40] and subsequent thermal remending,[41] have been shown, elaborating on the utility of retrocyclizations in mechanochemistry. Fernandez and co-workers have used force microscopy to quantify the mechanical acceleration of disulfide bond scission in polyproteins.[42] Furthermore, mechanical intervention has been observed to affect small molecule reaction kinetics such as electrocyclic ring openings and the bimolecular dissociation of disulfide bonds coupled to stiff-stilbene bearing macrocycles,[43-45] providing evidence that mechanical activation may not be strictly limited to macromolecules but may also be used to

understand small molecule reactivity and find potential applications in synthetic transformations.

The Craig group's activity and interest in this field dates back to 2006. While investigating the material properties of metallo-supramolecular gels based on a family of van Koten-type pincer complexes,[46-48] (see chapter 4) it became apparent that these complexes acted as defining motifs in supramolecular polymers; they were the active "force management" agents that dictated mechanical properties (Figure 1). This direct molecule-to-material relationship allowed for the use of the principles of physical organic chemistry to predict the behavior of supramolecular polymers and better understand the underlying mechanisms of their mechanical response.[49] The utility of this approach stemmed from the fact that the dynamic mechanical response of the polymers could be related back to the kinetics of ligand exchange in the isolated pincer complexes.[50-53] While many of the networks' dynamic mechanical properties could be related to the force-free kinetics of the pincer complexes, it was clear that under certain circumstances force could accelerate the dissociation in the macroscopic systems; the gels could be physically torn apart, for example, on timescales much shorter than the force-free ligand dissociation rate. Efforts therefore shifted to understand the extent to which force would accelerate the reaction, and whether macroscopic signatures could be quantitatively related to the force-induced kinetics, as had been done successfully with the force-free dissociation kinetics.

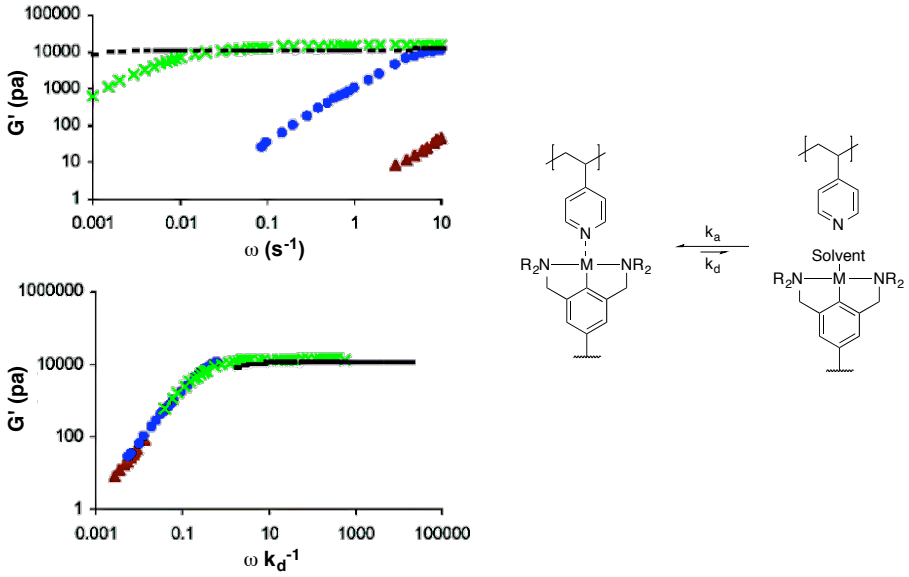

Figure 1 Variations in storage modulus (G′) are accounted for when normalized to the dissociation rates for a family of van Koten-type pincer ligands.[52]

Using single-molecule force spectroscopy (SMFS), Kersey and co-workers[26] determined that force does indeed accelerate the reaction, and that the rate of dissociation as a function of force extrapolated back to force-free reaction rates that match those of the model systems. These results demonstrate that the reaction under force (up to ~200 pN) could be viewed as a continuous perturbation of the force-free reaction mechanism.[26] Different ligands and pincer complexes were compared, and the relative dissociation rates in the force-free reactions persisted in the force-accelerated reactions, establishing a connection between the action of an applied force and the reaction mechanism.[54] Knowledge of these relationships has proven useful in interpreting the nonlinear viscoelasticity of supramolecular polymer networks,[55-57] itself a form of structural polymer stress-response. In this regard, Chapter 5 describes

continued efforts to use pincer coordination chemistry as a mechanism by which to look for signatures of force-induced reactions (covalent bond scission) in macroscopic polymer gels.

The timing of the BCB work by Moore and co-workers was therefore quite propitious. Having been thinking about the fundamentals and consequences of force-induced reactivity in polymers, the Craig group was inspired by the force-induced BCB reactivity, not only because of its implications for new types of reactions, but even more so because it proffered a vision of using mechanical forces to form new bonds to polymers. This pioneering work gave a first voice to the idea that mechanochemical activation could be the basis of constructive covalent bond formation for stress-responsive polymers. The following sections outline the Craig group's initial strategies in that area, and then review accomplishments and failures through the inception of the work contained in this dissertation. Ultimately, it was these contributions that inspired the vast majority of the work herein.

1.2 Mechanochemical Remodeling as a Platform for Stress-Responsive Materials

Stress distributions in polymeric materials are typically heterogeneous,[58] and regions of high stress concentration are generally regarded as the sites at which failure initiates.[59] The existence of these "at risk" regions create first an opportunity for material properties enhancement, but they also provide a critical challenge for the mechanophore strategy: the precise regions of high stress and failure initiation are difficult, and quite

frequently impossible, to predict in advance. It may therefore be desirable in many situations to disperse mechanophores at a high density throughout a polymer network. The thinking is that sufficiently high densities would ensure that a mechanophore is in the right place at the right time, without requiring *a priori* knowledge of stress distributions within a material. Relative to that of other activity in the field, the Craig lab has primarily focused on the incorporation and consequences of multiple, non-scissile mechanophores in a single polymer chain. The ability to place many mechanophores on each polymer molecule, and to systematically vary that content, therefore provides one guiding principle of the initial design strategy.

Two additional design principles arise from understanding the consequences of mechanically active functionalities that elicit constructive, and/or attenuate destructive, chemistry when exposed to a mechanical force. After high loading, the second design principle is motivated by the fundamental stress-strain behavior of single polymer molecules. Previous SMFS experiments[60-63] have confirmed the long appreciated theoretical picture of single polymer elasticity, in which the compliance of the polymer is initially determined by entropic, conformational degrees of freedom. The force required to extend a polymer in this regime is quite low (1-50 pN). Once the conformational entropy is nearly exhausted, however, the force necessary to extend the polymer further increases rapidly, growing over a relatively small strain range from ~50 pN at the undistorted contour length to several nN of force, at which covalent bonds are broken.[64]

Because forces on the order of hundreds of pN are necessary to have a dramatic influence on the rate of most covalent reactions, this means that mechanochemical activation without chain scission is only viable over a very narrow strain window in the extension of a polymer chain. To the extent that the goal is to prevent the bond breaking events that initiate macroscopic failure, then, a second design principle is to trigger processes that increase the "active strain window" prior to chain scission through molecular "stress relief" -a force-induced increase in the covalent contour length of the polymer, allowing individual polymer chains to survive strains that would otherwise be catastrophic (Figure 2).

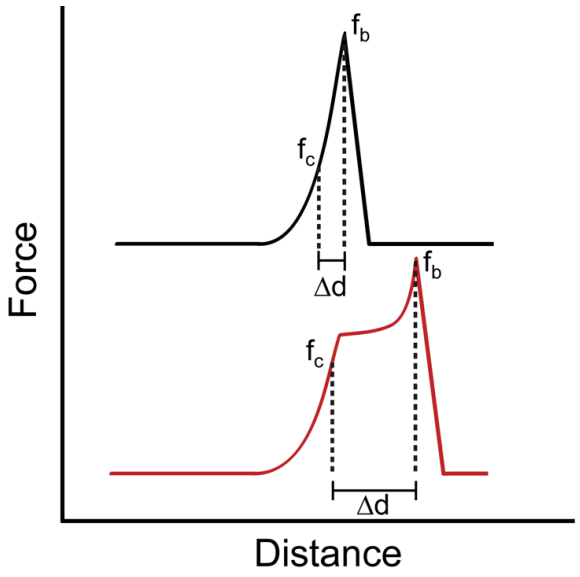

Figure 2 Once conformational entropy is exhausted covalent bonds begin to deform (f_c), resulting in bond scission (f_b) over a narrow strain window (Δd) (top). Molecular stress relief increases the "active strain window" (bottom).

The final design principle is that the activated mechanophores are able to form new bonds within the material in its load-bearing environment. Mechanochemically induced cross-linking could in principle serve either to prevent a loss in mechanical properties[13] under what is typically a destructive load, or to restore them during periods of relaxation between periodic stress events. In order to lead to improved properties, the number of constructive bond-forming events must also be effective on the macroscopic level. That is, they should create not only new bonds but also stress-bearing subchains akin to those lost or threatened due to the mechanical damage. These considerations tie to the two previous design criteria, because (a) multiple mechanophores per chain provide a mechanism for having multiple bond-forming events accompany each bond-breaking event (although triggering catalytic systems[36,37,65,66] also holds promise in this regard, see chapter 5), and (b) because it seems that forming a bond to a highly stressed chain prior to scission is unlikely to redistribute the force, as the formed bond must have some "slack", else it would be un likely to form. In this framework, creating additional slack in the highly stressed bond might prove quite useful. Depending on the nature of the applied load, the stresses experienced by the material may be highly localized, and mechanically active domains might need to be present in high concentration along the polymer backbone in order for an appreciable amount of chemical remodeling of the network to occur. There are obviously many layers of questions regarding these three design criteria (which, despite the arguments that motivate this approach, may not be

necessary nor sufficient). This includes fundamental questions about molecular stress distribution, the necessary density of mechanophores, the necessary extent of molecular stress relief, and the dynamics and time scale of all processes. When taken together, the successful realization of these criteria represents a potential pathway to stress-responsive, molecular scale properties that might permit what amounts to "mechanochemical annealing" -molecular responses that redistribute an applied stress to maximize the ultimate strength of a polymer or polymer composite (Figure 3).

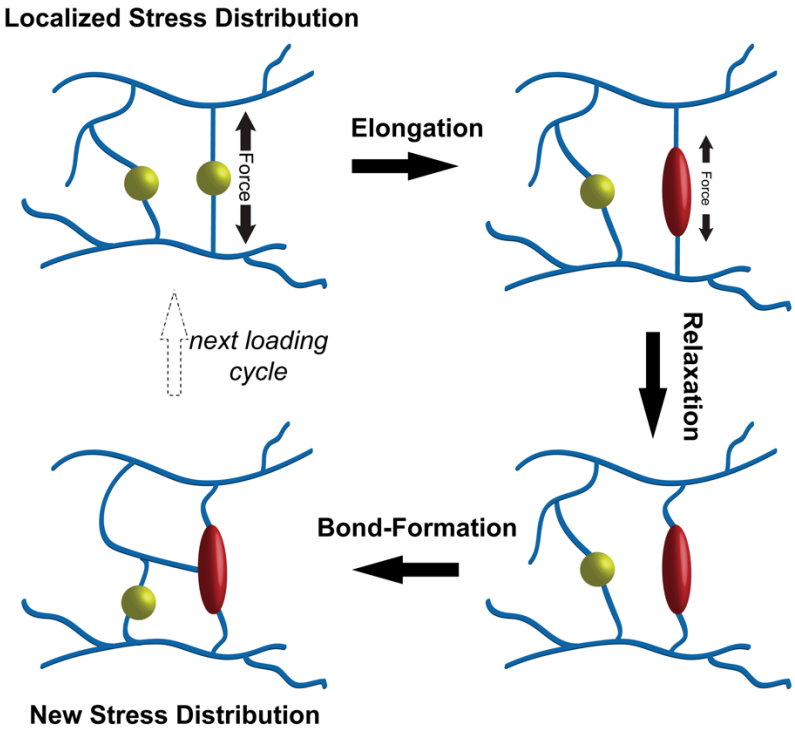

Figure 3 Schematic of the mechanophore strategy. Under stress, mechanophore activation leads to local elongation. Subsequent relaxation (either local or global) allows for new covalent bond formation. High mechanophore content then allows for stress response at the remodeled site or elsewhere in the material.

1.3 gem-Dihalocyclopropane Functionalized Polymers

The vision of reactions that occur along a polymer backbone under tension while leading to an increase in polymer contour length and mitigating molecular weight degradation is best satisfied by mechanophores that undergo ring opening reactions, since the reaction can occur without the polymer chain breaking. While early examples of mechanophores included those that undergo force-induced electrocyclic ring opening reactions,[30,33] the macroscopic consequences (if any) of creating mechanophore-rich polymers were unknown. Wanting to probe this idea, Lenhardt and co-workers looked initially to *gem*-dihalocyclopropane (*g*DHC) moieties because of their simple synthesis[67] and known ability to participate in thermally accelerated electrocyclic ring opening reactions to generate 2,3-dihaloalkenes[68-70] (Figure 4). In consideration of the first design criterion, the accessibility of these units enables their plentiful incorporation along the backbone of most alkene-containing polymers. *g*DHC-bearing polybutadiene was first reported by Pinazzi et al. in 1965,[71] and has been studied for decades[72-74] in part because of its potential as a flame retardant.[75] In addition, if the thermal rearrangement could be triggered mechanically, the *g*DHCs would satisfy the second and third mechanophore requirements: the product 2,3-dihaloalkene is longer than the parent *g*DHC, and it also possesses an allylic halide that, especially for the bromide, is susceptible to nucleophilic substitution reactions to which the *g*DHCs are relatively inert (Figure 4). Additionally, by varying the halogen atoms in *g*DHC polymers, a rich array of reactivity,

intermediates, and products can be accessed, a trait that can be exploited to gain insight into fundamental aspects of force-induced reactivity.

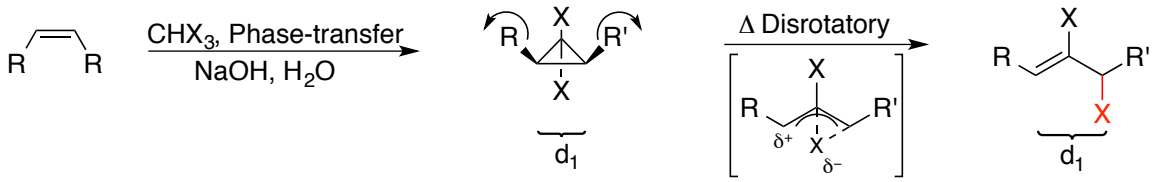

Figure 4 Synthesis and thermal activation of dihalocyclopropanes to 2,3-dihaloalkenes.

The history of work in the Craig group on these systems provides an outline for the remainder of this chapter, with each of the *g*DHCs playing its own unique role, from demonstrating that *g*DCCs undergo mechanically assisted ring opening reactions, to quantifying the ring opening of *gem*-dibromocyclopropanes (*g*DBCs) using single molecule force spectroscopy (SMFS), showing evidence of solid state activation, extending the lifetime of and subsequently trapping a *gem*-difluorocyclopropane (*g*DFC) isomerization transition state, and discovering the existence of one of the few known "mechanical only" reactions. The remainder of this chapter will further examine these studies and their relationship to each other. An in depth critique of how these results impact, reinforce, and challenge current views on force-coupled chemical reactivity in polymers will be presented. Finally, strategies to extend these implications to broader topics in polymer and material science will be offered. As described in the following sections, these non-scissile *g*DHC mechanophores have proven to be versatile, allowing for studies on their mechanical activity in single molecules, sheared polymer solutions,

and the solid state. They have provided insights into molecular stress distributions, the nature of chemomechanical coupling in polymers, and the mechanism and dynamics of mechanochemical reactions, and they have provided proof-of-concept examples of multi-mechanophore response, molecular stress relief, and mechanochemical strengthening under destructive load.

1.4. Mechanochemical Activity of poly(gDHCs)

1.4.1. Demonstrating Mechanical Activity

Several questions persisted at the outset of exploration into these compounds: (1) whether or not the thermal reaction (Figure 4) could be triggered mechanically, and, if so, (2) whether large numbers of *g*DHCs could be activated under conditions that led to a single chain scission event. To answer these questions, the sonochemistry of polymer solutions was initially employed. Polymer sonochemistry has a long tradition, dating back to studies by Schmid in the 1930s on the effect of sonication on the viscosity of polymer solutions.[76] In recent years, this method was re-popularized by Sijbesma as a method for studying a richer range of mechanical responses in polymers.[25] When solutions are exposed to ultrasound, oscillations from high to low pressure cause the formation of cavitation bubbles that, upon collapse, generate a radial flow field. Polymer chains that reside near the collapsing bubble wall experience a velocity gradient along the chain that can cause various levels of uncoiling, bond deformation, and scission. This fundamental mechanism has some ramifications for the response of polymers to

ultrasonic shear. First, bond scission occurs more readily in polymers of higher molecular weight[77,78] and this scission is more probable at the midchain.[79,80] These factors come into play for the poly(*g*DHC)s when discussing activation domains and ring opening efficiency. Second, environmental factors affect the sonication efficiency and the forces reached during cavitation events. In this category, it can be said that bond scission occurs more readily at low temperatures, in low vapor pressure solvents, at higher ultrasound intensity, and at lower polymer concentrations.[78,81] In some instances, additional solvation effects occur in solvents that encourage more stretched conformations, reducing the burden for mechanical work to overcome some of the conformational entropy and encourage a coil-stretched transition.[82] An empirical value referred to as "limiting molecular weight," defined roughly as the lower limit of molecular weight (typically ~40 kDa, although varying with conditions and the nature of the polymer) necessary to obtain shear forces that are significant enough to cause mechanochemical activation and chain scission, is particularly important in discerning between possible thermal and mechanical processes during sonication. For further reading, mechanochemical activation of polymers in elongational flow fields has been recently reviewed by May et al.[23] while the work of Price provides a comprehensive and historical overview.[77,78,81]

Sonication therefore provides a general method for screening the activity of mechanophores that are coupled to the main chain of polymers, and it was the basis for

the first investigations into the covalent mechanochemistry of *g*DHCs. Whereas sonochemistry is a robust method to effect mechanochemical transformations and qualitatively establish their viability, at present it has limited utility as a quantitative link to potential material applications and/or the determination of kinetic and thermodynamic parameters of mechanochemical events. Furthermore, because the applied shear forces are transient, sonication must be used thoughtfully when promoting changes that are reversible on the time scale of the experiment.

The synthesis of the *g*DHC polymers is straightforward, as the functionalization of polybutadiene and natural rubbers by dichlorocarbene has been known since the 1960s.[74,83] While it seems almost certain that these polymers were sonicated at some point during the early decades of their use, the force induced ring opening reaction remained unrecorded until 2009, when Lenhardt et al. first reported the mechanochemical activation of *g*DHC functionalized polymers under ultrasonic shear flow in solution.[84] Commercial polybutadiene was subjected to *gem*-dichlorocyclopropanation under aqueous phase transfer conditions using known procedures, resulting in polymers in which 5-72% of the alkenes were cyclopropanated. When subjected to ultrasound-generated elongational shear, the authors observed that *g*DCCs along the backbone underwent an electrocyclic ring opening to form the desired 2,3-dichloroalkenes in high quantity by ^{1}H NMR, with the ability to exceed 80% ring opening (based on initial *g*DCC content) at sufficient sonication times (Figure 5).

Because bubble collapse is known to generate enormous, localized temperature increases,[85] the potential role of thermal activation in sonochemical processes is often questioned. It is relatively straightforward, however, to rule out thermal effects through appropriate control experiments. In this system, for example, one telling control is the sonication of dichlorocyclopropanated polybutadiene (poly(*g*DCC)) with a high *1,2*-butadiene content. The *g*DCCs thus formed are not coupled to the polymer backbone, and therefore are also decoupled from the shear-induced tensile forces. No ring opening reaction of the side-chain mechanophores was observed under conditions in which main-chain mechanophores are highly activated, ruling out thermal contributions and supporting the mechanochemical nature of the reaction. In addition, when poly(*g*DCC) of molecular weight well below the "limiting molecular weight" was sonicated, no ring opening was observed. Again, thermal effects should be effectively the same for the lower molecular weight system, further supporting a mechanochemical mechanism for activation.

Approximately 35% of the *g*DCCs underwent ring opening by the time the average polymer chain had undergone one scission event, a result that held for several polymers of varying molecular weight and *g*DCC content. The magnitude of the response was especially encouraging, in that it demonstrated that the *g*DCC ring openings are triggered much more easily than destructive chain scission reactions. This activity corresponds to the generation of hundreds of reactive moieties per single chain

fracture, demonstrating that the platform might be useful as a highly efficient network-forming, stress-responsive system.

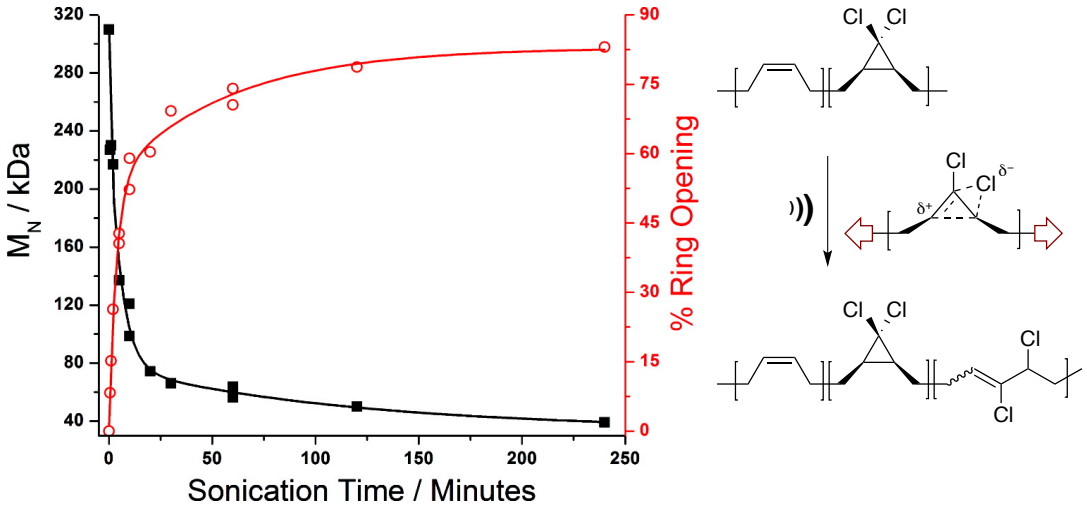

Figure 5 Sonochemical activation of *gDCC* polymer leads to the formation of 2,3-dihaloalkenes. Percent ring opening and molecular weight plotted vs. sonication time (left). Adapted with permission from Lenhardt et al., *J. Am. Chem. Soc.*, 131, 10818-10819. Copyright (2009) American Chemical Society.[84]

Comparing the relative reactivity of *cis* and *trans* *g*DCC isomers provided mechanistic insight. Previously reported data show that small-molecule *cis*-*g*DCC reacts 20 times faster than the *trans* isomer under thermal conditions.[86] Under sonochemical conditions, however, the extent of *cis* ring opening is only 1.35 times greater than the *trans*. Because the mechanical force is applied in a disrotatory fashion to the *cis* isomer but a conrotatory fashion to the *trans* isomer, it is expected that the thermal disrotatory reaction would be accelerated more at a given force for the *cis* isomer than the *trans*. In other words, the mechanochemical reaction should be even more selective for the *cis*

isomer, not less. The muted selectivity was attributed to the presence of very high forces that create large, localized regions of high stress in which virtually all *g*DCCs activate; that is, both reactions are accelerated to the point that they are quantitative, so that any additional acceleration in the *cis* does not matter. The size of the activation zone is larger for the *cis* isomer, due presumably to its greater inherent reactivity and better coupling between the direction of the applied force and the motion of the force-free reaction.

This model is supported by previous computational studies by Martinez and co-workers[87] showing non-degenerate force coupling along mechanistically different ring opening pathways. The large forces implicated, and presence of zones in which "everything reacts", further enforces the difficulty in programming selectivity into ultrasound based mechanochemistry.[24,27,28,36] This lack of selectivity is not, as will be discussed in the next section, characteristic of mechanochemistry in general, but rather is fairly specific to the exceptionally high shear forces generated during ultrasonication.

1.4.2 Quantifying Mechanochemical Activity

The sonochemical experiments were quite useful in verifying the innate mechanical activity of the *g*DCCs and establishing that they are more mechanochemically active than chain scission processes. The experiments did not, however, provide quantitative information regarding the force-vs.-rate relationships. A quantitative picture required a different method to apply known forces in a controlled manner, while simultaneously observing the induced reactivity in the mechanophores.

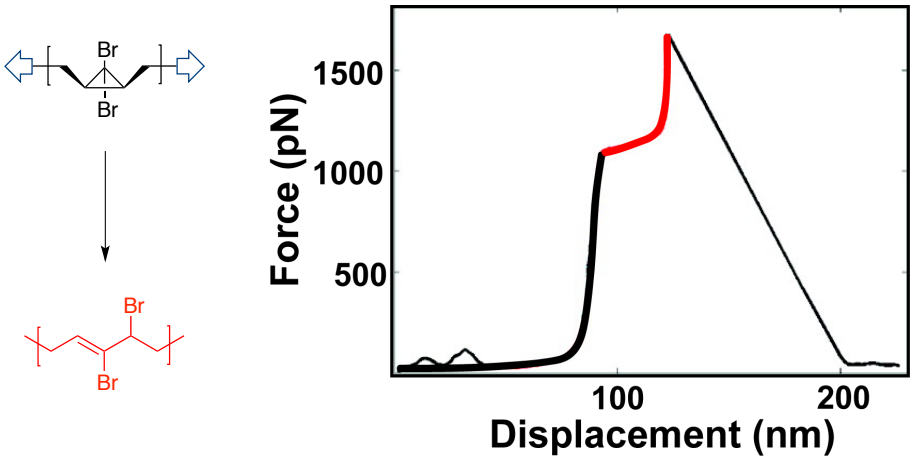

Figure 6 SMFS of *g*DBC polymer results in an expanded "strain window" due to the onset of ring opening (plateau at 88 nm). Adapted with permission from Wu et al., *J. Am. Chem. Soc.*, 132, 15936-15938. Copyright (2010) American Chemical Society.[88]

The Craig group therefore turned to single-molecule force spectroscopy (SMFS), implemented on an atomic force microscope (AFM). The experiment comprised of pulling individual *gem*-dibromocyclopropane-functionalized polybutadiene (poly(*g*DBC)) molecules that were adsorbed to both the tip of AFM and to a silicon surface anchored to a piezoelectric stage. As the stage is pulled away from the AFM tip, the growing tension along the polymer backbone increases and is recorded by observing the resulting displacement in the AFM tip. Up to around 1 nN of tensile force, the force curves associated with these polymers are typical of those for the elastic extension of a covalent polymer, as described in Figure 6: a low-force entropic elastic extension at low strains that gives rise to a rapid increase in force once conformational degrees of freedom have been exhausted and bond lengths and bond strengths have begun to be

distorted. What is noteworthy about the *g*DBC polymers is that, without exception, they undergo a conformational transition at approximately 1200 pN of force that is neither predicted nor observed in conventional polymer elasticity (Figure 6).

The observed plateau is consistent with a force-induced structural change that is coupled to an extension in the polymer contour length, as observed in conformational transitions of DNA,[89] although, in contrast to the B-to-S transition in DNA, the transition in these polymers is effectively irreversible. In the case of the synthetic *g*DHC polymers, the transition plateau can be attributed to the ring opening of the mechanophores. The width of the force plateau is in excellent agreement with the extension expected from the quantitative ring opening of the *g*DBCs to the 2,3-dibromoalkene products. Importantly, the observed extension is proportional both to the pre-transition contour length and mechanophore content of the polymer. For example, a fully functionalized polymer is observed to extend by 28% of its initial contour length, the same value obtained by computational models of *g*DBC dyads. The absolute extension corresponds to 1.28 Å per *g*DBC-to-2,3-dibromoalkene conversion, a value to which will return later in the discussion.

These observations have several implications in terms of materials property engineering. First, within the ability to discern it, the entire population of *g*DBC mechanophores is opened prior to chain detachment or chain scission. In fact, prior work by others suggests that forces of several nN are necessary to effect bond scission

on the millisecond time scale of the SMFS experiment,[64] and so the mechanophores are far more active under force than is the destructive scission event. The competition between mechanophore activity and chain scission in the ultrasound experiments is therefore attributed to the uneven force distribution along the polymers under extensional shear, a picture that is different from that generated by pure, static tension in the SMFS experiments.

Second, the observed extension potentially meets one of the challenges that may be critical for mechanophore-based self-strengthening polymers, in that there is a significant strain window between the onset of mechanical activity and the failure of the stress-bearing polymer subchain (Figure 2). A polymer subchain that would typically (without ring opening) have failed at a length of 88 nm, for example, was observed to survive to 112 nm thanks to the 28% extension, demonstrating the capacity for this architecture to have a dynamic contour length that can change on the time scale of destructive load.

Third, the observed covalent chemical response leads to a new form of "force management." Lake and Thomas[90] first pointed out over 50 years ago that the energy necessary to break a load-bearing polymer chain segment is far greater than the energy of the bond being broken, because it includes the elastic energy stored among all bonds that is lost when one of the bonds finally breaks. In relationship to the SMFS experiments, this toughness of an individual polymer subchain, or net energy absorbed

prior to rupture, is given by the total area under the force-distance curve up to the point of scission/detachment. In the case of poly(*g*DBC), both the magnitude of the force at the transition and the distance over which it is sustained are substantial, resulting in a toughness at the single molecule level that is several times larger than that of a typical covalent polymer. The toughness observed by SMFS in the *g*DBC polymers appears to be the largest demonstrated, and it is interesting to consider the consequences of such behavior for macroscopic material properties. Because the total energy absorbed by the material is spread over a large (relative to the molecular scale) volume, it seems likely that a significant effect can only result if the local "stress relief" allows nearby polymers to also reach the transition and absorb more energy. This in turn allows a third set of polymers to reach the transition and absorb more energy, and so on. Identifying the molecular design principles that create such non-linear macroscopic responses remains an open challenge.

The SMFS experiments also offer an opportunity for insight into mechanochemical coupling in polymers. The validity of the chemomechanical framework for covalent reactions across length and time scales has recently been confirmed via a thorough treatment by Boulatov,[43] but quantifying the effect of the coupling in various contexts (both in terms of the force transducer and the specific reaction) remains an important and ongoing challenge. For example, it is not clear whether isolated small molecule transduction, in which force of known directionality is

applied directly to specific atoms, is identical to force transduction in the same mechanophores embedded within polymers. Given the large number of observable ring opening events in even a single SMFS extension curve, the *g*DBC platform allowed us to rapidly obtain a statistically significant number of chemical reactions and extract the desired kinetic information. The force-coupled kinetics were inferred both from the time scale over which the transition occurred at the plateau force, and through a more comprehensive treatment in which the force curve was modeled as a monomer-by-monomer transition from one freely jointed chain to another. Both treatments yielded the same bottom line: the rate constant for ring opening at 1200 pN is approximately 102 s^{-1}, a factor of ~10^{13} greater than the extrapolated force-free value of 3 x 10^{-11} s^{-1}.[88] Fitting to the Eyring-Bell-Evans (EBE) model:

$$k(F) = k_0 e^{\frac{-F\Delta x^{\ddagger}}{k_B T}}$$

led to a value of $\Delta x^{\ddagger}$ = 1.05 ± 0.11 Å, a value that does not correspond to any relevant internuclear distances determined computationally for carbon atoms at or adjacent to the *g*DBC functionality or the polymer contour length. In the cases of cyclobutane ring opening at low to intermediate forces (< 1 nN), Boulatov and co-workers discovered that $\Delta x^{\ddagger}$ could be accurately interpreted as the change in internuclear distance between methylene carbons adjacent to the reactive groups based on the Eyring-Bell-Evans model.[91] This analysis benefited, however, from the fact that the projection of the force vector along the reaction coordinate could be computationally quantified.[45] In this case,

the measured force is the net tension applied along the vector defined by the entire length of the polymer chain. Because not all bonds (or even any bonds) are necessarily aligned with the overall chain direction, it may be difficult to interpret $\Delta x^{\ddagger}$ as a physically meaningful quantity. This idea was demonstrated computationally by Marx, who showed that the length of alkyl tethers influenced the extent of mechanochemical coupling to an embedded mechanophore.[92,93] Another possibility is that this discrepancy is inherent to the EBE model, namely the assumption that $\Delta x^{\ddagger}$ does not change based on the applied force. One can consider that the compliance of the system, and in particular the differential compliance of the ground state and transition state, might change as a function of force.[91,94] Force-dependent changes in the potential energy surface can be approximated by assuming a specific form of the potential energy surface, for example the cusp model. In the case of poly(gDBC), however, fitting the polymer extension curves assuming a cusp-like potential energy surface:

$$k(F) = k_0 \left(1 - \frac{F\Delta x^{\ddagger}}{2\Delta G^{\ddagger}}\right) e^{\Delta G^{\ddagger}\left[1-\left(1-F\Delta x^{\ddagger}/2\Delta G^{\ddagger}\right)^2\right]}$$

generated a value of $\Delta x^{\ddagger} = 1.28 \pm 0.14$ Å, roughly corresponding to the change in polymer contour length per ring-opened monomer between reactants and products.[95] For the case at hand, it should be noted that the net extension of the gDBC polymer upon ring opening is approximately 1.28 Å, and this ultimate extension puts an upper limit on the expectation for $\Delta x^{\ddagger}$. Because the transition state of the reaction is very late, it is

reasonable to expect that the effective value of $\Delta x^{\ddagger}$ would be close to, but slightly below, this value, in good agreement with the results from fitting the force curves.

1.4.3 Reactivity in the Bulk

The end-goal of the aforementioned design structure continues to be the creation of mechanically responsive materials, specifically via the use of mechanophores that will react constructively in the bulk thus altering the macroscopic properties of the target material. While the mechanical activity of the *g*DHC system was demonstrated under ultrasonic shear in solution, and rates were quantified under tension using SMFS, it is the behavior in the bulk that is most relevant to materials science, and the relevance of the former to the latter is not obvious. For example, different force distributions and active domain sizes depend strongly on the nature of the method of applying force: toward the center of the chain in sonication, and distributed throughout the entire sub-chain in AFM experiments. Though at the time, it was unclear how forces would be distributed in these polymers in the solid state.

In order to probe the reactivity of *g*DHCs in the solid state, we conducted compressions on bulk polymer samples in a steel press; the compressive force leads to large shear forces normal to the applied force. As observed in the sonochemical experiments, applied stress resulted in ring opening to the 2,3-dihaloalkenes.[96] As in solution, Lenhardt and co-workers[96] were able to utilize the varying reactivities of the different *g*DHC functionalities, as well as ^{1}H NMR characterizations of microstructure in

the ring opened products, to map force distributions in solid state poly(*g*DHC)s under stress. The macroscopic compression of polymer in a press led to large shear forces radiating out normal to the applied force vector, and those forces resulted in the same ring opening reactions observed in solution, but at much lower levels, typically on the order of tenths of a percent of monomer units. Greater pressures resulted in higher strain rates, and the extent of ring opening increased accordingly, although details of the specific dynamics at play are only speculative at this point.

In order to demonstrate the muted selectivity mentioned previously with the *g*DCC polymers,[84] *gem*-bromo-chloro-cyclopropanated polybutadiene (poly(*g*BCC)) was subjected to compression and pulsed ultrasound. In both cases, the stereochemistry of the *g*DHC had an effect on the ring opening activity. The *cis-anti-g*BCC mechanophore was approximately 1.8 times more reactive than its *cis-syn-g*BCC isomer. This is analogous to the sonochemical case and in contrast to the thermally obtained Woodward-Hoffman[97-99] allowed selectivity of 970:1 in previously reported solvolytic conditions.[100] Ring-opened dyads were distinguishable from isolated ring opened products by ^{1}H NMR, allowing for some determination of mechanically active domains in the solid state. The average length of these domains was on the order of 4 monomers. Given the small amount of opening overall, this is a higher degree of correlation than would be expected in a random thermal opening, but shorter than the entanglement spacing expected in a polymeric network.[101]

These results may be explained through several different effects, for example that entanglement spacings are polydisperse and the result may reflect that smaller spacings are more highly stressed than their larger counterparts. Second, it is possible that local stress relief occurs on the time scale of the deformation, reducing the load on other monomers within the entanglement region. Third, the forces may differ greatly due to topological structure, proximity to the direct entanglement point, knotting, etc..., all of which are difficult to analyze by conventional methods. Regardless of the origin, the presence of a high mechanophore density appears to be necessary in order to guarantee activation in regions of high stress; if only 1 out of 5 repeat units contained a mechanophore, there would be regions of high stress but perhaps no mechanochemical response.

1.4.4 Diblock Copolymers "In a Snap"

Encouraged by the ability to direct ring opening to specific domains along the polymer backbone, solution based sonochemistry was revisited in order to probe the domain effects where the degree of activation was large and presumably localized. In the ultrasonic degradation of poly(*g*DCC) to an average of one scission per chain, for example, it would be anticipated that on average the two resulting chains would possess AB diblock character, with an unactivated *g*DCC rich (A) block, and a 2,3-dichloroalkene rich (B) block (Figure 7a). The relative sizes and purity of the blocks would provide information as to the force distributions across the polymer chain during the course of

the scission event. The blocky character of activated regions was supported first by ^{1}H NMR analysis, where the chemical shifts of the 2,3-dichloroalkene varied depending on whether the product was adjacent to a *g*DCC or another 2,3-dichloroalkene. It was therefore necessary to chemically separate the blocks. This was accomplished by ozonolysis of the alkene products, allowing for the intact non-activated *g*DCC segments to be isolated (Figure 7b). The molecular weight of the *g*DCC blocks following ozonolysis matched the average *g*DCC content of a post-sonicated polymer chain, indicating that the *g*DCC blocks were effectively "pristine" within the limits of detection.

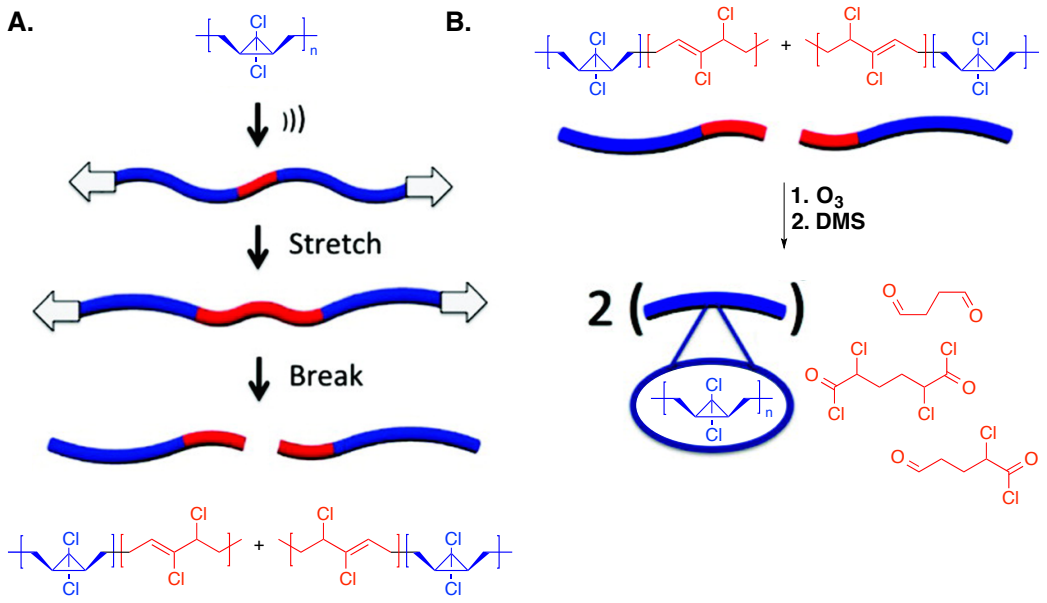

Figure 7 (a) Pulsed ultrasound of *g*DCC results in diblock copolymers. (b) Ozonolysis of diblocks allows for the isolation of pure *g*DCC fragments. Adapted with permission from Black Ramirez et al., *ACS Macro Lett.*, 1, 23-27. Copyright (2011) American Chemical Society.[102]

Given the range of distinct phase behavior known to exist in diblock copolymers, the bulk properties of the sonicated polymers were characterized by differential scanning calorimetry (DSC) and small-angle X-ray scattering (SAXS). DSC analysis of a 134 kDa *g*DCC polymer sonicated to 67 kDa showed the presence of two glass transition temperatures (T_g), which suggested the possibility of micro-phase separation into chemically distinct domains. This suggestion was confirmed by SAXS, which was performed above and below the T_m of the semicrystalline poly(*g*DCC) and showed well defined lamellar spacing of 27 nm (Figure 8).

This method of block copolymer synthesis (almost literally "in a snap") has interesting potential in the fields of polymer synthesis and material science. The formation of diblock copolymers via pulsed ultrasound can be viewed as an extreme example of regioselectivity. The many cyclopropanes along the polymer backbone have identical intrinsic reactivity, but only those located near the middle of the chain at the instant of chain rupture have been converted to 2,3-dihaloalkenes. This leads to the formation of discrete blocks, but it also serves as the basis for "on demand" activation in regions of high stress within macroscopic materials.

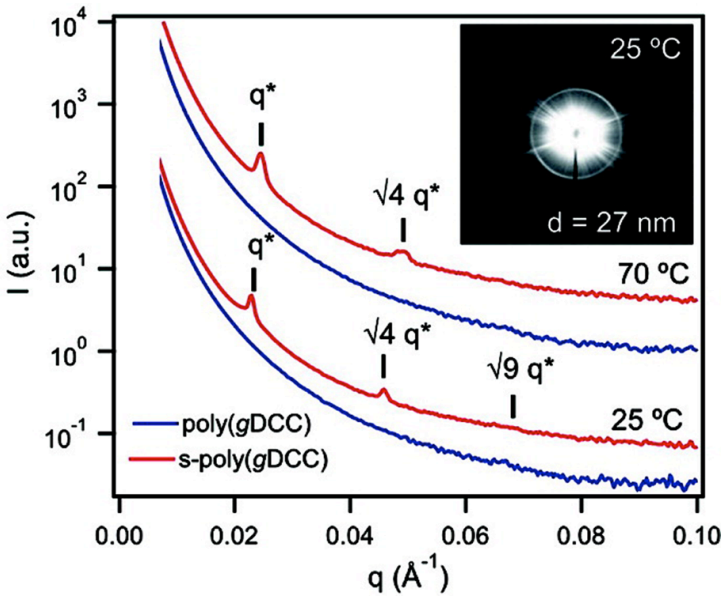

Figure 8 SAXS of sonicated poly(*g*DCC) shows long range order both above and below the T_m of the sample. Adapted with permission from Black Ramirez et al., *ACS Macro Lett.*, 1, 23-27. Copyright (2011) American Chemical Society.[102]

1.4.5 High Exchange Substitutions in the Bulk

As mentioned in the introduction, one long-term goal is to trigger constructive bond-forming chemistry in the solid state. An open question, however, was whether the activation of an intramolecular reaction could be coupled o a subsequent intermolecular reaction in the bulk. Given that the generation of 2,3-dihaloalkenes occurred in the bulk and at room temperature, Black Ramirez and co-workers[103] targeted nucleophilic substitution of the allylic halide as a viable bond-forming reaction. The concept was tested and established by extrusion, resulting in levels of ring opening of between 2 and 32% depending on the halogens, extrusion rate, time, and temperature.

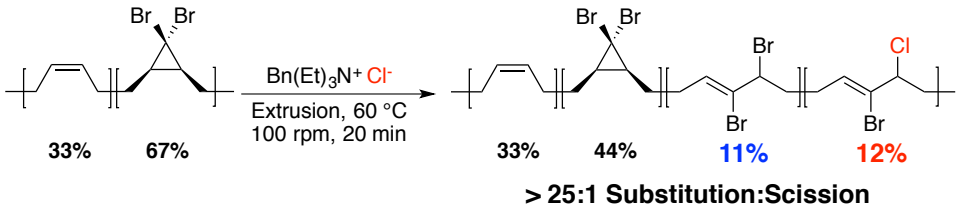

Figure 9 Extrusion of poly(*g*DBC) in the presence of a nucleophile results in high efficiency nucleophilic substitution in the solid state. Black et al., (2011) *J. Mater. Chem.*, 21, 8460-8465. - Reproduced by permission of The Royal Society of Chemistry.[103]

More importantly, however, was the observation of *in situ* nucleophilic substitution reactions occurring during the solid state extrusion process (Figure 9). When a *g*DBC polymer was extruded in the presence of benzyl triethylammonium chloride for 20 minutes at 60 °C and 100 rpm, subsequent ^{1}H NMR analysis established that substitution of the allylic bromide by chloride ion occurred in over half of the ring opened products. When molecular weight was analyzed, this corresponded to an average of over 500 ring openings and 250 substitution reactions for every 9 scission events per polymer chain (initial polymer: 67% *g*DCC, 490 kDa). This corresponds to over 25 new intermolecular covalent bond formations per covalent bond scission, and it represents the first example of tandem mechanochemical activation and substitution reaction in the bulk. This result provides a strong indication that it is possible to leverage stress-induced reactivity to trigger cross-linking chemistry in the solid state, a concept that has the potential to preserve or improve the integrity of a polymer network under destructive mechanical loads.

1.5 Tension Trapping and New Reactivity

1.5.1 *gem*-Difluorocyclopropanes

While a primary goal of polymer mechanochemistry is to enhance bulk material properties, there also exists the potential to create new chemistry that proceeds along pathways that are inaccessible in force-free regimes. As previously mentioned, this has been elegantly demonstrated by the Moore group in the Woodward-Hoffmann disallowed ring opening of BCB.[30] Fundamentally, this is based on the directionality of applied force, however the Craig and Martinez groups have recently demonstrated that reactions can be created that leverage the highly localized nature of this applied force.

In contrast to other *g*DHCs, which undergo electrocyclic ring opening reactions to form 2,3-dihaloalkenes, the *g*DFC moiety is known to undergo a thermal isomerization via a 1,3-diradical transition state.[104] This isomerization is observed when a poly(*g*DFC) is synthesized with a *cis* to *trans* ratio of 1:1.2. Subsequent thermal equilibration overnight at 210 °C gives a *cis* to *trans* ratio of 1:2.6, consistent with the ~1 kcal mol^{-1} stability difference between isomers. As with the ring opening reactions, the isomerization can be accelerated dramatically by mechanical force, nearing completion in less than an hour at ~5 °C when subjected to pulsed ultrasound. Surprisingly, however, the direction of the reaction is reversed. Sonochemical isomerization gives a *cis*:*trans* ratio of 3.5:1. Notably, the ultimate *cis*:*trans* ratio is limited largely by the size of

the mechanically active zone, and 95-98 % of activated *trans* isomers end up as *cis* cyclopropanes.[105]

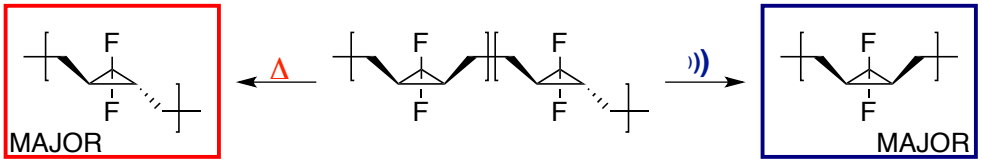

Figure 10 Thermal (*trans*) vs. sonochemical isomerization (*cis*) for poly(*g*DFC). From Lenhardt et al., (2010) *Science*, 329, 1057-1060. Reprinted with permission from AAAS.[105]

The result is qualitatively intriguing on two fronts. First, the mechanical isomerization leads to the less stable isomer, and so the covalent polymer structure can be reversibly switched between predominantly *cis* vs. *trans* states in response to ultrasound and heat, respectively. This behavior constitutes a reversible "mechanoswitch", reminiscent of azobenzene and other photoswitches. Second, the mechanically generated *cis*-*g*DFC has a shorter end-to-end distance than does the *trans*-*g*DFC, leading to the counterintuitive result that the mechanophore undergoes a net contraction in response to being pulled (Figure 10).[105]

This behavior is rooted in the formation and "tension trapping" of the *s*-*trans*/*s*-*trans* diradical transition state as a global minimum on the force-coupled potential energy surface under the transient shear induced tension. The diradical persists until the tension relaxes, either at the end of the bubble collapse or in response to chain scission, at which point the diradical undergoes an orbital-symmetry preferred disrotatory ring closing to the *cis*-*g*DFC. Extensive *ab initio* molecular quantum molecular dynamics

simulations were performed to determine the force regimes and time-scales over which these transformations occur. The application of 2 nN of force to *cis* attachments resulted in 6 out of 20 *g*DFCs opening in the disrotatory (allowed) pathway within 1 ps, whereas the remaining 14 did not open (though would be expected to over a longer timescale). The application of 3 nN was required to observe ring opening for the *trans* attachments, giving a result of 1 conrotatory (disallowed) opening out of 20 trajectories within 1 ps. Moreover, ring closure is not observed on the ps timescale, reinforcing the hypothesis that this occurs upon stress-free chain relaxation. Upon relaxation, the force-free ring closure is calculated to occur within 500 fs and proceeding through the thermally allowed (disrotatory) pathway in 95% of cases. A net contraction in contour length of ~7% per monomer occurs with each *trans* to *cis* isomerization event, in stark contrast (and perhaps complement) to *g*DCCs and *g*DBCs, for which contour length increases with each ring opening event. This counterintuitive result demonstrated the first evidence that the *g*DFC system was capable of undergoing mechanical-only reactions, in this case the selective formation of the isomer that is neither kinetically nor thermodynamically favorable under force-free conditions.

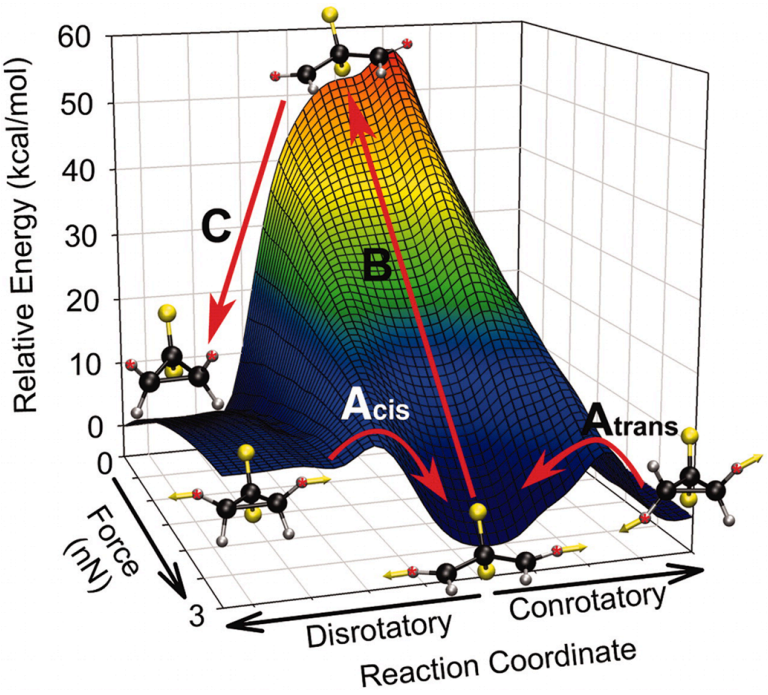

Figure 11 At high force, diradical transition state becomes a global minimum on the potential energy surface: (a) Upon relaxation (b) ring-closure occurs along the thermally allowed disrotatory pathway (c), resulting in the *cis* isomer. From Lenhardt et al., (2010) *Science*, 329, 1057-1060. Reprinted with permission from AAAS.[105]

The *ab initio* simulations indicated that the 1,3-diradical that results from *g*DFC ring opening becomes a local minimum on the force-modified potential energy surface at forces greater than 1 nN, and a global minimum above 3 nN (Figure 11). This near-inversion of the potential energy surface suggested that the 1,3-diradical may be stabilized sufficiently to participate in bimolecular addition chemistry. Gratifyingly, sonication of the *g*DFC polymer in the presence of coumarin-2,2,6,6-tetramethylpiperidine-1-oxyl (CT) adduct resulted in CT addition to the *g*DFC radical, a reaction that cannot occur on the force-free potential energy surface (Figure 12). The rate

constant for nitroxide addition is likely on the order of, or less than, 10^8 M^{-1} s^{-1},[106] and so the observed trapping efficiency of 1-2% corresponds to a diradical lifetime on the order of 10^{-9} s or longer.

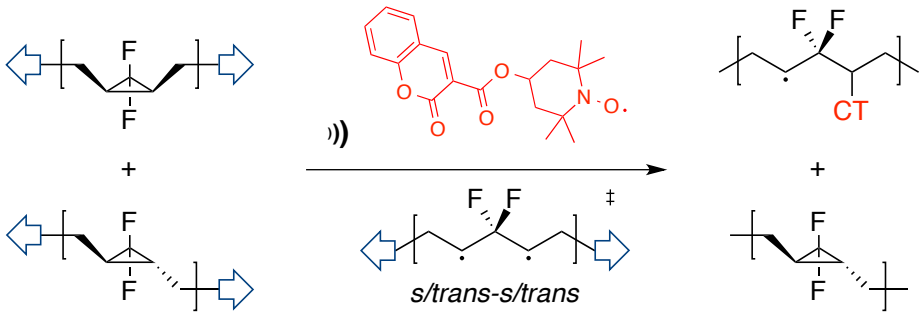

Figure 12 Sonication of poly(*g*DFC) in the presence of CT trap results in trapping of the diradical transition state. From Lenhardt et al., (2010) *Science*, 329, 1057-1060. Reprinted with permission from AAAS.[105]

Further work has recently shown that multiple diradicals can be trapped in proximity to one another, allowing a new radical elimination reaction to take place between them. The key observation is that the extent of isomerization relative to chain scission varied with the net *g*DFC content of the polymer; higher *g*DFC content gives lower levels of isomerizaton[107] (Figure 13). This behavior differs dramatically from that of the *g*DCCs and *g*DBCs, for both of which isomerization is independent of *g*DHC content, and it suggested that adjacent *g*DFCs might behave differently than *g*DFCs that are isolated between nascent butadiene monomer units.

The microstructure hypothesis was tested by synthesizing via ring opening metathesis polymerization (ROMP) a polymer of 33% *g*DFC content in which a *g*DFC

was on every third repeat unit, so that no adjacent *g*DFCs were present. The isolated *g*DFC polymer is a clear outlier from the trend established as a function of *g*DFC content with randomly functionalized polymers, as it exhibits a higher percent isomerization per scission cycle than even the lowest random content polymer tested (5% *g*DFC) (Figure 13). In contrast, when large numbers of adjacent *g*DFCs were introduced directly through synthesis, the extent of isomerization dropped to an extent that is consistent with a quantitative relationship established on the basis of the adjacent *g*DFC content of random copolymers. These experiments confirmed that polymer microstructure, and not simply the total *g*DFC content, is responsible for the observed reactivity trends.

The requirement for adjacent gDFCs and the detection of 3,3-difluoroalkene endgroup products by ^{1}H and ^{19}F NMR led to a proposed mechanism whereby adjacent 1,3-diradicals disproportionate via elimination of the central 1,4-diradical (Figure 14a). The scissile bond is weaker than a conventional covalent bond, and so chain scission occurs earlier in the stretching of the polymer chain, resulting in a lower extent of gDFC opening/closing and isomerizaton (Figure 14b). The mechanism is consistent with the experimental observations, intuitively satisfying, and, importantly, confirmed by ab initio simulations, which at 3 nN of simulated force showed the rapid formation of adjacent diradicals followed by the proposed disproportionation. The force-induced reactivity is somewhat remarkable, because the force-free transition state of this elimination (really a "transition state upon transition states") would correspond to an

activation energy in excess of 120 kcal mol-1, pointing further to the remarkable potential of mechanical force to create reaction pathways that are impossible by other means and presenting a framework for creating "mechanical only" response in materials.

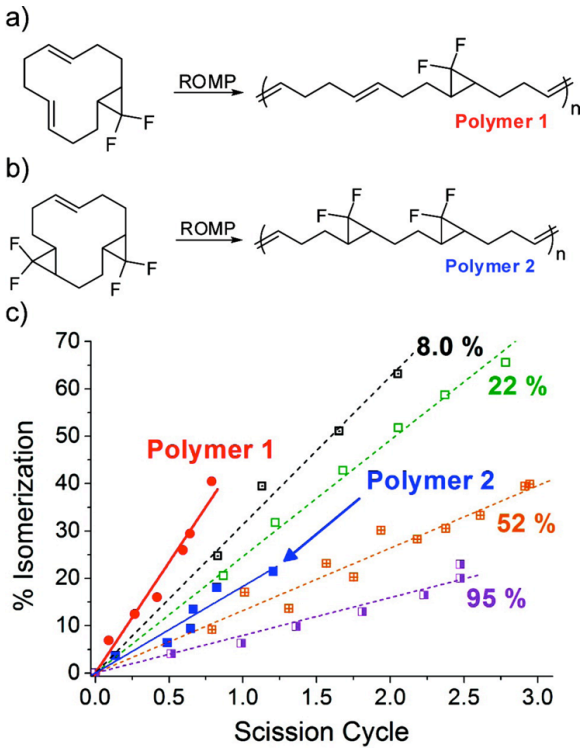

Figure 13 Percent isomerization vs. scission cycle decreases with increased *g*DFC incorporation. Polymers 1 and 2 are outliers from this trend. Adapted with permission from Lenhardt et al., *J. Am. Chem. Soc.*, 133, 3222-3225. Copyright (2011) American Chemical Society.[107]

The PB-co-*g*DFC polymer represents a versatile system that can potentially partake in a rich array of chemistry and be synthesized from relatively inexpensive commercially available components in one step. As with the *g*DBCs studied by AFM, the contour length modulation is particularly intriguing, although here it is a contractile,

rather than extensile, response. If a force regime can be reached where isomerization occurs and chain scission is eliminated, once can imagine the chain length contracting under a mechanical load and re-extending under subsequent thermodynamic equilibration (*cis* to *trans* thermal annealing). Furthermore, the mechanically generated radicals in this system are truly unique relative to force-free chemistry. The 1,3-diradical has been shown to exist long enough to participate in radical trapping, and this or similar non-scissile radical generation could be leveraged to induce interchain cross-linking under mechanical stress. From a mechanistic perspective, the disproportionation reaction is also unique relative to the molecular process, given that the steady-state concentration of diradicals is effectively zero under force-free conditions. In a broader sense, this demonstration of tension trapping an extremely transient species suggests a possible route to the spectroscopic observation of these and similarly elusive and exotic species and electronic states.

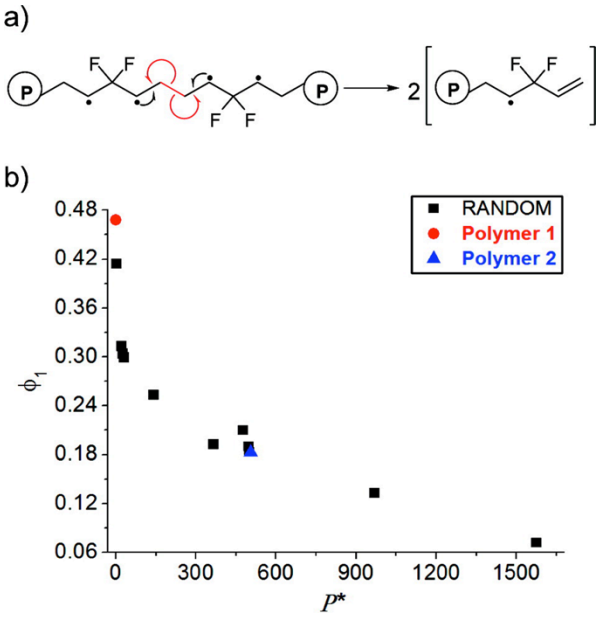

Figure 14 (a) Adjacent diradical intermediates allow for disproportionation and premature chain scission. (b) Percent isomerization per scission cycle (ϕ_1) correlates with the probability of adjacent *g*DFCs (P^*). Adapted with permission from Lenhardt et al., *J. Am. Chem. Soc.*, 133, 3222-3225. Copyright (2011) American Chemical Society.[107]

1.5.2 Thermally Remendable Perfluorinated Mechanophores

These studies on the *g*DFC system led to further exploration of the mechanochemical potential of polymers bearing polycyclic fluorinated backbones. For all of the *g*DHC polymers studied, the chain scission process is irreversible. The engineered mechanochemical outcomes produce ring-opened products, but molecular weight degradation is still predominantly caused by carbon-carbon bond scission. It may then be desirable to add a reversible scission "failsafe" onto the main chain. Previously, Wudl,[41] and later Bielawski,[39] showed the mechanochemically induced retro-Diels-Alder reactions along polymer backbones could be thermally reversed by subsequent heating. Additionally, the work of Sijbesma showed the indefinite

restoration of molecular weight after the mechanochemical rupture of coordination bonds[24,25,36]. To fulfill the requirement of high content and coupling to tension along the polymer backbone, Klukovich and co-workers looked to a family of perfluorocyclobutane polymers (pPFCBs).[108] The synthesis of these polymers is known to proceed through the step-growth dimerization of aryl bis-trifluorovinyl ethers (TFVEs) via a diradical intermediate at elevated temperatures (150-200 °C), but thermal degradation occurs primarily to hexafluorocyclobutene and phenol products. The authors sought to establish that under stress we could bias the degradation to the TFVE endgroups, which could subsequently be repolymerized (Figure 15).[108]

The pPFCB polymer was subjected to standard sonochemical conditions, with an observed drop in molecular weight from 115 kDa to 10 kDa, with the only detectable changes in structure being the conversion of PFCB groups to TFVE groups, as confirmed by both ^{1}H and ^{19}F NMR. Relative integrations of these transformations corresponded with the expected drop in molecular weight determined by gel permeation chromatography with multi-angle laser light scattering (GPC-MALS). Small scale thermal remending was then performed on the sonicated polymer, with an increase in molecular weight from 10 to 37 kDa and corresponding loss in TFVE end group, as characterized by ^{19}F NMR. Given that there is a rich array of available pPFCBs, it is worth noting that this effect was not unique to the biphenyl-ether based polymer (Figure

15), and similar results were observed for a biaryl hexafluoroisopropylidene based PFCB ether polymer.

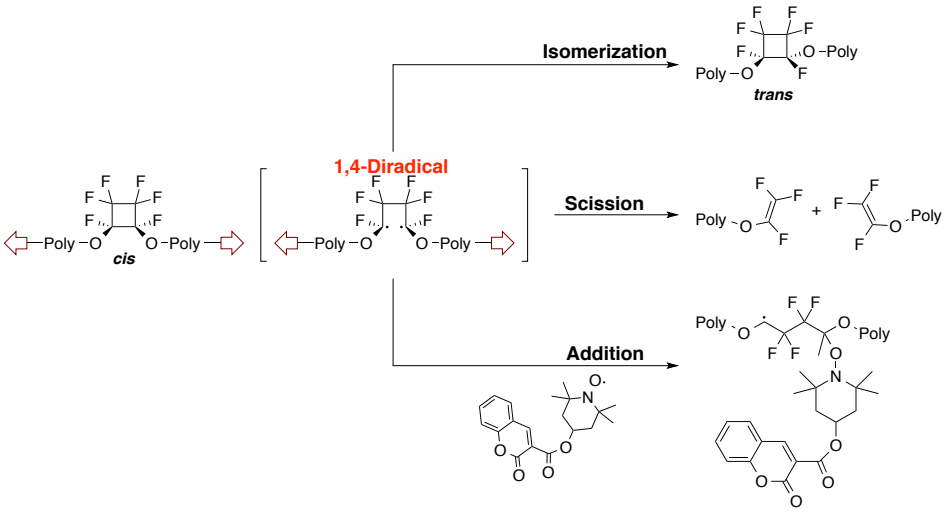

Figure 15 Sonochemical ring opening of *cis*-isomer (disrotatory) can result in chain scission, isomerization to the trans-isomer, or labeling in the presence of the CT trap. Adapted with permission from Klukovich et al., *J. Am. Chem. Soc.*, 133, 17882-17888. Copyright (2011) American Chemical Society.[108]

It was hypothesized that the mechanochemical conversion of PFCB to TFVE proceeds through a 1,4-diradical intermediate, the microscopic reverse of the step-growth polymerization. Mechanistic studies supported this hypothesis and analysis by ^{19}F NMR provided insight into and further proof of the proposed diradical mechanism. The thermal polymerization produces a stereorandom polymer (i.e. the initial polymer sample) with a *cis*:*trans* ratio of 48:52. An observed increase in the overall *trans* content with increased sonication time established that the C(3)-C(4) bond in many PFCBs must break without complete scission of the PFCBs to TFVEs. The isomerization might result

either from preferential ring opening of the *cis* isomers or preferential ring closure to the *trans* (or both), but in either case it offers an additional example of backbone remodeling in response to mechanical force. As in previous experiments, the polymer was sonicated in the presence of the CT radical trap, and CT incorporation was observed and quantified by GPC-UV-Vis. It is worth noting that the PFCB isomerization and associated tension trapping of main-chain radicals occurs here within a family of well-known commercial polymers, offering some hope that the concept of mechanochemical remodeling might be applicable outside of the academic laboratory.

1.6 Challenges

The success of the proposed approach to the construction of stress-responsive/self-healing materials relies on: the ability to construct polymers that (1) have high mechanophore content, (2) increase in contour length when stressed, and (3) generate the ability to participate in bond-forming reactions. In the past several years, this trajectory has proven fruitful, as the Craig group has developed working model systems that meet all of these criteria. In this regard, the demonstration of mechanical activity in *g*DHCs has proven to be quite enabling, given the ease of synthesis and high degrees of functionality attainable. With this system, dramatic increases in single-molecule contour lengths under stress (and corresponding increases in toughness at the single-molecule level) have been demonstrated, and extents of backbone remodeling that would have not been possible in polymers containing only one mechanophore.

Several discoveries have led to deviations from a linear path to the development of better materials. The *g*DFC system proved rather propitious in this regard, allowing for the first demonstration of trapping a force-free diradical transition state as a force-coupled ground state. Complementary to this, was the discovery of one of the few known "mechanical only" organic transformations, where the localized nature of applied stress allows for the disproportionation of adjacent, trapped diradical transition states.

Recently, Leibler and co-workers outlined design principles for supramolecular self-healing systems. They stated that the strength of the supramolecular associations (mechanically scissile bonds) must be lower than that of covalent bonds in order to ensure availability of mending sites. It was also suggested that self-healing efficiency relies on the number of groups available to associate after fracture.[109] Given the dynamic nature of the systems described, it is possible that purely covalent systems can fulfill the self-healing criteria set forth in the context of non-covalent networks. Traditionally, supramolecular systems with self-healing properties rely on dissociation rates that are favorable when compared to covalent bond scission and association rates that are favorable on the time scale where healing is required. As shown,[39,41,108] covalent bonds can be designed to break in a way that they are able to reform. This can be viewed as an extreme example of Leibler's dissociative scenario. In addition, however, the *g*DHCs[84,88,96] and BCB[30,33] demonstrate constructive mechanochemistry, in the form of

stress relief or increased reactivity, in the absence of chain rupture, allowing predominantly constructive outcomes to occur. The kinetics of ring opening (increase in contour length, and generation of functionality amenable to bond formation are also favorable with respect to homolytic bond scission. Relative to supramolecular systems, covalent networks can be completely static in a stress-free state and only undergo dissociation or activation only when stress is applied.

Moving forward, several hurdles had to be overcome as to better understand chemomechanical phenomena and create functional systems. The *g*DHC systems are rare examples of functional groups that can easily be embedded within a high molecular weight polymer backbone in high content. With architectural criteria for mechanical activity becoming more understood, many mechanophores with a wide range of potential transformations are sure to be demonstrated. The incorporation of a single mechanophore into a polymer chain will often be sufficient for many applications, but innovative ways to form high-content materials will remain an additional and important challenge.

To better understand the thermodynamics and kinetics of molecules under force, it is often desirable to apply precise amounts of static tension. Controlled force is typically applied either by SMFS, as in the seminal work of Fernandez and co-workers[42,63] and Craig and co-workers,[26,44,45,88,91] the strained macrocycles of Boulatov,[44,45,91] or through the adsorption of polymer bottle-brushes, as demonstrated by

Sheiko and Matyjaszewski.[110,111] While these methods are relatively robust, high throughput remains a challenge, particularly for SMFS. For example, the ability to efficiently create orthogonal but strong chemical and physical interactions between mechanophore laden polymers and a surface and force microscope tip is often a challenge. Although much of the work involving SMFS has probed interactions in the pN force regime, the activation of covalent bonds requires attachments that can withstand forces on the order of nN, a force regime that requires much more robust attachments.

Efforts transition towards reactions in the bulk, and especially in network formation, analysis becomes difficult. Mechanochemical systems that approach functional materials are realized; it becomes more difficult to probe fundamental mechanisms just as the behavior of interest becomes increasingly complex. This is perhaps particularly true when the goal is a macroscopic response that is generated by molecular and microstructural changes, requiring probes that work across decades of length and time scales. Despite these hurdles, the ability to systematically manipulate molecular structure combined with a firm understanding of relative mechanochemical reactivity, may allow for trends in the molecular to macroscopic property relationship to be established. Current work therefore aims to apply these design principles to as broad a range of polymer systems as possible, seeking to observe the manifestation of

mechanochemical response in bulk material properties such as toughness and self-healing.

1.7 Current Progress

The preceding sections largely outline the challenges and goals set out for me at the outset of this work. Specifically, the creation of mechanochemical systems that adhered to the aforementioned design principles, but beyond the *g*DHC system, was at the forefront of my motivation. Using *g*DHCs to develop stress-strengthening polymers was the primary focus of Ashley Black Ramirez's Ph.D. work, and when I joined the group, Ashley had already demonstrated bond formation in the bulk as shown in Figure 9.[103] Using *g*DBC-polybutadiene in conjunction with dicarboxylate salts, cross-linked polymers and aggregates were generated under extrusion (bulk) and pulsed ultrasound (solution) respectively (Figure 16).

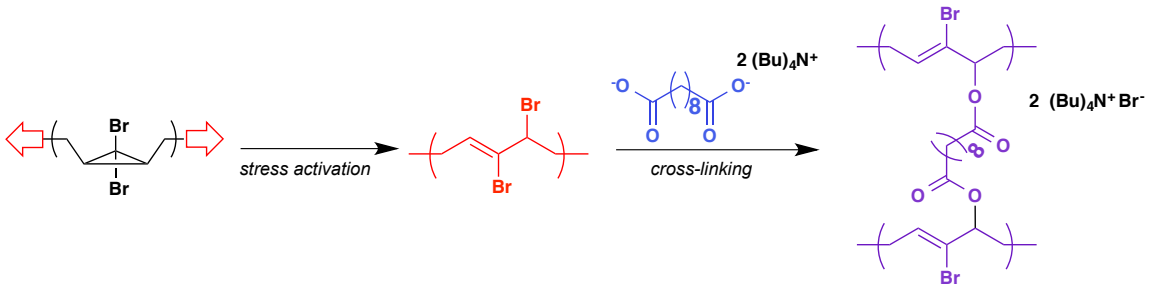

Figure 16 Stress activated *g*DBC reacts intramolecularly with a small molecule dicarboxylate to form cross-linked structures.[112]

Ultimately, we collaborated to develop a more robust ultrasound-responsive self-strengthening polymer, by incorporating tetrabutylammonium carboxylate groups along a *g*DBC-laden polymer backbone by ring-opening metathesis polymerization (ROMP). This new system enabled us to show that cross-linked polymer gels could be obtained by the application of otherwise destructive elongational flow forces to polymers in solution, effectively turning a viscous liquid solution into a solid elastic network (Figure 17).

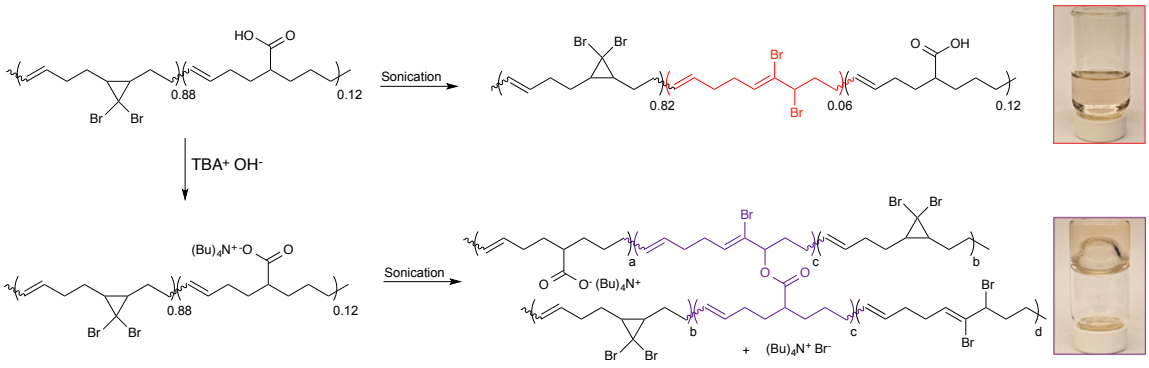

Figure 17 All-in-one stress-strengthening polymer reacts intramolecularly to form cross-linked networks only when deprotonated and subjected to pulsed ultrasound. The result is the stress-induced transformation from a polymer solution (top) to a cross-linked gel (bottom).[112]

As these experiments developed, much of the conversation involved addressing the "short-comings" of the gDHC mechanophores in materials applications. With respect to our design principles this included: limited elongation upon activation, limited activation without irreversible deformation in the bulk, and intermolecular reactions being limited to those with charged nucleophiles (i.e. carboxylates). The work

described in chapters 2 and 3 was ultimately inspired by the desire to develop mechanophores with rationally improved molecular level responses. To this end, Ashley and I adapted the cyclobutane motif as a "universal" mechanophore core. Building off the work of Kryger and Moore, which demonstrated the generation of reactive acrylate chain-ends via [2+2] cycloreversion of poly(methyl acrylate) chain-centered cyclobutane-diesters.[113,114] Chapters 2 and 3 describe cyclobutane-based mechanophores with improved or expanded molecular-level properties relative to the *g*DHC family. Additionally, chapter 3 (and appendix A) describes a new approach to the synthesis of high molecular weight (> 100 kDa) high mechanophore content polymers via carbodiimide polymerization of mechanophore containing diol monomers and aliphatic diacids.

As alluded to in section 1.1, chapter 4 describes the effect of weak non-covalent pincer-based cross-links on the bulk properties of polymer materials. Following the Ph.D. work of Jennifer Hawk, chapter 4 describes the effect of pincer cross-links have by increasing the macroscopic "strain window" of covalent polymer gels.[115] Not only does this serve to challenge the conventionally held notions relating dissipation and fracture toughness in polymer networks,[116,117] but may also suggest a strategy to increase mechanophore activation in otherwise weak materials. Increasing the nominal stress and strain, as well as time under load without catastrophic failure, may allow for greater opportunity for mechanophore activation.

Finally, chapter 5 describes the development and testing of force probe bound chiral ligands.[118] The results show that considerable changes in catalyst selectivity at forces that are readily accessible in bulk materials under non-catastrophic load.[119,120] This demonstrates that force-tuned catalysts may be used to perform covalent mechanochemistry in materials, an alternate yet complementary approach to producing "on-demand" reactivity in regions of high stress.

2. Bicyclo[3.2.0]Heptane Mechanophores for the Non-Scissile and Photochemically Reversible Generation of Reactive Bis-Enones*

2.1 Introduction

Mechanochemically active polymers have the potential to create a new generation of stress responsive and self-healing materials.[17,18] It has been proposed that stress-induced degradation of polymer chains on the molecular level, a mechanism that contributes to failure in bulk materials, could potentially be attenuated by incorporating latent reactive groups that can elicit constructive bond forming reactions in regions of high stress. Additionally, non-scissile mechanochemical ring-opening events may create "on demand" regions of local slack under applied mechanical load, thus preventing catastrophic failure.[88,121] Many examples of stress-responsive mechanophores have been reported,[25,30,33,36,39,66,84,105,108] and they have proved invaluable in studying the rich array of reactivity and stereochemical outcomes available through mechanochemistry. Despite this progress, most mechanophores to date, when activated, result in scission of their parent polymer chain. Examples of non-scissile mechanophores include: benzocyclobutenes (BCBs),[30,33] epoxides,[122] cyclobutene molecular force probes,[45] and *gem*-dihalocyclopropanes (*g*DHCs).[84] These generally offer only modest (1-2 Å) and

* This chapter adapted from: Kean et al. (2012) *J. Am. Chem. Soc.*, *134*, 12939-12942 (with Ashley Black Ramirez).

sometimes transient extensions, and only select *g*DHCs and cyclobutenes generate products with both good stability and significant elongations.

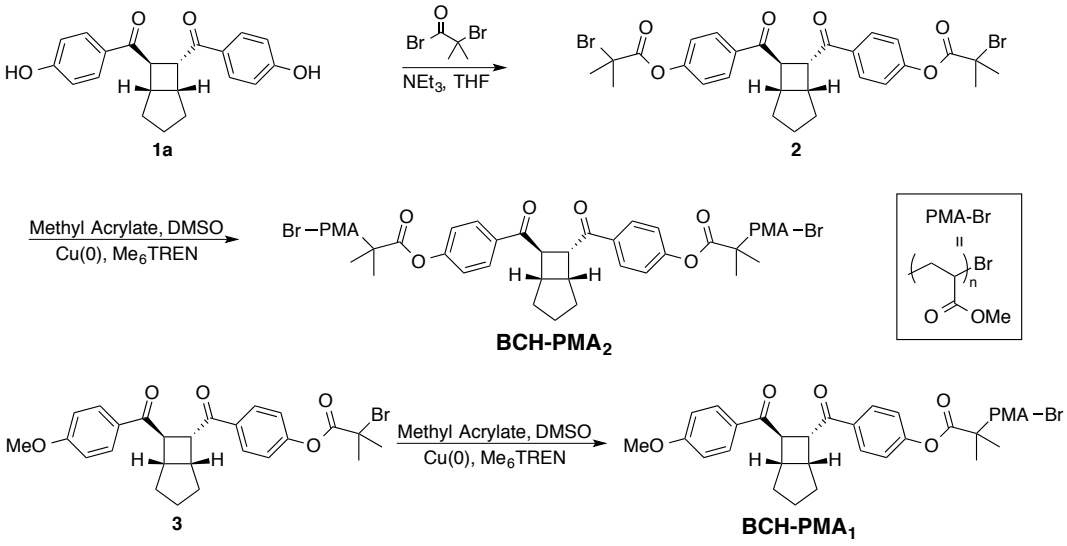

Scheme 1 Synthesis of BCH-linked initiators and PMA used in this chapter.

We therefore set out to construct a non-scissile mechanophore with substantial stored length and a stable activation product that is cross-reactive with uncharged reagents. The extensive palette of existing scissile mechanophores provided a rich set of reactivities from which to draw inspiration. In particular, we took note of the recent report by Moore,[123] in which cyclobutanes were mechanically cleaved to form functionalized acrylate chain-ends. We hypothesized that the mechanophores could be converted from scissile to non-scissile by incorporating them into a fused, bicyclic framework such as a bicyclo[3.2.0]heptane (BCH). In addition to non-scissile behavior and good product reactivity, we envisaged that this design would give large extensions compared to the aforementioned examples, as well as allow for new, two-way switching

behavior via photochemical reversion of the bis-enone products to the starting BCH mechanophore. Here, we report the synthesis and mechanochemical activation of a BCH mechanophore. Features of this system include non-scissile activation, generation of reactive enones, large local elongation, and photochemical reversibility.

2.2 Results and Discussion

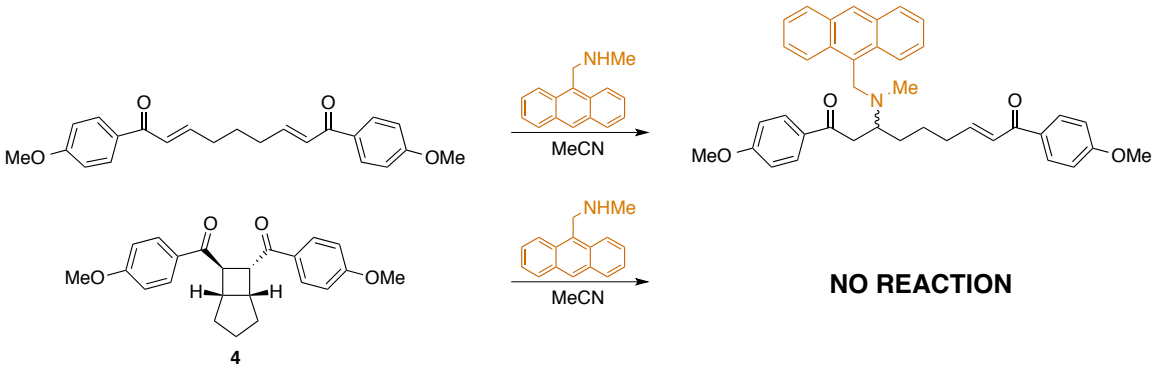

Scheme 2 Orthogonal labeling of BCH and bis-enone small molecule analogues by MAMA.

To access the BCH architecture, we looked to the simple and efficient synthesis of such molecules by Yoon.[124] Bisphenol **1a** was reacted with α-bromoisobutyryl bromide to yield **2**, a BCH-centered difunctional initiator (Scheme 1). Reaction of **2** under standard SET-LRP conditions[28,125] resulted in chain-centered **BCH-PMA$_{2,N}$** with various molecular weights (N = MW). Additionally, a similar strategy was used to access monofunctional initiator **3**, for the synthesis of end-functional control polymer **BCH-PMA$_1$** (Scheme 1). Chain-end linked mechanophores are commonly used as control systems in pulsed ultrasound as shear stresses accumulate towards the center of the

chain, precluding activation at the chain end. The low mechanophore content in these systems generally precludes direct observation of the reaction outcome by ^{1}H NMR, and the most common strategy to detect activation is to label the reaction products with UV active functionalities.[30,39,126] To ensure orthogonal labeling of the proposed bis-enone product over the starting BCH functionality, we explored the use of conjugate addition by secondary amines (Scheme 2).[127] When small molecule analogue **4**[126] was exposed to 9-methylaminomethyl anthracene (MAMA) (5 equiv, 0.25M) in MeCN overnight, no change was observed in the ^{1}H NMR spectrum. Alternatively, when a bis-enone analogue was subjected to identical conditions, the primary product observed was the mono-MAMA adduct (see experimental section). These observations motivated our experimental design, whereby activation of the BCH functionality by pulsed ultrasound could be tracked by the addition of MAMA to bis-enone products.

When BCH-PMA$_{2,151k}$ is subjected to pulsed ultrasound in acetonitrile (6-9 °C) and subsequently treated with MAMA, the integral of the UV absorbance (365 nm) increases with increasing sonication time (Figure 18). After 120 minutes this increase levels off at a ratio of 2.7:1 vs. the unsonicated sample (0 min) or a value of $\chi_{MAMA} = 0.81$ (Table 1), which we define as additional molecules of MAMA incorporated per initial chain relative to an unsonicated control (see experimental section). Because the MAMA concentration used with the polymers is lower than that used with the small molecule analogue, we expect that the labeling is dominated by formation of the mono-MAMA

adduct. Due to the non-scissile nature of the mechanophore, the change in absorbance does not directly correlate with molecular weight degradation, as mechanophore activation can occur independently from chain scission. For this reason, the absorbance is seen to increase in both high (unbroken chains) and low (broken chains) molecular weight regions of the GPC trace (see plot of UV absorbance vs. time, Figure 26 in experimental section), a first indication of non-scissile activation.

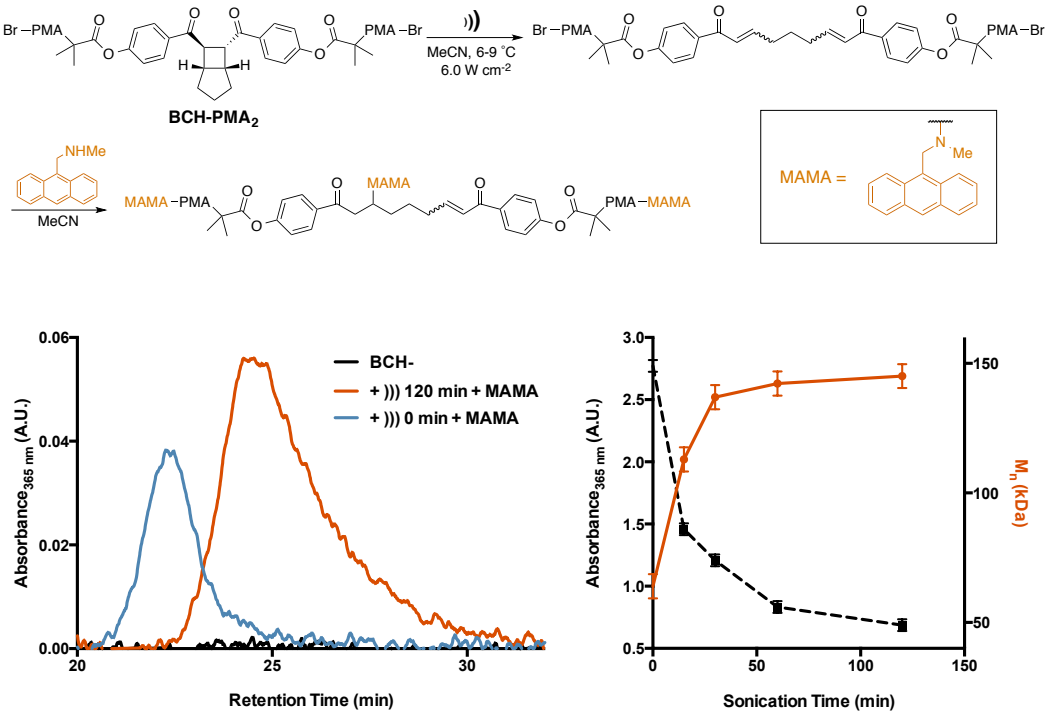

Figure 18 Sonochemical activation and subsequent labeling of bis-enone with MAMA (top). GPC-UV traces (365 nm, left) shows no absorbance in the native polymer (**BCH-PMA$_2$**) (black), the absorbance of the unsonicated polymer treated with MAMA (blue), and the absorbance of the sonicated (120 min) polymer treated with MAMA (orange). Increasing UV absorbance and concurrent MW degradation is plotted at various time points during sonication (right).

Table 1 Summary of **BCH-PMA** and control polymer sonication and labeling experiments

Polymer	M_n	PDI	$M_{n,)))}$	χ_{MAMA}
BCH-$PMA_{2,151k}$	151	1.11	49	0.81
PMA-CRP_{149k}	149	1.11	54	0.15
PMA-FRP_{157k}	157	2.12	51	0.12
BCH-$PMA_{2,23k}$	23	1.08	23	0.11
BCH-$PMA_{1,158k}$	158	1.12	61	0.09

We note the presence of UV absorbance in the control polymer after treatment with MAMA (Table 1, BCH-$PMA_{2,151k}$). This can be attributed to addition of the secondary amine to the chain end α-bromoesters that result from the SET-LRP process. This position is highly susceptible to nucleophilic attack as demonstrated by the "click" reaction with thiophenols described by the Percec group.[128] In support of this mechanism, PMA homopolymer ($PMA_{CRP,149k}$) produced by the same method shows a similar increase in absorbance when reacted with MAMA, with minimal additional increase after sonication (χ_{MAMA} = 0.15). We note that the modest increase in UV absorbance in the control sample is not unusual, and has been observed after sonication in similar labeling experiments.[126] Alternatively, PMA prepared by conventional free radical polymerization ($PMA_{FRP,157k}$) shows no UV absorbance due to lack of halogenated endgroups. Low molecular weight BCH-$PMA_{2,23k}$ also exhibits an increase in absorbance upon treatment with MAMA, and, upon purification by preparatory GPC, its ^{1}H NMR

spectrum shows no change in the BCH functionality. Upon sonication, this polymer exhibits only a mild increase in UV Absorbance (χ_{MAMA} = 0.11). Similar behavior is observed when control polymer BCH-PMA$_1$ bearing chain-end BCH functionality is subjected to identical conditions, yielding a χ_{MAMA} value of 0.09, both results indicating that mechanochemical, rather than thermal processes, drive this ring-opening reaction.

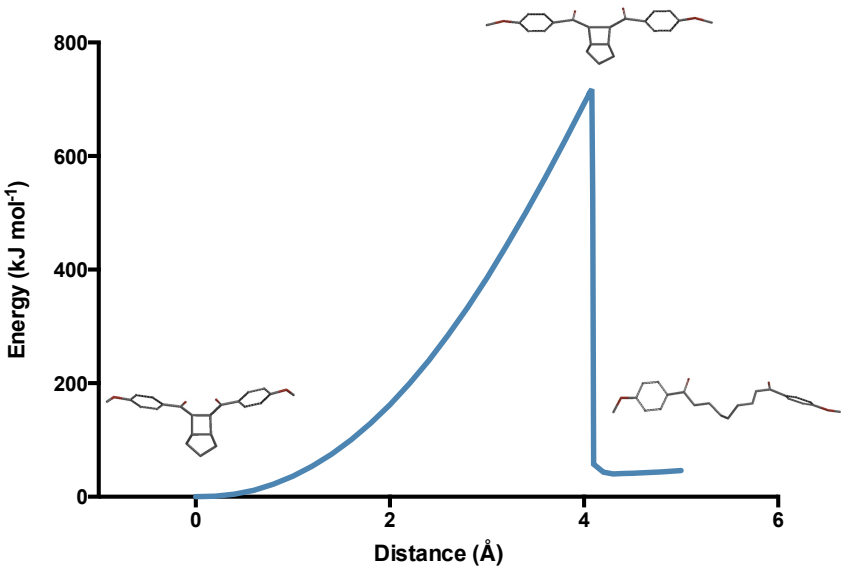

Figure 19 CoGEF energy vs. displacement curve simulating the extension of small molecule analogue **4**.

These results demonstrate that the mechanochemical activity of the fused BCH is qualitatively similar to that of Moore's cyclobutanes that inspired the design. Polymer[122] and mechanophore[123] architecture can have significant and sometimes unexpected effects on mechanical activity, however, and we turned to CoGEF calculations[129] to quantify the impact of the BCH framework on mechanical activity of the cyclobutane. In

the CoGEF calculations, the BCH functionality is seen to transform into the corresponding bis-enone product via a formal retro [2+2] cycloaddition at 4.08 Å elongation (Figure 19). Both this extension at break and the associated force (6.01 nN) are in excellent agreement with that of similar *trans* substituted cyclobutane mechanophores previously reported by the Moore group.[123]

The second ring system appears to fulfill its desired role as an otherwise inert source of stored length. That stored length has the potential to generate large amounts of local slack and increased strain windows between activation and rupture in polymer chains or sub-chains,[88] concepts that motivated our design. Quantitatively, we are able to estimate the elongation upon activation using our CoGEF force-displacement relationship:

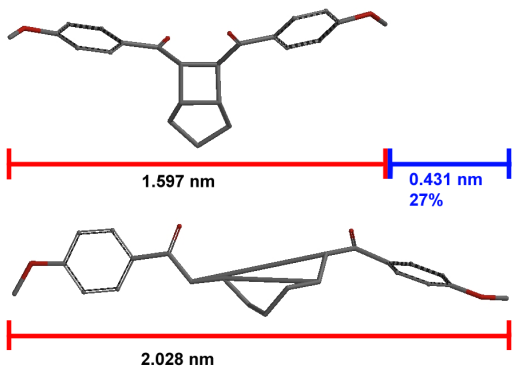

Figure 20 Illustration of change in contour length due to ring opening.

The contour lengths before and after activation were calculated at 100 pN of simulated force (estimating the force necessary to exhaust conformational entropy of a single

polymer chain), showing a local elongation of 4.31 Å, which to our knowledge is the largest extension of any non-scissile mechanophore to date (see experimental section for details).

That extension in contour length can only be realized, however, if the mechanophore is truly non-scissile. That is, the stored length that is released by the retro-cycloaddition must survive the forces required for ring opening. That this is the case is demonstrated by recyclizing the bis-enone under the same $Ru(bpy)_3Cl_2$ sensitized photocyclization used to generate the starting BCH small molecule **1a** (Product C).[124] Sonication and reaction with MAMA (Product B) generates a ~2.6 fold increase in absorbance over the control (Product A), whereas the final UV absorbance from Product C drops appreciably to ~0.8 vs. the control. The photoreversion occurs without a change in MW, confirming an intramolecular, rather than intermolecular, addition of the enones. The chain scission process is therefore spatially and temporally distinct from the BCH activation. Reversible mechanochemistry has been demonstrated for several scissile mechanophores,[39,41,108] but reversibility in non-scissile mechanophores has been limited to the mechanical/thermal *cis*/*trans* isomerization of gem-difluorocyclopropanes,[105,107] switching that comes with no significant difference in intrinsic reactivity between the two states. We believe the BCH mechanophore to be the first example of reversible, non-scissile mechanophores with states of qualitatively

different chemical reactivity, and the first example of photoreversion of an activated mechanophore of any type.

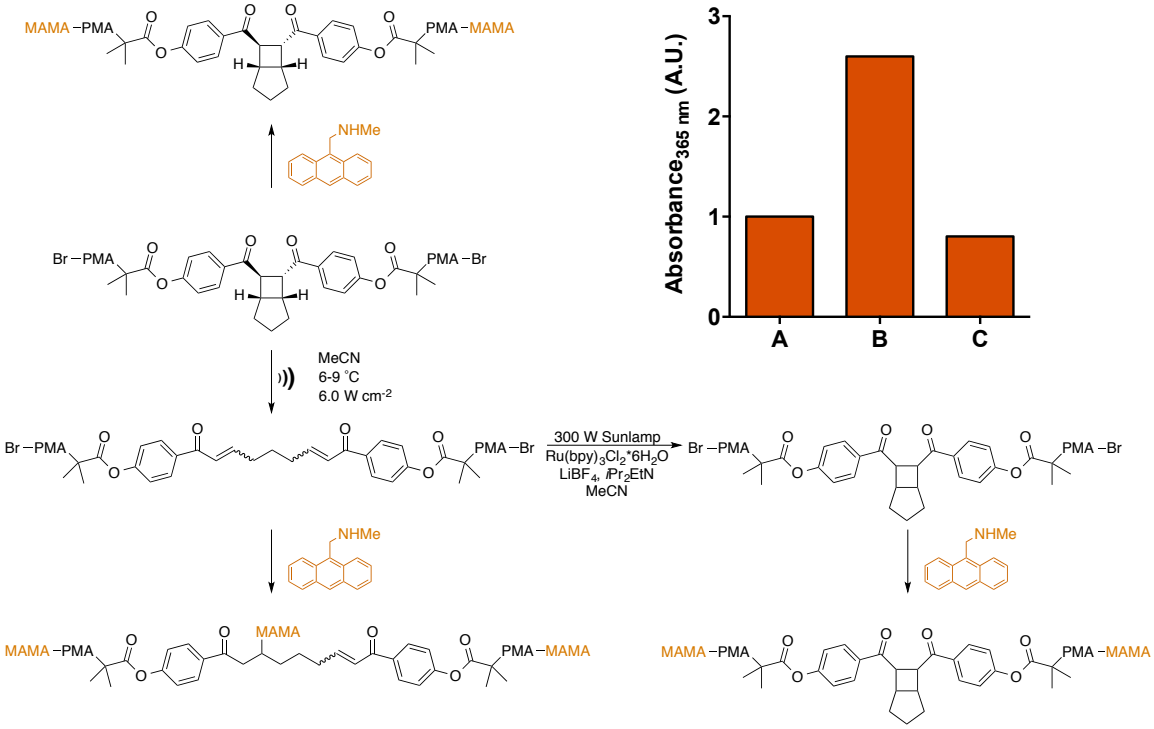

Figure 21 Summary of activation and recyclization experiment. [A] Initial polymer treated with MAMA. [B] After sonication and treatment with MAMA. [C] After recyclization and treatment with MAMA. Absorbance intensity returns to pre-sonication level after photochemical recyclization (inset).

2.3 Conclusion

In conclusion, we have demonstrated the mechanochemical generation of bis-enones via the formal retro [2+2] cycloaddition of a non-scissile bicyclo[3.2.0]heptane based mechanophore. The functionality generated upon activation can participate in conjugate additions that we envision could allow for application in stress-responsive and/or self-healing materials. Furthermore, this reaction is reversible under

photochemical conditions, demonstrating a platform where damage due to stress induced ring opening potentially could be reversed by ambient sunlight. In chapter 3 we continue this work, discussing the synthesis of high mechanophore content analogues of this system for applications along these lines and mechanistic inquiry. [130]

2.4 Experimental

2.4.1 General Procedures

Dry tetrahydrofuran (THF) was obtained from Sigma-Aldrich and purified with a Pure Solv™ solvent purification system before use. 2-(dimethylamino)ethanethiol hydrochloride (95%), α-bromoisobutyryl bromide (98%), triethylamine (99.5%, Sure/Seal™), potassium *tert*-butoxide (99.7%), ethylene bis(2-bromoisobutyrate) (97%), 1,8-diazabicyclo[5.4.0]undec-7-ene (DBU) (98%), and all other solvents were purchased from Sigma-Aldrich and used without further purification unless otherwise specified. 2,2'-azobis(2-methylpropionitrile) (AIBN) (98%) was purchased from Sigma-Aldrich and recrystallized from MeOH before use. Methyl acrylate (99%) was passed through a column of basic alumina to remove inhibitor before use. Cu wire (20 gauge) was purchased from McMaster-Carr and $CDCl_3$ and DMSO-d_6 were purchased from Cambridge Isotope Laboratories. Me_6TREN,[131] **1,** and **4**[124] were prepared as previously reported. All GPC experiments were performed using inhibitor free Chromasolv grade THF obtained from Sigma-Aldrich.

All ^{1}H and ^{13}C spectra were collected in either $CDCl_3$ (δ = 7.26) or DMSO-d_6 (δ = 2.50) and referenced to residual solvent peak on either a Varian 400 or 500 MHz spectrometer. Gel permeation chromatography (GPC) was performed on two in series columns (Agilent Technology PL gel 10^4 Å, 10^3 Å) with THF as the mobile phase at 0.5 mL min^{-1}. The flow rate was set using a Varian Prostar Model 210 pump, and molecular weights were determined using an inline Wyatt Dawn EOS multi-angle light scattering (MALS) detector and a Wyatt Optilab DSP Interferometric Refractometer (RI), while absorption spectra were collected using an inline Varian Prostar Model 320 UV-Vis detector. The dn/dc of PMA polymers was set to 0.068 as previously reported.[132] Preparatory GPC was performed using 3 columns in series (Waters Ultrastyragel 10^6 Å, 10^5 Å, 10^4 Å), with inhibitor free THF as the eluent. The flow rate was set to 6 mL min^{-1} with a Varian Prostar Model 210 pump, and peak detection was determined using a Waters 2414 RI detector. Data for Beer's law plot to determine ε ($MAMA_{365nm}$) was collected on a Varian model Cary 50 Conc UV-Visible Spectrophotometer. GPC peak integrations and normalizations were performed using Origin™ Software and CoGEF calculations were performed using Spartan™ software.

2.4.2 Synthesis and Characterization

Synthesis of Compound 1a:

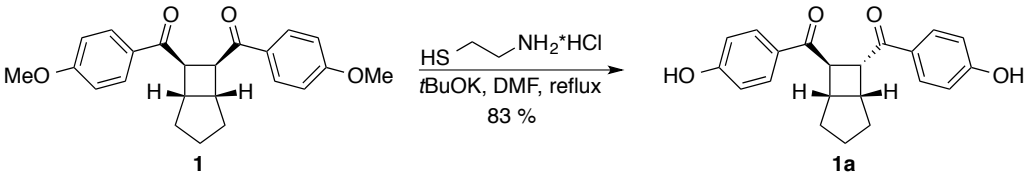

Compound **1** (364 mg, 0.865 mmol) was dissolved in 1.7 mL DMF in a flame-dried round bottom flask under argon. 2-(Dimethylamino)ethanethiol hydrochloride (292 mg, 2.08 mmol) was added as a solid and the resulting suspension was cooled to 0 °C in an ice bath. Potassium *tert*-butoxide (498 mg, 4.45 mmol) was added as a solid and the resulting red solution was stirred for 5 min at 0 °C, 15 min at room temperature, and then subjected to reflux at 153 °C for 3 h. The solution was allowed to cool, carefully acidified with 1 N HCl, and extracted with 2 x 100 mL EtOAc. The combined organics were washed with water, brine, and dried over $MgSO_4$. Upon evaporation under reduced pressure an orange residue was obtained which was then subjected to column chromatography (2:1 hexanes:EtOAc) to obtain 240 mg (0.714 mmol, 83 % yield) of **1a** as a white crystalline solid. **^{1}H NMR** (400 MHz, DMSO-d_6) δ 10.38 (s, 2H, OH), 7.83 (d, J = 8.0 Hz, 4H, ArH), 6.85 (d, J = 8.0 Hz, 4H, ArH), 4.37 (t, J = 9.2, 1H), 4.00 (t, J = 7.0, 1H), 3.18 (dd, J = 16.8, 8.0, 1 H), 2.91 (dd, J = 12.8, 6.4, 1H), 1.81 (m, 1H), 1.67 (m, 2H), 1.42 (m, 1H), 1.26 (m, 2H); **^{13}C NMR** (100 MHz, DMSO-d_6) δ 197.79, 196.04, 162.21, 162.18, 130.80, 130.68, 127.39, 126.70, 115.49, 115.41, 42.30, 39.61, 31.58, 27.89, 25.22; **HRMS-DART** (m/z): calcd for $C_{21}H_{20}O_4$ [MH^+], 337.1434; found, 337.1436.

Synthesis of Compound 1b (mixture of diastereomers):

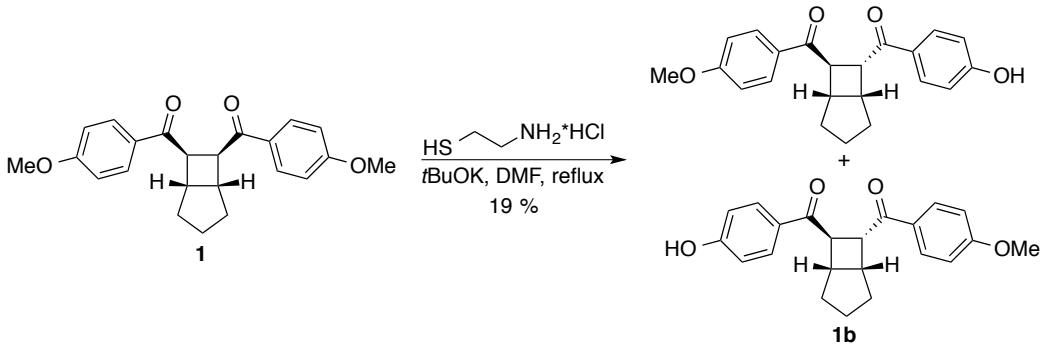

Compound **1** (434 mg, 1.20 mmol) was dissolved in 4 mL DMF in a flame-dried round bottom flask under argon. 2-(Dimethylamino)ethanethiol hydrochloride (142 mg, 1.20 mmol) was added as a solid and the resulting suspension was cooled to 0 °C in an ice bath. Potassium tert-butoxide (112 mg, 3.13 mmol) was added as a solid and the resulting red solution was stirred for 5 min at 0 °C, 15 min at room temperature, and then heated at reflux for 3 hr. The solution was allowed to cool, carefully acidified with 1 N HCl, and extracted with EtOAc (2 x 100 mL). The combined organics were washed with water, brine, and dried over $MgSO_4$. Upon evaporation under reduced pressure an orange residue was obtained which was then subjected to column chromatography (gradient elution: 4:1 to 2:1 hexanes:EtOAc) to obtain 80 mg (0.23 mmol, 19 % yield) of **1b** as a yellow oil (mixture of diastereomers) which was used without further purification. **^{1}H NMR** (400 MHz, $CDCl_3$) δ 8.30 (br s, 1H), 7.74-8.00 (m, 4H), 6.89-6.94 (m, 4H), 4.45-4.59(m, 1H), 4.19-4.27 (m, 1H), 3.84 (s, 3H), 3.13-3.17 (m, 1H), 2.99-3.03 (m, 1H), 1.74-1.86 (m, 3H), 1.36-1.51 (m, 3H); **^{13}C NMR** (100 MHz, $CDCl_3$) δ 200.59, 199.77, 198.15, 197.28, 163.85, 163.76, 161.39, 161.29, 131.29, 131.14, 130.89, 130.75, 128.91, 128.55, 128.41,

128.05, 115.66, 115.63, 113.96, 113.89, 55.48, 42.79, 42.71, 42.65, 40.80, 40.60, 40.42, 32.15, 32.10, 28.28, 25.56; **HRMS-DART** (m/z): calcd for $C_{23}H_{24}O_4$ [MH^+], 365.1747; found, 365.1738.

Synthesis of Compound 2:

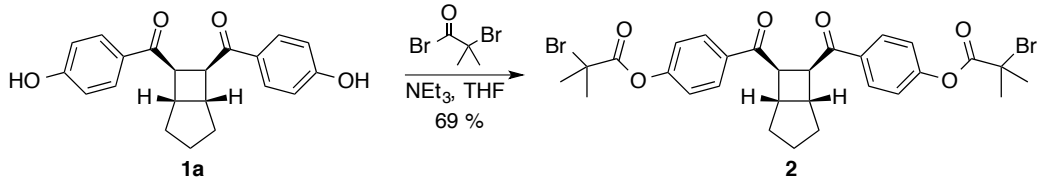

Compound **1a** (108 mg, 0.321 mmol) was dissolved in dry THF (5 mL) in a 10 mL round bottom flask under argon. Dry NEt_3 (0.22 mL, 1.7 mmol) was added by syringe and the solution cooled to 0 °C. α-Bromoisobutyryl bromide (0.12 mL, 0.96 mmol) was added dropwise by syringe. After 30 minutes, the solution was allowed to warm to room temperature and was stirred overnight under argon. The reaction mixture was taken up in 100 mL Et_2O and washed with 3 x 100 mL saturated aqueous K_2CO_3. The organic layer was dried over $MgSO_4$ and solvent removed under reduced pressure to afford a yellow residue. The crude residue was subjected to column chromatography (9:1 hexanes: EtOAc) to afford 140 mg (220 mmol, 69 % yield) of **2** as a white crystalline solid. **^{1}H NMR** (400 MHz, $CDCl_3$) δ 8.06 (d, J = 8 Hz, 2H), 7.99 (d, J = 8.0 Hz, 2H), 7.24 (d, J = 3.2 Hz, 2H), 7.22 (d, J = 3.2 Hz, 2H), 4.54 (t, J = 8.8 Hz, 1H), 4.24 (t, J = 6.8, 1H), 3.16-3.27 (m, 1H), 3.01-3.09 (m, 1H), 2.05 (s, 12H), 1.74-1.89 (m, 1H), 1.46-1.54 (m, 1H), 1.33-1.42 (m, 1H); **^{13}C NMR** (100 MHz, $CDCl_3$) δ 198.84, 196.77, 169.73, 169.68, 154.46, 154.44,

133.98. 133.51, 130.39, 130.05, 121.53, 121.43, 55.16, 43.08, 43.04, 40.40, 40.33, 32.14, 30.56, 28.46, 25.57; **HRMS-DART** (m/z): calcd for $C_{29}H_{30}Br_2O_6$ [MH^+], 633.0482; found, 633.0471.

Synthesis of Compound (mixture of diastereomers) 3:

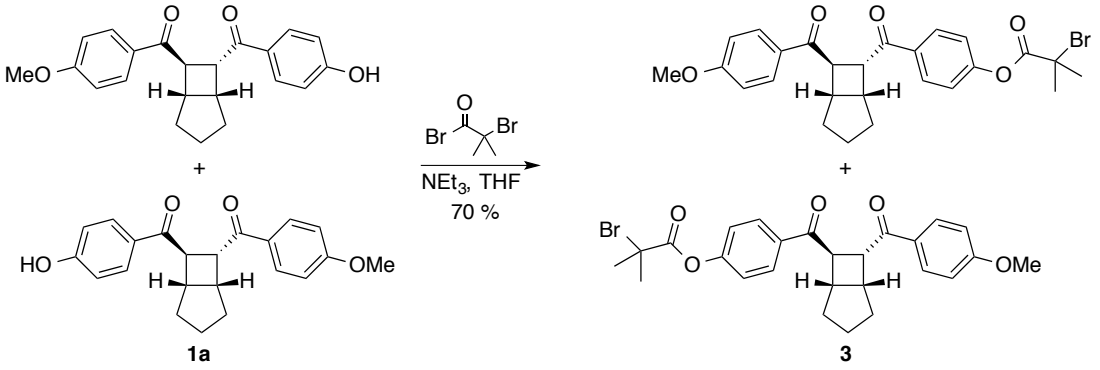

Compound **1b** (76 mg, 0.22 mmol) was dissolved in dry THF (4 mL) and transferred to an oven-dried round bottom flask under argon. Triethylamine (60 μL, 0.43 mmol) was added by syringe and the reaction mixture was cooled to 0 °C. α-Bromoisobutyryl bromide (40 μL, 0.33 mmol) was added dropwise and the solution was allowed to warm to room temperature and stir for 1.5 hours. The solvent was then evaporated under reduced pressure and subjected to column chromatography (silica gel, 9:1 hexanes: EtOAc) to yield 76 mg (0.15 mmol, 70% yield) of **3** as a white crystalline solid (mixture of diastereomers). **^{1}H NMR** (400 MHz, $CDCl_3$) δ 7.88-8.06 (m, 4H), 7.20-7.24 (m, 2H), 6.91-6.93 (m, 2H), 4.42-4.54 (m, 1H), 4.17-4.24 (m, 1H), 3.83-3.84 (m, 3H), 3.16-3.20 (m, 1H), 3.00-3.09 (m, 1H), 2.04-2.05 (m, 6H), 1.73-1.87 (m, 3H), 1.35-1.53 (m, 3H); **^{13}C NMR** (100 MHz, $CDCl_3$) δ 199.22, 198.77, 197.04, 196.49, 169.78, 169.74, 163.62, 154.40, 134.15, 133.65, 130.95, 130.63, 130.44, 130.04, 129.23, 128.64, 121.51, 121.39, 113.95,

113.87, 55.53, 55.16, 43.14, 43.06, 42.74, 40.54, 40.37, 40.08, 32.24, 32.15, 30.58, 28.49, 28.45, 25.66, 25.62; **HRMS-DART** (m/z): calcd for $C_{26}H_{27}BrO_5$ [MH^+], 499.1115; found, 499.1108.

Synthesis of Compound 4:

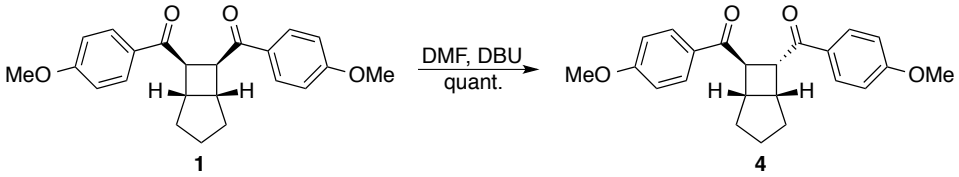

1 (231 mg, 0.634 mmol) was dissolved in 2 mL of DMF under argon. DBU (0.190 mL, 1.27 mmol) was added by syringe and stirred overnight. The solution was diluted with 50 mL ethyl acetate and extracted 3x with 1 N HCl, 1x with sat. aq. $NaHCO_3$, and brine. The organic layer was dried over $MgSO_4$, filtered, and evaporated under reduced pressure to afford **5** as a yellow solid in quantitative yield. **^{1}H NMR** (400 MHz, $CDCl_3$) δ 8.00 (d, J = 10 Hz, 2H), 7.91 (d, J = 10.0 Hz, 2H), 6.92 (d, J = 10 Hz, 4H), 4.47 (t, J = 9 Hz, 1H), 4.22 (t, J = 7, 1H), 3.85 and 3.84 (s, 3H), 3.16-3.22 (m, 1H), 3.01-3.10 (m, 1H), 1.71-1.89 (m, 3H), 1.37-1.54 (m, 3H); **^{13}C NMR** (100 MHz, $CDCl_3$) δ 200.70, 199.89, 198.27, 197.40, 163.97, 163.88, 161.51, 161.41, 131.41, 131.26, 131.01, 130.87, 128.67, 128.53, 128.17, 115.78, 115.74, 114.08, 114.01, 55.60, 42.91, 42.89, 42.83, 42.77, 40.92, 40.72, 40.54, 32.27, 32.22, 28.40, 25.68; **HRMS-DART** (m/z): calcd for $C_{22}H_{22}O_4$ [MH^+], 351.1591; found, 351.1599.

Synthesis of BCH-PMA$_{2,151k}$:

2 (20 mg, 0.032 mmol), methyl acrylate (6.6 mL, 73 mmol), and DMSO (13.3 mL) were combined in a 25 mL pear-shaped Schlenk flask with side-arm and a stirbar wrapped with 2 cm Cu wire (20 gauge). The solution was sparged via three freeze-pump-thaw cycles and placed in a thermostated water bath (25 °C) under argon. While stirring, Me_6TREN (9.5 μL, 0.064 mmol) was added by syringe to initiate the polymerization. After approximately 2.5 hours, the reaction was terminated by exposure to air, diluted with DCM, and twice precipitated into ice cold MeOH. The tacky solid was collected and dried under vacuum overnight to yield 3.61 g of polymer. **GPC-MALS**: M_n = 151 kDa, PDI = 1.11; **^{1}H NMR** (400 MHz, $CDCl_3$) δ 3.15-3.90 (br, 3H), 2.05-2.30 (br, 1H), 1.25-1.90 (br, 2H); **^{13}C NMR** (100 MHz, $CDCl_3$) δ 174.79, 51.68, 41.18, 34.84.

Synthesis of BCH-PMA$_{1,158k}$:

Mono-initiator **3** (3.0 mg, 0.0060 mmol), methyl acrylate (1.27 mL, 14.0 mmol), and DMSO (2.5 mL) were combined in a 10 mL pear-shaped Schlenk flask with side-arm and a stirbar wrapped with 2 cm Cu wire (20 gauge). The solution was degassed via three freeze-pump-thaw cycles and placed in a thermostated water bath (25 °C) under argon. While stirring, Me_6TREN (0.88 μL, 0.0060 mmol) was added by syringe to initiate the polymerization. After approximately 4 hours, the reaction was terminated by exposure to air, diluted with DCM, and twice precipitated into ice cold MeOH. The

tacky solid was collected and dried under vacuum overnight to yield 681 mg of polymer. **GPC-MALS**: M_n = 158 kDa, PDI = 1.12; **^{1}H NMR** (400 MHz, $CDCl_3$) δ 3.15-3.90 (br, 3H), 2.05-2.30 (br, 1H), 1.25-1.90 (br, 2H); **^{13}C NMR** (125 MHz, $CDCl_3$) δ 174.77, 51.63, 41.16, 34.82.

2.4.2.7 Synthesis of BCH-PMA$_{2,182k}$:

2 (8.6 mg, 0.014 mmol), methyl acrylate (2.9 mL, 32 mmol), and DMSO (5.7 mL) were combined in a 25 mL pear-shaped Schlenk flask with side-arm and a stirbar wrapped with 2 cm Cu wire (20 gauge). The solution was sparged via three freeze-pump-thaw cycles and placed in a thermostated water bath (25 °C) under argon. While stirring, Me_6TREN (4.1 μL, 0.027 mmol) was added by syringe to initiate the polymerization. After approximately 2.5 hours, the reaction was terminated by exposure to air, diluted with DCM, and twice precipitated into ice cold MeOH. The tacky solid was collected and dried under vacuum overnight to yield 1.53 g of polymer. **GPC-MALS**: M_n = 182 kDa, PDI = 1.11; **^{1}H NMR** (400 MHz, $CDCl_3$) δ 3.15-3.90 (br, 3H), 2.05-2.30 (br, 1H), 1.25-1.90 (br, 2H); **^{13}C NMR** (100 MHz, $CDCl_3$) δ 174.72, 51.60, 41.10, 34.76.

Synthesis of BCH-PMA$_{2,23k}$:

2 (20 mg, 0.032 mmol), methyl acrylate (1.0 mL, 11 mmol), and DMSO (2.0 mL) were combined in a 25 mL pear-shaped Schlenk flask with side-arm and a stirbar wrapped with 2 cm Cu-wire (20 gauge). The solution was sparged via three freeze-

pump-thaw cycles and placed in a thermostated water bath (25 °C) under argon. While stirring, Me_6TREN (9.6 μL, 0.064 mmol) was added by syringe to initiate the polymerization. After approximately 45 minutes, the reaction was terminated by exposure to air, diluted with DCM, and twice precipitated into ice cold MeOH. The tacky solid was collected and dried under vacuum overnight to yield 230 mg of polymer. **GPC-MALS**: M_n = 23.4 kDa, PDI = 1.08; **^{1}H NMR** (400 MHz, $CDCl_3$) δ 3.15-3.90 (br, 3H), 2.05-2.30 (br, 1H), 1.25-1.90 (br, 2H); **^{13}C NMR** (100 MHz, $CDCl_3$) δ 174.73, 51.60, 41.09, 34.77.

Synthesis of PMA-LRP $_{149k}$:

Ethylene bis(2-bromoisobutyrate) (5.0 mg, 0.014 mmol), methyl acrylate (3 mL, 32 mmol), and DMSO (6 mL) were combined in a 25 mL pear-shaped Schlenk flask with side-arm and a stirbar wrapped with 2 cm Cu wire (20 gauge). The solution was sparged via three freeze-pump-thaw cycles and placed in a thermostated water bath (25 °C) under argon. While stirring, Me_6TREN (4.2 μL, 0.028 mmol) was added by syringe to initiate the polymerization. After approximately 2.5 hours, the reaction was terminated by exposure to air, diluted with DCM, and twice precipitated into ice cold MeOH. The tacky solid was collected and dried under vacuum overnight to yield 1.34 g of polymer. **GPC-MALS**: M_n = 149 kDa, PDI = 1.10; **^{1}H NMR** (400 MHz, $CDCl_3$) δ 3.15-3.90 (br, 3H), 2.05-2.30 (br, 1H), 1.25-1.90 (br, 2H); **^{13}C NMR** (100 MHz, $CDCl_3$) δ 174.97, 51.83, 41.45, 35.00.

Synthesis of $PMA_{FRP,157k}$:

A solution of AIBN (9.5 mg, 0.058 mmol), methyl acrylate (1.2 mL, 0.060 mmol), and benzene (5 mL) was added to a 25 mL Schlenk flask with side-arm and a stirbar. The solution was sparged via three freeze-pump-thaw cycles and placed in a thermostated oil bath (60 °C) under argon for 17 hours. The solution was diluted with DCM, and twice precipitated into ice cold MeOH. The tacky solid was collected and dried under vacuum overnight to yield 891 mg of polymer. **GPC-MALS**: M_n = 157 kDa, PDI = 2.12; **^{1}H NMR** (400 MHz, $CDCl_3$) δ 3.15-3.90 (br, 3H), 2.05-2.30 (br, 1H), 1.25-1.90 (br, 2H); **^{13}C NMR** (100 MHz, $CDCl_3$) δ 174.83, 51.68, 41.23, 34.89.

2.4.3 Reactions of Small Molecule Analogues

2.4.3.1 Reaction of 4 with MAMA

4 (36 mg, 0.10 mmol) was dissolved in 2 mL MeCN and MAMA (110 mg, 0.50 mmol) was added as a powder. The solution was stirred overnight in a 5 mL vial flushed with nitrogen. The solution was evaporated under reduced pressure and redissolved in $CDCl_3$ for ^{1}H analysis. Stacked spectra below show no change in the peak shifts of **5** (red) or MAMA (green) after reaction (blue).

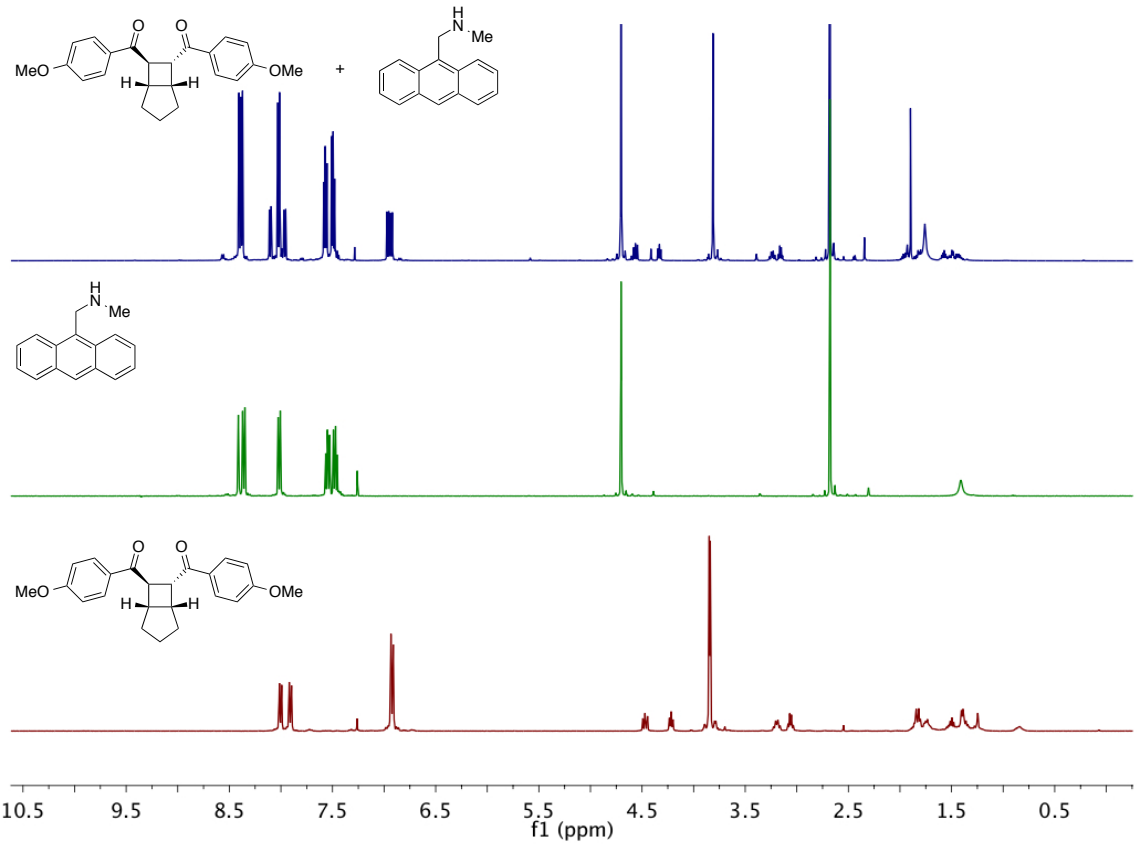

Figure 22 ^{1}H NMR of **4** (red), MAMA (green), and **4** treated with MAMA (blue). No detectable changes in chemical shifts are seen to occur.

2.4.3.2 Reaction of Bis-Enone with MAMA

Liquid chromatography-mass spectrometry was performed on an Agilent Technologies 6224 TOF LC/MS using an Ascentis 2 x 50 mm C_{18} column with a particle size of 2.6 μm. Gradient elution was performed for all runs from 70:30 (A:B) to 90:10 (A:B) over 10 minutes (A: 98% H_2O/2% MeCN/0.3% HCOOH, B: 98% MeCN/2% H_2O/0.3% HCOOH).

Bis-enone (150 mg, 0.412 mmol) was dissolved in 2 mL MeCN and MAMA (455 mg, 2.06 mmol) was added as a powder. The solution was stirred in a 5 mL vial flushed with nitrogen. The resulting solution was subject to analysis by LC-MS at 0.5, 5, and 6 hours. Chromatograph shown below illustrates relative content of mono and di-MAMA adducts.

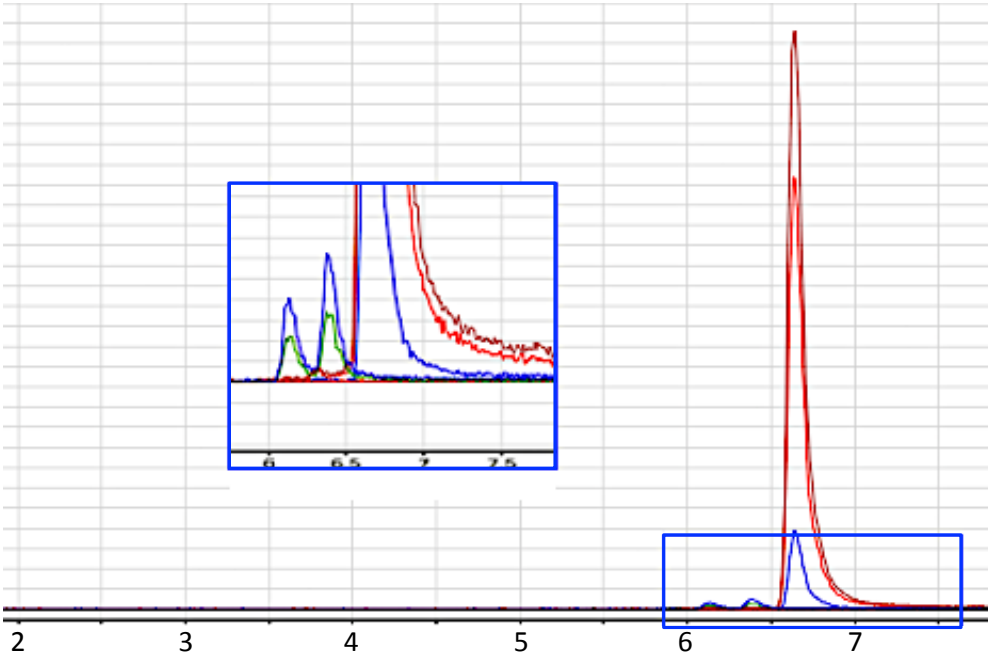

Figure 23 Chromatogram of MAMA addition to bis-enone at 0.5 (blue), 5 (red), and 6 (maroon) hours. Inset: minor peaks at 6-6.5 min correspond to diastereomeric di-adducts. Two peaks between 6.0 and 6.5 minutes correspond to species of identical mass, presumably the *R,S* and *R,R*/*S,S* diastereomeric products of the di-adduct.

2.4.4 Pulsed Ultrasound Studies

2.4.4.1 General procedure

A solution of 70 mg BCH-PMA$_2$ solution in 16 mL MeCN was transferred to a Suslick vessel. This was bubbled with nitrogen for 30 min. before sonication. The solution was sonicated under N_2 in an ice water bath (~6-9 °C) at 6.0 W cm^{-2} with a pulse sequence of 1 s on 2 s off. Aliquots were periodically withdrawn at various time points. In labeling experiments, the aliquots were reacted with MAMA overnight before being analyzed by GPC-MALS-UV-Vis. The sonicated solution was reacted directly with MAMA (20 mg/mL) in a 7 mL scintillation vial equipped with a stirbar. Labeling was performed after sonication to minimize any potential side reactions involving MAMA and to ensure homogenous reaction conditions across all experiments. Before GPC analysis the solutions were filtered through a 0.2 μm pore size PTFE syringe filter, evaporated under reduced pressure, redissolved in THF to an identical volume, and directly injected onto the GPC. Baselines and peak integrations were generated using Origin™ software. All UV integrations were normalized with respect to each other by setting the integral of the corresponding RI peak to unity and scaling the UV integrations accordingly. The results of all experiments are summarized in Table 2.

2.4.4.2 Sonication and Labeling of BCH-PMA$_{2,151k}$

Labeling of the unsonicated polymer BCH-PMA$_{2,151k}$ shows the presence of absorbance at 365 nm due to the incorporation of the anthracene moiety by nucleophilic substitution of α-bromoester bromine by MAMA amine:

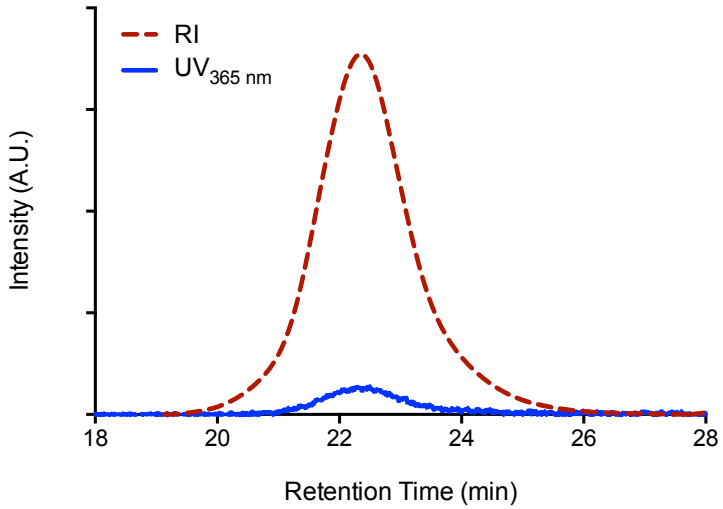

Figure 24 RI (red/dashed) and UV$_{365nm}$ (blue) traces for BCH-PMA$_{2,151k}$ reacted with MAMA without sonication (control).

When BCH-PMA$_{2,151k}$ is first subjected to pulsed ultrasound (120 min) and then reacted with MAMA, an increase in absorbance over that of the control (Figure 24) is observed:

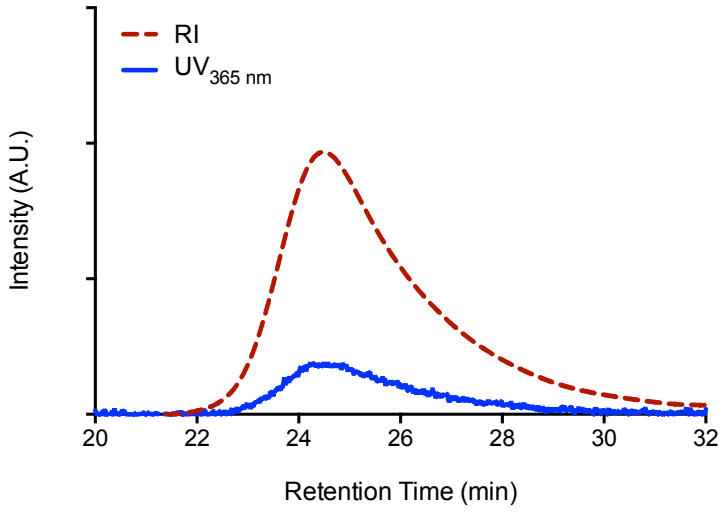

Figure 25 RI (red/dashed) and UV_{365nm} (blue) traces for BCH-$PMA_{2,151k}$ reacted with MAMA after 120 min sonication.

Change in UV absorbance as a function of sonication time as shown in Figure 18 was determined using the GPC-UV absorbance curves and equations shown below:

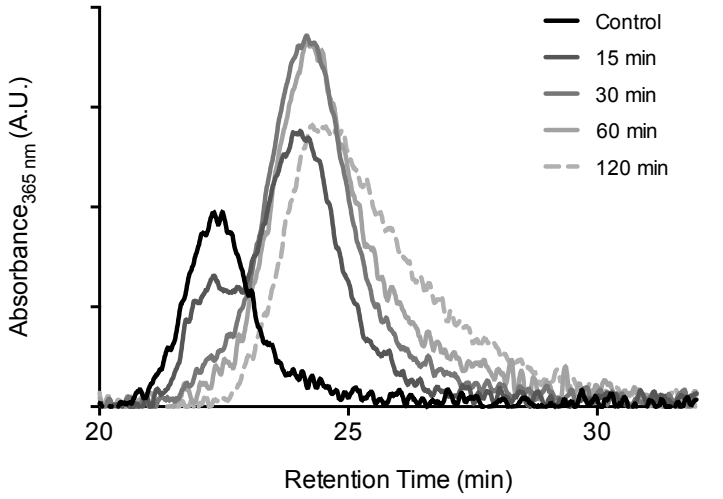

Figure 26 UV_{365nm} traces for BCH-$PMA_{2,151k}$ at various sonication times. Shown as moving average (50 pt) for clarity.

The raw RI integrals were normalized to 1 mg by dividing by the injected mass:

$$\frac{\int RI_{Raw}}{Mass\ Injected(mg)} = \int RI_{Norm}$$

or

$$\frac{\int RI_{Norm}}{\int RI_{Raw}} = N$$

Where the normalization factor N is used to normalize the raw integral UV absorbance:

$$N * \int UV_{Raw} = \int UV_{Norm}$$

The normalized integral UV absorbance for the control was then subtracted from that of the sonicated sample to generate a net UV absorbance due to sonication:

$$\int UV_{Norm,sonicated} - \int UV_{Norm,control} = \int UV_{Norm,net}$$

The moles of MAMA incorporated due to sonication was determined using the following relation:

$$\frac{\int UV_{Norm,net}\ (A * min) * flow\ rate(mL * min^{-1})}{7270\ (mol^{-1}L\ cm^{-1}) * 1cm * \frac{1000\ mL}{L}} = mol_{MAMA}$$

Moles of initial polymer were determined based on MW_N for 1 mg of polymer:

$$\frac{0.001\ g}{MW_{N,Polymer}} = mol_{Polymer}$$

Finally, the χ_{MAMA} value, defined as number of MAMA molecules per initial polymer chain was determined:

$$\frac{mol_{MAMA}}{mol_{Polymer}} = \chi_{MAMA}$$

2.4.4.3 Sonication and Labeling of BCH-PMA$_{1,158k}$

Experiment was performed as described in the general sonication and GPC-UV section. Data was analyzed in a fashion identical to that of BCH-PMA$_{2,151k}$ and results are summarized in Table 2.

2.4.4.4 Sonication and Labeling of BCH-PMA$_{2,23k}$

Experiment was performed as described in the general sonication and GPC-UV section. Data was analyzed in a fashion identical to that of BCH-PMA$_{2,151k}$ and results are summarized in Table 2. BCH-PMA$_{2,23k}$ (blue) was subjected to general sonication conditions and treated with MAMA (green). After typical GPC-UV analysis as described above, the polymer was purified by Preparatory GPC. The resulting ^{1}H NMR spectrum below (red) shows incorporated MAMA aromatic peaks due to chain-end functionalization, as well as unchanged BCH aromatic peaks. This indicates that no reaction occurs between the nascent BCH moiety and MAMA even though anthracene appears to be covalently attached to the polymer, presumably via addition to α-bromoester end-group.

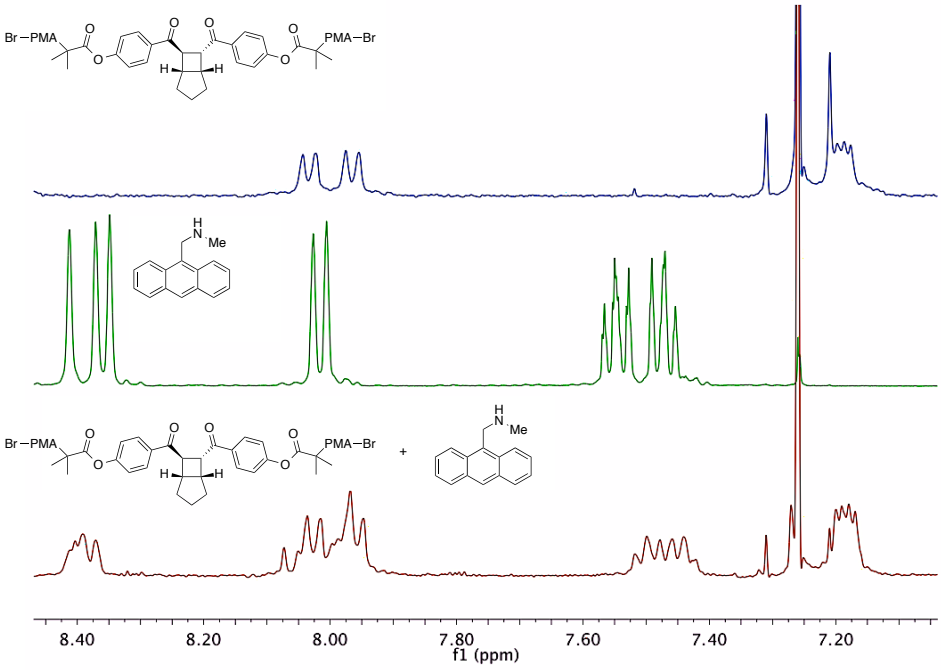

Figure 27 ^{1}H NMR of aromatic region showing no change (red) in peak patterns or shifts to the BCH aromatic protons (blue) after treatment with MAMA (green).

2.4.4.5 Sonication and Labeling of PMA-LRP$_{149k}$

Experiment was performed as described in the general sonication and GPC-UV section. Data was analyzed in a fashion identical to that of BCH-PMA$_{2,151k}$ and results are summarized in Table 2.

2.4.4.6 Sonication and Labeling of PMA-FRP$_{157k}$

Experiment was performed as described in the general sonication and GPC-UV section. Data was analyzed in a fashion identical to that of BCH-PMA$_{2,151k}$ and results are summarized in Table 2. Below is shown the UV and RI traces for PMA-FRP$_{157k}$ (control).

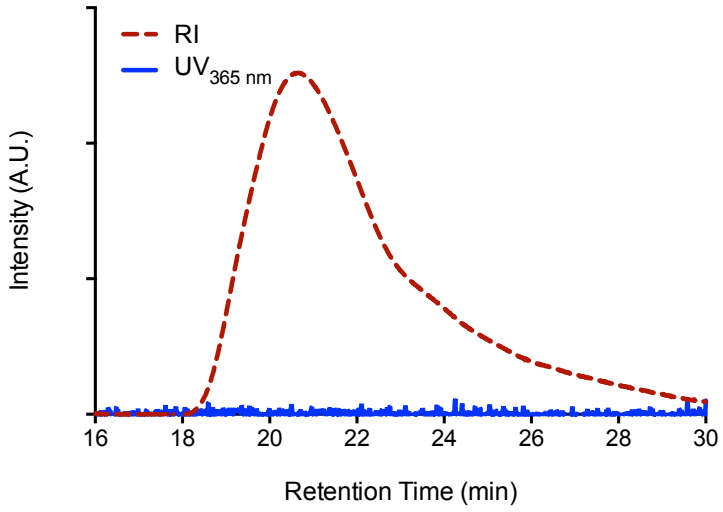

Figure 28 RI (red/dashed) and UV_{365nm} (blue) traces for PMA-FRP_{157k} reacted with MAMA. No discernible UV absorbance is present due to lack of reactive end groups preventing MAMA addition.

2.4.5 Recyclization of BCH-$PMA_{2,182k}$

BCH-$PMA_{2,182k}$ was subjected to sonication and MAMA labeling as described above to generate UV and RI curves "Control" and "Sonicated." A 50.3 mg (2.80 μmol BCH) portion of sonicated BCH-$PMA_{2,182k}$ was reserved (without exposure to MAMA) and subjected to the following conditions: dried Schlenk flask with sidearm under nitrogen. The Lithium tetrafluoroborate (61 mg, 0.65 mmol) and diisopropylethylamine (113 μL, 0.65 mmol) were added to a 10 mL flame sonicated BCH-$PMA_{2,182k}$ (50 mg) was added as a solution in 4 mL MeCN. The solution was subjected to three freeze-pump-thaw cycles, on the third cycle, while frozen, backfilling with nitrogen and adding $Ru(bpy)_3Cl_2 \cdot 6H_2O$ (12 mg, 16 μmol) as a solid while flushing with nitrogen. The flask was sealed with a rubber septum and subjected to three pump-backfill cycles while

frozen. After thawing, the flask was placed 20 cm from a 300 W sunlamp in a water bath and irradiated for 2 hr. The solution was concentrated to a minimal volume and precipitated into MeOH. This was repeated twice more before the polymer was dried in *vacuo* overnight. The polymer was then subjected to MAMA labeling and GPC-UV as described above to generate BCH-PMA$_{2,182k}$ (recyclized) (Table 2).

Table 2 Summary of sonication and labeling experiments.

Polymer	Entry	N	UV_{raw}	UV_{norm}	UV_{net}	M_n (kDa)	mol_{poly}	mol_{MAMA}	χ_{MAMA}
BCH-PMA2$_{151k}$	Control$_{Avg.}$	1.72	0.023	0.040		149	6.7E-09		
	15 min $_{Avg.}$	1.77	0.045	0.080	0.041	86		2.8E-09	0.42
	30 min	1.56	0.066	0.103	0.063	74		4.3E-09	0.65
	60 min	2.67	0.041	0.110	0.071	56		4.9E-09	0.73
	120 min	2.02	0.059	0.118	0.079	49		5.4E-09	0.81
PMA-CRP$_{149k}$	Control	1.49	0.049	0.074		148	6.8E-09		
	Sonicated	2.43	0.036	0.088	0.015	54		1.0E-09	0.15
BCH-PMA$_{2,23k}$	Control	1.56	0.134	0.210		23	4.3E-08		
	Sonicated	1.15	0.241	0.279	0.069	23		4.8E-09	0.11
BCH-PMA$_{1,158k}$	Control	1.70	0.013	0.022		158	6.3E-09		
	Sonicated	1.30	0.023	0.030	0.008	62		5.7E-10	0.09
PMA-FRP$_{157k}$	Control	2.80	0.000	0.000		157	6.4E-09		
	Sonicated	1.81	0.006	0.011	0.011	51		7.5E-10	0.12
BCH-PMA$_{2,182k}$ Recyclization	Control	1.78	0.016	0.028		171			
	Sonicated	1.84	0.040	0.074		55			
	Recyclized	3.73	0.006	0.024		65			

2.4.6 CoGEF Calculations

Procedure was performed similar to that described by Beyer.[133] All calculations were performed using DFT-B3LYP 6-31G* level of theory. After energy minimization, the structures were constrained at the terminal methyl carbons and the constraints were increased in increments of 0.2 Å, with increasingly smaller increments near rupture point as summarized in the table below. Relative energies were generated by setting that of the initial conformer to 0 kJ mol^{-1}. Failure was determined to be the precipitous drop in energy that occurred simultaneously with large elongations in cyclobutane C-C bond lengths (4.08 Å). The relationship between force and elongation was determined as the 1st derivative of a fit (2nd order polynomial) of the energy vs. distance curve (Figure 19).

3. Stress-Responsive Polymers Containing Cyclobutane Core Mechanophores: Reactivity and Mechanistic Insights*

3.1 Introduction

Covalent mechanochemistry has enabled the development of a wide array of stress-responsive polymers for application in the fields of catalysis,[37,65,66] synthesis,[134] stress-sensing,[96,135,136] and self-healing or self-strengthening materials[112] among others. Generally, these mechanochemical transformations are facilitated by polymeric handles, which act as force transducers to direct applied stress to the mechanophore of interest from bulk stress or shear flow,[17] but the relationship between macromolecular and intermolecular forces[137] has allowed molecular force probes to be used to productive effect as well.[44,45,138] Many of the reported mechanochemical transformations are inherently dissociative,[25,28,39,41,108] leading to the chain rupture and molecular weight degradation as a result of their activation. Non-scissile mechanophores allow for several unique molecular responses in the context of stress responsive material systems. First, because non-scissile activation events occur independently of molecular weight degradation, many reactive functional groups may be generated per chain rupture event (i.e. non-specific chain scission in pulsed ultrasound), giving the opportunity for

---

* This chapter adapted from: Kean et al. (2013) *J. Am. Chem. Soc.*, *135*, 13598-13604. Portions of this chapter were performed in collaboration with co-workers as noted where relevant.

constructive bond formation to outpace destructive bond scission in materials under load.[18,103] Second, high local elongations[88,95] can be engineered into these mechanophores, and may provide a basis for molecular level stress-relief in over-stressed subchains in bulk materials under load. These aspects of mechanophore design are heavily influenced by our goal of developing an "on-demand" response in materials under destructive stress in order to delay or prevent catastrophic failure.

Previously, we have explored the *gem*-dihalocyclopropanated (*g*DHC) polybutadiene platform to this end. The *g*DHC mechanophores elongate by ~1.5 Å per cyclopropane and generate reactive 1,3-diradicals or 2,3-dihaloalkenes upon activation.[121] Recently, we utilized this platform to demonstrate a liquid-to-solid transition in polymer solutions under destructive shear as well as stress-induced bond formation and crosslinking in the bulk.[112] Other reported non-scissile mechanophores include benzocyclobutenes,[30] epoxides,[122] spiropyrans,[33] pyrophosphates,[139] and oxanorbornadiene.[140] The Moore group has demonstrated that cyclobutane bearing acrylate polymers exhibit enhanced scission kinetics under the application of pulsed ultrasound leading to the production of functional chain-end acrylates in a net [2+2] cycloreversion.[123,126] We sought to utilize this transformation to develop a new class of non-scissile mechanophores based on fused-cyclobutane structures via the installation of a covalent tether. As described in chapter 2, we previously developed a photoreversible, single mechanophore system embedded in poly(methyl acrylate).[113] Here, we expand the

non-scissile mechanophore repertoire by incorporating the bicyclo[4.2.0]octane (BCO) moiety into high molecular weight (MW) polyesters via carbodiimide polyesterification[141] of BCO containing diester diols. We also use the BCO platform to analyze stereochemical effects on mechanochemical reactivity, for potential self-healing applications via stress-generated α,β-unsaturated ester functional groups, and as a tool for mechanistic inquiry through analysis of stereochemical product distributions.

3.2 Results and Discussion

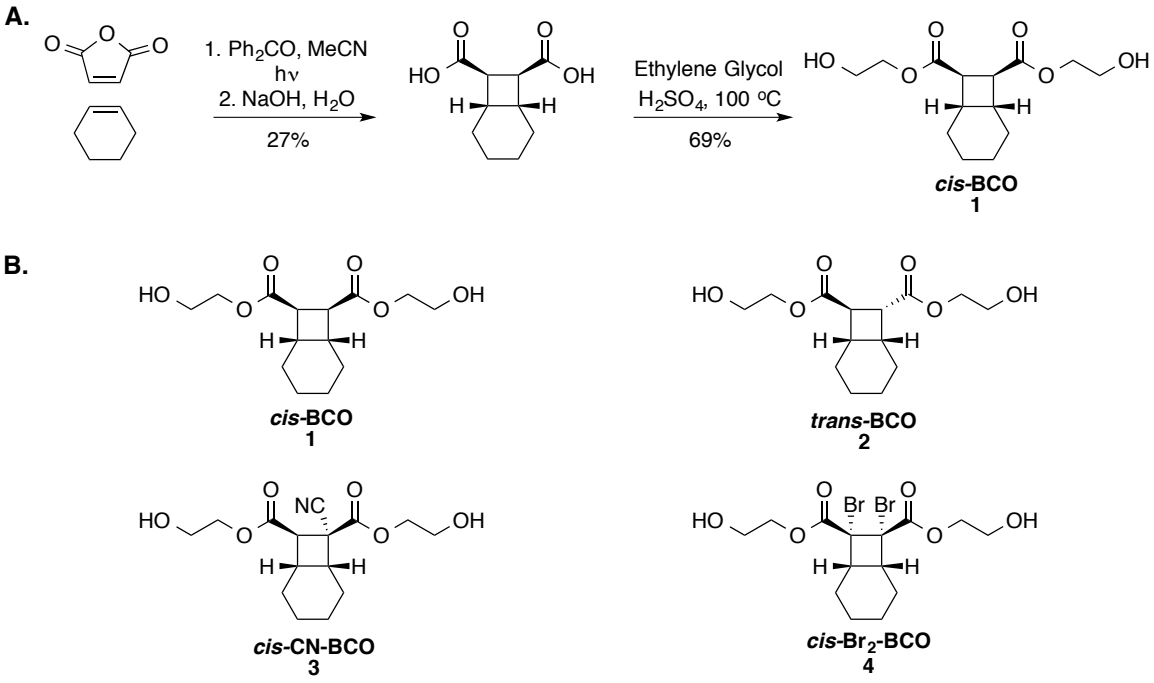

Scheme 3 (a) Representative synthesis of BCO diol monomers. (b) Structures of BCO diol analogues. Compounds synthesized as either *meso* compounds or racemic mixture.

Initially, we aimed to develop a modular and scalable (multi-gram) approach to synthesize fused-cyclobutane bearing monomers. As previously reported,[142] *cis*-BCO

dicarboxylic acid **1a** (Scheme 3) can be prepared in large quantities (~10 g, see experimental section) by photochemical [2+2] cycloaddition of maleic anhydride and cyclohexene in the presence of benzophenone. Basic hydrolysis of the anhydride followed by acidification allows for the precipitation of the carboxylic acid from water in high diastereomeric purity (95%, ^{1}H NMR, see experimental section). Acid-catalyzed esterification with ethylene glycol yields diol-functional *cis*-BCO **1**. Carbodiimide polyesterification, based on the method of Moore and Stupp,[141] of the diol monomer in the presence of glutaric acid, diisopropylcarbodiimide, and DPTS (dimethylaminopyridinium *p*-toluenesulfonate) in DCM (Scheme 3a) yields high-molecular weight polyester (179 kDa, Table 3). High MWs are routinely attainable with this method when polymerization is performed for 48 hours at high monomer concentration (~0.5-1 M). Polymers were characterized by gel permeation chromatography-multi-angle light scattering (GPC-MALS), and undergo multiple chain breaks per polymer chain (on average) during sonication experiments.

Mechanochemical activity was probed via the application of pulsed ultrasound (14.8 W cm^{-2}, 6-9 °C) to **P1 (***cis*-BCO) (179 kDa, MeCN, 2 mg mL^{-1}). Subsequent ^{1}H and ^{13}C NMR analysis revealed the presence of peaks consistent with α,β-unsaturated ester formation, the first direct spectroscopic observation of alkenes formed via the mechanochemical [2+2] cycloreversion of cyclobutanes (Figure 29, see experimental section):

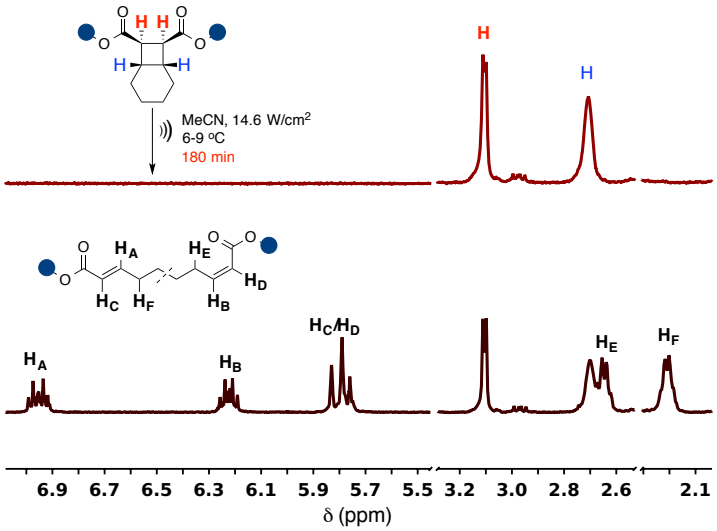

Figure 29 ^{1}H NMR of selected *cis*-BCO peaks before (top) and after (bottom) sonication for 180 minutes shows disappearance of cyclobutane resonances (red and blue) with concurrent appearance of alkene and allyl protons for *E* and *Z* isomers (black).

These resonances were observed to increase as a function of sonication time, reaching 48% ring opening after 180 minutes of sonication time, corresponding to the production of 450 alkenes per initial polymer chain. Due to the non-scissile nature of the mechanophore, many alkenes are formed per chain scission event, allowing for the quantification of percent ring opening (vs. initial BCO content, see the experimental section) at various sonication times with concurrent MW degradation via non-specific chain scission due to the high forces commonly generated during ultrasonication. Using established molecular modeling methods[95,129] (see experimental section), we estimate that elongations of ~7 Å per polymer repeat unit occur as the *cis*-BCO mechanophore unravels under applied stress. This magnitude of covalent stress relief per event exceeds

that reported previously,[88,113,135] and might permit survival of overstressed polymer subchains under strains that are otherwise catastrophic.[121]

Table 3 Summary of polymers used in this study. Polymers were synthesized according to the method outlined in **Scheme 4** from their respective diol monomers shown in **Scheme 3**. MWs (M_n) and PDI were determined by GPC-MALS (see experimental section).

Polymer Name	BCO Diol	M_n (kDa)	PDI
P1 (*cis*-BCO)	1	179	1.43
P2 (*trans*-BCO)	2	155	1.34
P1,2 (*cis/trans*-BCO)	1 & 2	161	1.32
P3 (*cis*-CN-BCO)	3	133	1.28
P4 (*cis*-Br_2-BCO)	4	51	1.35
PC (control)	1 & 2	13	1.28

To demonstrate the mechanochemical nature of the ring opening, we synthesized control polymer **PC** (13.3 kDa, Table 3). Flow forces experienced by low MW polymers are often insufficient to illicit many covalent mechanochemical transformations by pulsed ultrasound, while activation due to purely thermal processes presumably remains unaffected.[17] After 180 minutes of irradiation, polymer **PC** showed no ring opening or appreciable MW degradation (see experimental section).

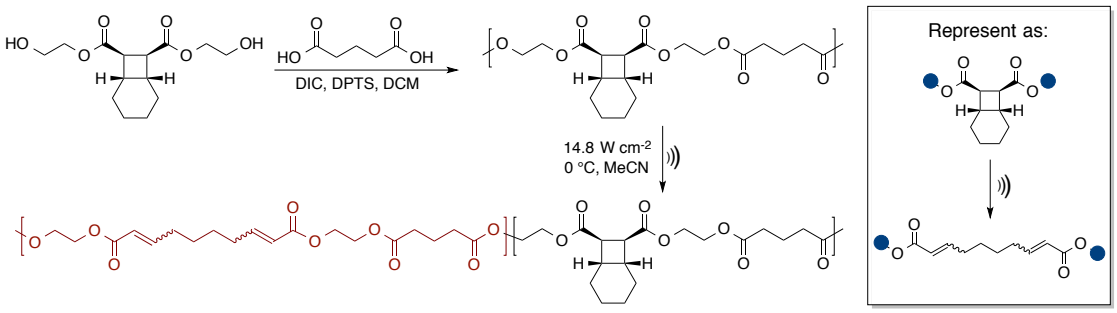

Scheme 4 Carbodiimide polyesterification of BCO-diol and mechanochemical activation by pulsed ultrasound. Blue dots symbolize the polymer structure surrounding BCOs in unactivated polymers and alkenes in activated copolymers (inset).

With the ability to quantify the extent of the mechanochemical [2+2] cycloreversion, we decided to use our platform to probe the relative reactivity of *cis* and *trans* handles to applied force. Previous observations have shown that mechanophores with *trans* attachment points display diminished activation kinetics when compared to their *cis* counterparts.[30,84,123] In the case of benzocyclobutene, this has been attributed to a combination of lower force-free activation energy, greater chemomechanical coupling efficiency, and larger changes in compliance along the reaction coordinate between ground and transition states for the *cis* isomer.[87,94,143] The *trans*-BCO monomer **2** was obtained by base-mediated epimerization of *cis*-BCO (dimethylester) with sodium methoxide and subsequent transesterification with ethylene glycol. The *cis* and *trans* diols were copolymerized into a single polymer **P1,2** (*47:53 cis:trans*, 161 kDa, Table 3) to ensure that the average forces experienced by each isomer were identical during sonochemical experiments. As shown in Figure 30, the percent ring opening for the *cis* isomer exceeded that of the *trans* at all times tested, further validating the observations

of Kryger et. al.[123] It should be noted that while the ring opening disparity diminishes throughout the sonication (from *cis:trans* 2.5:1 at 5 min to 1.6:1 at 180 minutes), this is consistent with exhaustion of the *cis* isomer in the mechanically susceptible region of the polymer chains.[28,80,102]

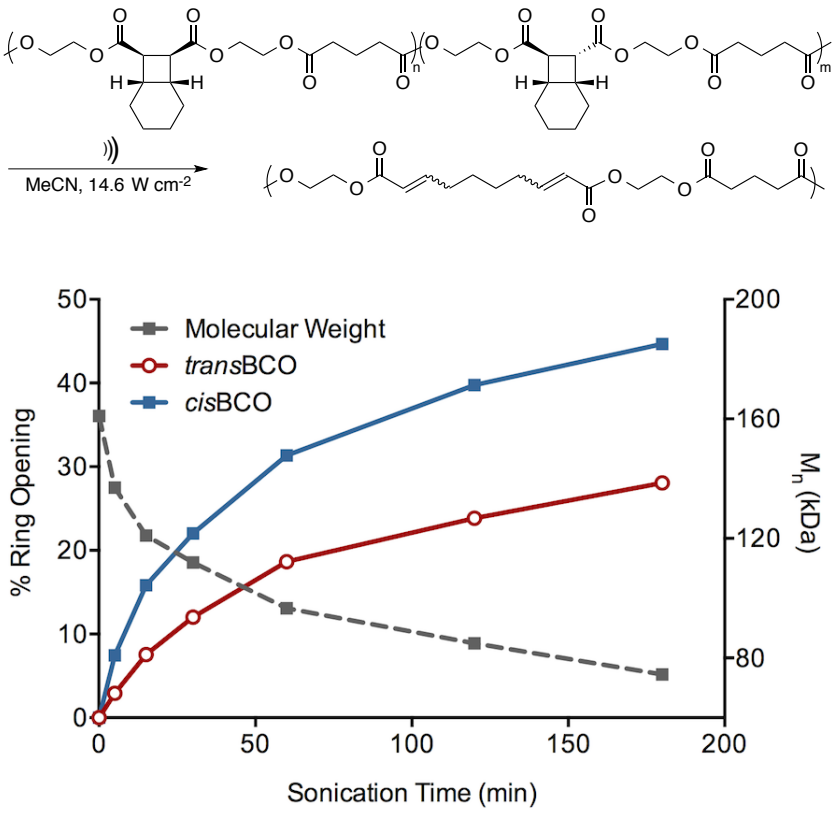

Figure 30 Sonochemical activation of *cis*/*trans*-BCO (**P1,2**) copolymer (top) results in different activation profiles for the two isomers as determined by ^{1}H NMR. MW degradation due to non-specific chain scission (grey) occurs due to high flow forces experienced in pulsed ultrasound.

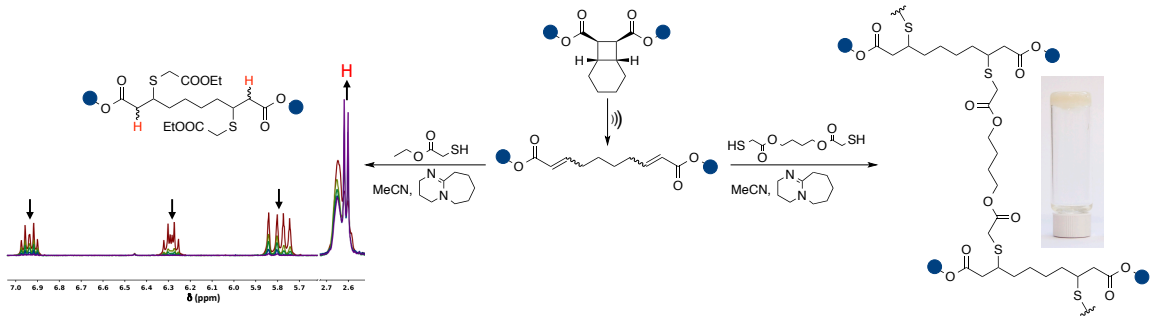

Figure 31 Stress-enabled reactivity of BCO polymers. Unsaturated esters react via nucleophilic thiol-ene conditions to form functionalized copolymers via reaction with mono-functional thiols (left) and network gels via reaction with bifunctional thiols (right).

The unveiled α,β-unsaturated esters are reactive toward a variety of conjugate addition conditions, allowing us to expand the repertoire of stress-induced bond forming reactions. To test the potential for our polymers as self-healing materials we targeted the nucleophilic thiol-ene reaction. *Cis*-BCO polymer **P1** was first sonicated for 180 min (4 mg/mL) to yield a 33% ring-opened polymer. To characterize the efficiency of the reaction, we first reacted the polymer with a mono-functional thiol, ethyl thioglycolate (1.5 eq. per alkene) in acetonitrile-d_3 (~0.1 mmol alkene), with 1,8-diazabicyclo[5.4.0]undec-7-ene (DBU, 0.5 mol%) catalyst. Time points were recorded by ^{1}H NMR and near complete conversion of the alkenes were observed in 65 minutes. Encouraged by the efficiency of the reaction, we subjected a 36% ring-opened *cis*-BCO polymer to identical reaction conditions in the presence of difunctional 1,4-butanediol bis(thioglycolate) (0.5 eq. per alkene) yielding an intractable polymer gel in less than 1 minute (Figure 31). These results demonstrate the potential of this system to participate

in an expanded array of bond forming reactions that occur rapidly under relatively mild (ambient) conditions. Current efforts focus on expanding this approach to *in situ* bond formation both in solution and in bulk materials. This involves both the construction of BCO-containing materials that encourage bulk mechanochemical activation as well as developing BCO analogues that increase the reactivity of the unveiled unsaturation to non-catalyzed conjugate addition.

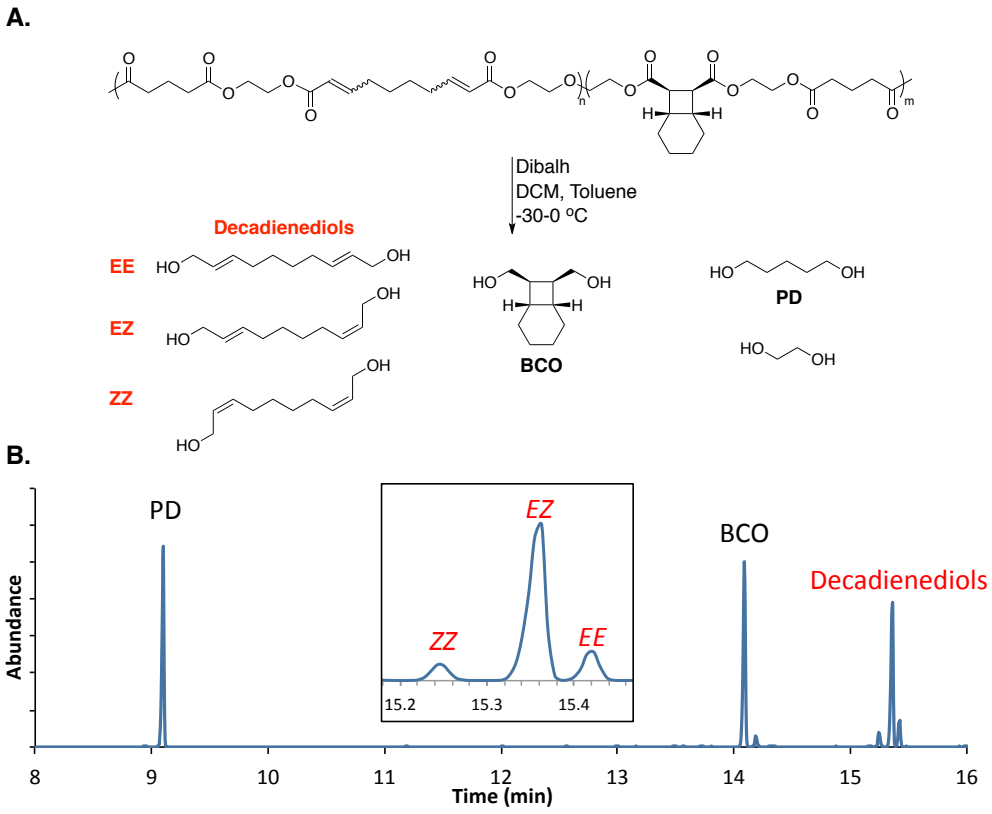

Figure 32 (a) Reduction of sonicated *cis*-BCO polymer **P1** (52% ring opening) yields constituent small molecule diols. (b) GC analysis of reduction mixture (as TMS-ethers derivatized with BSTFA) shows separation of *ZZ*, *EZ*, and *EE* decadienediol isomers confirmed by comparison with authentic compounds (see experimental section).

While exploring the sonochemical reactivity of the *cis*-BCO systems, we were intrigued by the stereochemistry of the mechanochemically generated alkenes (Figure 29). We observed two sets of overlapping peaks in the ^{1}H NMR spectrum (H_A, ~6.95 ppm) corresponding to the β,*E*-alkene proton. We presumed that this was due to differing shifts for *EE* and *EZ* pairs within a single monomeric diene. Lorentzian deconvolution of a representative peak (180 min sonication time, see experimental section) revealed that the major isomer accounts for 76% of the total β,*E*-alkene proton integration. Due to the relative total *E:Z* content (51:49) and less resolution between peak overlap for the remaining resonances, we were unable to obtain the stereochemical product distribution without ambiguity via this method (although the possibilities were narrowed to two possible outcomes, see experimental section). Instead, the identity of the major *E*-containing isomer was confirmed by reducing the esters of sonicated *cis*-BCO with Dibalh to diol derivatives of the constituent esters, specifically deca-2,8-diene-1,10-diols from the mechanochemically generated α,β-unsaturated esters (Figure 32a). Gas chromatography (GC) analysis of the TMS-derivatized product mixture versus authentic compounds showed that the *EZ*-isomer was produced as the major product (78%) followed by the *EE* (14%) and *ZZ* (8%) isomers (Figure 32b). This corresponded well to a possible product distribution of 77:13:10 previously determined by deconvolution of the ^{1}H NMR spectrum (see experimental section).

The opportunity to quantify a mixture of products in a mechanochemical reaction is unique among examples to date, and here the product stereochemistry provides an opportunity to experimentally probe the mechanism of mechanochemical cyclobutane cleavage, which was previously shown computationally to proceed through a sequential bond breaking process.[126] The generation of *EZ* products from *cis*-BCO represents a formal inversion of configuration at C(1) or C(2), facilitated by a formal rotation about either the C(1)-C(4) or C(2)-C(3) bonds prior to formation of the product alkenes. Though once the subject of debate,[144-146] it is generally accepted that [2+2] cycloreversions of cyclobutanes occur through highly non-concerted two step processes via a tetramethylene diradical intermediate.[147] Experimental[148] and theoretical[149] evidence, however, suggests that some preference exists for inversions (via bond rotation in the tetramethylene intermediate) that reflect the outcomes of hypothetical $2\pi_s+2\pi_a$ orbital symmetry allowed pathways, perhaps as a result of through-bond coupling in the diradical. Additionally, mechanochemical reaction mechanisms often deviate from canonical pathways[30,105] and deserve further interrogation. The most obvious deviation from force-free behavior in the present case is that the cycloreversion occurs with different regioselectivity from the force-free thermal process for bicyclo[4.2.0]octane, which degrades to cyclohexene and ethylene[148] (as opposed to 1,7-octadiene).

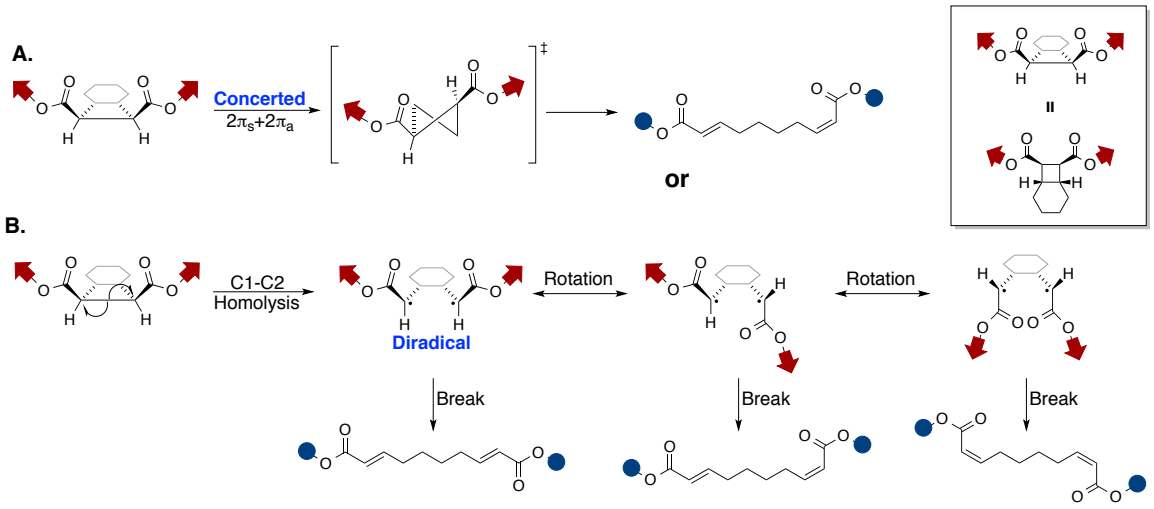

Figure 33 (a) Hypothetical concerted [2 + 2] cycloreversion of cis-BCO results in EZ diene product. (b) Diradical intermediate from C(1)−C(2) homolysis allows for conformational freedom and the formation of *EE*, *EZ*, and *ZZ* dienes.

We discuss the mechanism in terms of two limiting pathways: (a) inversion via a $2\pi_s+2\pi_a$ (Woodward-Hoffmann allowed) concerted [2+2] cycloreversion (Figure 33a) and (b) formation of a diradical intermediate via C(1)-C(2) homolytic cleavage and subsequent rotation in kinetic competition with product (alkene) formation (Figure 33b). We omit from consideration $2\pi_s+2\pi_s$ thermally disallowed concerted pathways due to the exceptionally high activation energy (~115 kcal mol^{-1}) determined by Woodward and Hoffmann[150] (in that this is significantly higher than the activation energy of cyclobutane ~62 kcal mol^{-1} [151]).

Taken alone, mechanochemical activation of *cis*-BCO leaves little room to comment on which pathway is primarily at play, as the *EZ* product might result from either mechanism (Figure 34a). We therefore synthesized a *trans*-BCO homopolymer **P2** (95% *trans*, 155 kDa) in order to observe whether the product stereochemistry has a memory of the reactant stereochemistry. After 180 min of sonication and reduction, the *trans*-BCO ring opening was analyzed by the GC and ^{1}H NMR deconvolution methods performed previously for **P1** (see experimental section). Again, the *EZ* isomer was observed to predominate (71%), though to a slightly lesser extent when compared with *cis*-BCO (Figure 34b). The formation of the *EZ* isomer from *trans*-BCO represents a formal retention of stereochemistry, versus a formal inversion from the *cis*-BCO isomer. The similar product distributions for the two isomers suggest that the two ring openings occur via a two-step process with a common intermediate (taken to be the tetramethylene diradical), followed by a stereochemistry-determining step (C(3)-C(4) homolysis, Figure 34b). In this scenario, the diradical is pulled into a preferred "*pro-EZ*" conformer prior to or concurrent with product formation (Figure 34c). We note that while most memory of the initial stereochemistry is lost, some remains; the relative product distributions for both isomers are skewed slightly toward the corresponding single inversion products (more *EZ* for *cis* and *EE*/*ZZ* for *trans*) predicted for $2\pi_s+2\pi_a$ cycloreversion pathways. It should also be pointed out that the diradical conformers shown in Figure 34c are meant to be *convenient representations of the dynamics involved*

during cycloreversion and do not necessarily represent all aspects of electronic and molecular structure involved.

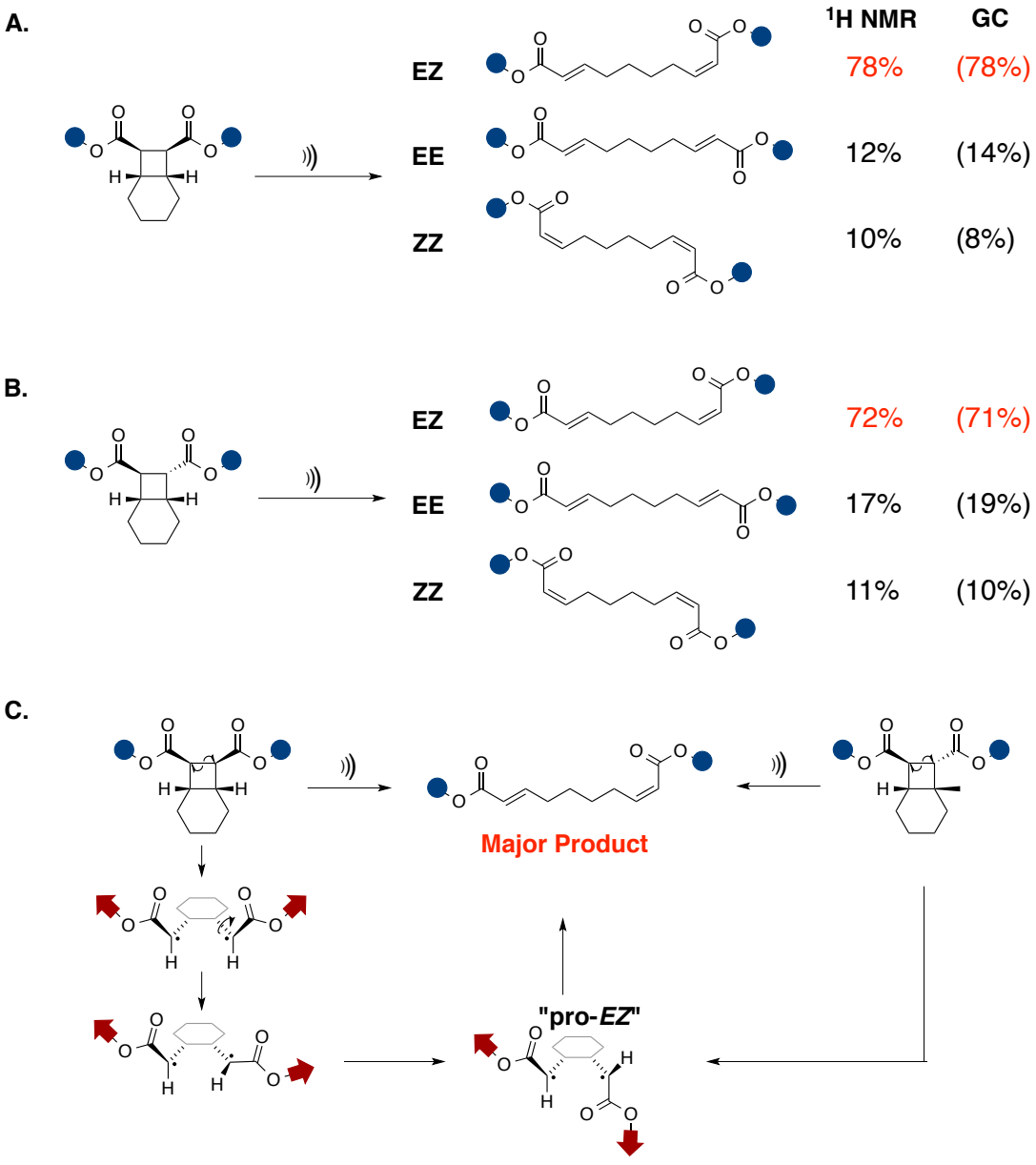

Figure 34 The *EZ*-diene is the major product of the mechanochemical [2+2] cycloreversion of both *cis*-BCO (a) and *tra*ns-BCO (b). (c) Both isomers are "pulled" into a single "pro-*EZ*" conformer after homolysis resulting in a single major product (red).

An alternate view of these "memory" effects is to couch them in terms of the dynamics of the diradical intermediate. Once the diradical forms (via C(1)-C(2) homolysis), alkene formation via C(3)-C(4) cleavage can occur either before or after conformational relaxation, for example through rotation about C(1)-C(4) or C(2)-C(3). Scission prior to relaxation ($k_{break} >> k_{rot}$) corresponds to an effectively concerted (if highly asynchronous) mechanism, whereas $k_{rot} >> k_{break}$ corresponds to the purely stepwise process. Within this framework, the *cis* vs. *trans* BCO reactivity is consistent with minor contributions from C(3)-C(4) scission prior to conformational relaxation; in other words, $k_{rot} > k_{break}$, but there is some competition between the processes. We therefore set out to hinder the rotation by increasing sterics at C(1) and/or C(2). Initially, we installed a single nitrile group on the cyclobutane ring. Purification by column chromatography yielded the asymmetrically substituted *cis*-CN-BCO dimethyl ester as the major product (single diastereomer **3a**, see experimental section), the structure of which was confirmed by X-ray crystallography (see experimental section). Transesterification with ethylene glycol yielded the diol monomer **3,** which was polymerized in the previously described fashion (Scheme 4) to yield a 133 kDa polyester **P3** (Table 3). The overall reaction stereochemistry was largely unchanged; Lorentzian deconvolution, which is sufficient to determine the product distribution unambiguously in this case, was utilized to determine the major product to be the EZ_{CN} diene (77%, Figure 35a, see experimental section). Little inversion was observed about the nitrile

functionalized C(1)-C(4) bond, with 98% of the cyanoalkenes obtained in the *Z*-configuration. Additionally, further support is given for the preference of a "pro-*EZ*" conformer in that the overall product ratios (*EZ*:*EE*:*ZZ*) is consistent with that of the unsubstituted *cis*-BCO and *trans*-BCO mechanophores (Figure 34c), indicating that the same preference for the formation of a "pro-*EZ*" conformer occurs even when rotation about one bond of the diradical is restricted. This outcome can be rationalized in the context of the non-concerted diradical intermediate where $k_{rot,H} > k_{rot,CN}$ but $k_{rot,H} > k_{break}$, as the initial configuration of the C(2)-C(3) bond is lost in the majority of cases. Similar effects are observed with respect to substitution in the thermolysis of aliphatic cyclobutane derivatives.[152]

We sought to determine whether additional substitution would further disfavor the formation of the *EZ* isomer and bias the reaction outcome towards net formal retention of initial configuration. By subjecting *cis*-BCO diacid **1a** to Hell-Volhard-Zelinsky conditions as previously reported,[153,154] we were able to isolate the dimethyl ester of *cis*-Br_2-BCO (*meso*) as a single diastereomer confirmed by X-ray crystallography (see experimental section). Analogous to previous diols, **4** was synthesized by acid-catalyzed transesterification with ethylene glycol. Polyesterification of **4** proved more challenging than previous examples, but we obtained polymer **P4** (51 kDa, Table 3) that was sufficient for sonochemical activation and product analysis. The polymer was subjected to pulsed ultrasound (180 min) in $CHCl_3$ (due to insolubility in MeCN), and

12% ring opening was observed by ^{1}H NMR. Unlike previous polymers, *Z*-alkene products predominated, accounting for 80% of all alkenes formed (note: due to a change of priority designation, the *Z*-configuration here is equivalent to the *E*-configuration of previous examples with respect to retention of stereochemistry). Again, Lorentzian deconvolution was sufficient to determine stereochemical product distributions. As hypothesized, the *ZZ* isomer was observed to be the major product (66%), corresponding to both a formal retention of stereochemistry, as well as a shift in preference away from the proposed "pro-*EZ*" conformer, in contrast with all preceding examples (Figure 35b and c). The differences in product distribution for **P4** are not due to its lower molecular weight, as verified by sonication of a lower MW **P1** (66 kDa) and the invariance of the product distribution with time as higher MW polymers are broken down into lower MW fragments (see experimental section).

This observation is consistent with the diradical model if steric congestion causes a loss of conformational freedom and $k_{rot} < k_{break}$, a shift in trend from the less substituted analogues. Here, rotation is further restricted by the bromine substituents, causing decomposition to the product alkenes with no rotation occurring in the majority of monomers. Comparing this result to unsubstituted *cis*-BCO, we see that any preference for single-inversion is highly suppressed, although the *EZ* product is formed in appreciable quantity (27%). Variations in k_{break} are unlikely to account for the differences. Prior estimates for radical stabilization due to bromine substitution are ~3.5 kcal mol^{-1}

for a carbon-centered radical, [155] or close to 7 kcal mol^{-1} for the diradical implicated here. We calculate that the di-acrylate product is stabilized by a similar value of 5 kcal mol^{-1}, we infer that the diradical-to-diacrylate bond-breaking step is not significantly impacted by bromination.

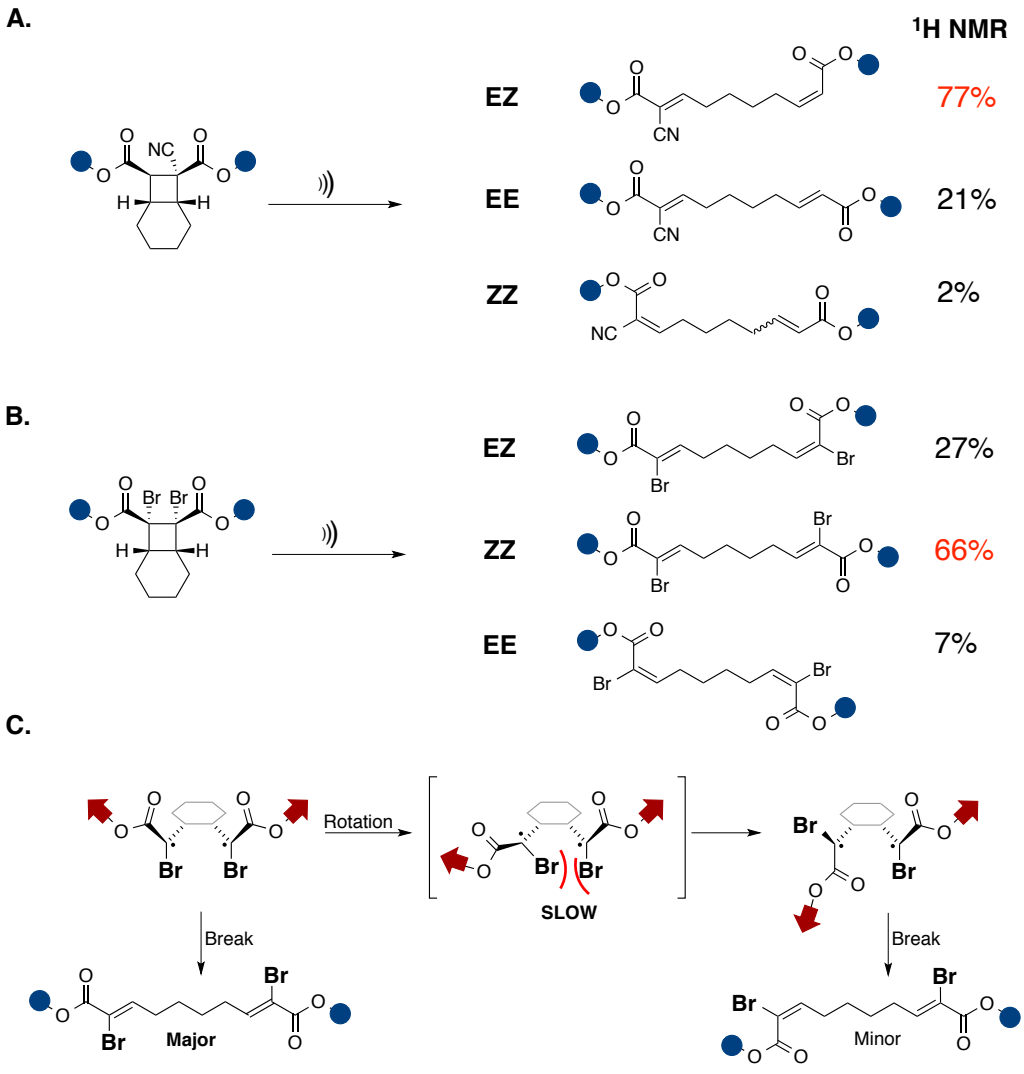

Figure 35 (a) Product distribution of mechanochemical activation of *cis*-CN-BCO polymer **P3**. (b) Product distribution of mechanochemical activation of *cis*-Br$_2$-BCO polymer **P4**. (c) Increased substitution hinders diradical rotation resulting in increased retention of stereochemistry. Major products shown in red.

As with most mechanistic considerations, the limiting cases provide a convenient framework for discussion, and we recognize that many subtleties are unresolved. For example, the tetramethylene diradical likely cannot be purely decoupled from C(3)-C(4) scission, as there will be mixing of the non-bonding and bonding orbitals. Likewise, restricted rotation about C(1)-C(4) or C(2)-C(3) might influence the true concertedness of the reaction by slowing C(1)-C(2) homolysis, rather than restricting rotation in the 1,4-diradicaloid intermediate. Nevertheless, these studies show how the outcomes, and presumably the rates, of mechanical BCO activation can be influenced by structural manipulation. Such control might be quite useful, given the potential utility of BCO as a mechanophore in stress-responsive materials.

3.3 Conclusion

The bicyclo[4.2.0]octane framework was exploited to develop a family of stress-responsive mechanophores. These functionalized cyclobutane bearing units were designed to undergo non-scissile ring opening to afford unsaturated products and high elongations under the application of stress for integration into stress-responsive materials. These mechanophores were incorporated as diol monomers into high molecular weight polyesters via carbodiimide polymerization and subsequently activated to form reactive α,β-unsaturated esters via the application of pulsed ultrasound. Due to the non-scissile nature of the activation, many cycloreversions occur per polymer chain (hundreds) allowing for quantification of reaction progress and

determination of products by conventional NMR methods. Small molecule functionalized copolymers as well as network structures were formed via rapid nucleophilic thiol-ene conjugation of mono and difunctional thiols respectively. Reactivity, along with high-elongations (~7 Å per monomer unit) demonstrates an improvement in stress-activated behavior of these mechanophores over that of the *g*DHC systems.[88,112] Moving forward, the BCO platform will be used to expand and compliment our efforts to develop self-healing materials based on the *g*DHC family of mechanophores. A qualitative assessment of the relative the reactivity of *cis* and *trans*-BCO was made by measuring percent ring opening as a function of sonication time. The stereochemical configurations of product dienes were unambiguously determined for all BCO derivatives and these observations were used to elaborate on a mechanistic description of the mechanochemical [2+2] cycloreversion of cyclobutanes. This model was used to guide our design of substituted BCO analogues, allowing us to tune the stereochemical product distributions. Moving forward, molecular dynamics (MD) simulations[87] might help to further address the factors that determine product stereochemistry in this system as well as a more detailed rationalization for the formation of a "pro-*EZ*" conformer. Additionally, efforts are underway to integrate these mechanophores into material platforms that will facilitate bulk activation and the development of mechanochemically stress-responsive materials.

3.4 Experimental

3.4.1 General Procedures

Dry solvents were obtained from Sigma-Aldrich and purified with a Pure Solv™ solvent purification system before use. $CDCl_3$ and DMSO-d_6 were purchased from Cambridge Isotope Laboratories. All GPC experiments were performed using inhibitor free Chromasolv grade THF obtained from Sigma-Aldrich. Ethyl thioglycolate (97%) and 1,4-butanediol bis(thioglycolate) (95%) were purchased from TCI and used without further purification. Maleic anhydride was recrystallized from chloroform and cyclohexene was washed with acidic aqueous ferrous sulfate and distilled over calcium hydride before use. All other reagents were purchased from Sigma-Aldrich and used without further purification unless otherwise noted.

All ^{1}H and ^{13}C spectra were collected in either $CDCl_3$ (δ = 7.26 (^{1}H) and 77.16(^{13}C)) or DMSO-d_6 (δ = 2.50 (^{1}H) and 39.52 (^{13}C)) and referenced to residual solvent peak on either a Varian 400 or 500 MHz spectrometer. All chemical shifts are given in ppm (δ) and coupling constants (J) in Hz as singlet (s), doublet (d), triplet (t), quartet (q), multiplet (m), or broad (br). Column (flash) chromatography was performed using Silicycle F60 (230-400 mesh) silica gel. Gel permeation chromatography (GPC) was performed on two in series columns (Agilent Technology PL gel 10^4 Å, 10^3 Å) with THF as the mobile phase at 0.5 mL min^{-1} with the flow rate set with a Varian Prostar Model 210 pump. Molecular weights were determined using an inline Wyatt Dawn EOS multi-

angle light scattering (MALS) detector and a Wyatt Optilab DSP Interferometric Refractometer (RI). The dn dc^{-1} values were determined in-line, assuming 100% mass recovery based on known injection mass. All dn/dc values for *cis* and *trans* BCO polymers (**P1, P2, P12, PC**) were determined to be within 0.058 ± 0.004 for both sonicated and unsonicated samples, a value of 0.058 was used for these polymers, while **P3** (dn dc^{-1} = 0.058 ± 0.003) and **P4** (dn dc^{-1} = 0.048 ± 0.001) were determined independently.

3.4.2 Synthesis and Characterization

Synthesis of *cis*-Bicyclo[4.2.0]octane-*cis*-7,8-dicarboxylic acid (1a):

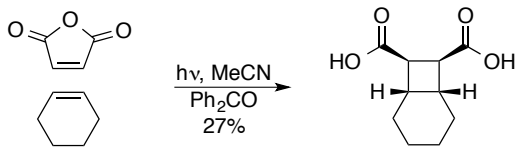

Using procedure modified from those previously reported,[142,153,154,156] benzophenone (5.00 g, 27.4 mmol), maleic anhydride (20.0 g, 197 mmol), and cyclohexene (100 mL, 987 mmol) were dissolved in 300 mL acetonitrile in a 500 mL photochemical reactor fitted with a water-cooled quartz emersion well. The solution was sparged with argon for 30 minutes then irradiated with a 450 W medium pressure mercury arc lamp through a Pyrex filter for 5 hours under argon. During the course of the reaction, the internal temperature stabilized at 35 °C. Acetonitrile and cyclohexene were removed under reduced pressure and resulting residue was distilled under high vacuum, collecting all volatiles distilling between 110 and 200 °C (200-500 mTorr). The distillate was stirred with 100 mL 2 N aqueous NaOH for 1 hour then extracted with 50

mL diethyl ether. The aqueous layer was then neutralized carefully with concentrated HCl at which point a white precipitate formed with was filtered and washed with MeOH (20 mL) to yield **1a** as a white powder in 27% yield (10.6 g, 53.5 mmol). Due to poor solubility, the compound was further characterized as the methyl ester. **^{1}H NMR** (400 MHz, DMSO-d_6) δ 2.92 (br d, 2H, J = 4.88 Hz), 2.48 (br, 2H), 1.64 (br, 2H), 1.43 (br, 4H), 1.24 (br, 2H); **^{13}C NMR** (125 MHz, DMSO-d_6) δ 174.86, 43.82, 34.07, 26.86, 21.92.

Synthesis of Compound Dimethyl *cis*-Bicyclo[4.2.0]octane-*cis*-7,8-dicarboxylate (1b):

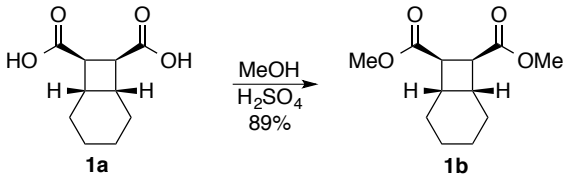

1a **1b**

Diacid **1a** (1.00 g, 5.05 mmol) was suspended in 20 mL dry MeOH in an oven dried 50 mL round bottom flask under argon. Concentrated H_2SO_4 (0.540 mL, 10.1 mmol) was carefully added and the solution was heated at reflux overnight, becoming homogenous after approximately 1 hour. The solution was cooled and carefully quenched with $NaHCO_3$ until effervescence ceased. Methanol was removed under reduced pressure and the residue was suspended in 100 mL water and extracted with EtOAc (3 x 50 mL), the combined organics were dried over $MgSO_4$ and solvent evaporated to give crude yellow oil which was purified by column chromatography (80:20 Hexanes:EtOAc) to give a clear oil in 88.5 % yield (1.01 g, 4.47 mmol). **^{1}H NMR (**400 MHz, $CDCl_3$) δ 3.67 (s, 6H), 3.10 (d, 2H, J = 4.88), 2.74 (br, 2H), 1.76 (br, 2H), 1.47 (br,

4H), 1.33 (br, 2H); **^{13}C NMR** (125 MHz, DMSO-d_6) δ 173.02, 51.28, 42.98, 33.07, 26.54, 21.67. **HRMS-ESI** (*m*/*z*): calcd for $C_{12}H_{18}O_4$ [MH+], 227.1278; found, 227.1279.

Synthesis of Bis(2-hydroxyethyl)-*cis*-Bicyclo[4.2.0]octane-*cis*-7,8-dicarboxylate (1):

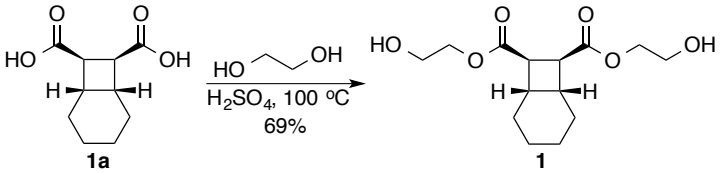

Diacid **1a** (4.02 g, 20.3 mmol) was suspended in 31 mL dry ethylene glycol in an oven dried 100 mL round bottom flask under argon. Concentrated H_2SO_4 (2.15 mL, 40.6 mmol) was carefully added at which point the mixture became homogenous. The solution was heated at 100 °C overnight under a stream of argon. After cooling, the reaction was quenched by pouring into 100 mL sat. $NaHCO_3$ and extracted with EtOAc (4 x 100 mL). The combined organics were washed with 200 mL water and dried over Na_2SO_4, then evaporated under reduced pressure to give a light yellow oil which was subjected to column chromatography (gradient, DCM to 98:2 DCM:MeOH) to give **1** as a clear yellow oil in 69.4 % yield (4.03 g, 14.1 mmol). **^{1}H NMR** (400 MHz, $CDCl_3$) δ 4.26-4.32 (m, 2H), 4.12-4.18 (m, 2H), 3.80 (br, 4H), 3.19 (d, 2H, J = 5.08), 2.78 (br, 2H), 2.63 (br, 2H), 1.72-185 (m, 2H), 1.42-1.55 (m, 4H), 1.27-1.41 (m, 2H); **^{13}C NMR** (125 MHz, $CDCl_3$) δ 173.68, 66.10, 60.37, 43.72, 33.53, 26.99, 21.99. **HRMS-ESI** (*m*/*z*): calcd for $C_{14}H_{22}O_6$ [M+Na]+, 309.1309; found, 309.1306.

Synthesis of Dimethyl *cis*-Bicyclo[4.2.0]octane-*trans*-7,8-dicarboxylate (racemic) (2a):

Under argon, methyl ester **1b** (1.50 g, 6.64 mmol) was dissolved in dry MeOH (5 mL) in a 25 mL oven dried round bottom flask with reflux condenser and stir bar. A 50% (wt/wt) solution of sodium methoxide in methanol was added and the solution heated at reflux overnight. After cooling, the solution was poured into 100 mL of 1N HCl and extracted with DCM (3 x 50 mL), dried over $MgSO_4$, and evaporated to yield an 5:1 mixture of trans:cis diester. Purification by flash chromatography (SiO_2, 95:5 Hexanes:Ethyl Acetate) yielded pure trans isomer as a clear oil in 13.3 % yield (200 mg, 0.885 mmol). **^{1}H NMR** (400 MHz, $CDCl_3$) δ 3.67 (s, 3H), 3.66 (s, 3H), 3.29 (m, 2H), 2.50 (m, 2H), 0.95-1.82 (m, 8H); **^{13}C NMR** (125 MHz, $CDCl_3$) δ 174.24, 172.28, 51.79, 51.57, 42.03, 40.67, 34.54, 33.17, 25.25, 24.42, 22.73, 21.70; **HRMS-ESI** (*m*/*z*): calcd for $C_{12}H_{18}O_4$ [M+Na]+, 249.1097; found, 249.1094.

Synthesis of Bis(2-hydroxyethyl)-cis-Bicyclo[4.2.0]octane-trans-7,8-dicarboxylate (racemic) (2):

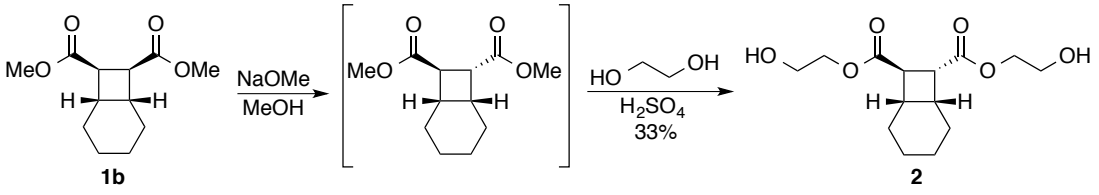

1b 2

Dimethyl ester **1b** (3.83 g, 17.0 mmol) was transferred to an oven dried 50 mL round bottom flask fitted with a reflux condenser under argon. Dry MeOH (12 mL) was added, followed by a solution of NaOMe in MeOH (25%, 7.6 mL). The solution was

heated at reflux for 18 hours. After cooling, $NaHSO_4$ (6.3 g) was added carefully and solution evaporated under reduced pressure. The mixture was suspended in 30 mL dry ethylene glycol and concentrated H_2SO_4 (0.41 mL) was added dropwise. The solution was heated at 100 °C overnight under a stream of argon. After cooling, the reaction was quenched by pouring into 100 mL sat. $NaHCO_3$ and extracted with EtOAc (4 x 100 mL). The combined organics were washed with water (2 x 150 mL) and dried over Na_2SO_4, then evaporated under reduced pressure to give a light yellow oil which was subjected to column chromatography (gradient, DCM to 2% MeOH in DCM) to give **2** as a clear yellow oil in 32.7 % yield (1.59 g, 5.56 mmol, 95:5 dr), two steps. **^{1}H NMR** (400 MHz, $CDCl_3$) δ 4.13-4.32 (m, 4H), 3.77-3.83 (m, 4H), 3.30-3.43 (m, 2H), 2.50-2.60 (m, 2H), 2.30 (br, 2H), 0.92-1.89 (m, 8H); **^{13}C NMR** (125 MHz, $CDCl_3$) δ 174.14, 172.20, 66.25, 66.11, 61.00, 42.52, 40.97, 34.20, 33.23, 25.23, 24.62, 22.74, 21.75; **HRMS-ESI** (*m*/*z*): calcd for $C_{14}H_{22}O_6$ [M+Na]+, 309.1309; found, 309.1299.

Synthesis of Dimethyl 7-cyano-cis-Bicyclo[4.2.0]octane-cis-7,8-dicarboxylate (racemic) (3a):

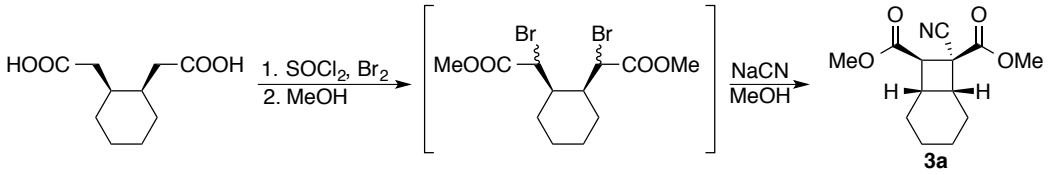

Cis-cyclohexanediacetic acid[157] (12.2 g, 60.8 mmol) was loaded into an oven dried 250 mL round bottomed flask with stir bar, addition funnel, and reflux condenser fitted with a N_2 bubbler. Thionyl chloride (30.0 mL, 413 mmol) was carefully added by

addition funnel and the suspension was heated at reflux for 2 hours at which point the solid had completely dissolved. Bromine (6.92 mL, 134 mmol) was then added dropwise and the solution heated at 80 °C overnight then allowed to cool to 60 °C and excess thionyl chloride and bromine were removed under a stream of N_2. The brown oil was allowed to cool to room temperature and 30 mL of MeOH was carefully added followed by heating at reflux for 2 hr. After cooling, the mixture was poured into 1 L of cold water. The aqueous layer was decanted from the brown residue, which was dissolved in Et_2O and washed with aqueous sodium bisulfite (10%), potassium carbonate (10%), water, and brine. Drying over magnesium sulfate and evaporation under reduced pressure yielded a yellow oil, which was used for the next step without further purification (90.8 % crude yield, 21.2 g, 55.2 mmol). **HRMS-ESI** (*m*/*z*): calcd for $C_{12}H_{18}Br_2O_4$ [MH+], 384.9645; found, 384.9647.

The dibromide (21.0 g, 55.3 mmol) and finely ground potassium cyanide (10.8 g, 166 mmol) were loaded into a 250 mL round bottomed flask with stir bar and subsequently suspended in 20 mL of dry MeOH. The suspension was heated at reflux for 3 days under N_2. The resulting black oil was allowed to cool then diluted with 400 mL EtOAc and stirred over celite and filtered. The brown solution was then washed with water (3 x 150 mL) and brine (100 mL), dried over $MgSO_4$ and concentrated under reduced pressure. The dark brown oil was then subjected to column chromatography (SiO_2, 9:1 Hexane/EtOAc, R_f ~ 0.15) to give white crystals of X as a single diastereomer in

14.9 % yield (two steps, 2.07 g, 8.25 mmol). **^{1}H NMR** (500 MHz, $CDCl_3$) δ 3.82 (s, 3H), 3.69 (s, 3H), 3.50 (d, 1H, J = 10.8), 3.19 (m, 1H), 2.65 (q, 1H, J = 8.59), 2.11 (m, 1H), 1.69 (m, 4H), 1.54 (m, 1H), 1.35 (m, 1H), 1.13 (m, 1H); **^{13}C NMR** (125 MHz, $CDCl_3$) δ 170.78, 167.95, 117.29, 53.77, 52.25, 46.63, 46.53, 37.63, 33.17, 26.09, 24.88, 22.15, 20.92; **HRMS-ESI** (*m*/*z*): calcd for $C_{13}H_{17}NO_4$ [MH+], 252.1230; found, 252.1232.

Synthesis of Compound 3: Bis(2-hydroxyethyl)-7-cyano-*cis*-Bicyclo[4.2.0]octane-*cis*-7,8-dicarboxylate (racemic):

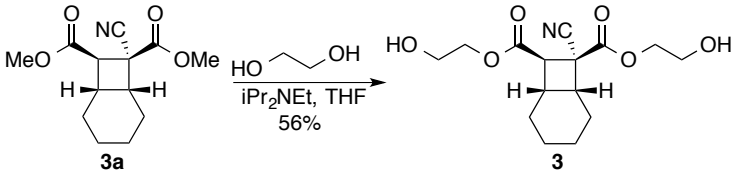

3a (1.38 g, 5.50 mmol) was dissolved in dry THF (5 mL) in a flame dried 25 mL under Argon. Ethylene glycol (10.2 mL, 165 mmol) and diisopropylethylamine (0.960 mL, 5.50 mmol) were subsequently added and the solution was stirred at room temperature for 72 hours. The solution was directly purified by column chromatography (SiO_2, gradient elution 1:1 to 4:1 EtOAc/Hexane) to yield **3** as a clear oil in 56 % yield (950 mg, 3.05 mmol). **^{1}H NMR** (400 MHz, $CDCl_3$) δ 4.92 (m, 4H), 3.85 (t, 2H, J = 4.48), 3.79 (t, 2H, J = 4.55), 3.59 (d, 1H, J = 11.0), 3.22 (m, 1H), 2.80 (br, 2H), 2.72 (q, 1H, J = 8.59), 2.13 (m, 1H), 1.66 (m, 5H), 1.37 (m, 1H), 1.15 (m, 1H); **^{13}C NMR** (125 MHz, $CDCl_3$) δ 170.87, 167.76, 117.33, 68.65, 66.92, 60.67, 60.43, 46.93, 46.75, 37.64, 33.21, 26.07, 24.88, 22.09, 20.88; **HRMS-ESI** (*m*/*z*): calcd for $C_{15}H_{21}NO_6$ [MH+], 312.1442; found, 312.1443.

Synthesis of Dimethyl *7,8-dibromo-cis*-Bicyclo[4.2.0]octane-*cis*-7,8-dicarboxylate (4a):

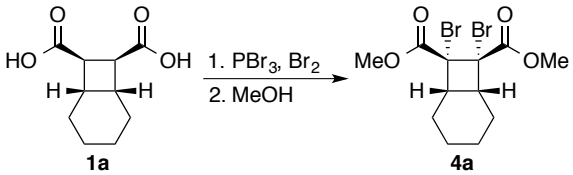

4a was synthesized as previously reported.[153] **^{1}H NMR** (400 MHz, $CDCl_3$) δ 3.77 (s, 6H), 3.04 (m, 2H), 1.93 (m, 2H), 1.79 (m, 4H), 1.32 (m, 2H); **^{13}C NMR** (125 MHz, $CDCl_3$) δ 169.98, 68.90. 53.54, 38.54, 25.50, 21.27; **HRMS-ESI** (*m*/*z*): calcd for $C_{12}H_{16}Br_2O_4$ $[M+NH_4]+$, 399.9754; found, 399.9746.

Synthesis of Compound 4: Bis(2-hydroxyethyl)-*7,8-dibromo-cis*-Bicyclo[4.2.0]octane-*cis*-7,8-dicarboxylate:

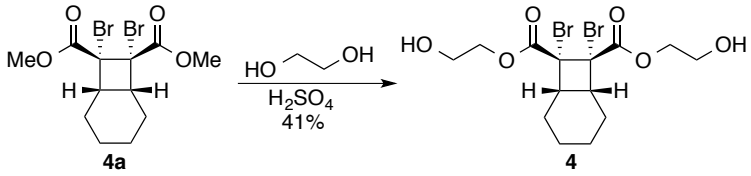

4a (1.04 g, 2.71 mmol) was suspended in ethylene glycol (10 mL) in a 25 mL round bottomed flask under argon. H_2SO_4 (0.2 mL) was added and the biphasic solution was heated at 100 °C for 24 hours (until 1 phase was formed) then 90 °C for 48 hours. The solution was then allowed to cool, was diluted with 125 mL EtOAc, and washed with 50 mL dilute $NaHCO_3$ and 50 mL brine, dried over magnesium sulfate and concentrated under reduced pressure. The light yellow oil was then subjected to column chromatography (SiO_2, gradient elution 1:1 to 4:1 EtOAc/Hexane) to yield **4** as a clear oil in 40.5 % yield (487 mg, 1.10 mmol). **^{1}H NMR** (400 MHz, $CDCl_3$) δ 4.35 (m, 2H), 4.24 (m,

2H), 3.83 (t, 4H, J = 4.52), 3.07 (m, 2H), 2.60 (br, 2H), 1.92 (m, 2H), 1.80 (m, 4H), 1.32 (m, 2H) ; **^{13}C NMR** (125 MHz, $CDCl_3$) δ 169.96, 69.23, 68.37, 60.63, 38.70, 25.60, 21.27. **HRMS-ESI** (*m*/*z*): calcd for $C_{14}H_{20}Br_2O_6$ [M+NH_4]+, 459.9965; found, 459.9967.

3.4.3 Polymer Synthesis

All polyesterifications were performed using a method modified from that of Moore and Stupp.[141]

Synthesis of P1 (*cis*-BCO):

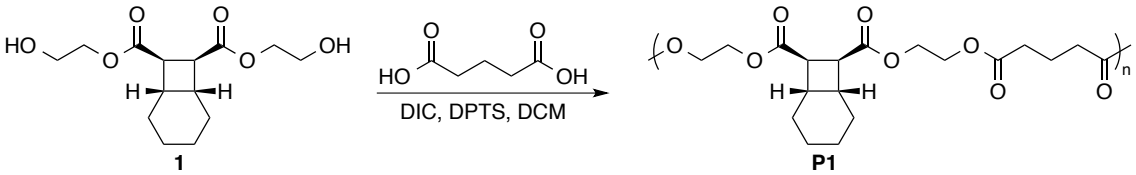

Diol **1** (3.77 g, 13.2 mmol), glutaric acid (1.74 g, 13.2 mmol), and DPTS (1.55 g, 5.28 mmol) were weighed into a 50 mL oven dried round bottom flask. The flask was purged with argon for 30 minutes, then 15 mL of dry DCM was added by syringe. The solution was heated to 37 °C and stirred until homogenous, then allowed to cool to room temperature. DIC (6.63 mL, 39.6 mmol) was added dropwise by syringe, and the polymerization was allowed to proceed for 48 hours. The viscous mixture was then precipitated three times from DCM into MeOH and dried under high vacuum to yield 3.47 g of white gummy polymer. **^{1}H NMR** (400 MHz, $CDCl_3$) δ 4.21-4.30 (m, 8H), 3.13 (d, 2H), 2.73 (br, 2H), 2.41 (t, 4H, J = 7.32), 1.94 (quintet, 2H, J = 7.49), 1.70-1.82 (br, 2H), 1.42-

1.54 (br, 4H), 1.26-1.40 (br, 2H); **^{13}C NMR** (125 MHz, $CDCl_3$) δ 173.03, 172.77, 62.29, 43.67, 34.00, 33.09, 27.31, 22.32, 19.99; **GPC-MALS**: M_n = 179 kDa, PDI = 1.43.

Synthesis of P2 (*trans*-BCO):

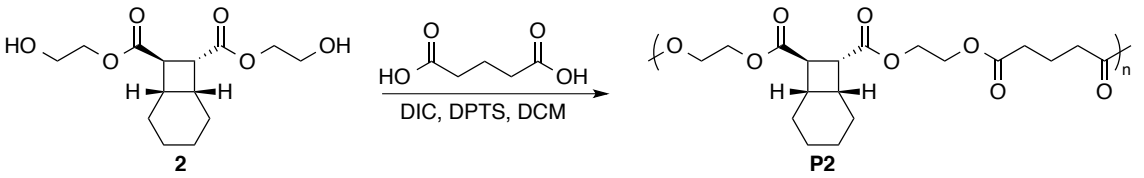

Diol **2** (1.12 g, 3.90 mmol), glutaric acid (0.515 g, 3.90 mmol), and DPTS (0.459 g, 1.56 mmol) were weighed into a 25 mL oven dried round bottom flask. The flask was purged with argon for 30 minutes, then 6 mL of dry DCM was added by syringe. The solution was heated to 37 °C and stirred until homogenous, then allowed to cool to room temperature. DIC (1.82 mL, 11.7 mmol) was added dropwise by syringe, and the polymerization was allowed to proceed for 48 hours. The viscous mixture was then precipitated three times from DCM into MeOH and dried under high vacuum to yield 692 mg of a tacky clear solid. **^{1}H NMR** (400 MHz, $CDCl_3$) δ 4.20-4.33 (m, 8H), 3.34 (m, 2H), 2.45-2.56 (m, 2H), 2.38 (t, 4H, J = 7.33), 1.94 (quintet, 2H, J = 7.36), 1.74-1.79 (br, 1H), 1.58-1.66 (br, 3H), 1.16-1.47 (m, 3H), 0.95-1.04 (m, 1H); **^{13}C NMR** (125 MHz, $CDCl_3$) δ 173.50, 172.66, 171.61, 62.30, 62.19, 41.82, 40.65, 34.81, 33.26, 33.10, 25.25, 24.48, 22.77, 21.75, 20.00; **GPC-MALS**: M_n = 155 kDa, PDI = 1.34.

Synthesis of P1,2 (*cis*/*trans*-BCO):

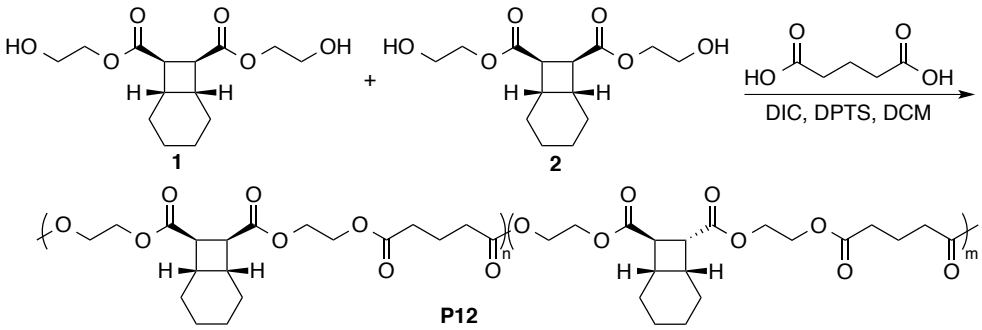

Diol **1** (576 mg, 2.01 mmol), diol **2** (578 mg, 2.03 mmol), glutaric acid (532 mg, 4.03 mmol), and DPTS (473 mg, 1.61 mmol) were added to a 25 mL oven dried round bottom flask. Dry DCM (6 mL) was added by syringe and the solution was heated to 37 °C and stirred until homogenous, then allowed to cool to room temperature. DIC (1.88 mL, 12.1 mmol) was added dropwise by syringe, and the polymerization was allowed to proceed for 48 hours. The viscous mixture was then precipitated three times from DCM into MeOH and dried under high vacuum to yield 1.015 g of white gummy polymer. **^{1}H NMR** (400 MHz, $CDCl_3$) δ 4.16-4.34 (m, 8H), 3.32 (m, 1.06H), 3.10 (d, 0.94H), 2.70 (br, 0.94H), 2.45-2.56 (m, 1.06H), 2.38 (m, 4H), 1.91 (quintet, 2H, J = 7.34), 0.92-1.83 (m, 8H); **^{13}C NMR** (125 MHz, $CDCl_3$) δ 173.44, 172.94, 172.64, 171.55, 62.22, 62.13, 43.59, 41.73, 40.54, 34.72, 33.91, 33.17, 33.01, 27.23, 25.17, 24.42, 22.70, 22.24, 21.68, 19.91; **GPC-MALS**: M_n = 161 kDa, PDI = 1.32.

Synthesis of P3 (CN-*cis*-BCO):

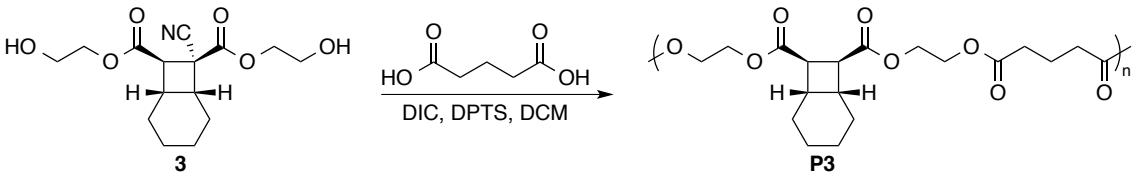

Diol **3** (906 mg, 2.91 mmol), glutaric acid (384 mg, 2.91 mmol), and DPTS (342 mg, 1.16 mmol) were added to a 25 mL oven dried round bottom flask. The flask was purged with argon for 30 minutes, then 4 mL of dry DCM was added by syringe. The solution was heated to 37 °C and stirred until homogenous, then allowed to cool to room temperature. DIC (1.35 mL, 8.73 mmol) was added dropwise by syringe, and the polymerization was allowed to proceed for 48 hours. The viscous mixture was then precipitated three times from DCM into MeOH and dried under high vacuum to yield 640 mg of solid white polymer. **^{1}H NMR** (400 MHz, $CDCl_3$) δ 4.16-4.48 (m, 8H), 3.52 (d, 1H, J = 10.98), 3.16 (m, 1H), 2.65 (m, 1H), 2.39 (m, 4H), 2.11 (m, 1H),1.93 (quintet, 2H, J = 7.35), 1.47-1.80 (m, 6H), 1.36(m, 1H), 1.13(m, 1H); **^{13}C NMR** (125 MHz, $CDCl_3$) δ 172.66, 172.63, 170.00, 167.25, 116.87, 64.43, 62.74, 61.86, 61.54, 46.57, 46.42, 37.81, 33.22, 32.97, 26.07, 24.82, 22.11, 20.86, 19.89; **GPC-MALS**: M_n = 133 kDa, PDI = 1.28.

Synthesis of P4 (Br$_2$-*cis*-BCO):

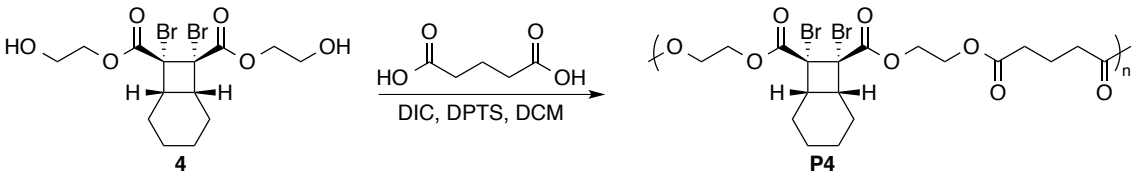

Diol **4** (417 mg, 0.940 mmol), glutaric acid (124 mg, 0.940 mmol), and DPTS (110 mg, 0.376 mmol) were added to a 10 mL oven dried round bottom flask. The flask was purged with argon for 30 minutes, and then 2 mL of dry DCM was added by syringe. The solution was heated to 37 °C and stirred until homogenous, then allowed to cool to room temperature. DIC (0.440 mL, 2.82 mmol) was added dropwise by syringe, and the polymerization was allowed to proceed for 48 hours. The viscous mixture was then precipitated three times from DCM into MeOH and dried under high vacuum to yield 276 mg of clear tacky polymer. **^{1}H NMR** (400 MHz, $CDCl_3$) δ 4.22-4.44 (m, 8H), 3.00 (br, 2H), 2.41 (t, 4H, J = 7.30), 1.86-2.02 (m, 4H), 1.70-1.86 (br, 4H), 1.26-1.40 (br, 2H); **^{13}C NMR** (125 MHz, $CDCl_3$) δ 172.66, 169.30, 68.66, 64.04, 61.68, 38.66, 33.09, 25.58, 21.35, 19.98; **GPC-MALS**: M_n = 51.0 kDa, PDI = 1.35.

Synthesis of Control Polymer (PC):

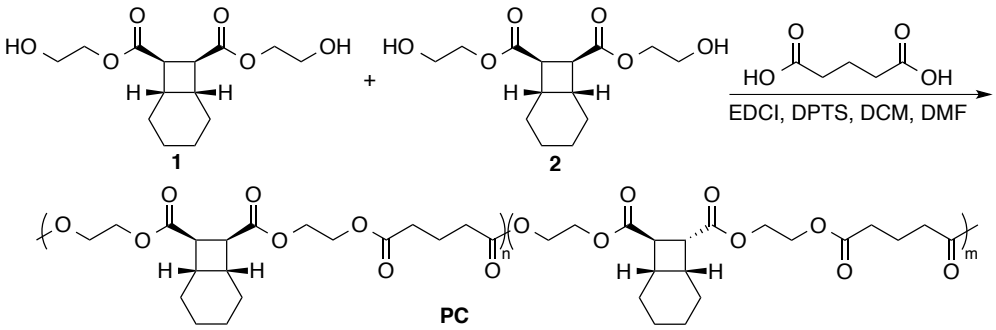

Diol **1** (285 mg, 1.00 mmol), Diol **2** (285 mg, 1.00 mmol), glutaric acid (250 mg, 1.89 mmol), and DMAP (97 mg, 0.80 mmol) were dissolved in 3 mL DCM and 3 mL DMF in a 25 mL round bottom flask and subsequently purged with argon. EDCI (1.14 g, 5.97 mmol) was added as a solid and the solution allowed to stir overnight. The solution was diluted with 150 mL DCM and washed with water (2 x 100 mL), and brine (100 mL), dried over Na_2SO_4 and evaporated under reduced pressure. The residue was dissolved in a minimal amount of DCM and passed through a plug of neutral alumina, eluting with DCM to yield 198 mg of clear viscous polymer. **^{1}H NMR** (400 MHz, $CDCl_3$) δ 4.16-4.34 (m, 8H), 3.33 (m, 1.08H), 3.12 (d, 0.92H), 2.71 (br, 0.92H), 2.43-2.58 (m, 1.08H), 2.38 (m, 4H), 1.93 (quintet, 2H, J = 7.36), 0.93-1.83 (m, 8H); **^{13}C NMR** (125 MHz, $CDCl_3$) δ 173.50, 172.99, 172.70, 171.60, 62.28, 62.18, 43.67, 41.80, 40.63, 34.79, 33.91, 33.98, 33.24, 33.09, 27.29, 25.23, 24.47, 22.76, 22.30, 21.74, 19.99; **GPC-MALS**: M_n = 13.3 kDa, PDI = 1.28.

Synthesis of P1,66kDa (*cis*-BCO)

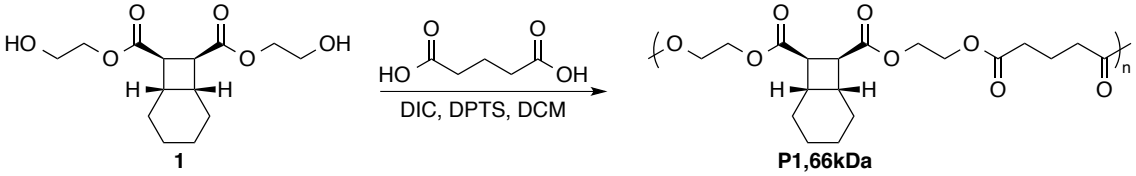

Diol **1** (1.24 g, 4.32 mmol), glutaric acid (0.570 g, 4.32 mmol), and DPTS (0.508 g, 1.73 mmol) were weighed into a 25 mL oven dried round bottom flask. The flask was purged with argon for 30 minutes, then 7 mL of dry DCM was added by syringe. The solution was heated to 38 °C and stirred until homogenous, then allowed to cool to room temperature. DIC (2.00 mL, 13.0 mmol) was added dropwise by syringe, and the polymerization was allowed to proceed for 48 hours. The viscous mixture was then concentrated to half volume and precipitated three times from DCM into MeOH and dried under high vacuum to yield 1.18 g of clear tacky polymer. **^{1}H NMR** (400 MHz, $CDCl_3$) δ 4.19-4.33 (m, 8H), 3.13 (d, 2H, J = 3.12), 2.72 (br, 2H), 2.41 (t, 4H, J = 7.32), 1.95 (quintet, 2H, J = 7.30), 1.71-1.83 (br, 2H), 1.42-1.53 (br, 4H), 1.26-1.40 (br, 2H); **^{13}C NMR** (125 MHz, $CDCl_3$) δ 172.93, 172.68, 62.23, 43.63, 33.94, 33.04, 27.24, 22.25, 19.95; **GPC-MALS**: M_n = 66.1 kDa, PDI = 1.52.

3.4.4 Activation of P1 (*cis*-BCO)

3.4.4.1 General Sonication Conditions and GPC-MALS Analysis

Ultrasound experiments were performed in dry acetonitrile on a Vibracell Model VCX500 (20 kHz frequency) with a 12.8 mm titanium probe. For polymer **4**, $CHCl_3$ was used due to insolubility in acetonitrile while all other conditions were identical. Solutions were irradiated at a concentration of 2 mg/mL in 16 mL of solvent unless otherwise noted. Prior to sonication, the solution was transferred to a 3-necked Suslick cell in an ice bath and sparged with nitrogen for 30 minutes prior to sonication. Irradiations were performed at 14.8 W cm^{-2} with a pulse sequence of 1s on/1s off while maintaining a temperature of 6-9 °C under a nitrogen atmosphere. Power calibration was performed using the method of Berkowski et al.[28]

Individual sonication experiments were performed for each time point. 32 mg of **P1** was dissolved in 16 mL MeCN, subjected to irradiation for the times indicated. The solution was filtered and evaporated under reduced pressure. 2 mg was dissolved in 1 mL of THF for GPC analysis, while the remainder was dissolved in 0.5 mL $CDCl_3$ for NMR analysis.

Molecular weight was observed to decrease as a function of sonication time, indicated by an increase in retention time with prolonged irradiation. MWs are reported as number average molecular weight (M_n). **P1** sonication overlay below (Figure 36) is representative of all polymers tested unless otherwise noted:

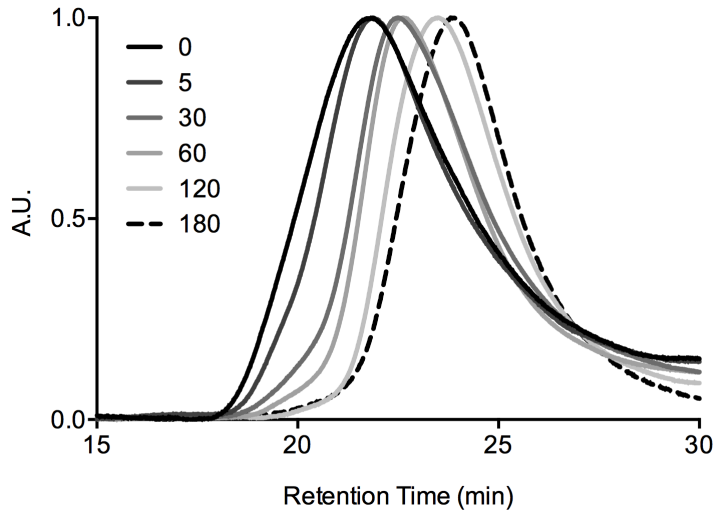

Figure 36 GPC overlay of **P1** molecular weight degradation at various sonication times.

3.4.4.2 ^{1}H and ^{13}C Product Analysis

Assignment of mechanochemically generated products are shown below, peaks are consistent with expected shifts for substitution and stereochemical arrangement of analogous reported compounds.[158]

3.4.4.3 Determination of P1 % Ring Opening vs. Sonication Time

% Ring Opening was calculated via integration as shown below. Protons H^{*} (red) and $H_{c,d}$ were chosen due to good resolution from neighboring peaks and because their resonances represent an equal number of protons (2) in both BCO and diene monomer units:

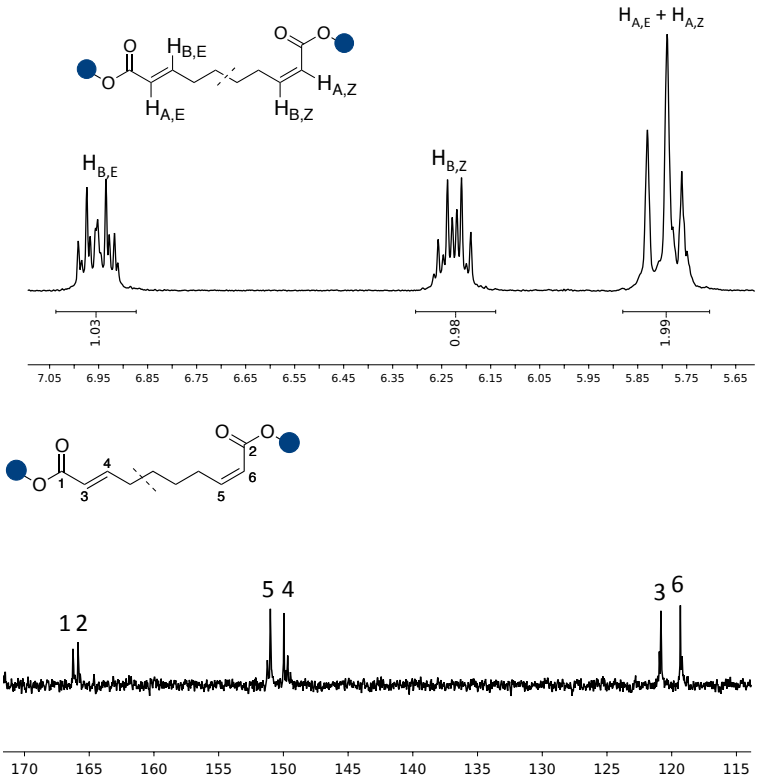

Figure 37 ^{1}H and ^{13}C NMR assignments for unsaturated products of **P1** activation.

The % ring opening was determined by the integration of diagnostic protons H^{*} (red) and $H_{c,d}$ as shown in Figure 38 according to the following:

$$\%\ Ring\ Opening = \frac{\int H_{c,d}}{\int H_{c,d} + \int H^{*}} \cdot 100$$

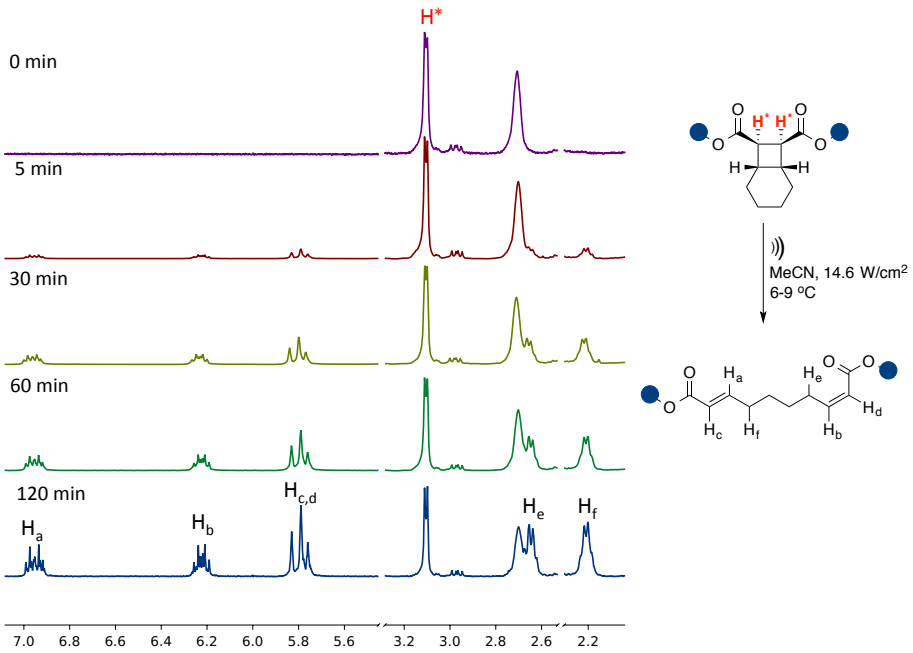

Figure 38 Peak assignments and equation used in the calculation of % ring opening of *cis*-BCO (**P1**) as a function of sonication time.

P1 % ring opening and corresponding molecular weight (M_n) is plotted below:

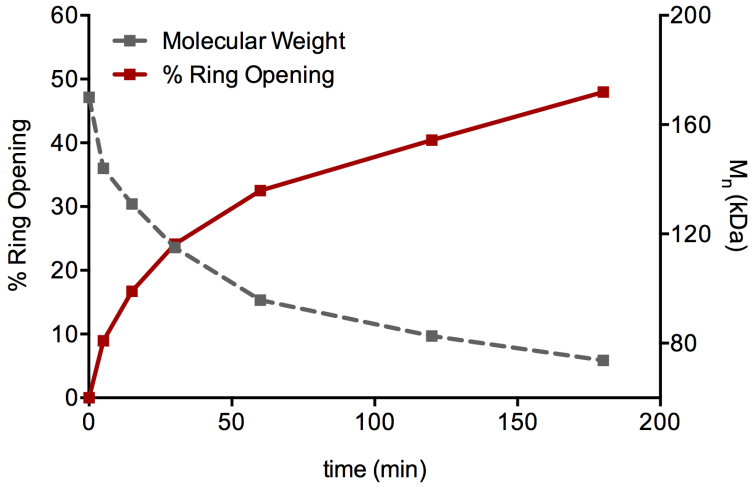

Figure 39 % Ring Opening and M_n of **P1** as functions of sonication time.

3.4.4.4 Determination of Product Distribution by Deconvolution

Lorentzian peak fitting was performed using Mestrelab Mnova (Mestrelab Research S.L., Santiago de Compostela, Spain) peak fitting function. β,*E*-Protons were deconvoluted into two peak distributions, corresponding to major (*EZ*) and minor (*EE*) monomeric product dienes:

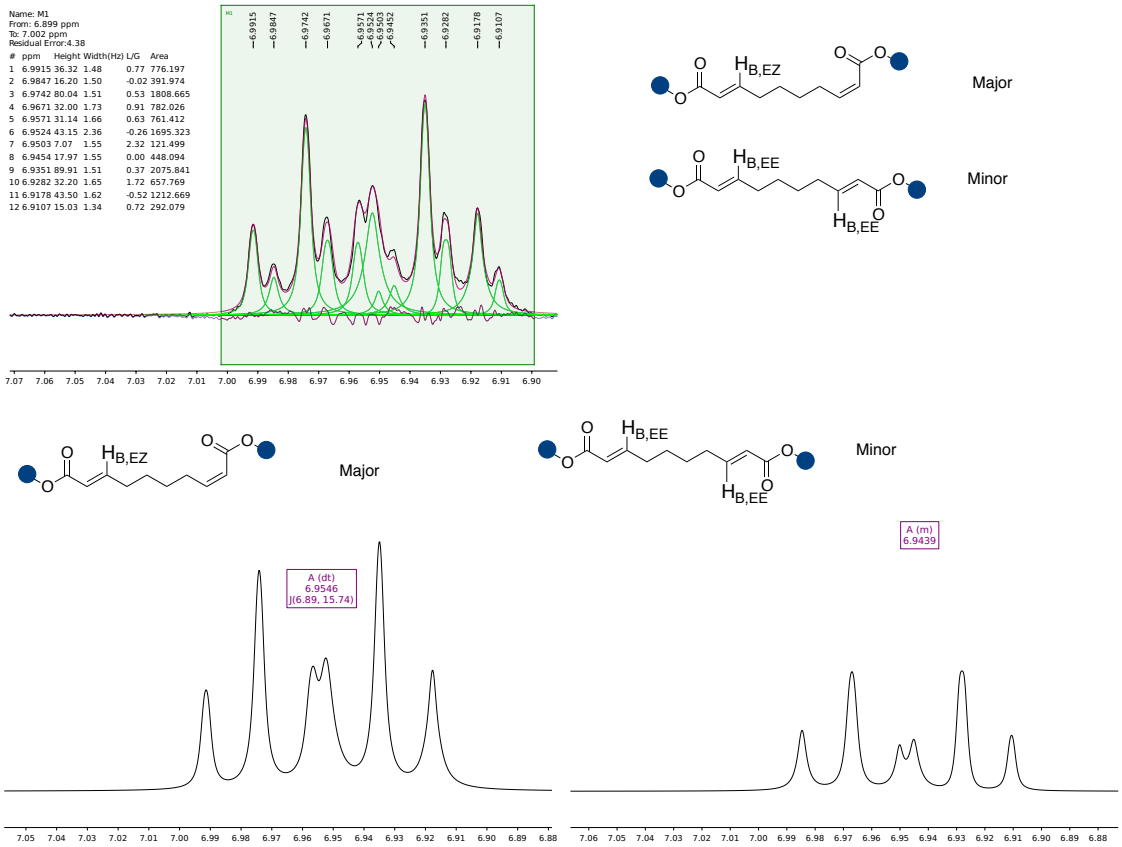

Figure 40 Sample deconvolution of *E*-alkene peaks in sonicated polymer **P1** used to determination of major and minor isomer content.

Deconvolutions were performed for all time points. The equations and Table 4 below detail determination of individual isomer ratios. $\%E_{total}$ and $\%Z_{total}$ are the percent of total alkenes generated in the *E* and *Z* configurations respectively:

$$\%E_{total} = 100 \cdot \frac{\int H_{B,E}}{\int H_{B,E} + \int H_{B,Z}}$$

$$\%Z_{total} = 100 \cdot \frac{\int H_{B,Z}}{\int H_{B,E} + \int H_{B,Z}}$$

$\%E_{major}$ and $\%E_{minor}$ are the percent of E_{total} integration that is attributed to each isomer respectively:

$$\%E_{major} = \%E_{total} \cdot \frac{\int H_{E,major}}{\int H_{E,major} + \int H_{E,minor}}$$

$$\%E_{minor} = \%E_{total} \cdot \frac{\int H_{E,minor}}{\int H_{E,major} + \int H_{E,minor}}$$

Total isomer content in terms of % of monomeric diene generated are calculated as follows:

$$\%EZ = \frac{2 \cdot \%E_{major} \cdot \%E_{total}}{100}$$

$$\%EE = \frac{\%E_{minor} \cdot \%E_{total}}{100}$$

$$\%ZZ = 100 - \%EZ - \%EE$$

Note: Product ratios shown in Table 4 (e.g. 77:13:10, 180 min) are based on the assumption that the E_{major} isomer is *EZ*. Without prior knowledge, another product ratio is possible if E_{major} is *EE* (e.g. 25:39:36). Given that E_{total} ~ Z_{total} and unsatisfactory deconvolution of $H_{B,z}$ we were unable to distinguish between the two by ^{1}H NMR. This

necessitated GC analysis. For CN and Br derivatives, asymmetry within the monomer unit and different E_{total}:Z_{total} content allowed for full characterization by ^{1}H NMR.

Table 4 Summary of product ratios by deconvolution for **P1**.

Sonication Time [min]	E_{total}	$E_{major,(EZ)}$	$E_{minor,(EE)}$	Z_{total}	*EZ*	*EE*	*ZZ*
5	49.4	80.6	19.4	50.6	79.7	9.6	10.8
15	50.2	73.1	26.9	49.8	73.4	13.5	13.1
30	50.9	81.2	18.8	49.1	82.6	9.6	7.8
60	50.8	70.5	29.5	49.2	71.6	15.0	13.4
120	51.2	73.4	26.6	48.8	75.2	13.6	11.2
180	51.2	75.5	24.5	48.8	77.4	12.5	10.1

3.4.4.5 Determination of Product Distribution in Sonicated P1 by GC

P1 was sonicated using standard conditions to achieve a 52% ring opening by ^{1}H NMR. The polymer (31 mg, 0.649 mmol ester groups) was transferred to a 25 mL Schlenk flask with a stir bar and dried under high vacuum. Under argon, 3.5 mL dry DCM was added and the solution was cooled to -30 °C. A 1M solution of Dibalh in toluene (2.60 mL, 2.60 mmol) was added dropwise with the solution first turning to a gelled suspension and eventually a homogenous solution upon completion of addition. The solution was allowed to warm to 0 °C over 1.5 hr. The reaction was quenched by addition of 50 μL water, 100 μL 2 N NaOH, and 75 μL water in succession. $MgSO_4$ was

then added and the suspension stirred for 15 minutes. The mixture was then filtered and evaporated to yield 12 mg of a clear oil, which was then subjected to GC analysis.

All GC analysis was performed using a Shimadzu QP2010 GC/MS with autosampler. All samples were derivatized before injection by the following method: A 2 mg/mL sample in dry DCM was prepared in an oven dried 4 mL scintillation vial. BSTFA (5:1 mol% vs. hydroxyl content) was added via microsyringe and the vial was sealed and heated in a sand bath at 60 °C then immediately subjected to GC analysis.

Retention times were confirmed by comparing with authentic samples[158] as shown in red and green curves below. Blue curve shows result of analysis of **P1** sample after reduction and derivatization. Percent content of each isomer was determined by integration of the decadienediol peaks:

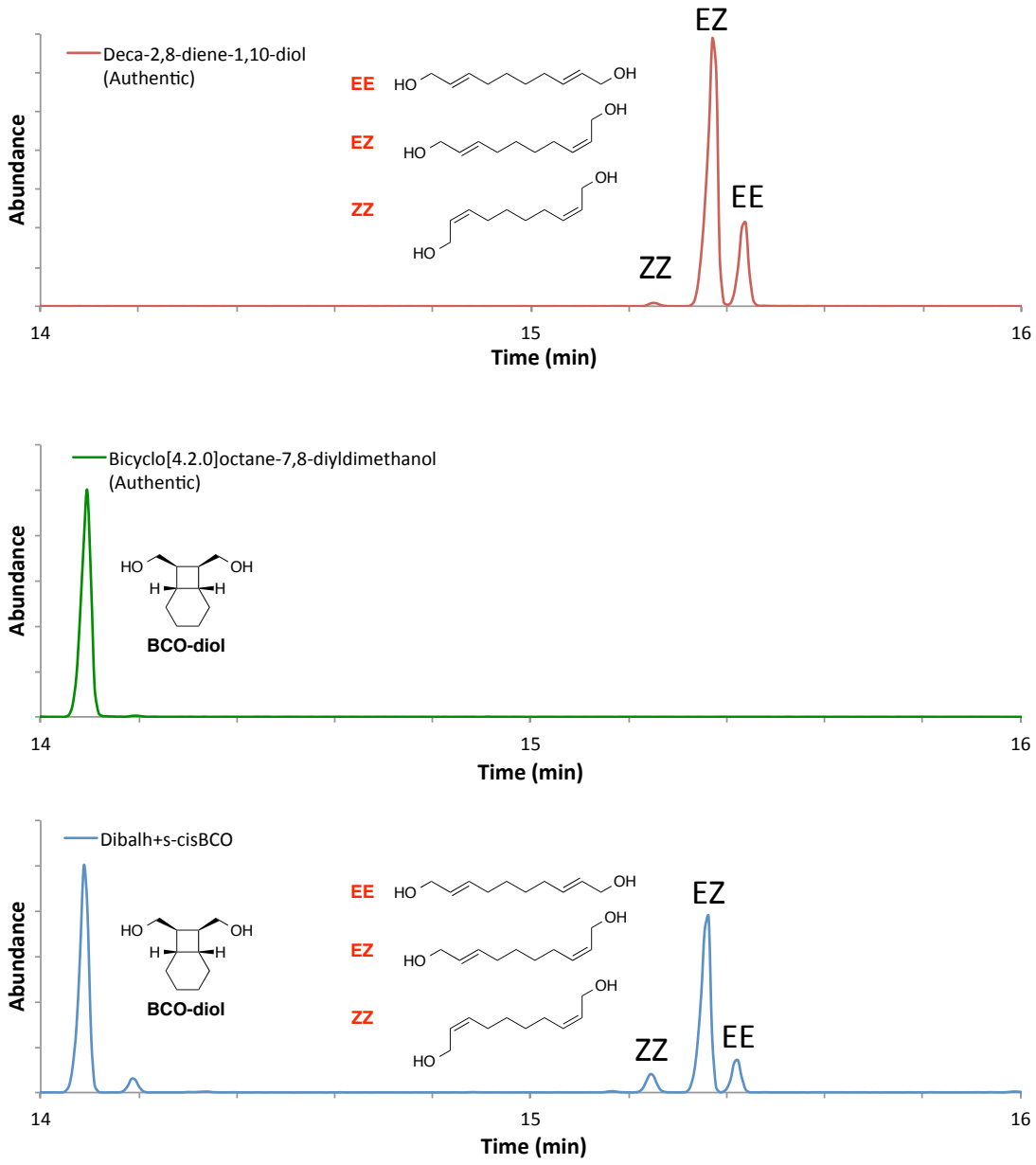

Figure 41 GC chromatograms for authentic decadienediols (red), reduced *cis*-BCO (green), and **P1** after sonication and reduction (blue). Content based on integration: *EZ* (77.5%), *EE* (13.6%), *ZZ* (8.9%).

3.4.5 Activation of P2 (*trans*-BCO)

Activation of **P2** by pulsed ultrasound was done in an identical fashion to **P1**.

3.4.5.1 Determination of P2 % Ring Opening vs. Sonication Time

The % ring opening was determined by the integration of diagnostic protons H^* (red) and $H_{c,d}$ as shown in Figure 42 according to the following:

$$\% \; Ring \; Opening = \frac{\int H_{c,d}}{\int H_{c,d} + \int H^*} \cdot 100$$

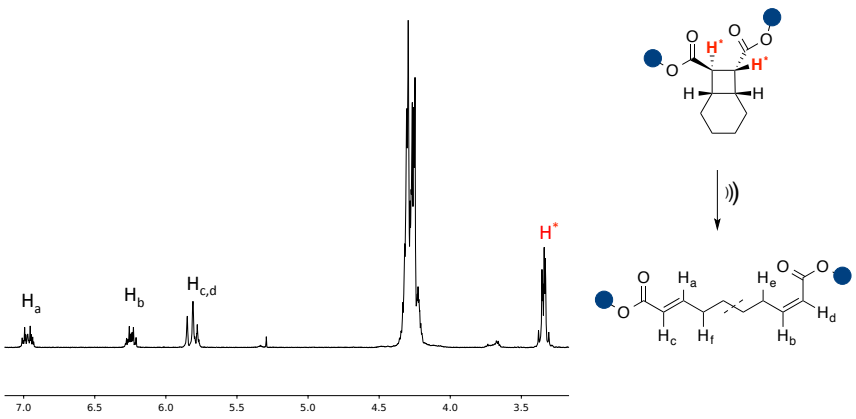
H*
H*
H*
H
H
O
O
O
O
O
H
H
H

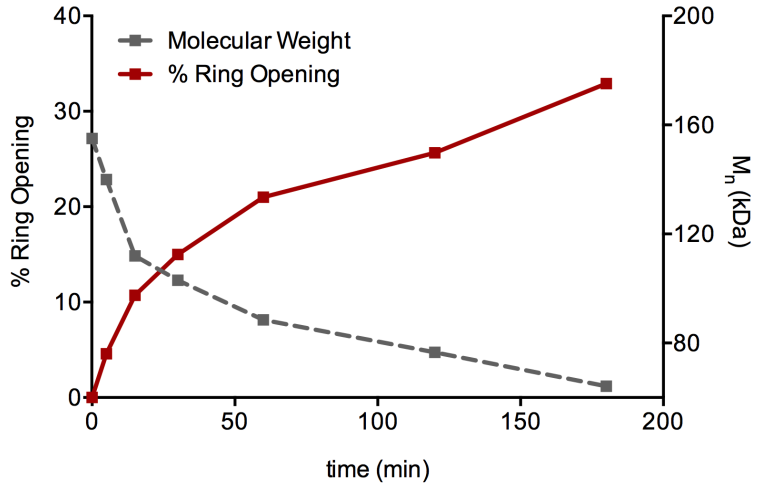

Figure 43 Evolution of % Ring Opening and M_n of **P2** as functions of sonication time.

3.4.5.2 Determination of Product Distribution by Deconvolution

Deconvolution was performed in a manner identical to that of **P1**. The results are summarized in Table 5 below:

Table 5 Summary of product ratios by deconvolution for **P2**.

Sonication Time [min]	E_{total}	$E_{major,(EZ)}$	$E_{minor,(EE)}$	Z_{total}	*EZ*	*EE*	*ZZ*
5	53.0	70.2	29.8	47.0	74.4	15.8	9.8
15	52.9	70.0	30.0	47.1	74.0	15.9	10.1
30	52.7	69.2	30.8	47.3	73.0	16.2	10.8
60	53.0	64.6	35.4	47.0	68.4	18.8	12.8
120	54.0	69.7	30.3	46.0	75.3	16.3	8.3
180	53.2	68.1	31.9	46.8	72.5	17.0	10.6

3.4.5.3 Determination of Product Distribution in sonicated P2 by GC

The **P2** product distribution was determined in an identical fashion to **P1**:

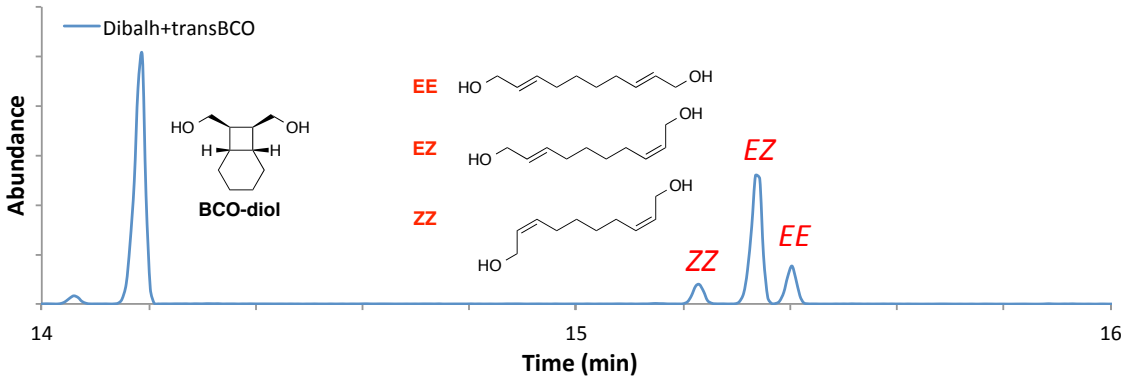

Figure 44 GC chromatogram of **P2** after sonication and reduction. Content based on integration: *EZ* (70.7%), *EE* (18.8%), *ZZ* (10.5%).

3.4.6 Activation of P1,2 (cis/*trans*-BCO)

Activation of **P1,2** by pulsed ultrasound was done in an identical fashion to **P1**.

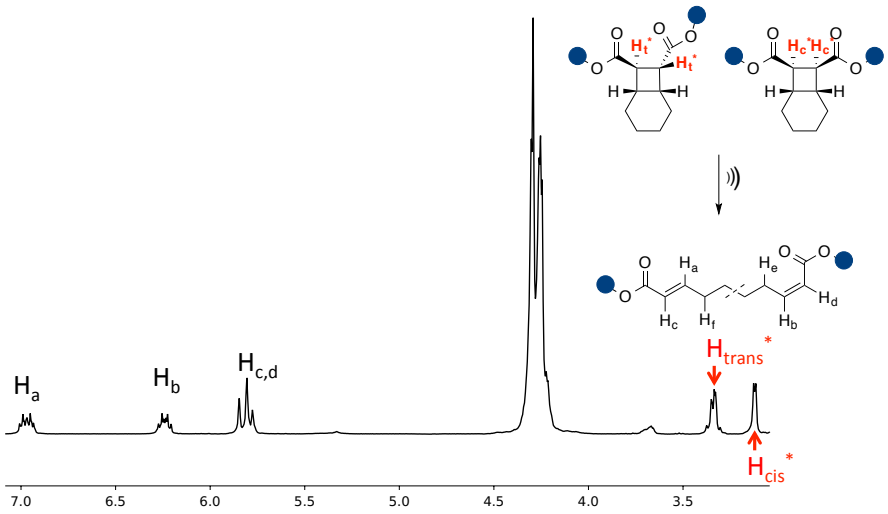

Figure 45 Peak assignments used in the calculation of % ring opening of *cis and trans* isomers in **P1,2** as a function of sonication time.

^{1}H NMR spectra for all time points were normalized based on peak integration to –OCH_2CH_2O- shifts from ethylene glycol subunits at 4.2-4.4 ppm. % Ring Opening as a function of time (t) was calculated based on change in H_{trans} and H_{cis} integrals from initial values $H_{trans,0}$ and $H_{cis,0}$:

$$\%RO_{trans}(t) = \frac{\int H_{trans,0} - \int H_{trans,t}}{\int H_{trans,0}} \cdot 100$$

$$\%RO_{cis}(t) = \frac{\int H_{cis,0} - \int H_{cis,t}}{\int H_{cis,0}} \cdot 100$$

3.4.7 Activation of P3 (*cis*-CN-BCO)

Activation of **P3** by pulsed ultrasound was done in an identical fashion to **P1**.

3.4.7.1 ^{1}H and ^{13}C Product Analysis of P3

Assignment of mechanochemically generated products are shown below, peaks are consistent with expected shifts for substitution and stereochemical arrangement of analogous reported compounds.[159]

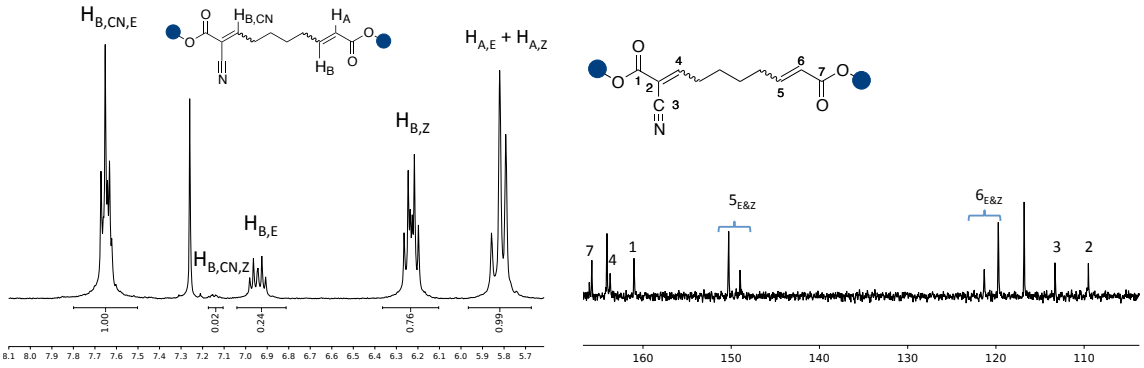

Figure 46 ^{1}H and ^{13}C NMR assignments for unsaturated products of **P3** activation.

3.4.7.2 Determination of % Ring Opening vs. Sonication Time

The % ring opening was determined by the integration of diagnostic protons H* (red) and H_B as shown in Figure 47 according to the following:

$$\% \; Ring \; Opening = \frac{\int H_B}{\int H_B + \int H^*} \cdot 100$$

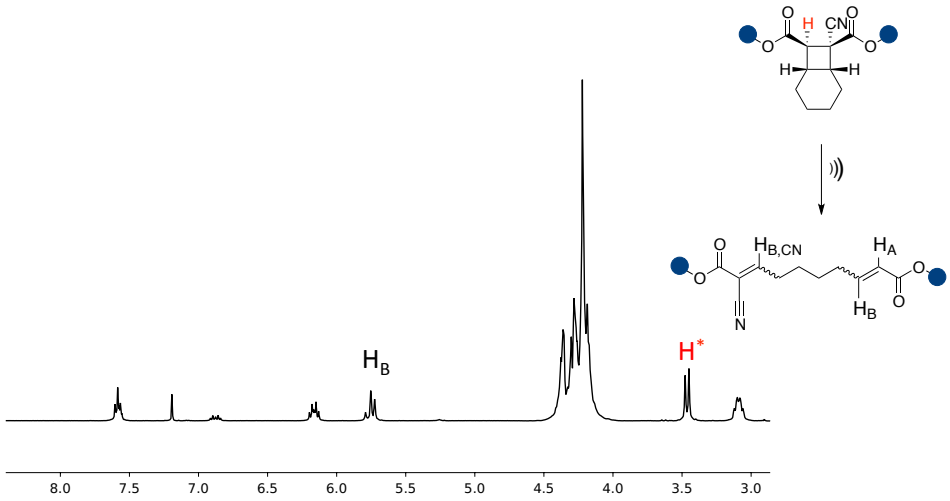

Figure 47 Peak assignments and equation used in the calculation of % ring opening of *cis*-CN-BCO as a function of sonication time.

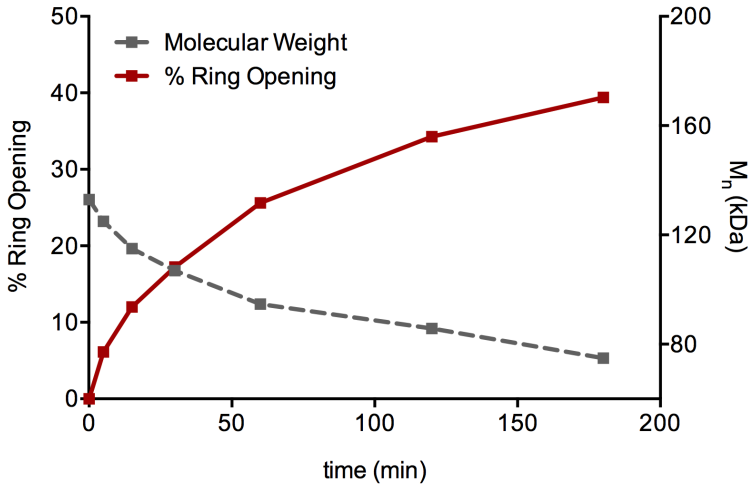

Figure 48 Evolution of % ring opening and M_n of **P3** as functions of sonication time.

3.4.7.3 Determination of Product Distribution of Sonicated P3 by Deconvolution

Deconvolution was performed using methods similar to those used in the deconvolution of **P1**. β,CN,*E*-Protons (Figure 47) were deconvoluted into two peak distributions, corresponding to major (*EZ*) and minor (*EE*) monomeric product dienes:

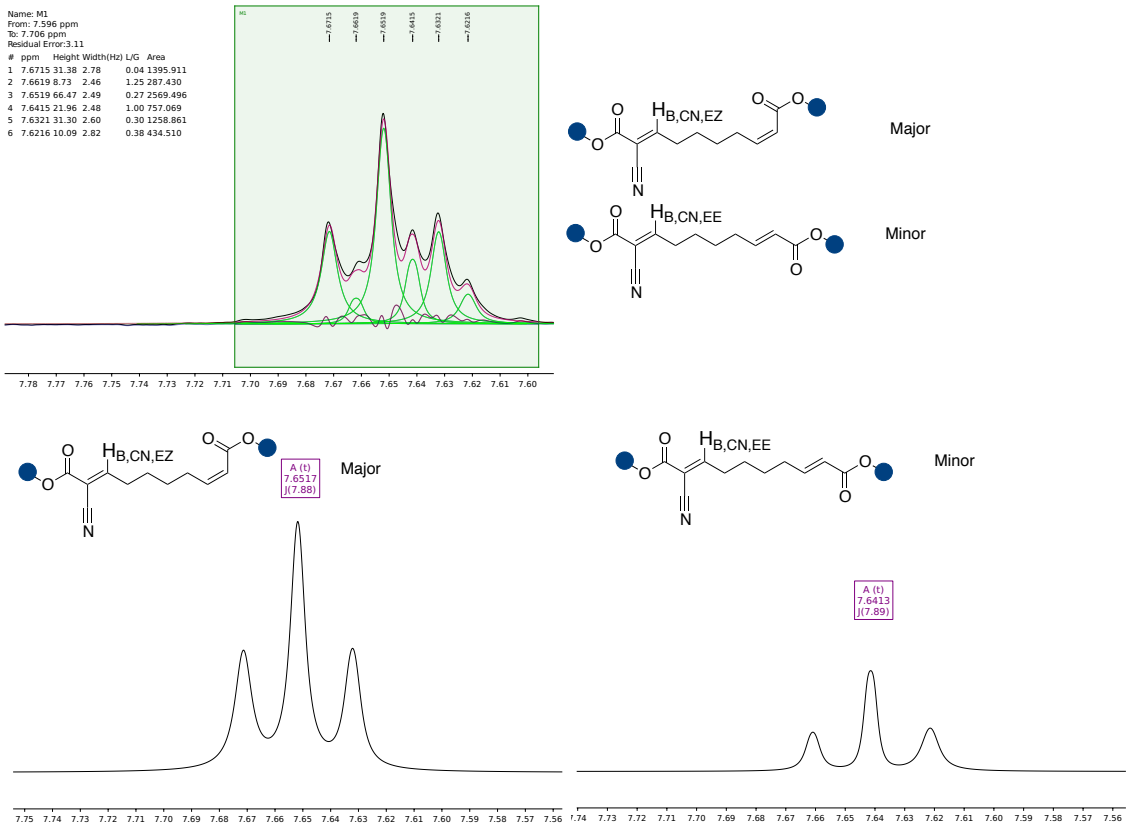

Figure 49 Sample deconvolution of *E*-alkene peaks in the determination of major and minor isomer content.

Deconvolutions were performed for all time points. Table 6 and equations below detail determination of individual isomer ratios:

$\%E_{CN,\text{total}}$ and $\%Z_{CN,\text{total}}$ are the percent of total cyano-alkenes generated in the E and Z configurations respectively:

$$\%E_{CN,total} = 100 \cdot \frac{\int H_{B,CN,E}}{\int H_{B,CN,E} + \int H_{B,CN,Z}}$$

$$\%Z_{CN,total} = 100 \cdot \frac{\int H_{B,CN,Z}}{\int H_{B,CN,E} + \int H_{B,CN,Z}}$$

$\%E_{\text{major}}$ and $\%E_{\text{minor}}$ are the percent of $E_{CN,\text{total}}$ integration that is attributed to each isomer respectively:

$$\%E_{CN,major} = \%E_{CN,total} \cdot \frac{\int H_{E,CN,major}}{\int H_{E,CN,major} + \int H_{E,CN,minor}}$$

$$\%E_{CN,minor} = \%E_{CN,total} \cdot \frac{\int H_{E,CN,minor}}{\int H_{E,CN,major} + \int H_{E,CN,minor}}$$

$\%E_{\text{unsub,total}}$ and $\%Z_{\text{unsub,total}}$ are the percent of total unsubstituted unsaturated esters generated in the E and Z configurations respectively:

$$\%E_{unsub,total} = 100 \cdot \frac{\int H_{B,E}}{\int H_{B,E} + \int H_{B,Z}}$$

$$\%Z_{total} = 100 \cdot \frac{\int H_{B,Z}}{\int H_{B,E} + \int H_{B,Z}}$$

Total isomer content in terms of % of monomeric diene generated are calculated as follows:

$$\%EZ = \frac{\%E_{CN,major} \cdot \%E_{CN,total}}{100}$$

$$\%EE = \frac{\%E_{CN,minor} \cdot \%E_{CN,total}}{100}$$

$$\%ZX = 100 - \%EZ - \%EE$$

Table 6 Summary of product ratios by deconvolution for P3.

Sonication Time (min)	$E_{CN,total}$	$E_{CN,EZ}$	$E_{CN,EE}$	$Z_{CN,total}$	$E_{unsub,total}$	$Z_{unsub,total}$	*EZ*	*EE*	*ZX*
5	91.3	83.0	17.0	8.7	22.5	77.5	75.7	15.5	8.7
15	93.4	80.7	19.3	6.6	22.2	77.8	75.4	18.0	6.6
30	94.3	79.2	20.8	5.7	22.3	77.7	74.7	19.6	5.7
60	91.5	78.2	21.8	8.5	22.9	77.1	71.6	19.9	8.5
120	94.0	79.2	20.8	6.0	23.6	76.4	74.4	19.5	6.0
180	98.4	77.9	22.1	1.6	24.0	76.0	76.7	21.7	1.6

3.4.8 Activation of P4 (*cis*-Br2-BCO)

3.4.8.1 ^{1}H Product Analysis

Assignment of mechanochemically generated products are shown below, peaks are consistent with expected shifts for substitution and stereochemical arrangement of analogous reported compounds.[160]

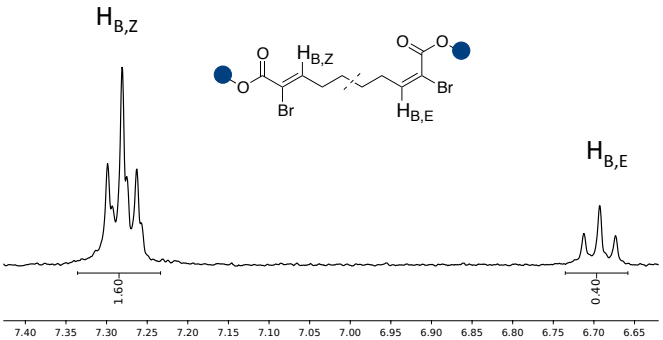

Figure 50 ^{1}H assignments for unsaturated products of **P4** activation.

3.4.8.2 Determination of % Ring Opening

The % ring opening was determined by the integration of diagnostic protons H* (red) and $H_{B,Z}$ and $H_{B,E}$ as shown in Figure 51 according to the following:

$$\%\ Ring\ Opening = \frac{\int H_{B,Z} + \int H_{B,E}}{\int H_{B,Z} + \int H_{B,E} + \int H^*} \cdot 100$$

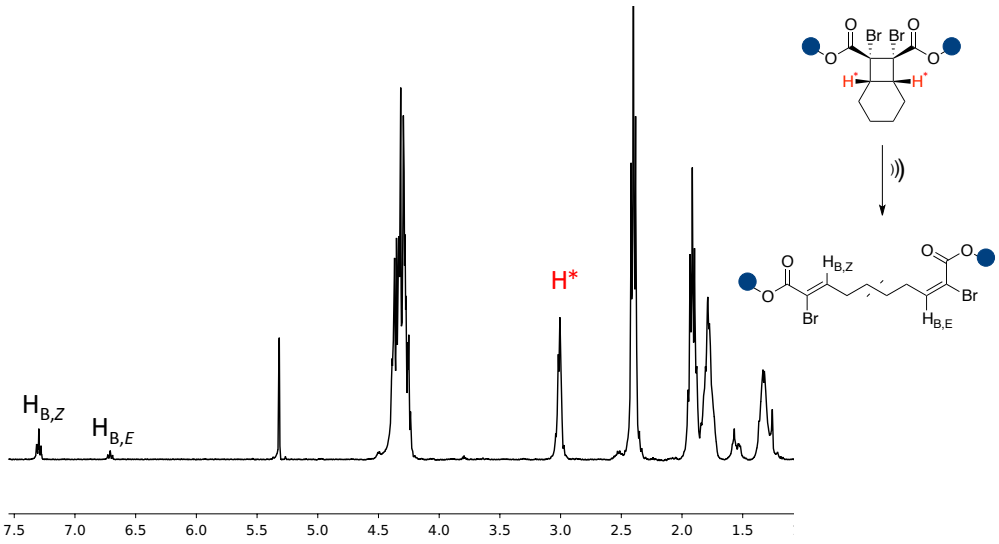

Figure 51 Peak assignments and equation used in the calculation of % ring opening of *cis*-Br_2-BCO as a function of sonication time.

3.4.8.3 Determination of Product Distribution by Deconvolution

Deconvolution was performed using methods similar to those used in the deconvolution of **P1**. β,*E*-Protons (Figure 50) were deconvoluted into two peak distributions, corresponding to major (*ZZ*) and minor (*Ze*) monomeric product dienes:

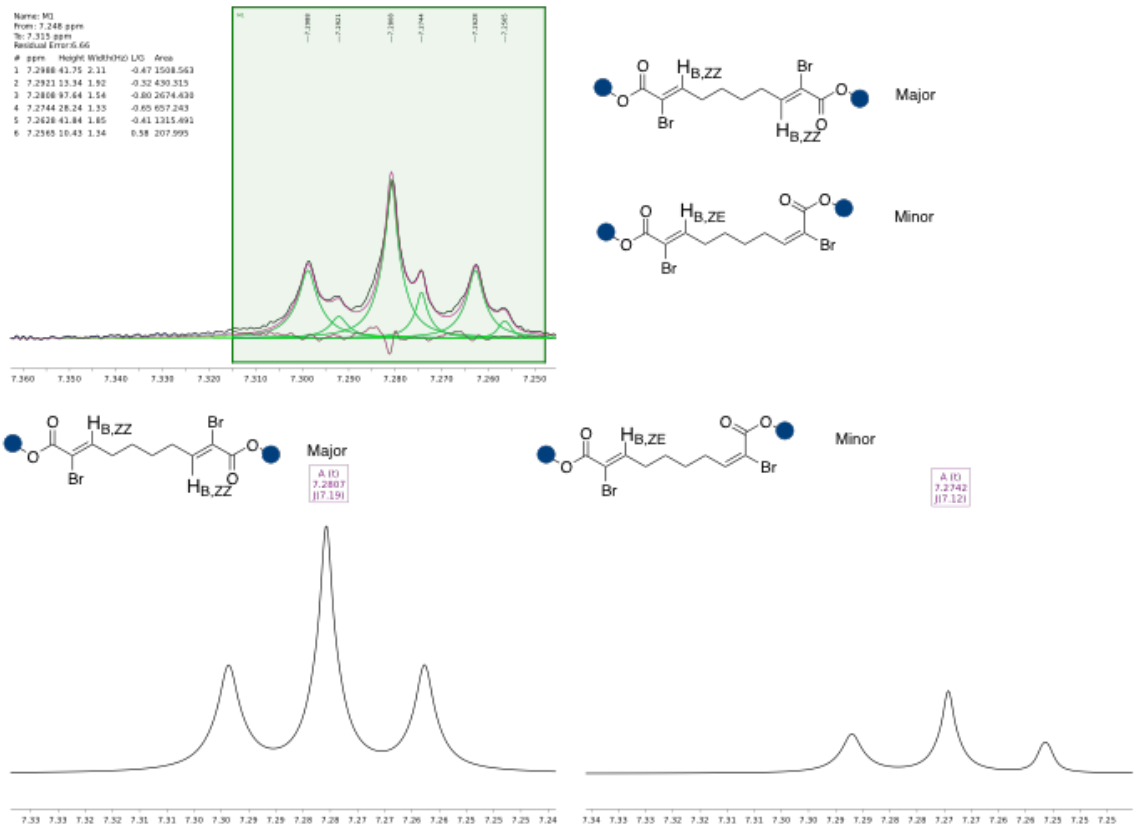

Figure 52 Sample deconvolution of *Z*-alkene peaks in the determination of major and minor isomer content.

Table 7 and the equations below detail determination of individual isomer ratios. $\%E_{total}$ and $\%Z_{total}$ are the percent of total alkenes generated in the *E* and *Z* configurations respectively:

$$\%E_{total} = 100 \cdot \frac{\int H_{B,E}}{\int H_{B,E} + \int H_{B,Z}}$$

$$\%Z_{total} = 100 \cdot \frac{\int H_{B,Z}}{\int H_{B,E} + \int H_{B,Z}}$$

%E_{major} and %E_{minor} are the percent of E_{total} integration that is attributed to each isomer respectively:

$$\%Z_{major} = \%Z_{total} \cdot \frac{\int H_{Z,major}}{\int H_{Z,major} + \int H_{Z,minor}}$$

$$\%Z_{minor} = \%Z_{total} \cdot \frac{\int H_{Z,minor}}{\int H_{Z,major} + \int H_{Z,minor}}$$

Total isomer content in terms of % of monomeric diene generated are calculated as follows:

$$\%EZ = \frac{2 \cdot \%Z_{minor} \cdot \%Z_{total}}{100}$$

$$\%ZZ = \frac{2 \cdot \%Z_{major} \cdot \%Z_{total}}{100}$$

$$\%EE = 100 - \%EZ - \%ZZ$$

Table 7 Summary of product ratios by deconvolution for **P**4.

Sonication Time (min)	%Z_{major} (*ZZ*)	%Z_{minor} (*ZE*)	%Z_{total}	%E_{total}	*ZZ*	*EZ*	*EE*
180	83.3	16.7	79.8	20.2	66.4	26.7	6.8

3.4.9 Sonication of PC (control-*cis*-BCO)

Polymer **PC** was sonicated using the standard procedure. Due to the low molecular weight (13.3 kDa) forces experienced by the polymer would be insufficient for ring opening, supporting the mechanical nature of the reaction. No ring opening was observed by ^{1}H NMR and the final MW was determined to be 12.6 kDa as shown in Figure 53.

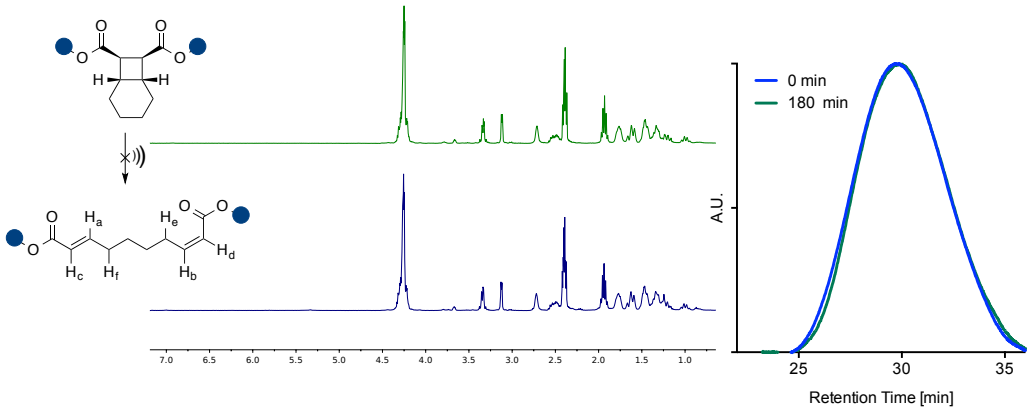

Figure 53 ^{1}H NMR (left) and GPC trace (right) of 13.3 kDa control polymer PC before (green) and after (blue) 180 minutes of sonication.

3.4.10 Product distribution vs. MW Evolution and Activation of P1$_{77kDa}$

While the **P4** product distribution is dramatically different from all other examples, the M_n is also significantly lower. To show a lack of sensitivity of mechanochemical product distributions to initial MW a lower MW *cis*-BCO polymer (**P1**$_{77kDa}$) was tested (Deconvolution of **P1**$_{77kDa}$ was performed in a manner identical to that of **P1**):

Table 8 Summary of product ratios by deconvolution for **P1**$_{77kDa}$.

Sonication Time (min)	E_{total}	$E_{major,\ EZ}$	$E_{minor,\ EE}$	Z_{total}	*EZ*	*EE*	*ZZ*
30	56.0	69.0	31.0	44.0	77.2	17.4	5.4
60	57.2	71.5	28.5	42.8	81.8	16.3	1.9
120	56.7	68.5	31.5	43.3	77.7	17.8	4.4
180	55.7	68.8	31.2	44.3	76.6	17.4	6.0

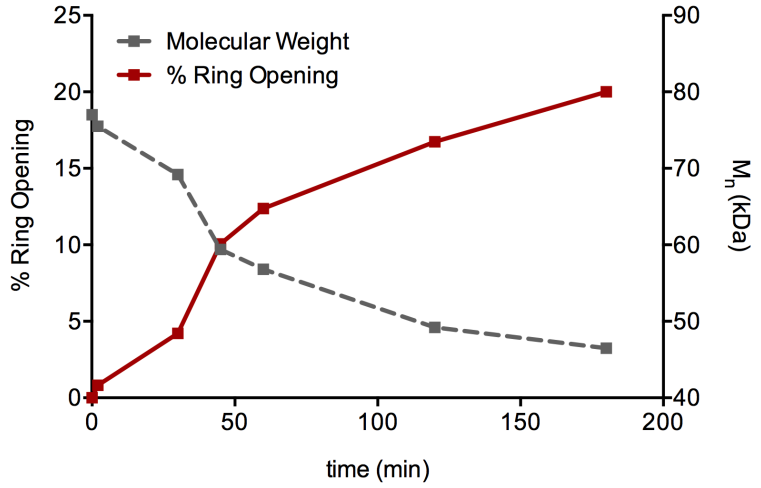

Figure 54 Evolution of % Ring Opening and M_n as functions of sonication time for $P1_{77kDa}$.

While a slight increase in % *EE* is observed, this is at the cost of *ZZ* isomer content, which is not reflected in the product distribution of **P4**. If a decrease in *EZ* predominance in the product distribution is a product of low MW, one might anticipate that % *EZ* content would decrease throughout sonication. No such trend is observed, and **P4** *EZ* content (pink) is significantly lower than all other polymers tested at all time points:

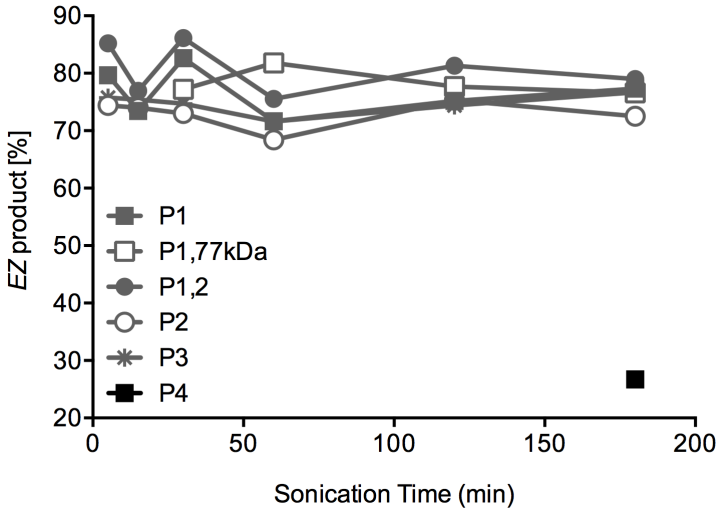

Figure 55 Evolution of % *EZ* product and vs. sonication time for all polymers tested.

3.4.11 Functionalization of P1 by Thiol-ene Addition

3.4.11.1 Small Molecule Conjugation

P1 was sonicated for 3 hr as a 4 mg mL^{-1} solution in MeCN to obtain 53 mg of 33% ring opened (0.092 mmol alkenes). Polymer was dissolved in 0.75 mL MeCN-d_3 and ethyl thioglycolate (16.4 mg, 0.137 mmol) was added. DBU (0.6 mg, 0.004 mmol) was added from a stock solution in 0.1 mL of MeCN-d_3 to initiate reaction and time-points were recorded.

3.4.11.2 Formation of Cross-linked Polymer Networks

P1 was sonicated for 3 hr as a 4 mg mL^{-1} solution in MeCN to obtain 55 mg of 36% ring opened (0.10 mmol alkenes). The polymer was dissolved in 0.5 mL MeCN in a 7 mL vial. 1,4-butanediol dithioglycolate (12 mg, 5.0 mmol) was added followed by DBU

(0.80 mg) from a stock solution in 0.1 mL MeCN. The vial was vortexed for 1 second and allowed to stand for 1 minute at which time a gel was formed (left).

An identical experiment was run with unsonicated **P1** as a control. No gelation was observed and the solution remained free flowing upon inversion (right). No change was observed over the course of two weeks.

3.4.12 X-ray Crystallography*

3.4.12.1 X-ray Crystal Structure of Compound 3

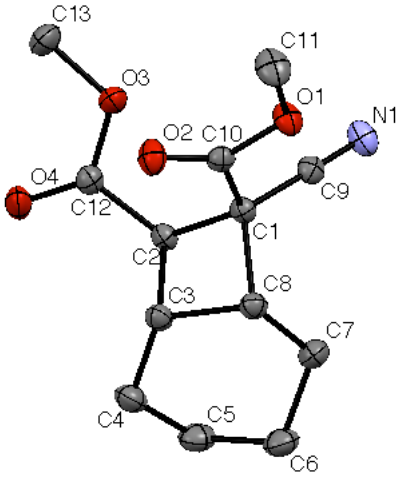

Colorless prisms crystallized from pentane/acetone at 3-6°C by employing liquid/liquid diffusion method. Crystal data: Prism, colorless, crystal size = 0.4157 x 0.3474 x 0.1977 mm^3, $C_{13}H_{17}NO_4$, FW 251.28, monoclinic, space group $P\ 1\ 2_1/c\ 1$, a = 8.89070(11), b = 12.16463(14), c = 12.12008(14) Å, α = 90°, β = 93.0379(10)°, γ = 90°, V = 1308.97(3) $Å^3$, Z = 4, D_c = 1.275 mg/m^3, T = 100(1) K, μ = 0.785 mm^{-1}, 11312 measured

*Compounds 3 and 4 were crystallized by Zhenbin Niu, Craig Lab. Crystallographic data was obtained and the structure solved by Prof. Arnold Rheingold, UC San Diego.

reflections, 2689[R(int) = 0.0238] independent reflections, 2689 / 0 / 165 Data / restraints / parameters, *F(000)* = 536, *R1* = 0.0381, *wR2* = 0.0950, *R1* = 0.0362, *wR2* = 0.0934[I>2sigma(I)], Max. residual density 0.358 e.Å^{-3}, Max. and min. transmission 1.894 and 0.821, and goodness-of-fit (F^2) = 1.048.

3.4.12.2 X-ray Crystal Structure of Compound 4

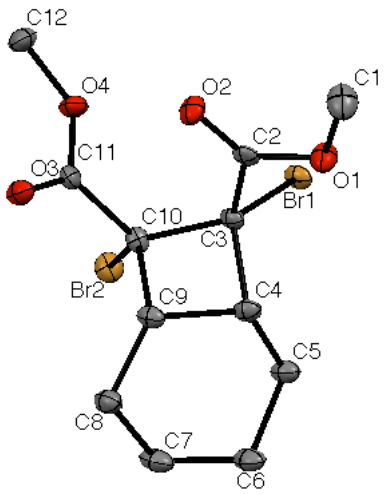

Colorless plates crystallized from pentane/acetone at room temperature by employing vapor diffusion method. Crystal data: plates, colorless, crystal size = 0.24 x 0.24 x 0.10 mm^3, $C_{12}H_{16}Br_2O_4$, FW 384.07, Monoclinic, space group P2(1)/c, *a* = 8.4288(2), *b* = 13.7579(4), *c* = 12.3099(3) Å, α = 90°, β = 106.9400(10)°, γ = 90°, *V* = 1365.55(6) Å^3, *Z* = 4, D_c = 1.868 mg/m^3, *T* = 100(2) K, μ = 7.588 mm^{-1}, 8416 measured reflections, 2391[R(int) = 0.0519] independent reflections, 2391 / 0 / 165 Data / restraints / parameters, *F(000)* = 760, *R1* = 0.0450, *wR2* = 0.1017, *R1* = 0.0409, *wR2* = 0.0988 [I>2sigma(I)], Max. residual density 1.090 e.Å^{-3}, Max. and min. transmission 0.5175 and 0.2632, and goodness-of-fit (F^2) = 1.074.

3.4.13 Determination of Elongation

Modeling to determine change in monomer length was performed using Spartan® software as previously described.[95] In short, Molecular Mechanics (MMFF) was performed for both closed (*cis*-BCO dimethyl ester) and opened (*EZ* dimethyl ester) to generate a CoGEF[129]-type constrained potential relating molecular energy to end-to-end distance (left plot). This was fitted to a second order polynomial, the derivative of which relates force to end-to-end distance (right). By solving the linear equation of force vs. distance for f = 0 N a contour length was obtained, the difference of which between the opened and closed form equals the net elongation upon ring opening.

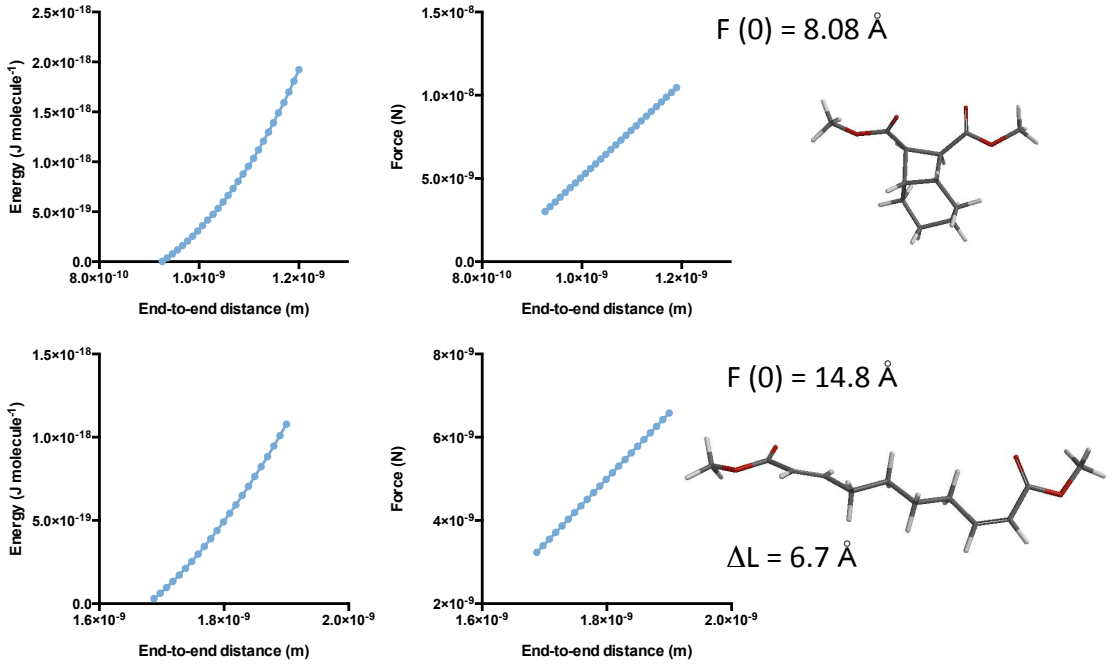

Figure 56 Force-elongation curves of *cis*-BCO and ring-opened *EZ* product used in the determination of change in contour length. Contour lengths were determined by extrapolating the force-distance curves to force = 0.

4. Impacting the Bulk Properties of Covalent Gels by Incorporating Weak and Transient Non-Covalent Bonds*

4.1 Introduction

Polymer organogels and hydrogels are important materials for applications ranging from biomedical implants and tissue engineeering[161] to soft, active devices. For many of these applications, a high range of motion (i.e., achieving high strains) is desirable, but the network defects of polymer gels often limit the maximum strain they can achieve.[117,162] Many biological and device applications would benefit from gels that withstand high strains without having to pay the energetic costs associated with added, highly dissipative interactions in current stretchable gels.[163-165] Structurally homogeneous "precision" networks constructed from monodisperse molecular elements result in a smooth network stress distribution[166] that can accommodate high strains[167,168] with minimal energy dissipation.[169-171] This approach, however, typically cannot be transferred to existing gels made from easily accessible random biopolymer or synthetic polymer networks. An ideal solution would be to identify modifications that have no discernable impact on the modulus of a gel and maintain high levels of elastic recovery, while permitting the gel to achieve otherwise inaccessible strains repeatedly over

* This chapter adapted from: Kean et al. (2014) *Adv. Mater.*, 26, 6013-1018. Portions of this chapter were performed in collaboration with co-workers as noted where relevant.

multiple loading cycles without a loss in mechanical properties. Here, we build on earlier observations by Jennifer Hawk[172] to show that the addition of transient, supramolecular cross-links to a covalent polymer gel can provide dramatic increases in the maximum achievable strain at break, even when the added supramolecular cross-links are so weak and dynamic as to be effectively invisible in terms of their contribution to modulus or energy dissipation in materials. The results suggest that classes of "very weak" supramolecular interactions might play an important, previously overlooked, role in developing next generation gels.

4.2 Results and Discussion

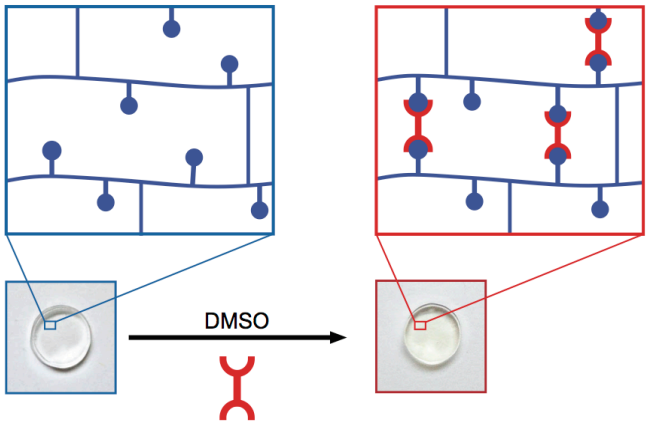

Figure 57 Cylinders (typical diameter = 4.4-5.0 mm, typical height = 1.6-1.8 mm) of covalent organogel **PN1** (left) incorporate transient pincer cross-links (right) by coordination with pyridine side-groups (blue circles) in P4VP-based networks (**PN1•PdEt** [5 mM]) shown.

Model organogels were synthesized by reaction of poly(4-vinylpyridine) (P4VP) with a dibromide functional cross-linker in DMSO (Scheme 5). The P4VP has an M_n of 33 kDa and a polydispersity of 1.35 (see experimental section), and cross-linking was

introduced by selectively alkylating a small fraction of the pyridine groups along the polymer backbone (~315 average repeat units), resulting in a heterogeneous network mesh. Cross-linking with 1,6-dibromohexane (1 per 50 pyridines) led to network **PN1**, which was subsequently punched into cylinders and swollen to equilibrium in DMSO (polymer volume fraction $\phi \sim 0.03$). The fragile nature of the nascent **PN1** gels necessitated the use of unconfined uniaxial compression (hereafter compression) for the majority of our characterization. Consistency in the compression results was achieved by restricting studies to low strain values (<0.8)[173] and maintaining proper sample geometry to avoid buckling.[174] The failure point from the stress-strain curves was validated through the use of a chemiluminescent probe (see below). Weak, transient supramolecular cross-links were introduced into the **PN1** network cylinders by solution uptake (5 mM in DMSO) of bifunctional van Koten-type[175] pincer complexes, which coordinate reversibly on either end to free pyridines along the polymer side chain (Figure 57).

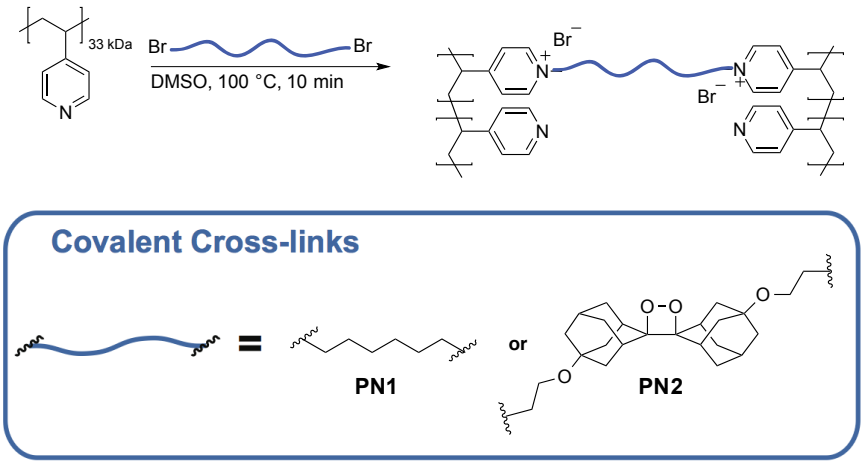

Scheme 5 Synthesis of **PN1** and **PN2** organogels by alkylation of P4VP with dibromide cross-linkers in DMSO.

Mechanical testing (see Figure 59, below) shows that the number of reversible cross-linkers introduced in this way is comparable to the number of covalent cross-linkers, consistent with the concentrations and associations constants of the pincer complexes. The pincers were chosen because they are versatile probes of dynamic molecular contributions to bulk macromolecular properties;[52,176,177] small structural changes in the metal and ligand adjust the lifetime of the cross-linker across a range from milliseconds to minutes (Figure 58). This control element is critical for our strategy,[178] as it provides access to hybrid gels in which the reversible component rearranges so rapidly that it makes a negligible contribution to the compressive mechanical properties on typical experimental timescales.

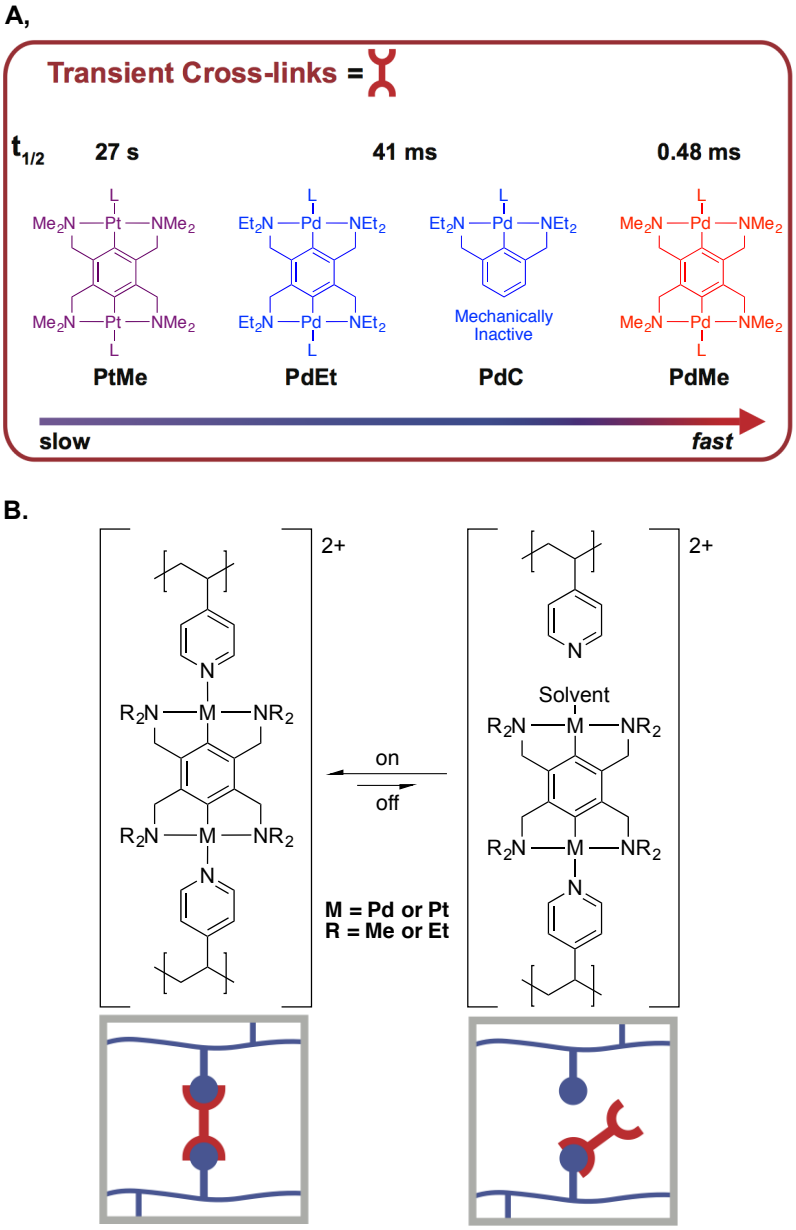

Figure 58 (a) Structure and metal-pyridine half-lives of pincer-based cross-linkers in DMSO (solvent).[178] (b) Solvent mediates the reversible dissociation of metal-pyridine bonds.

The consequences of the weak cross-linking on hybrid gel properties are shown in Figure 59. When **PN1** is compressed rapidly (~8 mm s^{-1}, 4 s^{-1}) to 20% strain and held

for 1 s, the stress is stored in its covalent network, and minimal relaxation is observed. When the **PdEt** cross-linker ($t_{1/2}$ = 41 ms) is added, some additional stress is stored in the reversible cross-linker, and that stress dissipates over a few tenths of seconds. The even more rapidly dissociating **PdMe** ($t_{1/2}$ = 0.48 ms) accumulates even less additional energy. When the loading rate is reduced to 80 μm s^{-1}, the amount of additional stress stored in the reversible component of **PN1•PdEt** drops to ~2%, and that stored in the reversible component of **PN1•PdMe** is too small to be detected. Slowing the compression further to 8 μm s^{-1} led to indistinguishable relaxation behavior among the nascent covalent and both hybrid gels.

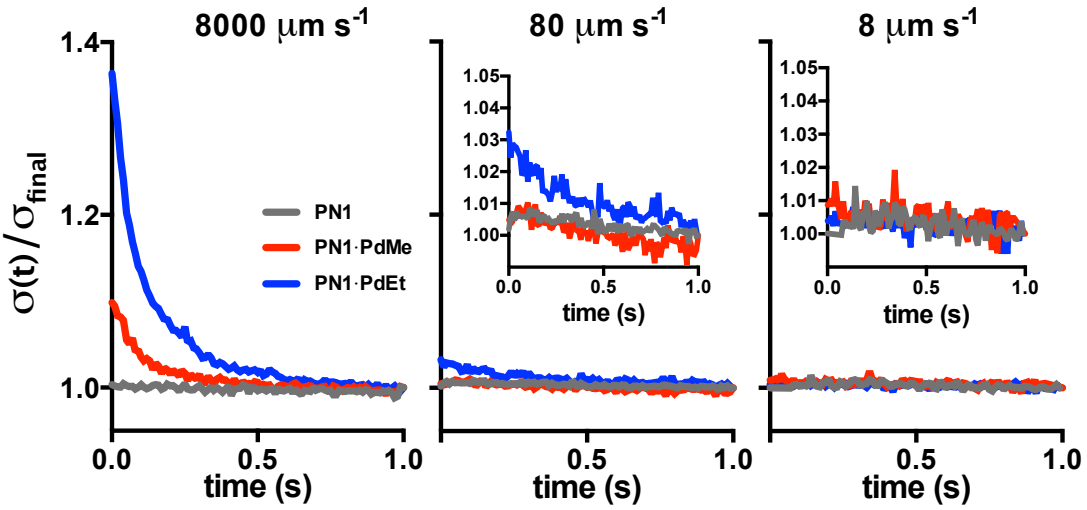

Figure 59 Time-dependent low-strain (ε = 0.2) relaxation behavior of **PN1** (grey), **PN1•PdEt** (blue), and **PN1•PdMe** (red) organogel cylinders showing decreased mechanical activity of pincer cross-links with decreased loading rate. Stress as a function of time after loading (t) is normalized by the stress at t = 1 s (σ_{final}) and insets show magnified relaxation curves.

As expected, therefore, the hybrid networks store minimal additional energy relative to **PN1**, and subsequent characterization shows that the same is true for the amount of energy dissipated. Stress-strain hysteresis (Figure 60b) reveals that the amount of energy dissipated in **PN1•PdEt** is measurably larger than that of **PN1** at 80 μm s^{-1} but not at 8 μm s^{-1}, while the hysteresis energy of **PN1•PdMe** is indistinguishable from that of **PN1** at both loading rates. Hysteresis energies shown in Figure 60b amount to between 18 and 34% at low strain (ε = 0.2) and between 21 and 46% at high strain (ε= 0.4).

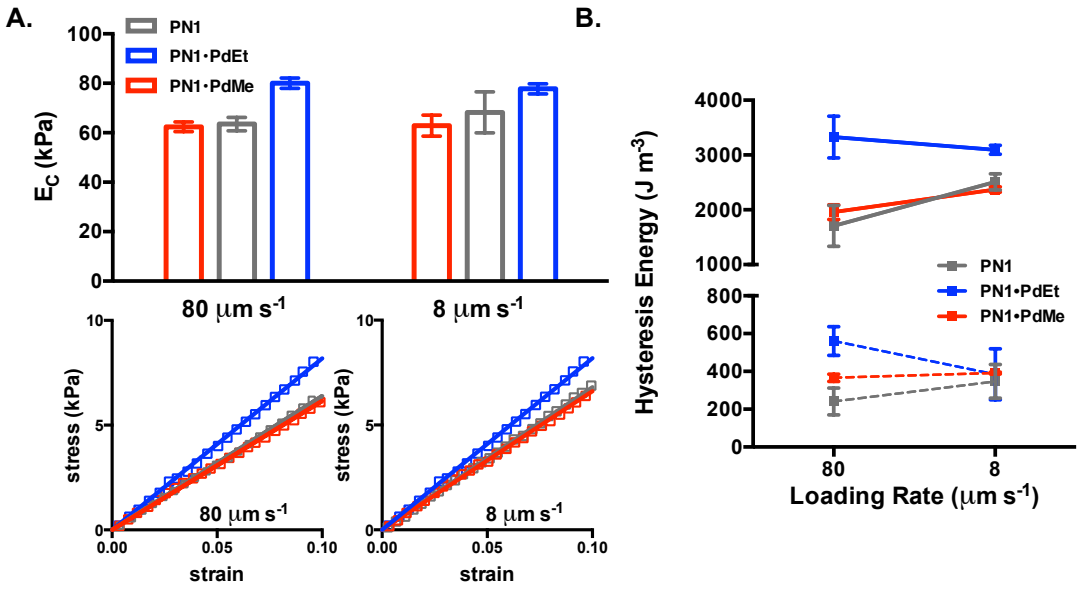

Figure 60 (a) E_C of **PN1**-based networks as a function of loading rate, determined by stress-strain curves under compression (squares) and linear fit (ε = 0-0.1, solid). **PdEt** cross-links make minor contributions to E_C while **PdMe** crosslinks are mechanically "invisible." (b) Hysteresis energy for **PN1**-based networks under compression (ε_B = 0.4 (solid), 0.2 (hashed)) at different loading rates. Error bars denote SEM, n= 3. T = 25 °C for all experiments.

Measurements of compressive moduli (E_C, taken as the initial slope of the stress-strain curves) further confirm that additional energy input is needed to strain **PN1•PdEt** relative to **PN1** (E_C = 80 vs. 64 kPa at 80 μm s^{-1}). Conversely, the modulus of **PN1•PdMe** (62 kPa) was indistinguishable from that of the parent gel, consistent with the short lifetime of the **PdMe** cross-linkers relative to the timescale of the compression. The three gels have the same covalent network, the active chains of which contribute roughly 62-64 kPa to the modulus of each system. The supramolecular component of the **PN1•PdEt** network contributes an additional 25% to the modulus, whereas the contribution of the supramolecular component of **PN1•PdMe** is too small to be measured (Figure 60a). The minimal contributions of these elements are seen as well in low strain oscillatory rheology (see experimental section, Figure 70).

The overlay of the red (**PN1•PdMe**) and gray (**PN1**) data, especially the stress-strain curves in Figure 60a, is particularly compelling. For a given strain, the same energy is being stored in the same covalent framework, and so the behavior of the hybrid networks as the gels were compressed further came as a surprise. The **PN1** gels are fairly weak, with an average compressive strain-at-break (ε_B) of 0.46, and stress-at-break (σ_B) of 103 kPa at the 80 μm s^{-1} loading rate. In comparison, **PN1•PdEt** showed a dramatic increase in ε_B (0.73 vs. 0.46) and σ_B (816 kPa vs. 103 kPa) (Figure 61a), somewhat surprising given the otherwise modest mechanical activity of the transient **PdEt** cross-linker. Given this result, we then examined the effect of introducing **PdMe**

that, due to increased lability ($t_{1/2}$ = 0.48 ms) makes no measurable contribution to modulus and bears no measurable stress. Unexpectedly, these hybrid gels also demonstrated dramatic increases in stress and strain at break (ε_B = 0.68, σ_B = 492 kPa; 5 mM **PdMe**) (Figure 61b).

The observed effect is due to the introduction of dynamic cross-links, as supported by several observations. First, the strain (and stress) at break increases monotonically as a function of **PdEt** or **PdMe** loading (Figure 61d and e). Second, while some deswelling occurs upon introduction of pincer complexes, the effect of differential swelling was ruled out by compression testing of **PN1** gels swollen to a wide range of polymer volume fractions (ϕ ~ 0.03-0.08, varied by addition of co-solvent; see experimental section) that encompass those observed in all **PN1•Pd** samples (ϕ ~ 0.03-0.04). Differential swelling has only a minimal impact on ultimate properties, relative the impact of added pincer complex (Figure 61g). To ensure that the effect is due to cross-linking rather than simply chemical modification, we introduced the mechanically inactive monofunctional control **PdC** (10 mM, equivalent [Pd] to 5 mM **PdEt**). Again, only a minimal effect was observed (ε_B = 0.51, σ_B = 122 kPa), consistent with the minor effect of differential swelling (Figure 61c and g). Additional experiments reveal that dynamic rearrangement of the network is required for enhanced ε_B in this system; for example, replacing the metal center with platinum increases the cross-linker lifetime by five orders of magnitude (**PtMe** vs. **PdMe**) to ~38 s, which is on the order of the

compression experiment (1-10 s^{-1}). Though it may be expected that **PN1•PtMe** would display increased ε_B with increased E_C, we instead observed diminished ε_B (0.07) with increased modulus (E_C = 354 kPa), reminiscent of increasing the concentration of covalent or strong ionic cross-links (Figure 61f). Based on these observations, it is apparent that rapid dissociation of supramolecular cross-links (**PdMe** and **PdEt**) is required to increase ε_B.

To probe directly how the fracture behavior of the underlying covalent network changed as a function of the added supramolecular component, we employed **PN2**. **PN2** bears a bis(adamantyl) dioxetane mechanophore cross-linker, which behaves as a chemiluminescent indicator of covalent failure[179,180] (Figure 62a). Upon rupture, the dioxetane mechanophore breaks to form electronically excited adamantanone chain ends that rapidly transfer energy to the singlet acceptor 9,10-bis(phenylethynyl) anthracene, which ultimately emits a photon at ~600 nm. **PN2•PdEt** was subjected to compression testing at various **PdEt** concentrations, and the emission was simultaneously recorded using a CMOS-based sensor at 33 FPS. As seen in Figure 62b, the onset of emission due to failure of the covalent network shifts in concert with strain-at-break, while the integral emission intensity and duration of emission remains constant. The reversible interactions, even when not bearing stress within the network, therefore inhibit the scission of the underlying covalent network that is actively bearing greater stresses in their presence.

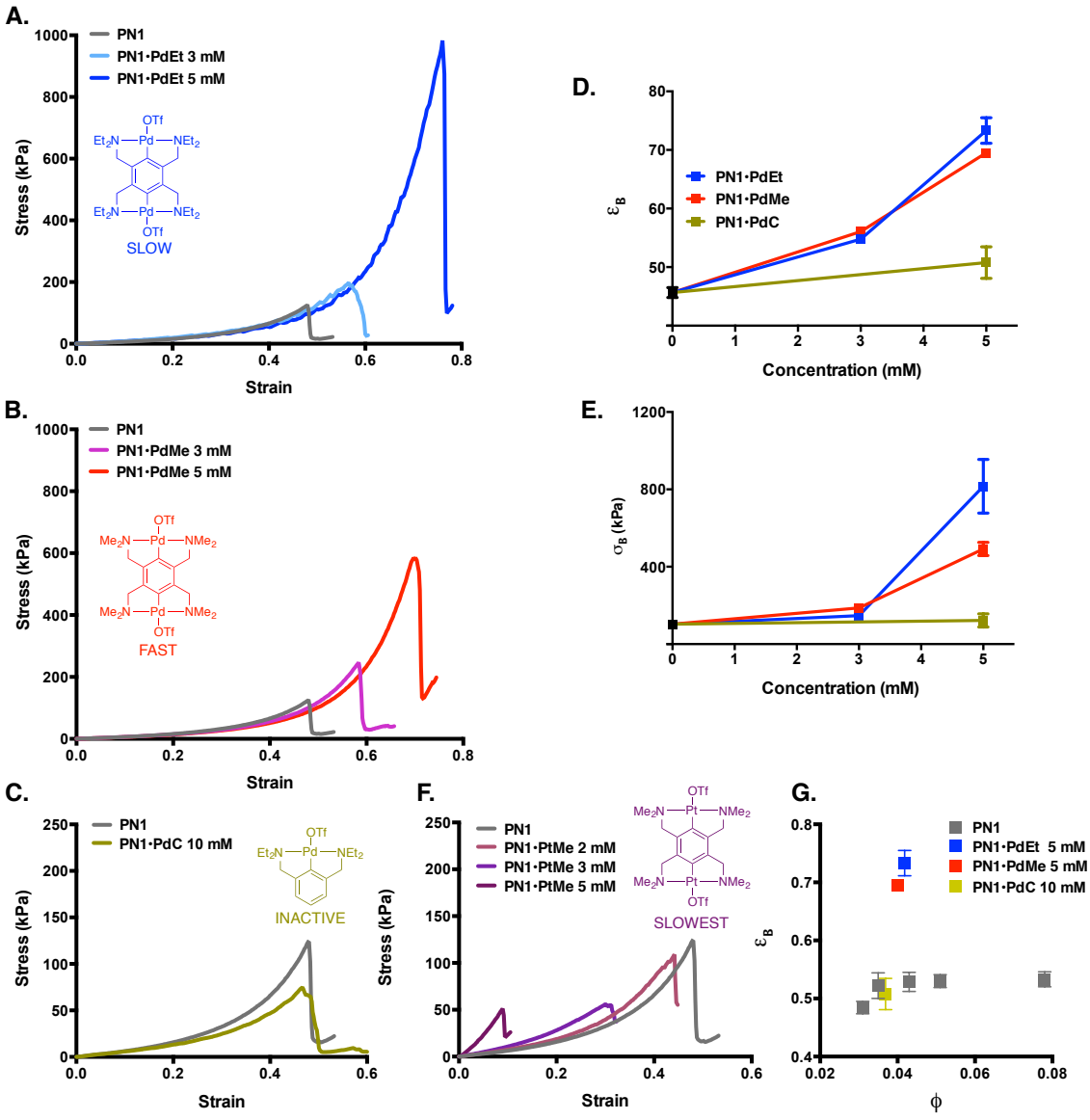

Figure 61 (a,b) Representative stress-strain behavior of **PN1** (grey), **PN1•PdEt** (blue), and **PN1•PdMe** (red) as a function of pincer concentration. (c) Monotonic increases in ε_B and σ_B of **PN1** network with increasing pincer concentration. (d) Strain at break (ε_B) vs. polymer volume fraction (ϕ) showing only minimal change in properties of PN1 due to differential swelling. Error bars denote SEM, n = 5. (e) Stress-strain behavior of **PN1•PtMe** gels bearing the slowest dissociating cross-links. In contrast to the more transient pincers, samples become increasingly brittle with increased **PtMe**

concentration. (f) Representative stress-strain curve showing the effect of added mechanically inactive control pincer **PdC**. Loading rate = 80 μm s^{-1}, T = 25 °C.

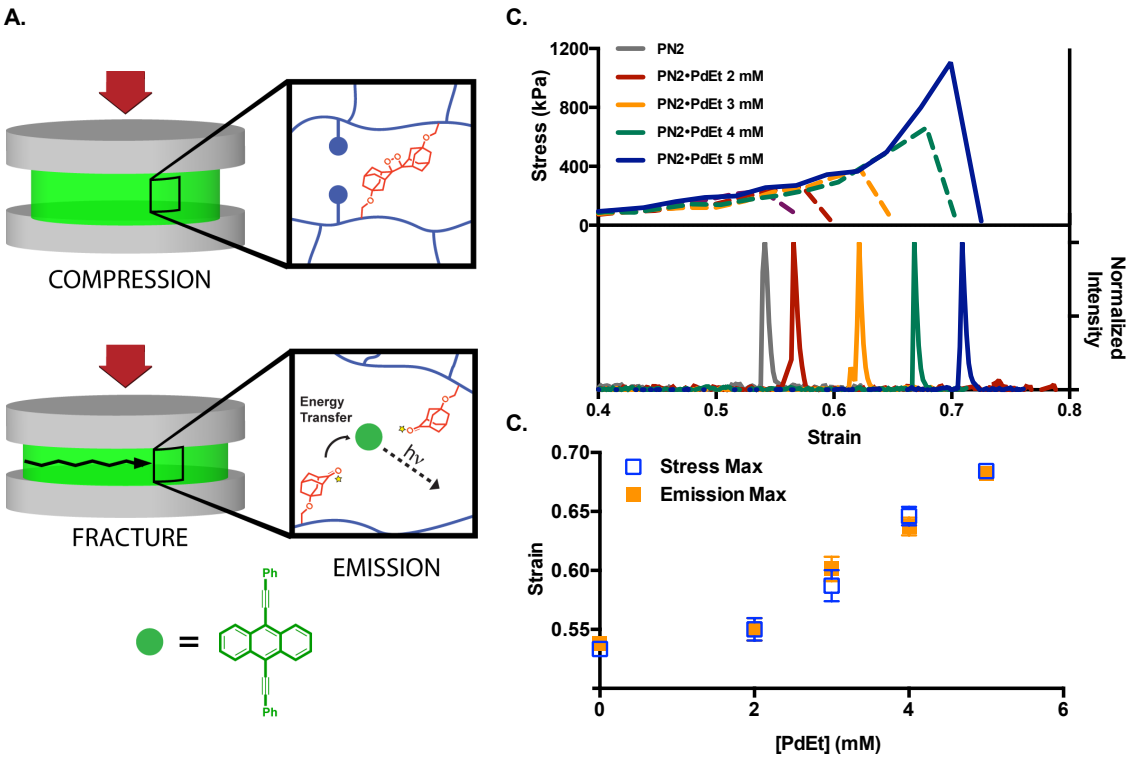

Figure 62 (a) **PN2** network structure bearing dioxetane-functional crosslinks. Samples are video recorded under loading in a compression geometry. Photons are emitted upon failure (crack propagation) of the underlying covalent network, allowing for the collection of emission-strain data simultaneously with stress-strain data. (b) Representative stress-strain and emission intensity-strain plots of **PN2•PdEt** gels as a function of [**PdEt**]. (c) Strain at Emission max and stress max vs. [**PdEt**]. Microscopic failure emission max) is observed to occur in concert with macroscopically observe failure (stress max). Error bars denote SEM, n = 10. Loading rate = 80 μm s^{-1} T = 25 °C (Experiments performed in collaboration with Jennifer Hawk).

Given that the underlying covalent framework survives high strains in the hybrid networks, we examined the elastic recovery of **PN1•Pd** under deformations (ε = 0.6) that would be catastrophic for the pure covalent network (ε_B = 0.46). In contrast to

most dissipative gels reported to date,[116,181,182] the enhanced stress/strain at break comes without significant loss upon immediate reloading, as shown in Figure 63. The dissipation in hybrid networks obviously cannot be compared to that of **PN1** at these high strains, but qualitatively we see that the area between the loading (solid color) and unloading (dashed) curves is small, especially for **PN1•PdMe**. While **PN1•PdEt** exhibits consistently higher dissipation, this loss is recoverable, with both systems showing near complete recovery of modulus upon immediate reloading (~99%). Both **PN1•PdEt** and **PN1•PdMe** were subjected to instantaneous cyclic loading cycles under compression:

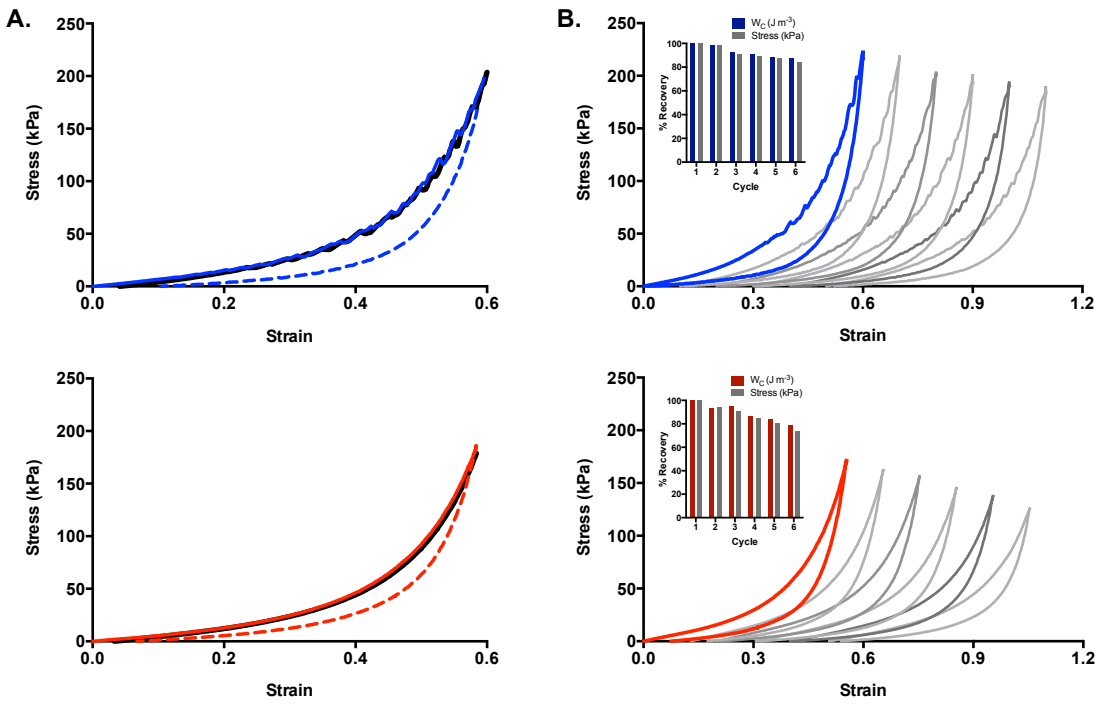

Figure 63 (a) Loading (solid, ε = 0.6), unloading (dashed), and immediate reloading (black) curves for **PN1•PdMe** [5 mM] (blue) and **PN1•PdEt** [5 mM] (red) cylinders under compression. (b) Representative cyclic loading curves (ε = 0.6) for **PN1•PdMe** [5

mM] (blue) and **PN1•PdEt** [5 mM] (red). Inset shows work of compression (W_C, J m^{-3}) and peak stress (kPa) for each cycle. Strain axis offset for clarity. Loading rate = 80 μm s^{-1}, T = 25 °C.

Comparing the stress reached and work of compression (W_C, J m^{-3}) on each loading cycle, both recovered ~93% of their W_C after three cycles. At six cycles, **PN1·PdEt** achieved 87% recovery while **PN1•PdMe** showed 79%, indicating a slightly higher level of fatigue resistance in the case of **PdEt**. Increases in ultimate strain are not unknown in systems where added non-covalent cross-links contribute considerably to the stress-bearing properties of the network.[163,183] It is remarkable though, that the addition of **PdMe,** which does not contribute to E_C, has such a profound effect on the survivability of the otherwise identical **PN1** network. This indicates that these labile non-covalent cross-links are able to prevent network failure under conditions where they bear virtually zero stress.

4.3 Conclusion

Here, we have demonstrated that mechanically "invisible" elements can have a profound effect on the stress-strain behavior of an otherwise unremarkable random network. These added dynamic cross-links have a negligible effect on nascent properties and structure, but allow for much greater stress and strain to be borne within the same covalent network that typically fractures at much lower strains. The impact is realized even with transient cross-links that neither store nor dissipate measurable macroscopic stress within the network under the conditions tested. These benefits come from a range

of supramolecular interactions that are relatively unexploited in polymers, where the focus has historically been on strong association constants and/or slow dissociation rates.[109,183-187] Here, cross-linking interactions that are both thermodynamically (association constants ~30 M^{-1}) and kinetically ($t_{1/2}$ < 1 ms) weak[178] lead to gels that are ultimately not only more deformable, but also stronger, than comparable networks formed from stronger and slower interactions (**PtMe**, 8000 M^{-1} and 27 s, respectively). We speculate that dynamic material properties on the timescale of crack propagation, rather than loading, might be critical, and we observe substantial enhancements in fracture energies that are consistent with this interpretation (**PN1** ~1.2 J m^{-2}, **PN1•PdEt** ~5.7 J m^{-2}, **PN1•PdMe** ~29.4 J m^{-2}; see experimental section). Alternatively, the dynamic supramolecular topology might serve to "smooth out" structural heterogeneity on the molecular level throughout the network, minimizing as a consequence the stress concentrations that initiate crack formation and propagation.[117,188,189] Regardless of mechanism, however, these results suggest that there might be contributions toward the effects observed when reversible interactions are added to polymer gels for the different objective of increased toughness, which is typically obtained by maximizing energy dissipation as quantified by the hysteresis observed in the loading cycles. Higher strains at break are often observed in such systems,[163,181,183] and while previously alluded to,[190,191] the results presented here provide some evidence that the effect often assumed to be tied to the extent of energy dissipation under load might, in fact, have contributions from

other mechanisms. The results motivate further study of how polymer networks can be modified in a way that decouples contributions to fracture energy from the contributions to deformation energy (modulus). To that end, the networks presented here, and related systems, might prove useful in developing and testing quantitative relationships. Such modifications have practical implications as well, because in contrast to common approaches, here high strains are achieved without paying additional energy costs to dissipation. This feature is particularly attractive for soft active devices and biomaterials where a high range of motion is required.

4.4 Experimental

4.4.1 Synthetic Methods

4.4.1.1 Representative Organogel Synthesis

P4VP (600 mg, 5.7 mmol) was weighed into a 2 dr glass vial and dissolved in 2 mL dry DMSO. Cross-linker (0.11 mmol, 17 μL of 1,6-dibromohexane for **PN1** or 62 mg of **S2** for **PN2**) was added and solution was mixed by vortexer. Bubbles were removed by briefly applying vacuum (~100 Torr) to the solution vial and the solution was poured into a 1 mm deep glass mold and sealed with a glass slide. The gels were cured by heating at 100 °C on a ceramic hotplate for 10 minutes. After cooling to room temperature, the gel was carefully removed from the mold and soaked in DMSO for 24 hours at room temperature in a desiccator in the absence of light.

4.4.1.2 Representative Preparation of Organogel Cylinders

Organogels were cut into cylinders using a 5 mm stainless steel biopsy punch. Cylinders were transferred to glass vials and allowed to soak for an additional 48 hr in a desiccator in the absence of light. An excess of DMSO (~20:1 wt/wt) was used for soaking and was replaced 4 times over the 48 hr period.

4.4.1.3 Representative Preparation of PN and PN•Pincer Cylinders

Cylinders were partitioned into 2 dram glass vials (10 cylinders/vial). Stock solutions of pincer complex in DMSO were prepared according to Table 9 by dissolving the respective bis(triflate) pincer complex in dry DMSO. "5 mM" Samples were prepared by adding 2 mL (200 μL/cylinder) of the stock solution to the vials containing organogel cylinders. Vials were then flushed with nitrogen and sealed before allowing soaking for 72 hours in the absence of light in a desiccator. Pincer-free **PN1** and **PN2** samples were treated in the exact same manner using the same crop of cylinders and substituting the pincer solutions for pure DMSO. Samples used for concentration studies were prepared by appropriately diluting the stock solutions with DMSO before adding to the cylinders. In the case of **PN2** gels pure DMSO solutions were substituted with a saturated solution of 9,10-bis(phenylethynyl)anthracene in DMSO.

Table 9 Summary of stock solutions used for the preparation of **PN•Pincer** gels.

Pincer	Molecular Weight ($g\ mol^{-1}$)	Concentration ($mg\ mL^{-1}$) in DMSO	Concentration (mM) in DMSO
PdEt	928	4.6	5
PdMe	815	4.1	5
PdC	503	5.0	10
PtMe	992	5.0	5

Synthesis of 5,5′/7′-(2-Bromoethylenoxy) adamantylideneadamantane (S1):

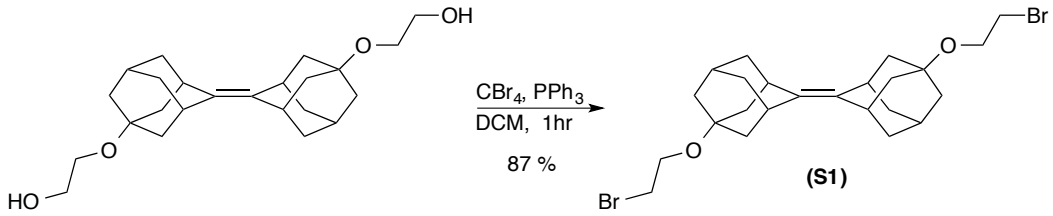

5,5′/7′-(2-Hydroxyethylenoxy) adamantylideneadamantane (400 mg, 1.03 mmol) and tetrabromomethane (856 mg, 2.57 mmol) were dissolved in DCM (5 mL) in an oven dried 25 mL round bottom flask under N_2 and placed in a water bath at room temperature. Triphenylphosphine (675 mg, 2.57 mmol) was dissolved in DCM (2 mL) and added dropwise by syringe over 30 min. After 1 hr, H_2O_2 solution (0.1 mL, 35 wt%) was added and allowed to stir for ten minutes. Anhydrous $MgSO_4$ was added until clump free, followed by 10 mL of Et_2O. The mixture was then filtered, thoroughly washing with Et_2O. The filtrate was then evaporated under reduced pressure and purified via column chromatography (4:1 Hexanes/Et_2O, SiO_2) to afford 461 mg **S1** (0.897

mmol, 87%) as a pale yellow solid (mixture of isomers). **^{1}H NMR** (400 MHz, $CDCl_3$) δ 3.70 (t, J = 6.6, 4H), 3.39 (t, J = 6.6, 4H), 3.10 (br, 4H), 2.22 (br, 2H), 1.82-1.55 (br m, 20H); **^{13}C NMR** (100 MHz, $CDCl_3$) δ 132.28, 73.12, 73.02, 61,00, 42.78, 42.69, 41.29, 41.22, 38.50, 38.41, 33.56, 31.84, 30.97; **HRMS** (ESI) *m*/*z*: [M] calcd for $C_{24}H_{34}Br_2O_2$, 514.0905; found, 514.0905.

Synthesis of 5,5′/7′-(2-Bromoethylenoxy) adamantylideneadamantane 1,2-dioxetane (2):

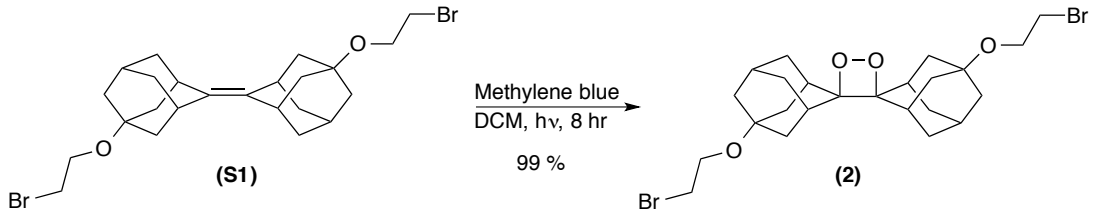

S1 (871 mg, 1.69 mmol) and methylene blue (87 mg, 0.27 mmol) were dissolved in dichloromethane (170 mL) in a 3-neck jacketed flask fitted with a reflux condenser and stir bar. Oxygen was bubbled through the solution while irradiating with a 600 W high-pressure sodium lamp (distance ~ 6 cm) for 8 hours, periodically monitoring for complete conversion by ^{1}H NMR. After completion, the solution was stirred with ~100 mg of activated charcoal and filtered through a 0.2 μm PTFE filter, repeating if necessary to remove any remaining blue color. Evaporation under reduced pressure yielded 910 mg (1.67 mmol, 99%) of **2** as a yellow oil which crystallized upon standing. The product is a mixture of three isomers as illustrated below:

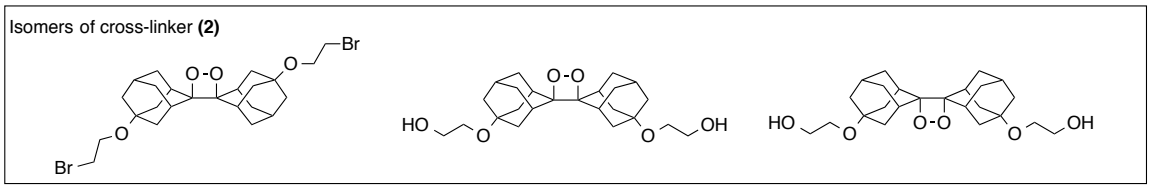

^{1}H NMR (400 MHz, $CDCl_3$) δ 3.68 (m, 4H), 3.38 (m, 4H), 2.82 (s, 4H), 2.21-1.42 (m, 22H); **^{13}C NMR** (125 MHz, $CDCl_3$) δ 94.33, 93.99, 72.17, 71.53, 71.48, 61.32, 61.14, 61.08, 41.36, 41.32, 41.10, 41.07, 40.70, 38.65, 38.54, 36.33, 36.24, 34.22, 34.17, 34.08, 34.04, 33.92, 33.80, 33.70, 33.59, 33.54, 31.71, 31.62, 29.62, 29.54, 28.92, 28.86, 28.68; **HRMS** (ESI) *m*/*z*: [M+H] calcd for $C_{24}H_{34}Br_2O_4$, 545.0897; found, 545.0907.

4.4.2 Compression Testing

General compression and extension testing was carried out on a RSA III (TA Instruments) micro-strain analyzer. Gel dimensions (thickness (t) and diameter (d)) were measured prior to testing. Compression tests were performed using a 15 mm parallel plate geometry at the specified loading rate. All experiments were performed at 25 °C. Hysteresis and cyclic loading experiments were performed in the same manner with a 1 s pause at the end of each loading cycle. Strain-at-break (ε_B) and stress-at-break (σ_B) were defined by the point in the stress-strain curve where a dramatic drop in stress occurs indicating failure of the gel. As shown in Figure 62, this method generates values consistent with the occurrence of crack propagation as determined by emission in **PN2**

networks. Stress (σ) was defined as engineering stress using instantaneous normal force and the initial cross sectional area:

$$stress = \frac{Force}{Area_{initial}}$$

Strain was defined as engineering strain based on the initial (t_o) and instantaneous thickness (t) of the sample:

$$strain = \frac{t_0 - t}{t_0}$$

Compressive modulus (E_C) was determined as the slope of the initial linear region ($r^2 > 0.96$) of the stress-strain curve, generally at strain < 0.15. Cylinder aspect ratios (d/t) were ~2.8, and all strain-at-break values were < 0.8, well within the ISO 604 parameters[27] to avoid buckling:

$$\left(\frac{d}{t}\right)^2 \times 0.4 > \varepsilon_{break}$$

Compression to failure was collected as 5 compressions per data point. Raw stress-strain curves used in Figure 61 are shown below with failure point marked by a + sign:

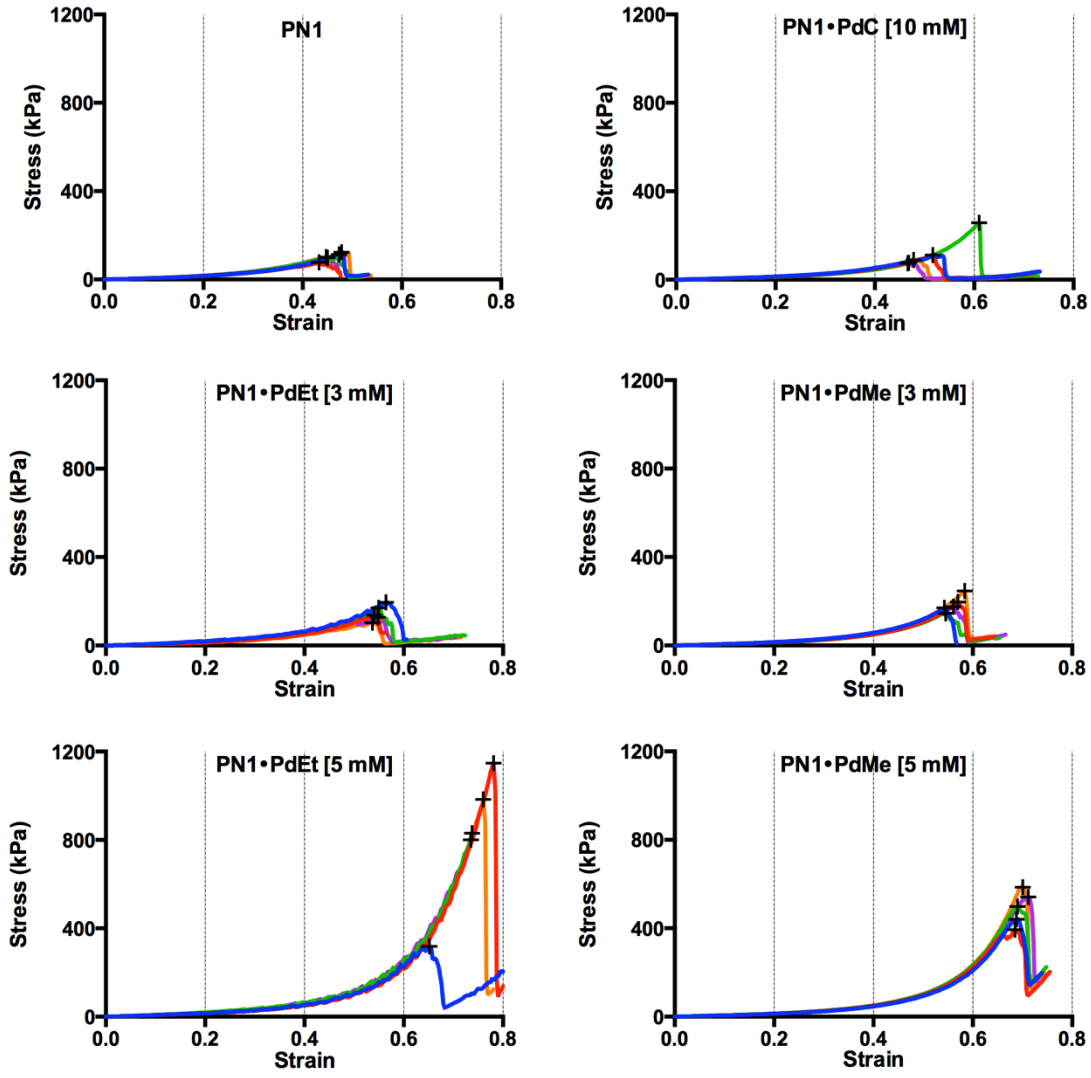

Figure 64 Stress-strain curves and failure points (black +) of **PN1**, **PN1•PdMe**, **PN1•PdEt**, and **PN1•PdC** used to generate the average values and representative curves shown in **Figure 61**.

PN1•PtMe samples were tested in the same manner with the exception that the cylinders were allowed to soak for 7 days before testing.

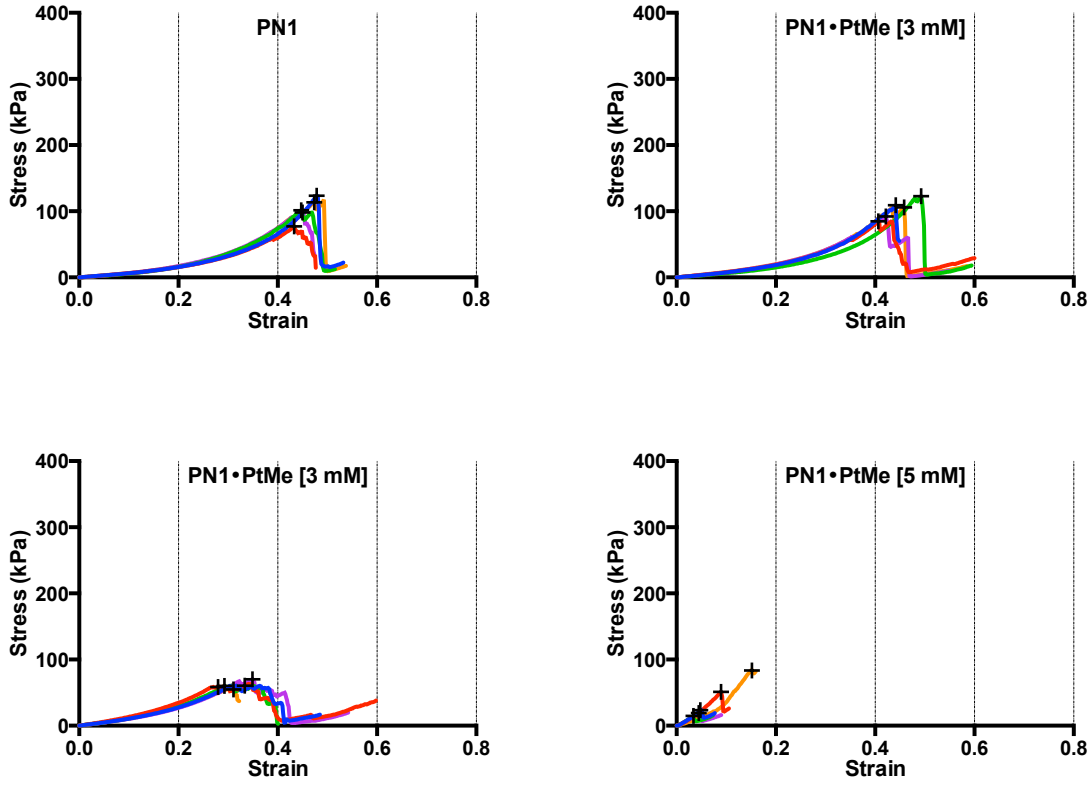

Figure 65 Stress-strain curves and failure points (black +) of **PN1•PtMe** gels used to generate the average values and representative curves shown in **Figure 61**.

4.4.3 Determination of Polymer Volume Fraction

Swollen gels were dried in a 2 dr vial at 80 °C for 2 days then under high vacuum (~ 20 mTorr) until a constant mass was reached. The mass loss do to evaporation was attributed to DMSO and was converted to volume using the density at 25 °C (ρ_{DMSO} =

1.10 g mL^{-1}). The remaining mass was attributed to polymer using the density of P4VP at 25 °C (ρ_{P4VP} = 1.11 g mL^{-1}) to convert to volume. The polymer volume fraction (ϕ) was determined according to the following equation in triplicate for both **PN1** and **PN2** gels (Table 10):

$$\phi = \frac{V_{Polymer}}{V_{Polymer} + V_{Polymer}}$$

Table 10 Summary of drying data used for the determination of polymer volume fraction in **PN1** and **PN2** gels.

PN1 Sample	**$Mass_{swollen}$** mg	**$Mass_{polymer}$** mg	**$Mass_{DMSO}$** mg	**$V_{Polymer}$** mL	**V_{DMSO}** mL	**V_{total}** mL	**ϕ**
1	541	17	524	0.015	0.476	0.491	0.032
2	616	20	596	0.018	0.542	0.560	0.032
3	609	17	592	0.016	0.538	0.553	0.029
						Avg.	**0.031**
						St.Dev.	0.002
PN2 Sample	**$Mass_{swollen}$ mg**	**$Mass_{polymer}$ mg**	**$Mass_{DMSO}$ mg**	**$V_{Polymer}$ mL**	**V_{DMSO} mL**	**V_{total} mL**	ϕ
1	**293**	**16**	**277**	**0.014**	**0.252**	**0.266**	**0.056**
2	337	18	320	0.016	0.290	0.306	0.055
3	296	16	281	0.014	0.255	0.269	0.055
						Avg.	**0.055**
						St.Dev.	0.001

4.4.4 The Effect of Swelling on Ultimate Properties

PN1 gels were synthesized as usual and swollen to equilibrium. Cylinders were then partitioned and soaked in a mixture of DMSO and triethyleneglycol dimethylether (TEG) at the ratios given below (200 μL per cylinder). After 3 days, the cylinders were subjected to compression testing and analyzed as usual. Volume fractions ϕ were determined by scaling ϕ of the nascent gel (**PN1** ~ 0.031) by the change in measured volume (area x height) upon de-swelling:

$$\phi_{deswollen} = \phi_{PN1}\left(\frac{V_{deswollen}}{V_{PN1}}\right)$$

Raw data (below) is summarized in Table 11, showing minimal effect that deswelling has on the stress-strain behavior compared to that of the introduction of pincer complexes.

Table 11 Summary of compression results (**Figure 66**) for samples deswollen by the addition of TEG as described above.

Sample	Fraction DMSO	Fraction TEG	Avg. ε_{break}	Avg. σ_{break}	Avg. E_C	Avg. ϕ
	v/v	v/v	ε	kPa	kPa	v/v
1	1	0	0.484	116	60.3	0.0309
2	0.8	0.2	0.522	144	61.8	0.0353
3	0.7	0.3	0.529	139	60.4	0.0426
4	0.6	0.4	0.530	130	68.0	0.0542
5	0.5	0.5	0.533	142	72.9	0.0777

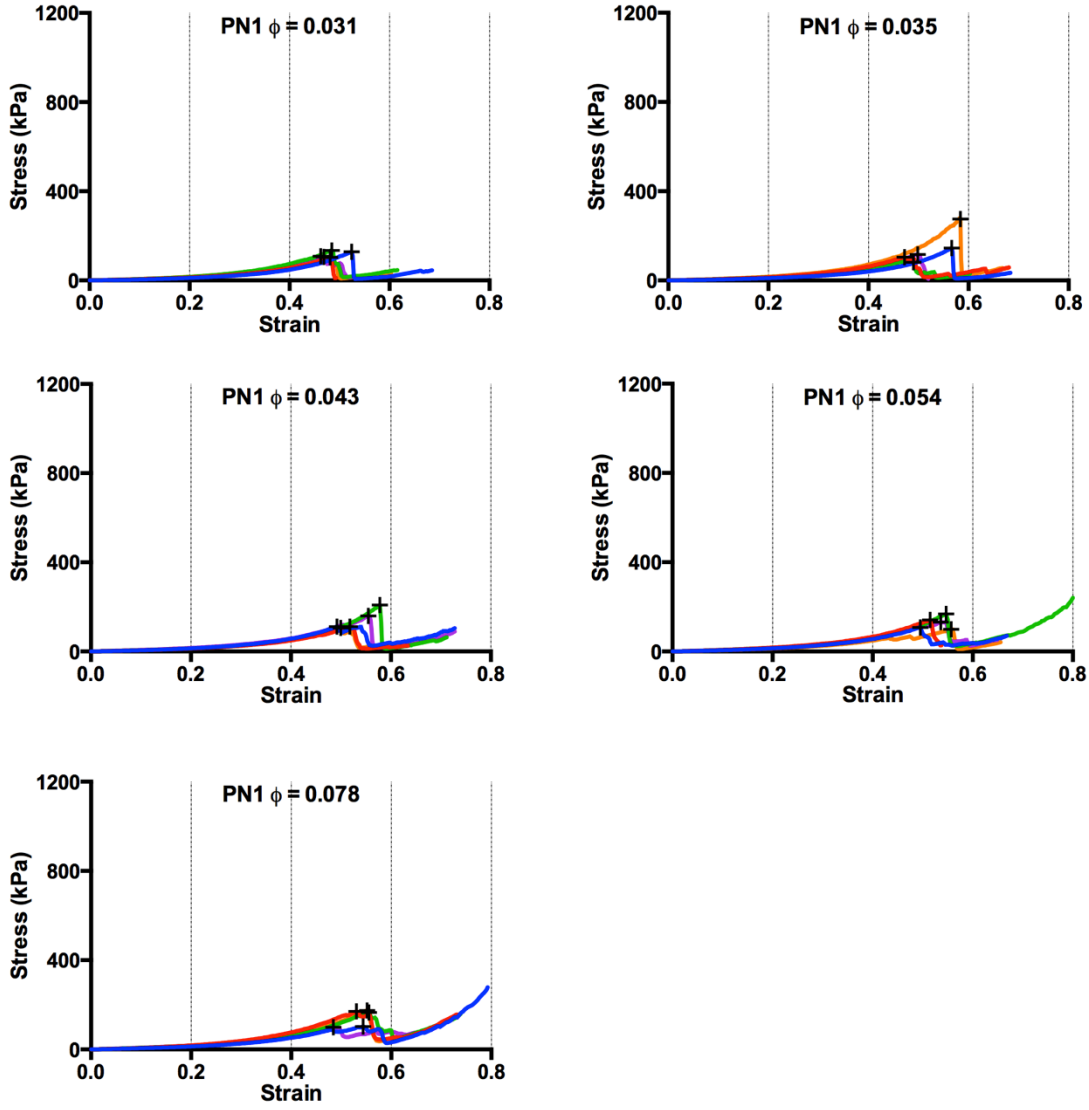

Figure 66 Stress-strain curves and failure points (black +) of **PN1** gels at various polymer volume fractions (ϕ) used to generate the average values and representative curves shown in **Figure 61**.

4.4.5 Compression-Emission Experiments

Compression-emission testing of **PN2** samples was performed using an AR G2 rheometer (TA Instruments) with a concentric cylinder geometry (8 mm diameter) at 25 ^{o}C in Squeeze/Pull-off mode. Images were recorded using a pco.edge 4.2 CMOS camera (PCO AG, Kelheim, Germany) with a 50mm f/1.4D AF Nikkor lens at f =1.4 and a 33 ms shutter speed with the BW dynamic range set at 80 min and 170 max. Sample was placed in the geometry then the camera was mounted with a custom built barrel and enclosure to exclude ambient light. A custom trigger circuit allowed for synchronization between the acquired video and stress-strain data acquired by the AR G2. Camera time (1 frame = 33 ms) was converted to strain by multiplying by (loading rate/sample height) (units = strain/s). Images were processed using Fiji software.[192] Each image was cropped to a size of 160 x 20 pixels then average intensity was measured and plotted vs. strain while setting the baseline to zero using Origin software (Originlab, Northampton, MA).

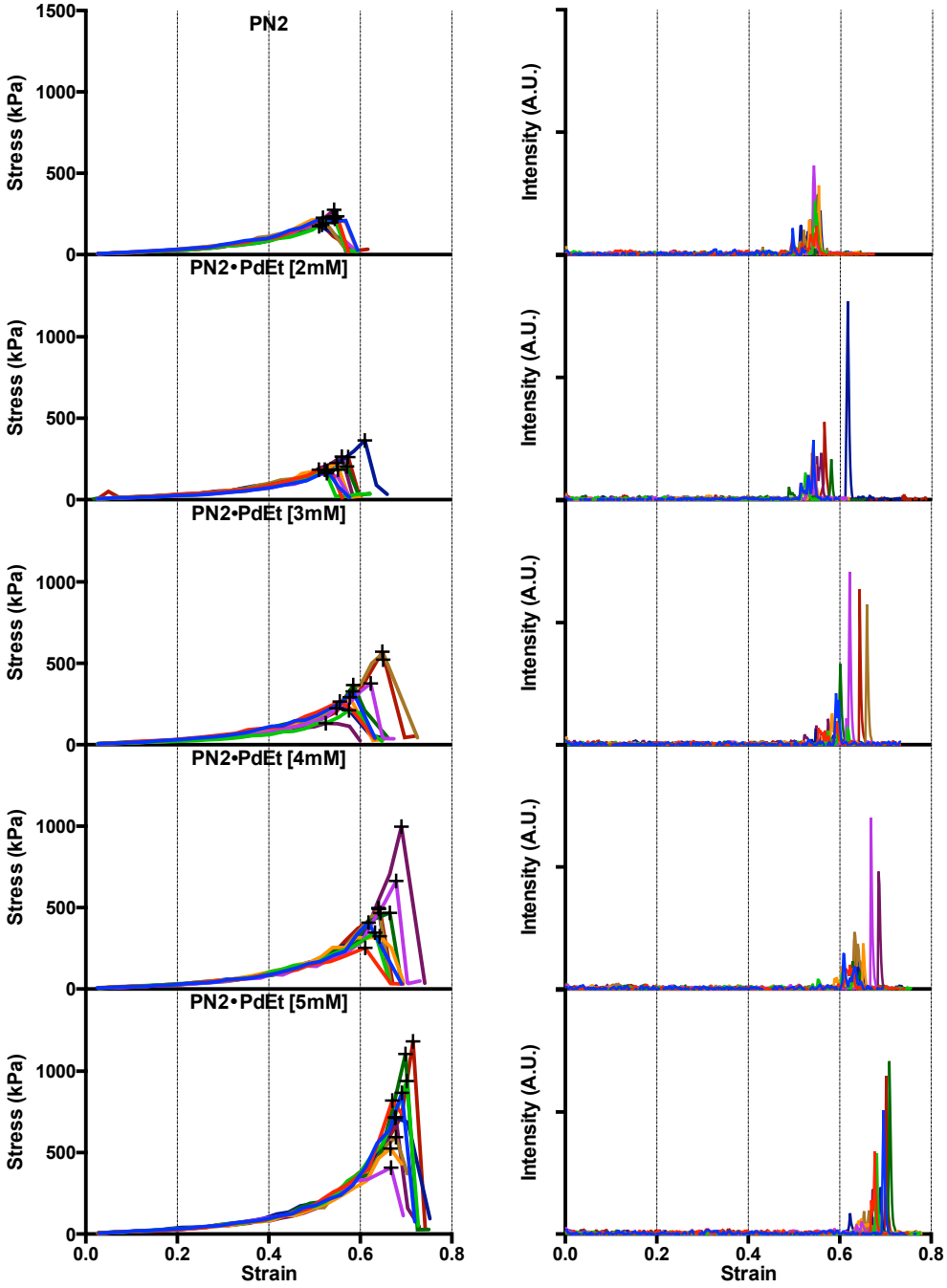

Figure 67 Stress-strain curves and failure points (black +) of **PN2** and **PN2•PdEt** gels used to generate the average values and representative curves shown in **Figure 67** of the main text. Figures on the right show the overlay of all emission curves generated for the corresponding compression experiment.

Overall trends in emission/stress-strain data are consistent with dioxetane emission occurring only during brittle fracture of the **PN2** gels. Integral emission and maximum emission say constant regardless of [**Pincer**], therefore independent of stress, strain, and time at which the emission occurs. Additionally, the duration of emission, related to the timescale of crack propagation, is insensitive to the loading rate.

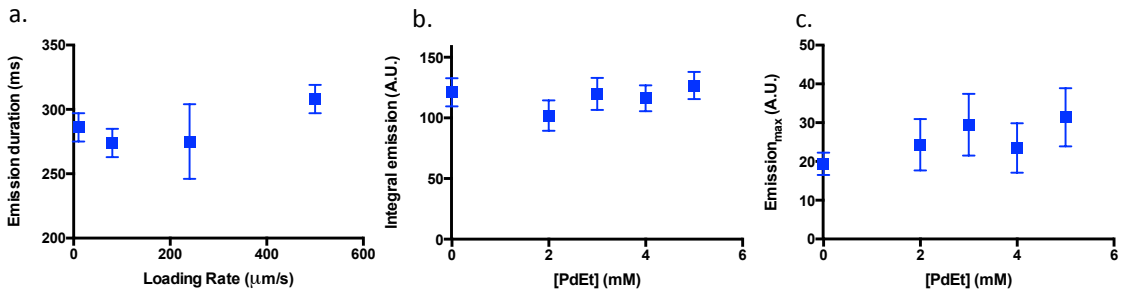

Figure 68 (a) **PN2** samples were subjected to compression testing at various loading rates (x-axis) while recording dioxetane emission as described above. Emission duration was determined from the number of frames over which emission occurred (1 frame = 33 ms), n = 3. (b) Integral emission vs. **PdEt** concentration as determined as described above, n = 10. (c) Peak emission vs. **PdEt** concentration as determined as described above, n = 10. Error bars denote SEM.

4.4.6 Determination of Fracture Energy*

Fracture energy is measured from pure-shear test as follows: (Figure 69a) a piece of a hydrogel with a notch with stretched to a critical stretch of λ_C until the crack propagates; (Figure 69b) the same piece of sample but without notch was stretched to λ_C with the nominal stress σ recorded:

* Experiments performed in collaboration with Shaoting Lin, Xhao Group, Duke University.

$$\sigma = \frac{F}{WT}$$

Where T is the thickness of the sample. The fracture toughness (Γ) of the hydrogel can be calculated as:

$$\Gamma = AH \int_1^{\lambda_c} \sigma d\lambda$$

Fracture energy of **PN1•PdMe** (~29.4 J m^{-2}) out performed both **PN1** (~1.2 J m^{-2}) and **PN1•PdEt** (~5.7 J m^{-2}) by roughly a factor of 25 and 5 respectively, which indicates that the introduction of the "weaker" **PdMe** cross-linkers can enhance a greater degree of fracture energy compared with **PdEt** cross-linkers.

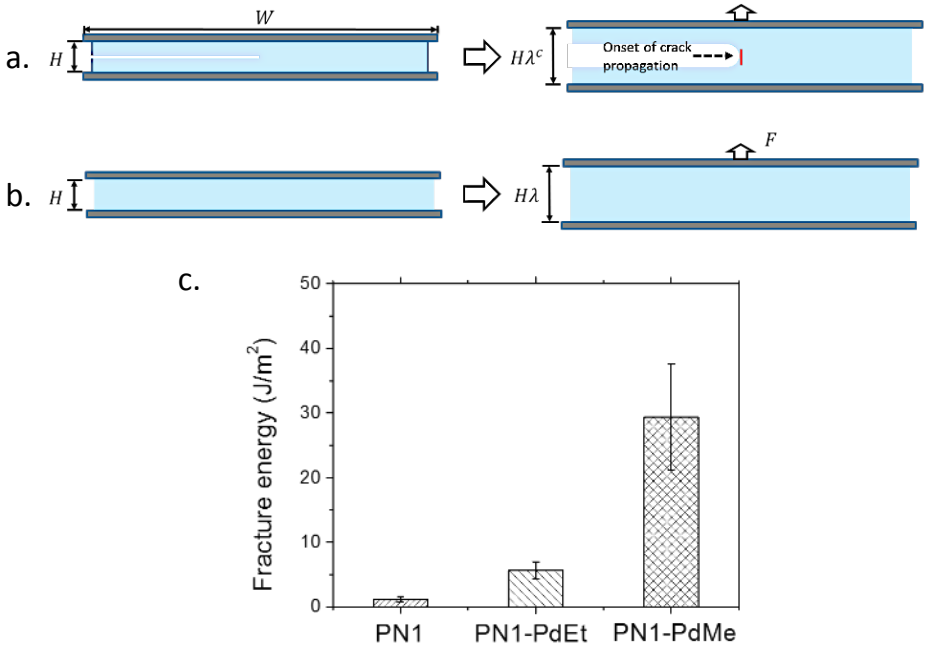

Figure 69 Summary (c) of (a) notch and (b) extension tests used to determine the fracture energy of **PN1**, **PN1•PdEt** [5 mM], and **PN1•PdMe** [5 mM] gels. Figure provided by Shaoting Lin and Xuanhe Zhao.

4.4.7 Oscillatory Shear Measurements

Rheological testing of **PN2** samples was performed using an AR G2 rheometer (TA Instruments) with a concentric cylinder geometry (8 mm diameter) at 25 °C. The fixed strain (1%) was determined to be within the linear viscoelastic region by strain-sweep analysis. Samples were loaded into geometry and compressed to 0.1 nN and the remainder of the gap was filled with DMSO to prevent evaporation. Data is consistent with rate-dependent dissipation due to the incorporation of **PdEt** and **PdMe** cross-links as evidenced by the increases in loss modulus (G“) at moderate (**PdEt**) and high (**PdMe**) frequencies. Consistent with compression data, only small variations in G’ are observed. Overall dissipation is small, with G“ only a few percent of G’ at intermediate frequencies:

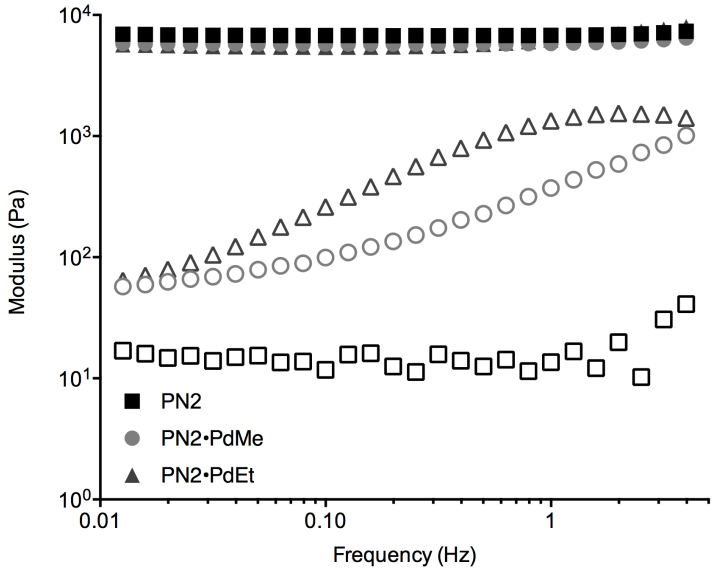

Figure 70 Oscillatory shear frequency sweep of **PN2** cylinders at 1% strain and 25 °C. G' (storage modulus) is shown as solid shapes and G'' (loss modulus) as hollow shape.

5. Photomechanical Actuation of Ligand Geometry in Enantioselective Catalysis*

5.1 Introduction

"Switchable" catalytic systems have generated considerable interest because of their potential to trigger and/or optimize activity *in situ* with spatiotemporal control. This external modulation of chemical processes may benefit fields ranging from nanofabrication to biologically relevant therapeutics and diagnostics.[193-195] Ultimately, such systems might enable otherwise inaccessible reactivity by switching between multiple active forms on the timescale of catalytic turnover[194] or polymer enchainment.[196,197] A potentially useful, but heretofore untapped, trigger is the application of a mechanical force. Whereas mechanical force has been used to activate latent catalysts,[37,38,65] it should also be capable of modulating an active catalyst, for example by distorting ligand geometry. As a first step toward that end, we sought a catalyst whose activity could be modulated[198,199] (rather than turned on/off or reversed) externally, but through purely mechanical/geometric effects as opposed to electronic changes. Our design employs a stiff stilbene (1,1′-biindane) photoswitch that offers good quantum efficiency, large geometry changes, molecular rigidity, and thermal stability.[200]

---

*This chapter adapted from: Kean et al. (2014) *Angew. Chem., Int. Ed., DOI: 10.1002/anie.201407494.* Portions of this chapter were performed in collaboration with co-workers as noted where relevant.

Stiff stilbenes have been used in light-driven molecular machines,[201] including Feringa's rotor-based catalyst for photoswitchable asymmetric thiol-Michael additions.[202] Additionally, the *Z* to *E* isomerization of stiff stilbene has been used to generate highly strained macrocycles that function as molecular force probes for quantitative studies of mechanochemical reactivity.[45,203-206] Given this foundation, we set out to construct a ligand that was switchable between two states that would have differential reactivity,[207-209] as has been well characterized in the C_n-TunePhos ligands[210-212]: a "compressed" state with a biaryl dihedral angle (ϕ, Scheme 7) that is more acute than that of the acyclic analogue (MeOBiphep, ϕ = 97°), and an "extended" state with a more obtuse dihedral angle.

5.2 Results and Discussion

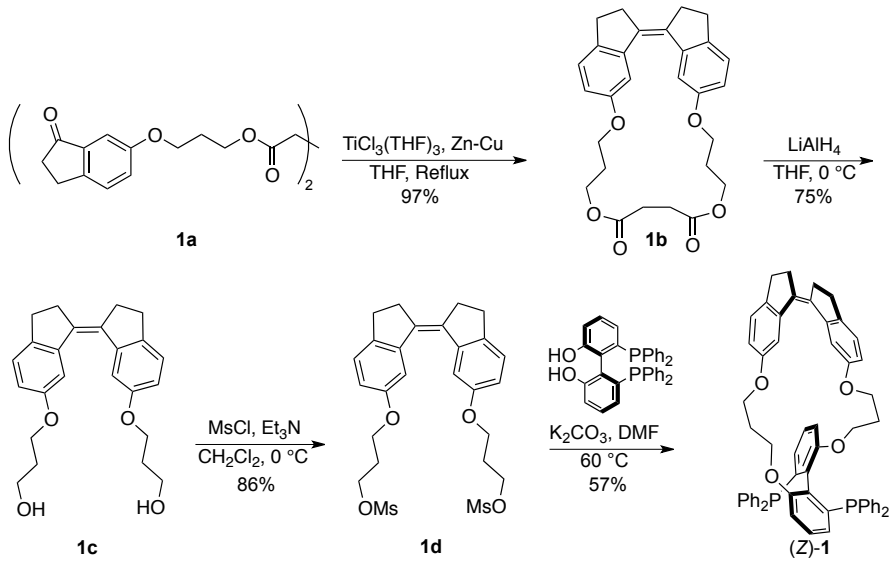

Scheme 6 Synthesis of photoswitchable chiral bisphosphine (*Z*)-**1**.

Synthesis of macrocyclic ligand (*Z*)-**1** (Scheme 6) followed modifications of previously described procedures (see the experimental section).[204,211,213] DFT calculations predict that (*Z*)-**1** is "compressed" (ϕ = 83°), (*E*)-**2** is extended (ϕ = 106°), and (*E*)-**2'** is virtually undistorted in terms of biaryl geometry (ϕ = 98°) relative to untethered MeOBiphep. The natural dihedral angle (as well as the related natural bite angle) of bis(phosphine) ligands is a geometric parameter commonly referenced in regard to catalyst selectivity.[211,212,214-216] When irradiated at 365 nm in dichloromethane, bisphosphine (*Z*)-**1** yielded a photostationary 68:23:9 (^{1}H NMR; see experimental section) mixture of (*Z*)-**1**:(*E*)-**2**:(*E*)-**2'** within minutes (Scheme 7). Each isomer was isolated from the mixture using conventional flash or medium pressure liquid chromatography, allowing for further study of pure (*Z*)-**1** and (*E*)-**2**. When embedded in a macrocycle, *E* stiff stilbenes assume axial chirality, such that both (*E*)-**2** and (*E*)-**2'** are diastereomers of atropisomers. X-ray crystallography of the derivative phosphine selenides of (*E*)-**2** and (*Z*)-**1** confirmed the stereochemistry of all three isomers and the expected greater dihedral angle in (*E*)-**2** relative to (*Z*)-**1** (see experimental section). The isolated ligands (entries 1-3) were employed in the asymmetric Heck reaction between 2,3-dihydrofuran (DHF) and either phenyl[217,218] (Table 12) or 1-naphthyl[219] (Table 13) triflate to form 2-aryl dihydrofurans. In the case of arylation with phenyl triflate, (*E*)-**2** yields **3a** in 79% *ee* (*er* = 89:11) (GC) and high conversion (GC, 95%), whereas the distortion in ligand dihedral angle (ϕ) in (*Z*)-**1** yields **3a** in 96% *ee* (*er* = 98:2) and 55% conversion. Here, the "stretched"

ligand (*E*)-**2** results in a decreased enantioselectivity relative to the acyclic MeOBiphep (90% *ee*), while the "compressed" ligand (*Z*)-**1** exhibits higher selectivity. In contrast to prior photoswitchable catalysts,[198,199] ligands (*Z*)-**1** and (*E*)-**2** differ in their shape but not their electronics (σ-donating ability) at the phosphorus atoms, as indicated by the identical ^{31}P-^{77}Se coupling constants ($^{1}J_{P,Se}$, both 739 Hz) of the corresponding phosphine selenides[220-223] and supported by a comparison with the C_n-TunePhos ligands (see experimental section)[212,224]. This evidence suggests that geometric/steric effects predominate, and that the contribution of the stiff stilbene moiety can be considered from a purely mechanical point of view.

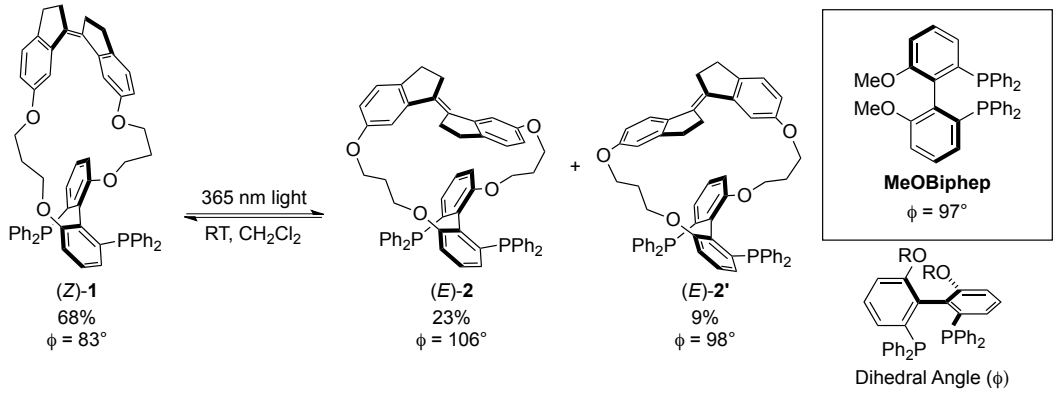

Scheme 7 Irradiation of (*Z*)-**1** at 365 nm generates a photostationary mixture (given as %) of (*Z*)-**1**, (*E*)-**2**, (*E*)-**2'**. (*E*)-**2** and (*E*)-**2'** are isolable diastereomers due to the combination of atropisomerism in the tethered stiff stilbene and fixed chirality of the bis(phosphine). (*Z*)-1 also exists as a pair of diastereomers (effectively diastereomeric conformers) that are unresolvable because of the low barrier for isomerization across the alkene (~6 kcal mol^{-1} in untethered *Z*-stiff stilbene[45]). Distortion of ligand geometry is evaluated using the calculated (DFT) "natural" dihedral angle (ϕ) defined by the biaryl carbons at the positions shown in bold (bottom right). All ligands used in this study are axially chiral about the biaryl backbone in the (*S*)-configuration.

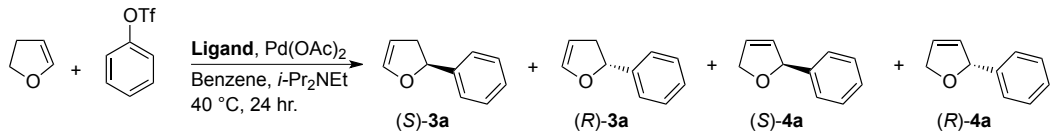

Table 12 Summary of ligand screen in the asymmetric Heck reaction of phenyl triflate and 2,3-dihydrofuran.[a]

Entry	Ligand	Conv. [%][b]	3a:4a[c]	Total (*S*) Products [%]	(*S*)-3a *ee* [%][d]
1	MeOBiphep	23	95:5	91	90
2	(*Z*)-**1**	55	97:3	96	96
3	(*E*)-**2**	95	98:2	88	79
4[e]	(*E*)-**2** + 365 nm	93	97:3	93	90

[a] Reaction carried out using phenyl triflate (1 equiv., 0.6 M), Ligand (0.06 equiv.), $Pd(OAc)_2$ (0.03 equiv.), 2,3-DHF (5.6 equiv.), *i*-Pr_2NEt (3.4 equiv.) in Benzene at 40 °C for 24 hr. All values are averages of duplicate runs. [b],[c] Determined by GC. [d] Determined by GC on chiral stationary phase (Supelco β-Dex). Absolute configuration determined by comparison with sign of optical rotation as previously reported.[217 225]

For arylation with 1-naphthyl triflate, qualitatively similar effects are observed (Table 13), with (*Z*)-**1** yielding **3b** in 60% *ee* (HPLC), vs. only 13% *ee* from (*E*)-**2**. Both reactions proceed to high conversion (*ee* is independent of conversion, see experimental section), although, in contrast to the reaction with phenyl triflate, ligand distortion now has a substantial impact on regioselectivity (for (*E*)-**2**, **3b:4b** = 88:12; for (*Z*)-**1, 3b:4b** = 72:28). The selectivity of Heck arylations has been attributed to two sequential processes[217,218]: the initial irreversible insertion of DHF at C(2) into the Pd–aryl bond (which determines the total *S*/*R* ratio at C(2) in all regioisomers), and then the isomerization and regiodetermining displacement of the metal to generate either the 2,3

or 2,5-DHF product. Here, as the natural dihedral angle of the ligand increases, selectivity of the initial enantiodiscriminating step decreases, as reflected in an overall decrease in the percentage of (*S*)-**3b** + (*S*)-**4b** obtained. Further, the wider dihedral angle slows ligand displacement to form (*S*)-**3b** and/or accelerates the insertion/*β*-hydride elimination processes that lead to isomerization and formation of the 2,3-dihydrofuran isomers **3**, as evidenced by the greater total content of **3** (both enantiomers) relative to **4** with increasing ligand dihedral angle.

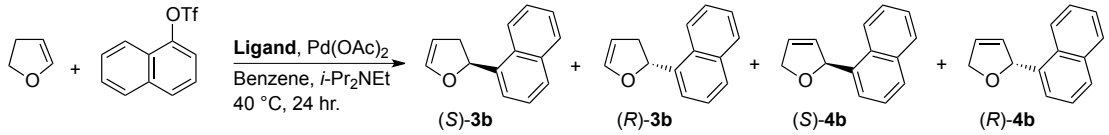

Table 13 Summary of ligand screen in the asymmetric Heck reaction of 1-naphthyl triflate and 2,3-dihydrofuran.[a]

Entry	Ligand	Conv. [%][b]	3b:4b[c]	Total (*S*) Products [%][d]	(*S*)-3b *ee* [%][d]
1	MeOBiphep	98	79:21	64	54
2	(*Z*)-**1**	91	72:28	63	60
3	(*E*)-**2**	>99	88:12	52	13
4	(*E*)-**2** + 365 nm	>99	85:15	69	42

[a] Reaction carried out using 1-naphthyl triflate (1 equiv., 0.6 M), Ligand (0.06 equiv.), $Pd(OAc)_2$ (0.03 equiv.), 2,3-DHF (5.6 equiv.), *i*-Pr_2NEt (3.4 equiv.) in Benzene at 40 °C for 24 hr. [b],[c] Determined by GC [d] Determined by HPLC on chiral stationary phase (Daicel CHIRALPAK AD-H) and GC on normal stationary phase (see the experimental section). Absolute configuration determined by comparison with sign of optical rotation as previously reported.[219]

In contrast to the Heck arylations examined, Trost allylic alkylations using standard substrates (Table 4) showed more modest changes in selectivity between

ligands *Z*-(**1**) and *E*-(**2**), demonstrating a lower sensitivity to the geometric changes we are able to achieve via photomechanical actuation.

Table 14 Summary of ligand screen in Trost asymmetric allylic alkylations.[a]

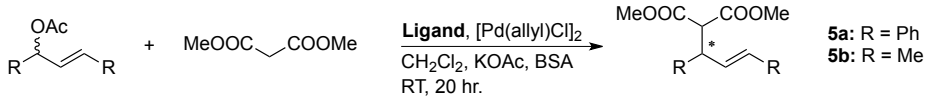

Entry	Ligand	Yield [%][b]	Product	*ee* [%]
1	MeOBiphep	98	(*R*)-**5a**[c]	93[d]
2	(*Z*)-**1**	95	(*R*)-**5a**[c]	93[d]
3	(*E*)-**2**	96	(*R*)-**5a**[c]	91[d]
4	**MeOBiphep**	96	**5b**	37[e]
5	(*Z*)-**1**	92	**5b**	45[e]
6	(*E*)-**2**	96	**5b**	40[e]

[a] Reaction carried out using allyl acetate substrate (1 equiv., 0.2 M), Ligand (0.05 equiv.), $[Pd(allyl)Cl]_2$ (0.025 equiv.), dimethyl malonate (3 equiv.), BSA (3 equiv.), and KOAc (cat.) in CH_2Cl_2 at RT for 20 hr. [b] Isolated yield after column chromatography. [c] Absolute configuration determined by comparison with sign of optical rotation as previously reported.[226] [d] Determined by HPLC on chiral stationary phase (Daicel CHIRALPAK AD-H). [e] Determined by ^1H NMR with $Eu(hfc)_3$ chiral shift reagent. Absolute configuration not determined.

Importantly, the changes in reactivity are a consequence of an applied mechanical distortion, and the relevant forces can be quantified. Following previously described methodology,[139,203] calculations at the B3LYP/6-311+G(d) level of DFT on complete conformational ensembles of MeOBiphep with constraining potential imposed across the C atoms of the Me groups yielded a calibration curve that relates the O···O

bond distance to the force applied to adjacent carbon atoms (indicated by arrows in Figure 2) for (*Z*)-**1**, (*E*)-**2**, and (*E*)-**2'**.

The O···O distance was chosen because it best represents the pulling coordinate through which the dihedral angle is compressed or widened by stiff stilbene. This approach has been validated previously[203] against single molecule force spectroscopy data[88] in the context of *gem*-dibromocyclopropane ring opening. As summarized in Table 3, the compression of the dihedral angle in (*Z*)-**1** to 83° requires the equivalent of 130 pN of compressive force applied to MeOBiphep, whereas the extension of the dihedral angle of (*E*)-**2** to 106° would be observed if a tensile load of 140 pN were applied in the opposite direction. The highest energy isomer, (*E*)-**2'**, shows negligible distortion along the O···O coordinate, a minimal compressive force (14 pN), and only 1° distortion about the dihedral angle relative to MeOBiphep; illustrating that even in such fairly small molecule, local restoring force is a better predictor of reactivity than strain energy.[45,200,204] The magnitude of these forces provides a first benchmark for the design and implementation of catalysts and catalyst platforms that are mechanically tunable and/or switchable *in situ*:

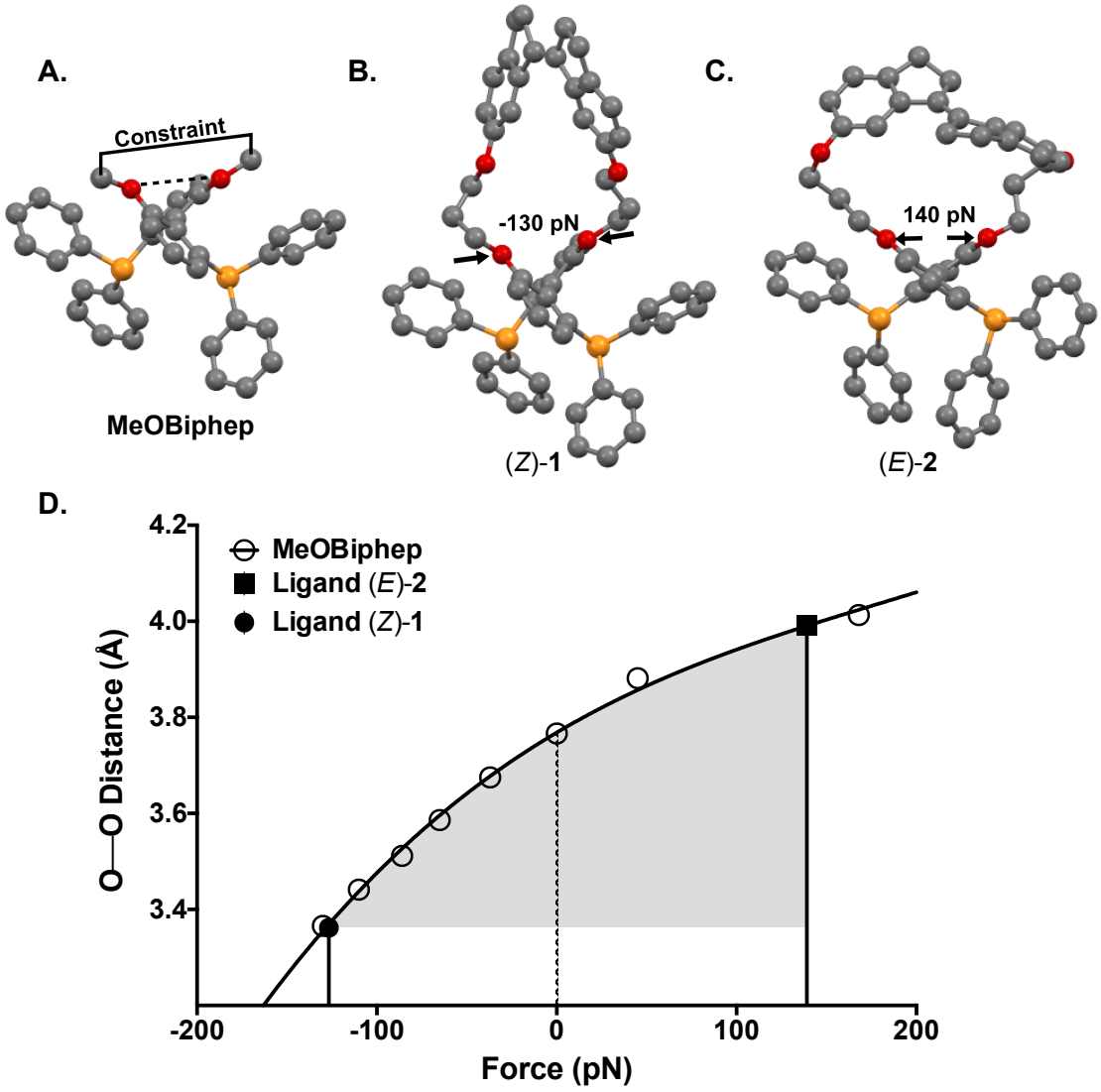

Figure 71 (a) Constraint applied to terminal methyls on **MeOBiphep** generates a calibration curve (solid curve in d) of O···O distance (dashed line) vs. force. (b) and (c) Calibration yields a compressive force of -130 pN and an extensional force of 140 pN for (*Z*)-**1** and (*E*)-**2** respectively. (d) Calculated O···O distance of (*Z*)-**1** and (*E*)-**2** plotted on MeOBiphep calibration curve yields force values. Shaded area illustrates the work done along the O···O between (*Z*)-**1** and (*E*)-**2**. The data in this figure was provided by Dr. Yancong Tan and Dr. Roman Boulatov, Boulatov Group, University of Liverpool.

Table 15 Summary of geometric and force parameters of ligands used in this study. Negative sign corresponds to compressive force.

Ligand	Photostationary Content [%]	Dihedral Angle (ϕ)	O···O Distance [Å]	Force [pN]
MeOBiphep	-	97	3.77	0
(*Z*)-**1**	68	83	3.36	-130
(*E*)-**2**	23	106	3.99	140
(*E*)-**2'**	9	98	3.74	-14

Interestingly, although secondary to our purposes, photoswitching also occurs in the presence of $Pd(OAc)_2$ in benzene (Figure 72c). Irradiating (*E*)-**2** (365 nm, 3W, 60 s) presumably gives a photostationary mixture of isomers, and the ensuing Heck reactions proceed with a selectivity that is intermediate to that of (*E*)-**2** and (*Z*)-**1** (Figure 72a,b).

5.3 Conclusion

Looking ahead, we note that the forces required to effect significant perturbation of the dihedral angle of ligands (*Z*)-**1** and (*E*)-**2** ($\Delta\phi = 23°$) are small relative to those necessary to trigger covalent chemistry in many mechanophores whose activity has been previously characterized.[87] In particular, similar forces (< 500 pN) are believed to be operative in the mechanically driven ring opening reaction of spiropyran to merocyanine on the time scale of seconds,[120] and so the forces demonstrated here are directly relevant to those experienced by molecules in a range of material platforms.[31-34] In such materials, the MeOBiphep based catalysts, and other modulated

mechanocatalysts, might therefore provide an amplified chemical response to localized stress and/or access to new reversibly tunable reactions. Materials and soft devices in which the necessary forces can be generated reversibly and repeatedly[119,227] are especially attractive in this regard, because of the potential to toggle between multiple active forms of the same catalyst.

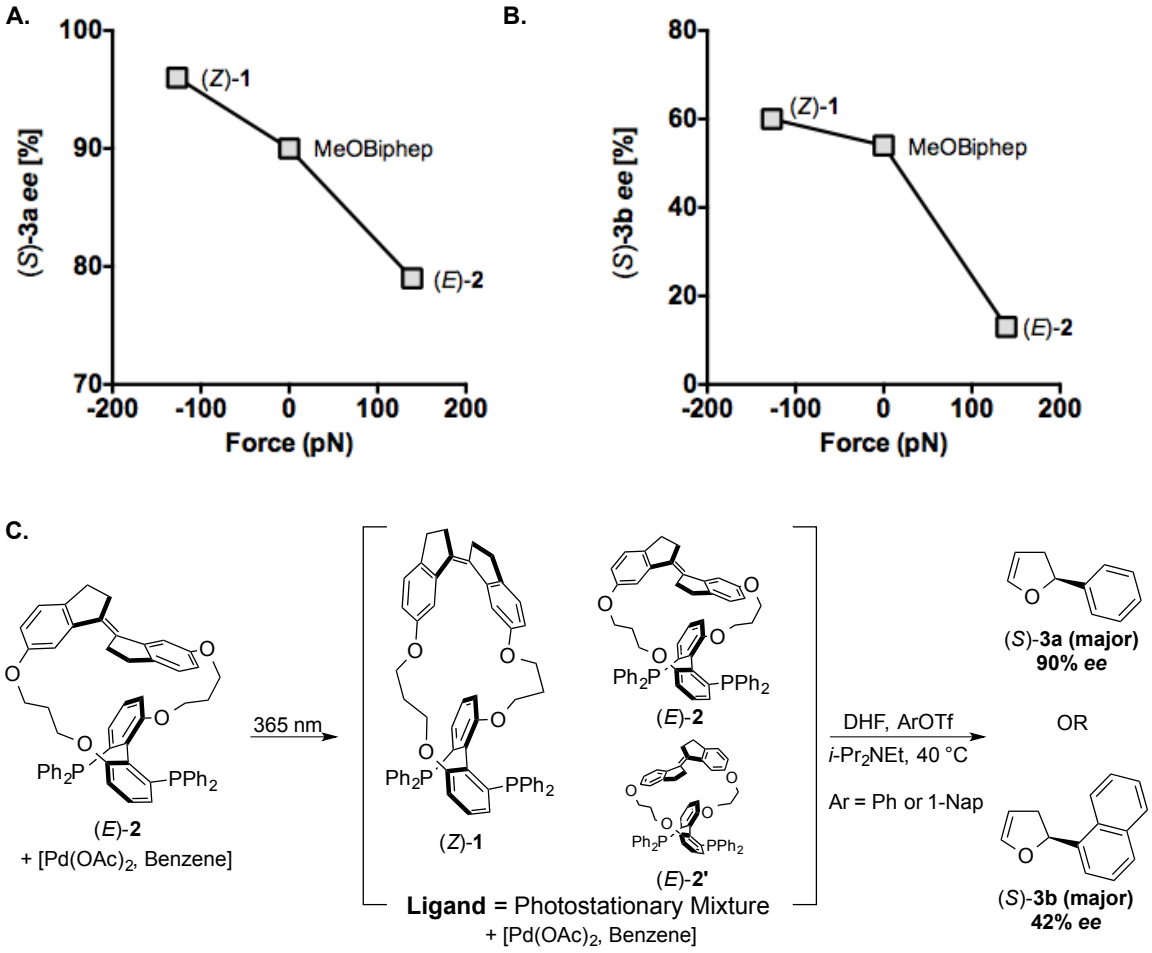

Figure 72 The *ee* of (*S*)-**3a** (a) and (*S*)-**3b** (b) as a function of force for ligands used in this study. (c) Irradiation of catalyst solution [(*E*)-**2**, Pd(OAc)2, in benzene] *in situ* at 365 nm yields a presumed photostationary mixture of ligands, changing the selectivity in asymmetric Heck arylations.

5.4 Experimental

5.4.1 Materials and Methods

All reactions were performed under argon atmosphere using standard Schlenk techniques unless otherwise noted. 6-Hydroxy-1-indanone (>98%) was purchased from TCI America, $TiCl_3(THF)_3$ was synthesized as previously described,[228] all other reagents were purchased from Sigma-Aldrich and used without further purification. Tetrahydrofuran and dichloromethane were purified using an Innovative Technology solvent purification system. DMF was stored over molecular sieves and degassed prior to use. $CDCl_3$ and CD_2Cl_2 were purchased from Cambridge Isotope Laboratories. All other reagents were purchased from Sigma-Aldrich and used as received unless otherwise noted. Flash chromatography was performed on Silicycle F60 (230-400 mesh) silica gel. Medium pressure liquid chromatography (MPLC) was performed on a Teledyne ISCO CombiFlash Rf 200. ^{1}H and ^{13}C NMR spectra were referenced to the residual solvent peak ($CDCl_3$ δ = 7.26 (^{1}H) and 77.16(^{13}C)) were collected on either a Varian INOVA 400 MHz or 500 MHz spectrometer as noted. ^{31}P NMR spectra were referenced to the respective ^{1}H NMR spectra using absolute frequency referencing[229] in Mnova software. Chemical shifts are given in units of ppm (δ) and coupling constants (J) in Hz. Multiplicities are assigned as singlet (s), doublet (d), triplet (t), quartet (q), multiplet (m), or broad (br). Gas chromatography (GC) was performed on a Shimadzu GCMS-QP2010 using TIC detection. For standard GC an Agilent Technologies HP-1MS

UI (30 m x 0.25 mm x 0.25 μm) column was used and for chiral GC a Supelco b-Dex 325 (30 m x 0.25 mm x 0.25 μm) column was used. HPLC was performed on a Shimadzu LC-2010A HT Liquid Chromatograph equipped with a Chiralpak AD-H (0.46 cm x 25 cm) column and a UV detector operating at 210/220 nm using a hexanes–isopropanol eluent system.

5.4.2 Synthetic Procedures

General Procedure for the Synthesis of 1b:

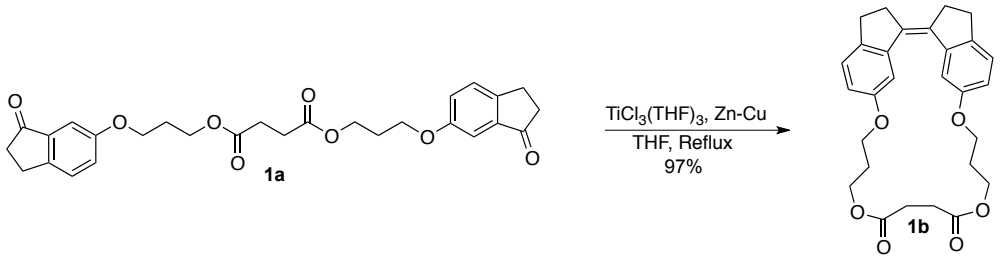

Zinc-copper couple[230] (1.42 g, 21.8 mmol) and $TiCl_3(THF)_3$[231] (2.70 g, 7.28 mmol) were transferred as solids to an oven dried 500 mL 2-neck flask fitted with reflux condenser and septum under argon. Dry and degassed THF (80 mL) was added by cannula and the suspension was heated at reflux for 1.5 hr with vigorous stirring to generate a black suspension. In a separate oven dried pear flask, **1a** (600 mg, 1.21 mmol) was dissolved (with the help of mild heating) in dry and degassed THF (120 mL). While maintaining a rapid reflux, the solution of **1a** was added to the McMurry reagent by syringe pump over a period of 6 hr. Once addition was complete, the solution was allowed to cool and poured into 300 mL of stirring sat. NH_4Cl (aq.). The organic layer

was decanted off and the aqueous layer was extracted 2 x 150 mL THF. The combined organic layers were evaporated to approximately 20 mL then taken up in 200 mL DCM and washed with water (100 mL) then brine (100 mL), dried over $MgSO_4$ and evaporated under reduced pressure. The light yellow (can be pink) product was subjected to column chromatography (SiO_2, Gradient DCM to 2% EtOAc in DCM) to yield pure **1b** as a white solid (549 mg, 1.18 mmol) in 97 % yield. Scaling-up by a factor of two yielded 931 mg (2.02 mmol) from 1.20 g (2.43 mmol) **1a** in 93 % yield. Spectroscopic data matched those previously reported.[44]

Synthesis of 1d:

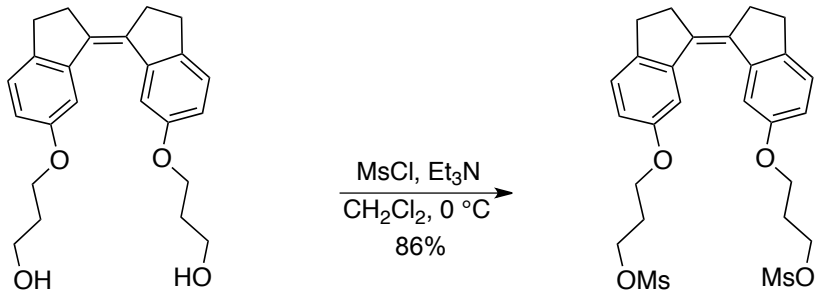

1c **1d**

1c[44] (1.60 g, 4.21 mmol) was dissolved in dry DCM (65 mL) in an oven dried 125 mL round bottom flask with stirbar under argon. The solution was cooled to 0 °C and triethylamine (1.75 mL, 12.6 mmol) was added by syringe followed by dropwise addition of methanesulfonyl chloride (0.98 mL, 12.6 mmol). The solution was allowed to stir for 30 min while monitoring by TLC. The reaction mixture was diluted with DCM (200 mL) and washed with 1N HCl (50 ml), water (100 mL), $NaHCO_3$ (sat. aq., 50 mL),

and brine (100 mL), then dried over Na_2SO_4 and evaporated under reduced pressure. The yellow oil was then purified by flash chromatography (SiO_2, DCM) to yield **1d** as a white solid in 86% yield (1.96 g, 3.64 mmol). **^{1}H NMR** (400 MHz, $CDCl_3$): δ 7.54 (d, *J* = 2.0 Hz, 2H), 7.13 (d, *J* = 8.2 Hz, 2H), 6.68 (dd, *J* = 8.2, 2.2 Hz, 2H), 4.36 (t, *J* = 6.1 Hz, 4H), 3.99 (t, *J* = 5.8 Hz, 4H), 2.90 (s, 6H), 2.89–2.82 (m, 4H), 2.80–2.69 (m, 4H), 2.14 (m, 4H). **^{13}C NMR** (126 MHz, $CDCl_3$): δ 156.91, 141.79, 141.29, 135.61, 125.89, 114.37, 109.35, 67.11, 63.57, 37.27, 35.51, 29.98, 29.23. **HRMS**-ESI (*m*/*z*) Calcd for ($C_{26}H_{32}O_8S_2$) ([M+H]+): 537.1612; found: 537.1633.

Synthesis of (*Z*)-1:

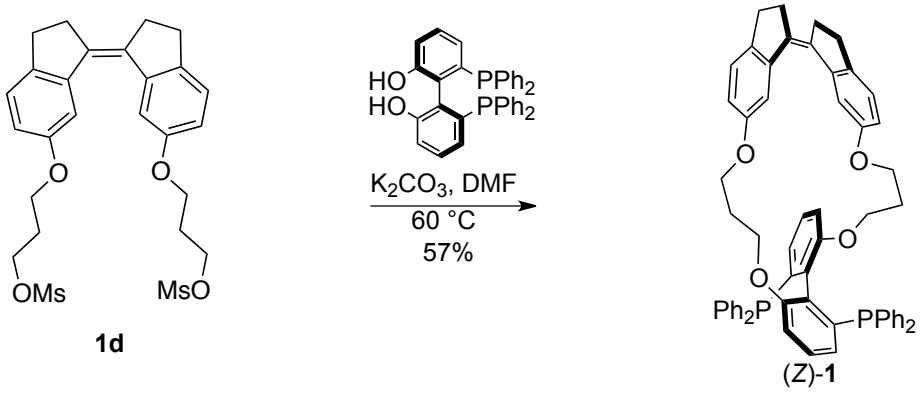

(*S*)-**(HO)$_2$-Biphep*** [synthesized as previously described[211] from (S)-MeOBiphep (Solvias, ≥ 99% *ee*)] (825 mg, 1.49 mmol) was dissolved in dry and degassed DMF (20 mL) in a flame dried 100 mL 2-neck round bottom flask with stirbar then sparged with argon for 30 minutes. In a separate flame dried vial fitted with a septum, **1d** (800 mg, 1.49 mmol) was dissolved in DMF (12 mL) and sparged with argon for 30 min.

Potassium carbonate (1.03 g, 7.45 mmol) was added to the solution of (S)-**(HO)$_2$-Biphep** as a solid and the pale-yellow suspension was stirred at room temperature for 30 minutes then heated to 60 °C at which time the solution of **1d** in DMF was added dropwise by syringe pump over 2 hr. After an additional 5 hr, the reaction was complete by TLC. Solvent was removed by vacuum distillation at 40 °C and the residue was suspended in ~50 mL degassed DCM. Degassed LiCl (5% aq.) was added by cannula and the mixture stirred gently until two translucent layers formed. The aqueous layer was removed by cannula and the washing step was repeated with degassed water. The organic layer was then transferred to a flask containing Na_2SO_4 under argon and stirred for 10 min before evaporation under reduced pressure. The brown oil was then purified by flash chromatography (SiO_2, 1:1 Hex/DCM) to yield (*Z*)-**1** as an amorphous white solid in 57% yield (766 mg, 0.852 mmol). ***rac**-(*Z*)-**1** was synthesized in an identical manner starting from *rac*-MeOBiphep which was synthesized according to the procedure of Schmid et al.[232] forgoing chiral resolution. **^{1}H NMR** (400 MHz, $CDCl_3$): δ 7.44 (d, *J* = 2.3 Hz, 2H), 7.29–7.12 (m, 22H), 7.09 (d, *J* = 8.3 Hz, 2H), 6.69 (d, *J* = 7.4 Hz, 2H), 6.61–6.54 (m, 4H), 3.69–3.49 (m, 6H), 3.23 (dt, *J* = 8.5, 4.1 Hz, 2H), 2.95–2.76 (m, 4H), 2.75–2.64 (m, 4H), 1.69–1.54 (m, 2H), 1.54–1.41 (m, 2H). **^{13}C NMR** (126 MHz, $CDCl_3$): δ 156.91, 156.71, 141.64, 140.47, 138.92, 137.64, 135.44, 134.52, 133.32, 128.67, 128.26, 128.24, 127.92, 127.86, 126.20, 125.82, 115.07, 111.60, 108.62, 64.33, 63.87, 35.31, 30.02, 28.72. **^{31}P NMR**

(162 MHz, $CDCl_3$): δ -14.28. **HRMS**-ESI (*m*/*z*) Calcd for ($C_{60}H_{52}O_4P_2$) ([M+H]+): 899.3414; found: 899.3437.

Photochemical preparation of *(E)-2 and* (*E*)-2'

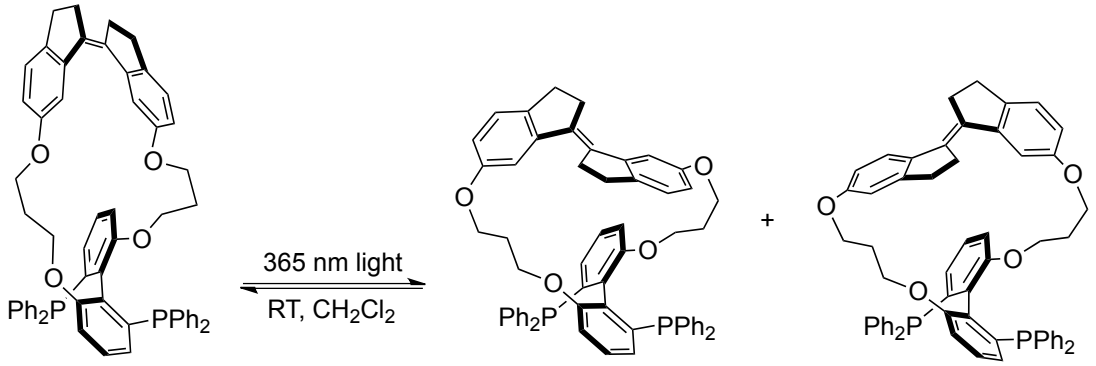

(*Z***)-1** (198 mg, 0.220 mmol) was transferred to a flame dried 500 mL single-neck round bottom flask with stirbar under argon. Dry DCM (200 mL) was added and the solution sparged with argon for 30 min. With vigorous stirring, the solution was irradiated with a 3W 365 nm single diode high-powered LED (~17.5 mW cm^{-2}) in contact with the bottom of the flask for 40 min. The solvent was removed under reduced pressure and the white solid was purified by conventional flash chromatography or MPLC (SiO_2, gradient Hexanes to 80:20 Hexanes/EtOAc). Yield: 72% **(***Z***)-1** (143 mg, 0.160 mmol), 6% (*E*)-**2'** (11 mg, 0.012 mmol), and 18% (*E*)-**2** (35 mg, 0.039 mmol) with 95% overall recovery.

(*E*)-2 (major *E*-isomer):

^{1}H NMR (400 MHz, $CDCl_3$): δ 7.25–7.08 (m, 14H), 7.08–6.96 (m, 6H), 6.82 (d, *J* = 2.3 Hz, 2H), 6.74 (t, *J* = 6.6 Hz, 4H), 6.69 (d, *J* = 8.1 Hz, 4H), 6.65 (dd, *J* = 8.1, 2.1 Hz, 2H), 4.02–3.77 (m, 4H), 3.50–3.38 (m, 2H), 3.31–3.20 (m, 2H), 2.96 (dd, *J* = 13.2, 7.3 Hz, 2H), 2.91–2.72 (m, 6H), 1.34–1.22 (m, 2H), 0.88–0.71 (m, 2H). **^{13}C NMR** (126 MHz, $CDCl_3$): δ 156.99, 155.46, 144.99, 141.45, 139.05, 138.56, 134.98, 133.96, 133.79, 133.13, 132.97, 128.41, 128.15, 127.65, 127.08, 125.99, 118.31, 113.12, 111.02, 66.75, 64.97, 35.64, 31.78, 26.60. **^{31}P NMR** (162 MHz, $CDCl_3$): δ -14.97. **HRMS**-ESI (m/z) Calcd for ($C_{60}H_{52}O_4P_2$) ([M+H]+): 899.3414; found: 899.3176.

(*E*)-2' (minor *E*-isomer):

^{1}H NMR (500 MHz, $CDCl_3$): δ 7.37–7.23 (m, 12H), 7.17–7.07 (m, 8H), 7.02 (d, J = 1.4 Hz, 2H), 6.91-6.88 (m, 4H), 6.76 (dd, J = 8.1, 1.7 Hz, 2H), 6.70 (dd, *J* = 7.6, 2.8 Hz, 2H), 6.13 (d, *J* = 8.2 Hz, 2H), 4.11–4.01 (m, 2H), 3.81–3.70 (m, 2H), 3.21–3.02 (m, 3H), 3.01–2.86 (m, 3H), 1.41–1.19 (m, 4H). **^{31}P NMR** (162 MHz, $CDCl_3$): δ -15.09. **HRMS**-ESI (m/z) Calcd for ($C_{60}H_{52}O_4P_2$) ([M+H]+): 899.3414; found: 899.3411.

Synthesis of Phosphine Selenides:

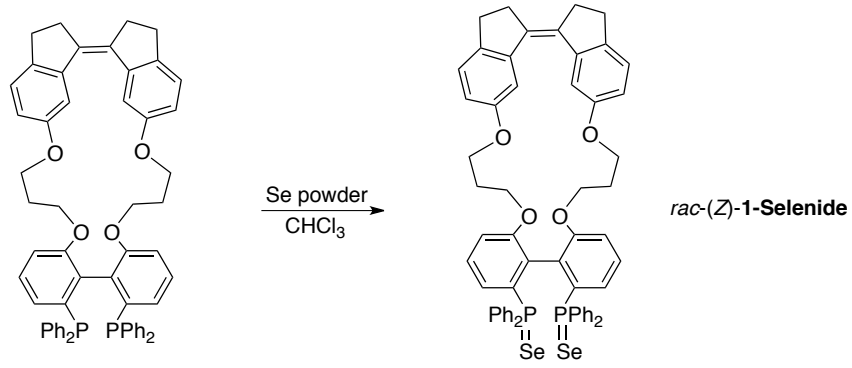

Bisphosphine *rac*-**(***Z***)-1** (62 mg, 0.070 mmol) and selenium (110 mg, 1.4 mmol) were transferred to an oven dried 10 mL round bottom flask under argon. Dry and degassed chloroform (3.5 mL) was added by syringe and the suspension was stirred for 4 hours in the dark. The mixture was then filtered through celite, rinsing through with dichloromethane and evaporated under reduced pressure to yield the *rac*-**(***Z***)-1** selenide (64 mg, 0.061 mmol) as a white solid in 86% yield. **^{1}H NMR** (400 MHz, $CDCl_3$): δ 7.87 – 7.80 (m, 4H), 7.73 – 7.65 (m, 4H), 7.37 (d, *J* = 2.4 Hz, 2H), 7.31–7.19 (m, 11H), 7.18–7.16 (m, 1H), 7.12–6.95 (m, 6H), 6.55–6.42 (m, 4H), 3.57–3.46 (m, 2H), 3.44–3.27 (m, 6H), 2.97–2.59 (m, 8H), 1.67–1.47 (m, 2H), 1.46–1.31 (m, 2H). **^{31}P NMR** (162 MHz, $CDCl_3$): δ 32.61. **HRMS**-ESI (m/z) Calcd for ($C_{60}H_{52}O_4P_2Se_2$) ([M+H]+): 1059.1750; found: 1059.1750.

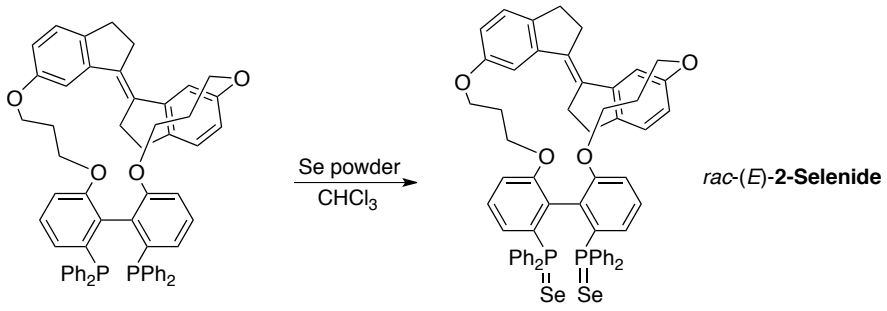

Bisphosphine *rac*-(*E*)-**2** (55 mg, 0.062 mmol) and selenium (98 mg, 1.2 mmol) were transferred to an oven dried 10 mL round bottom flask under argon. Dry and degassed chloroform (3 mL) was added by syringe and the suspension was stirred for 4 hours in the dark. The mixture was then filtered through celite, rinsing through with dichloromethane and evaporated under reduced pressure to yield the (*rac*)-(*E*)-**2-**selenide (54 mg, 0.051 mmol) as a white solid in 82% yield. **^{1}H NMR** (400 MHz, $CDCl_3$): δ 7.89 (m, 4H), 7.66 (m, 4H), 7.51–7.42 (m, 2H), 7.35 (m, 4H), 7.31–7.25 (m, 2H), 7.25–7.17 (m, 6H), 7.10 m, 2H), 7.06–6.99 (m, 2H), 6.86 (d, *J* = 2.3 Hz, 2H), 6.74 (m, 2H), 6.53 (d, *J* = 8.1 Hz, 2H), 4.07–3.94 (m, 2H), 3.93–3.79 (m, 2H), 3.26–3.14 (m, 4H), 3.10–2.81 (m, 8H), 1.19–1.05 (m, 2H), 0.99–0.82 (m, 2H). **^{31}P NMR** (162 MHz, $CDCl_3$): δ 32.75. **HRMS**-ESI (m/z) Calcd for ($C_{60}H_{52}O_4P_2Se_2$) ([M+H]+): 1059.1750; found: 1059.1754.

5.4.3 Determination of Photostationary State*

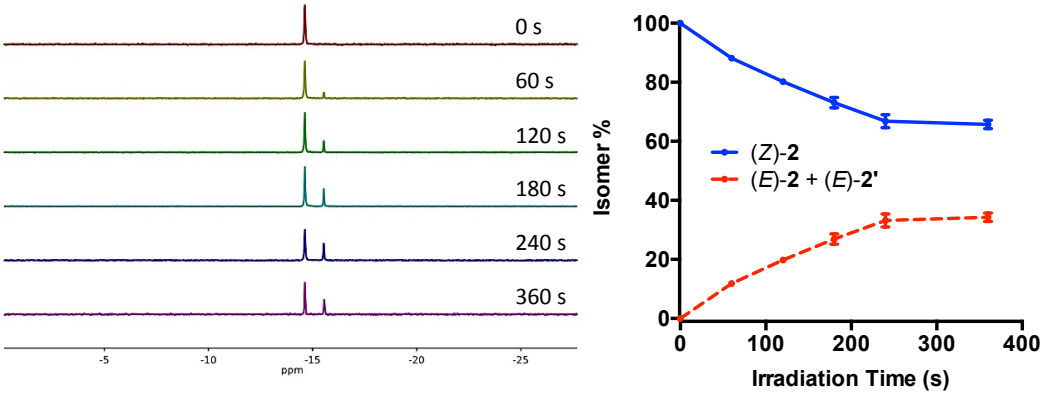

Figure 73 ^{31}P NMR spectra (left) was used to monitor equilibration of (*Z*)-1 by observing a decrease in the integration of (*Z*)-1 peak at ~14.7 ppm and an increase in the peak at ~15.5 ppm corresponding to the *E*-isomers.

An NMR tube was charged with **(*Z*)-1** (15 mg) followed by 0.5 mL dry and degassed (sparged) CD_2Cl_2. Tube was irradiated (365 nm, 3W, 17.5 mW cm^{-2}) for time intervals specified below. Distinct shift between the ^{31}P NMR shifts of the Z-isomer **(*Z*)-1** (14.67 ppm) and E-isomers (*E*)-**2** and (*E*)-**2'** (15.49 and 15.58 ppm respectively) were used to track the progress of the reaction. Experiment was performed in triplicate. After 360 s, all three samples had reached (approximately) photostationary equilibrium.

Resolvable ^{1}H NMR resonances attributable to a specific isomer as determined by authentic samples (black boxes), were used to determine the composition of the photostationary mixture based on integration.

---

* Preliminary determination of PS ratio (not shown) determined by Dr. Sergey Akbulatov, Boulatov Group, University of Liverpool.

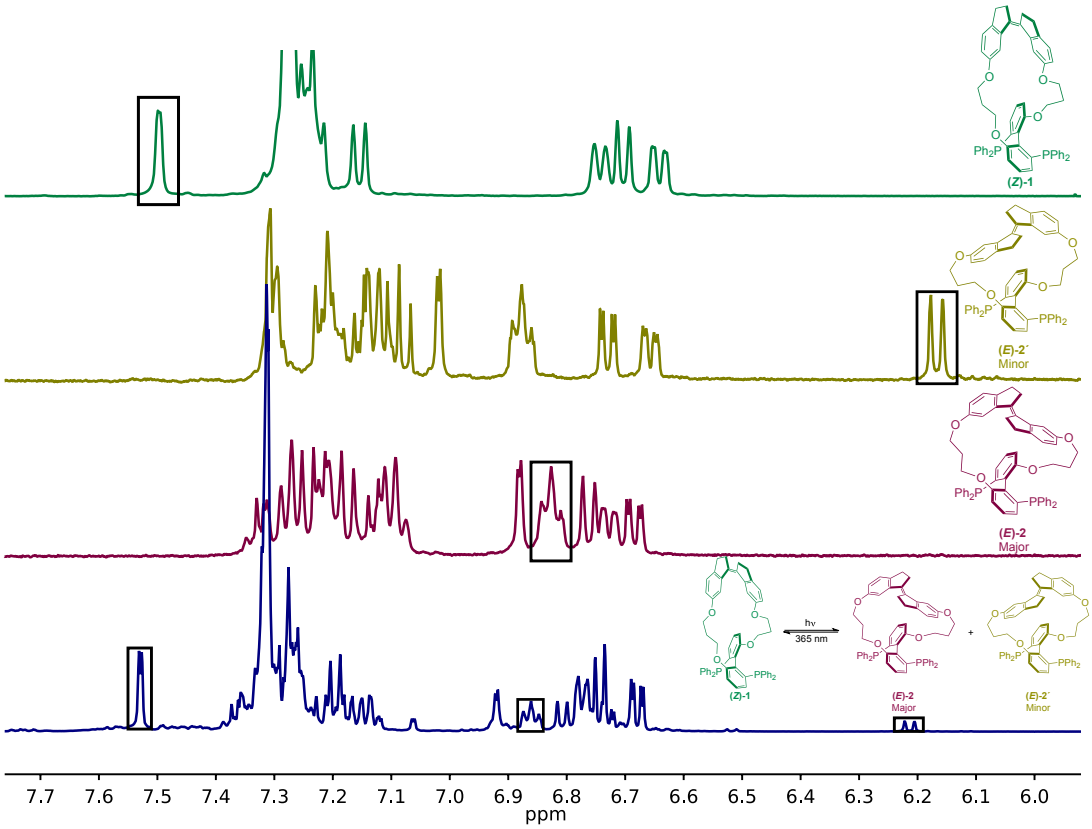

Figure 74 Resolvable peaks for each isomer (shown in black boxes) used to calculate the composition of the photostationary mixture by ^{1}H NMR (blue trace shows a representative spectrum).

5.4.4 Catalysis Procedures

5.4.4.1 General Procedure for Asymmetric Heck Reaction with 2,3-Dihydrofuran and Aryl Triflates

Ligand (0.013 mmol, 0.06 equiv.) was added to an oven dried 4 mL amber glass screw top vial with stirbar sealed with a septum cap under argon. $Pd(OAc)_2$ (1.5 mg, 0.0067 mmol, 0.03 equiv.) was added as a stock solution in dry and degassed benzene (370 μL) and stirred for ten minutes. ArOTf (0.22 mmol, 1 equiv.), N,N-

diisopropylethylamine (130 μL, 0.75 mmol, 3.4 equiv.), and 2,3-dihydrofuran (94 μL, 1.2 mmol, 5.6 equiv.) were then added sequentially by syringe. The vial was sealed under argon and heated at 40 °C for 24 hr in the dark. The reaction was allowed to cool then diluted with 4 mL hexane and filtered to remove precipitate. The yellow-orange solution was then passed through a small plug of silica gel and evaporated under reduced pressure. *In situ* photoswitching experiments were performed identical to that described with the following modifications: After stirring for 10 minutes, the $Pd(OAc)_2$/**Ligand**/Benzene solution (in a clear vial) was irradiated for 1 min (3W, 365 nm) under vigorous stirring.

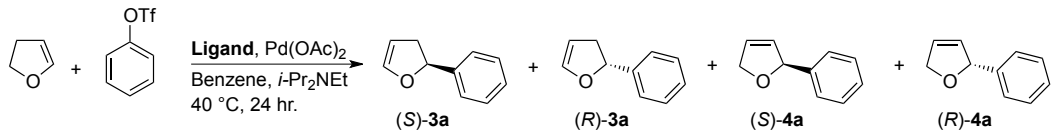

The enantiomeric excess and diastereomeric ratio were determined by GC analysis on chiral stationary phase (Supelco b-Dex 325): t_R = 12.5 min for (*S*)-**3a**, t_R = 12.6 min for (*R*)-**3a,** t_R = 13.1 min for (*S*)-**4a**, t_R = 13.2 min for (*R*)-**4a**.

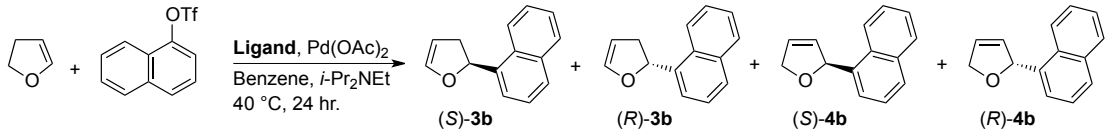

Composition of diastereomers as a percent of total products (**3b** $[\%]_{GC}$ and **4b** $[\%]_{HPLC}$) was determined by GC [normal stationary phase (Agilent Technologies HP-1MS UI): t_R = 10.9 min for **3b**, t_R = 11.2 min for **4b**]. The enantiomeric excess was determined

by HPLC analysis on chiral stationary phase (Daicel Chiralcel AD-H column, Hexanes:*i*PrOH = 99:1, flow rate 1 mL min^{-1}, λ = 210 nm): t_R = 6.11 min for (*S*)-**3b**, t_R = 8.02 min for (*R*)-**3b,** t_R = 12.1 min for (*R*)-**4b**. (*S*)-**4b** elutes near the front of (*R*)-**3b (**t_R ~ 7.5 min) and is generally resolvable, however, at low concentration the peak is not observed. The total area of all products by HPLC is: $Product_{total,HPLC}$ = ∫(*S*)-**3b** + ∫[(*S*)-**4b** + (*R*)-**3b**] + ∫(*R*)-**4b.** The total percentages of each product (Table S4) are calculated as follows: (*S*)-**3b** [%] = (*S*)-**3b** $[\%]_{HPLC}$; (*R*)-**3b** [%] = [**3b** $[\%]_{GC}$ - (*S*)-**3b** $[\%]_{HPLC}$]; (*R*)-**4b** [%] = (*R*)-**4b** $[\%]_{HPLC}$; (*S*)-**4b** [%] = 100%-**3b** $[\%]_{GC}$ - (*R*)-**4b** $[\%]_{HPLC}$.

Degree of conversion, defined by depletion of ArOTf (GC) had no effect on the observed *ee* independent trials using MeOBiphep as ligand:

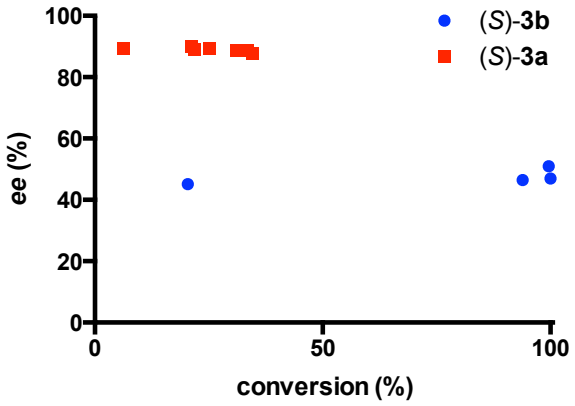

Figure 75. Conversion vs. ee for asymmetric Heck reaction of phenyl triflate (red) and 1-naphthyl triflate (blue) under standard conditions using MeOBiphep as ligand.

5.4.4.2 General Procedure for Asymmetric Allylic Alkylation of (+/-)-*E*-Allyl Acetates

Allylpalladium (II) chloride dimer (2.4 mg, 0.067 mmol, 0.025 equiv.) was added as a stock solution in dry and degassed DCM (250 μL) to an oven dried 4 mL amber

glass screw top vial with stirbar under argon. **Ligand** (0.013 mmol, 0.05 equiv.) was added as a stock solution in dry and degassed DCM (1 mL), and the solution allowed to stir for 1 hr. Racemic allyl acetate substrate (0.27 mmol, 1 equiv.) was added as a stock solution in DCM (250 μL), followed by dimethyl malonate (91 μL, 0.80 mmol, 3 equiv.). *N,O*-bis(trimethylsilyl)acetamide (195 μL, 0.80 mmol, 3 equiv.) was added dropwise followed by a catalytic amount of KOAc. The vial was then sealed under argon and stirred at ambient temperature for 20 hr in the dark. The reaction mixture was diluted with Et_2O (7.5 mL) and passed through celite then washed with 3 x 5 mL NH_4Cl (10%, aq.), water (10 mL), and brine (10 mL). The solution was dried over $MgSO_4$ and filtered before evaporation under reduced pressure. The crude orange oil was purified by flash chromatography (SiO_2, gradient elution Hexanes to 95:5 Hexanes:EtOAc) to yield **5a** or **5b** as a clear oil.

5a:

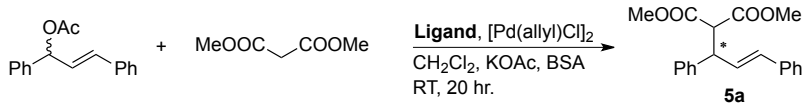

The enantiomeric excess was determined by HPLC analysis on chiral stationary phase (Daicel Chiralcel AD-H column, Hexanes:*i*PrOH = 98:2, flow rate 1 mL min^{-1}, λ = 220 nm): t_R = 24.0 min for (*S*)-**5a**, t_R = 16.5 min for (*R*)-**5a**. Spectral data and the sign of optical rotation (determined to be +) match that previously reported consistent with the *R* enantiomer as the major isomer.[226]

5b:

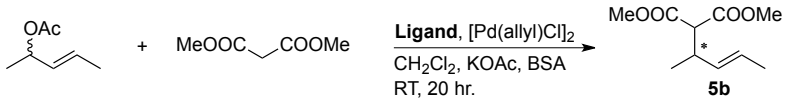

The enantiomeric excess was determined by ¯H NMR by titrating product with Eu(hfc)$_3$ chiral shift reagent.[233] Briefly, 5 mg of **5b** was dissolved in an NMR tube in 0.5 mL $CDCl_3$. Eu(hfc)$_3$ was titrated in ~20 μL portions in solution (100 mg/mL) from a gas-tight syringe. Spectra were acquired with each addition until peaks were sufficiently resolved. The average of all resolved peaks from multiple spectra were used to calculate the % *ee* for each trial.

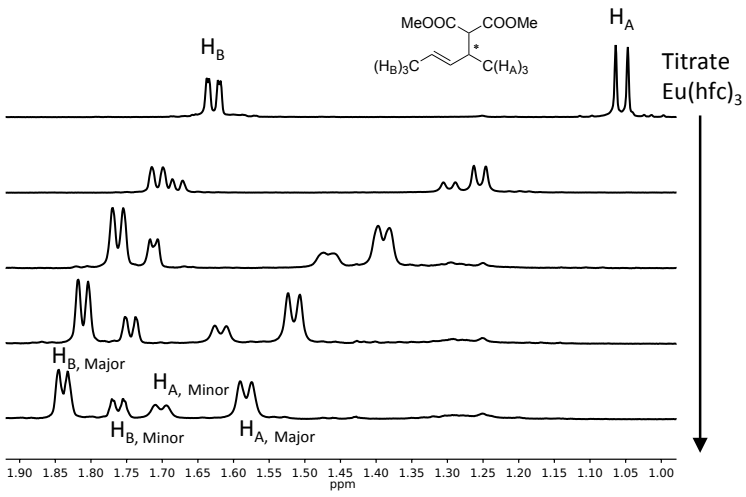

Figure 76 Resolution of 5b enantiomers by ^{1}H NMR [chiral shift titration with Eu(hfc)$_3$ in $CDCl_3$].

5.4.4.3 Comparison with Previously Reported Results

A previous report by Zhang demonstrates the effect of ligand dihedral angle on the reaction outcomes of both Heck arylation of phenyl triflate to produce **3a**.[224] Natural

dihedral angles (ϕ) in these studies were calculated using CAChe with force field MM2 and are not directly comparable to our study. Figure S6 shows results (% *ee* of **3a**) from this study (blue) with dihedrals calculated as described in the main text for (*Z*)-**1**, MeOBiphep, and (*E*)-**2** (ϕ = 83, 97, 106° respectively), transcribed data from previously reported TunePhos results (blue) and MeOBiphep (red) with dihedral angles calculated by MM2.[224] Given the discrepancy in MeOBiphep dihedral angle as plotted (black arrow connects the previous and present MeOBiphep results), it is reasonable that our trend reflects the decrease in *ee* with increasing dihedral between ~80 and 100°.

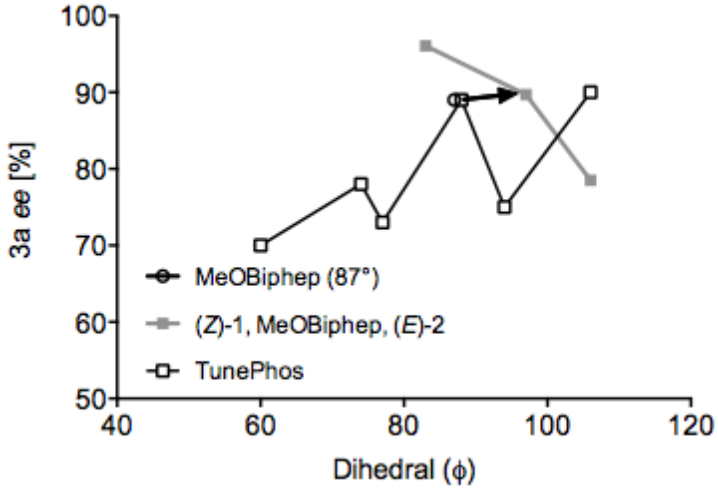

Figure 77 Natural dihedral angle (ϕ) plotted vs. 3a *ee* [%] from this work (grey squares), and a previous report[224] (hollow squares). The result for MeOBiphep calculated at MM2 level of theory (hollow circle) is shown connected (black arrow) to the present result for MeOBiphep calculated as a conformational ensemble at DFT level of theory.

5.4.5 Quantum-chemical Calculations*

All calculations were performed in the gas phase with the Gaussian09.B01 software package on trestles.sdsc.edu HPC resource supported by the NSF as part of the XSEDE computational network. The Berny algorithm was used to locate stationary points. Because of the large size of the molecules, frequencies were not calculated. Boltzmann averaging used relative electronic energies. Conformers were searched and force-dependent parameters were calculated as previously described.[139,234] Force-dependent ensemble average parameters of MeOBiphep are listed in Table 16. Key parameters of individual conformers of the stiff stilbene macrocycle are tabulated in Table 17.

* Performed by Dr. Yancong Tian, Boulatov Group, University of Liverpool

Table 16 Force-dependent ensemble average parameters of MeOBiphep.

Rel. electronic energy [kcal mol^{-1}]	**Applied force** [pN]	**Constrained distance** [Å]	**O$^{\cdots}$O distance** [Å]	**(P)-C-C-C-C-(P) torsion of biaryl** [^{o}]	**C_{Ar}-C=C-C_{Ar} torsion of stiff stilbene** [^{o}]
1.088	-130	4.855	3.36585	-92	-82
0.736	-110	5.055	3.44128	-94	-85
0.445	-86	5.255	3.51136	-96	-87
0.221	-65	5.455	3.58614	-98	-90
0.075	-37	5.655	3.67515	-101	-93
0.000	0	5.855	3.76625	-109	-97
0.047	45	6.155	3.88146	-111	-101
1.814	52	4.955	4.00872	-107	-103
1.040	159	6.755	4.11702	-112	-111
2.083	354	7.055	4.29484	-116	-115
4.446	783	7.355	4.52585	-119	-120
9.063	1372	7.655	4.78243	-124	-125

Table 17 Key parameters of individual conformers of the stiff stilbene macrocycles.

Isomer	**Rel. electronic energy** [kcal mol^{-1}]	**(P)-C-C-C-C-(P) torsion of biaryl** [^{o}]	**C_{Ar}-C=C-C_{Ar} torsion of stiff stilbene** [^{o}]	**O$^{\cdots}$O distance** [Å]
Z	0.00	85	11	3.395
	0.34	83	11	3.288
	2.30	-102	-8	3.768
	2.70	77	10	3.138
	3.19	-98	-11	3.608
	4.46	-106	-10	3.972
E1	15.14	92	-162	3.741
	16.47	-90	158	3.617
	21.50	-111	154	4.293
E2	11.90	106	159	4.031
	12.05	103	159	3.948
	13.35	106	162	4.060
	14.02	-90	-155	3.689
	14.61	89	156	3.668
	15.03	-100	-157	3.846
	15.99	-97	-162	3.847
	16.36	-106	-158	3.972
	22.79	-113	-155	4.294

5.4.6 X-ray Crystallography*

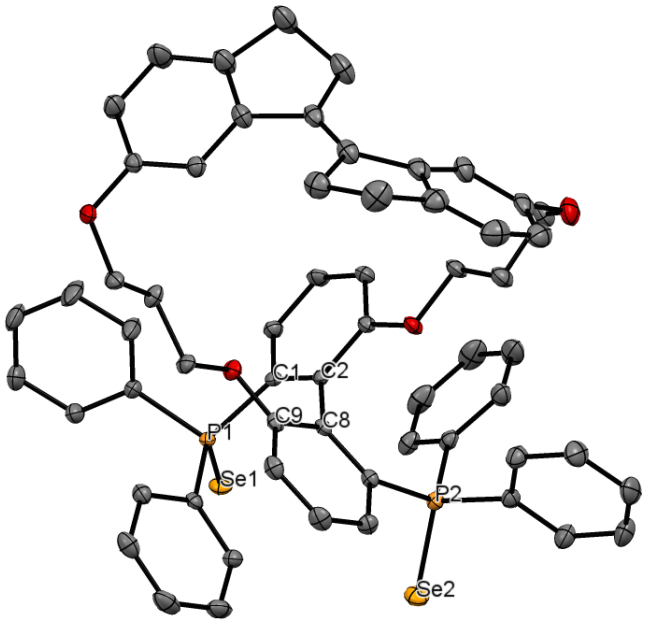

Figure 78 X-ray crystal structure of *rac*-(*E*)-**2**-selenide (thermal ellipsoids shown at 50% probability level). Solvent removed for clarity. One indene moiety is disordered over two positions, of which the one of higher occupancy is shown. Solvent removed for clarity.

Compound *rac*-(*E*)-2 (CCDC 1014253):

Colorless plates crystallized from diisopropyl ether/acetone at RT by vapor diffusion. Crystal data: Plate, colorless, crystal size = 0.155 x 0.188 x 0.288 mm^3, $C_{72}H_{76}O_8P_2Se_2$, FW 1289.18, monoclinic, space group $P\ 1\ 2_1/c\ 1$, a = 22.1463(10), b = 17.8980(8), c = 16.6303(7) Å, α = 90°, β = 105.871(2)°, γ = 90°, V = 6340.(5) $Å^3$, Z = 4, D_c = 1.351 mg/m^3, T = 110(2) K, μ = 1.273 mm^{-1}, 104192 measured reflections, 17782 [R(int) =

* Crystallographic data was collected and structure solved by Dr. Roger Sommer, NCSU Department of Chemistry.

0.0367] independent reflections, 17782 / 876 / 883 Data / restraints / parameters, *F(000)* = 2680, *R1* = 0.0502, *wR2* = 0.0971, *R1* = 0.0361, *wR2* = 0.0904[I>2sigma(I)], Max. residual density 1.156 e.Å^{-3}, Max. and min. transmission 0.8270 and 0.7110, and goodness-of-fit (F^2) = 1.016.

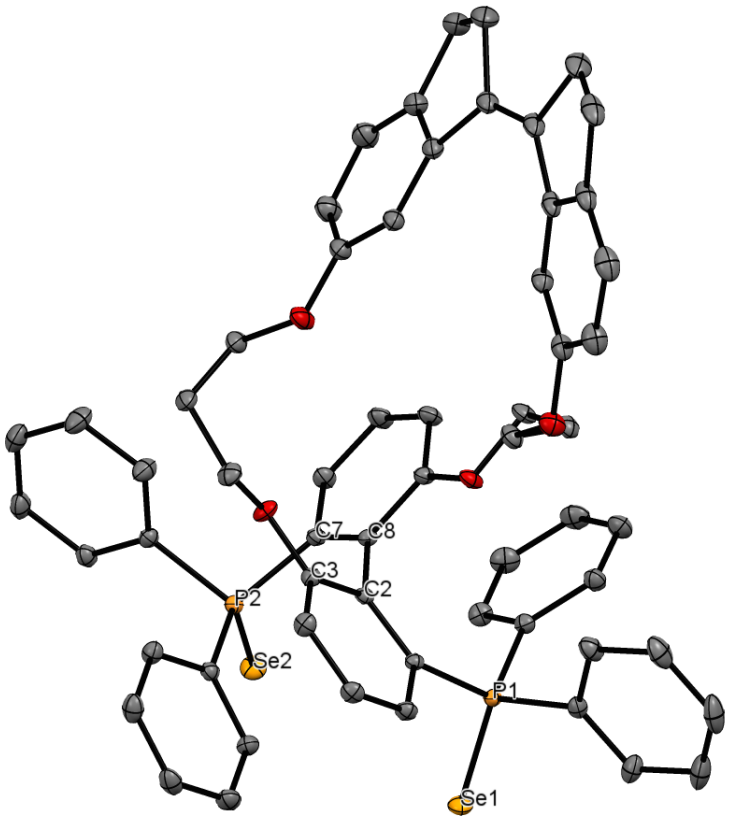

Figure 79 X-Ray crystal structure of *rac*-(*Z*)-**1**-selenide (thermal ellipsoids shown at 50% probability level). Solvent removed for clarity.

Compound *rac*-(*Z*)-1 (CCDC 1014182):

Colorless blocks crystallized from diisopropyl ether/acetonitrile at RT by vapor diffusion. Crystal data: Blocks, colorless, crystal size = 0.438 x 0.534 x 0.604 mm^3,

$C_{62}H_{55}NO_4P_2Se_2$, FW 1097.93, triclinic, space group *P* - 1, *a* = 11.6658(3), *b* = 12.6980(3), *c* = 176338(5) Å, α = 97.2890(10)°, β =98.1190(10)°, γ = 90.0040(10)°, *V* = 2564.63(12) Å^3, *Z* = 2, D_c = 1.422 mg/m^3, *T* = 110(2) K, μ = 1.555 mm^{-1}, 232835 measured reflections, 22704 [R(int) = 0.0373] independent reflections, 22704 / 0 / 641 Data / restraints / parameters, *F(000)* = 1128, *R1* = 0.0360, *wR2* = 0.0711, *R1* = 0.0264, *wR2* = 0.0676[I>2sigma(I)], Max. residual density 0.643 e.Å^{-3}, Max. and min. transmission 0.5490 and 0.4540, and goodness-of-fit (F^2) = 1.038.

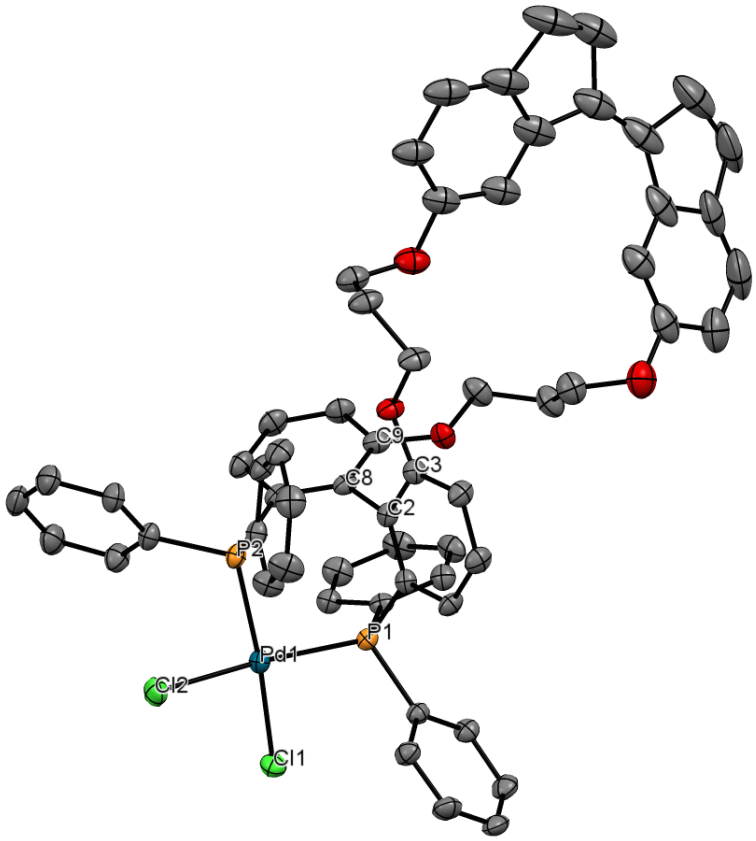

Figure 80 X-Ray crystal structure of (*S*)-(*Z*)-**1**-$PdCl_2$ complex (thermal ellipsoids shown at 50% probability level). Solvent removed for clarity.

(*S*)-(*Z*)-1-$PdCl_2$:

Yellow needles crystallized from pentane/THF at RT by vapor diffusion. Crystal data: Blocks, colorless, crystal size = 0.146 x 0.168 x 0.458 mm^3, $C_{72}H_{76}Cl_2O_7P_2Pd$, FW 1292.56, hexagonal, space group *P 65*, *a* = 27.9768(13), b = 27.9768(13), *c* = 13.9743(7) Å, α = 90°, β = 90°, γ = 120°, *V* = 9472.3(10) $Å^3$, *Z* = 6, D_c = 1.360 mg/m^3, *T* = 110(2) K, μ = 0.484 mm^{-1}, 191508 measured reflections, 18306 [R(int) = 0.0596] independent reflections, 18306 / 57 / 757 Data / restraints / parameters, *F(000)* = 4044, *R1* = 0.0510, *wR2* = 0.0986, *R1* = 0.0379, *wR2* = 0.0917 [I>2sigma(I)], Max. residual density 0.690 $e.Å^{-3}$, Max. and min. transmission 0.9330 and 0.8090, and goodness-of-fit (F^2) = 1.068.

6. Summary and Outlook

This dissertation describes the development of new systems that respond to mechanical force through molecular level changes. These effects are observed across many orders of magnitude, from bulk material properties (chapter 4)[115] to the stereochemistry of single carbon—carbon bonds (chapter 5).[114] The initial motivation, whereby covalent mechanochemistry could be utilized to construct better stress-responsive materials, is described in chapter 1. Three molecular design criteria are outlined: "on-demand" activation via high-mechanophore content polymers, large local elongations upon activation for local stress relief, and the generation of reactive functional groups for stress strengthening.[121] The inspiration for non-scissile cyclobutane-based mechanophores, improving upon the molecular-level stress-response of the established *g*DHC mechanophores, was based on these criteria.

In chapter 2, a bicyclo[3.2.0]heptane mechanophore is developed that demonstrated, at the time, the largest local elongations of any non-scissile mechanophore (4 Å vs. ~1.3 for *cis*-*g*DHCs). Additionally, the ring-opened bis-enone products were demonstrated to be reactive towards neutral amines via aza-Michael addition. Finally, the ring opening was shown to be photo-reversible, the first such demonstration in a covalent mechanophore.[113] Chapter 3 expands on these themes utilizing a bicyclo[4.2.0]octane diester (BCO) framework. It was shown that high molecular weight polyesters could be synthesized using a general carbodiimide

polyesterification method, a new approach to high mechanophore content polymers for "on-demand" activation, potentially opening the door for a wide variety of structurally diverse high-mechanophore content polymers. Additionally, this system possessed even larger elongations (7 Å) and reactivity toward nucleophilic thiol-ene conjugate addition. The development of high BCO-content polymers allowed for the first direct spectroscopic (^{1}H and ^{13}C NMR) observation of alkenes mechanochemically generated from the [2+2] cycloreversion of cyclobutanes. As a result, detailed stereochemical analysis was performed on the product bis-α,β-unsaturated esters for a variety of BCO analogues, allowing for the development of a working model of the radical dynamics involved in the non-concerted cycloreversion.

In chapter 4, an alternative, though potentially complementary approach was applied to enhance bulk material properties via dynamic molecular level interactions. Weak, fast-exchanging coordination cross-links were incorporated into covalent poly (4-vinylpyridine) organogels. While "mechanically invisible" on the timescale of the experiments performed, these weak cross-links imparted vastly improved stress and strain at failure to these materials.[115] Historically,[116,117] a great deal of emphasis has been placed on the magnitude of energy dissipation in engineering tougher materials. These results may serve to challenge the classically held notions in regard to the relationship between toughening that occurs due to dissipation on the timescale of deformation and dissipation which occurs much faster, perhaps on the timescale of crack propagation.

While we demonstrate some preliminary data that suggests that crack propagation occurs on the order of 100 ms in these experiments, further studies are required to fully construct a molecular level interpretation of these results.

Finally, chapter 5 describes the first studies that directly relate force to reactivity in a mechanocatalytic system. Stiff stilbene based force probes were tethered to a chiral biaryl bis(phosphine)–based ligand. Using DFT, the *Z*-stilbene moiety was determined to exert a compressive force of ~130 pN on the biaryl backbone. Through photochemical switching, the *E*-stilbene is also accessible, and was determined to exert an extensional force of ~140 pN along the same coordinate. Through this parameterization, the effect of force and the resulting geometric changes could be correlated to changes in selectivity for a variety of asymmetric Heck arylations and Trost alkylations.[118] Importantly, these results show that forces on the order of 100 pN, which are readily accessible in solid materials under elastic deformation, can have large impacts on catalyst activity. Moving forward, these results may inspire the development of polymer-bound "fluxional mechanocatalysts," that are tunable in response to bulk deformation. Such systems could allow us to access new materials, such as polymers with regularly alternating microstructures, resulting from cyclic deformation of a "fluxional" catalyst on the timescale of polymerization.

Though several different strategies to develop force-responsive systems were undertaken in this dissertation, the approaches are complementary and their overall

impacts may be interwoven. The cyclobutane work (chapters 2 and 3) demonstrates a general approach to engineering mechanophores with greatly improved molecular level properties. Regardless, application of the design criteria described in chapter 1 is still hampered by the limited ability to efficiently activate these mechanophores in bulk materials. This will likely require more advanced and thoughtful choice of material architecture, an active area of research in the Craig lab. To achieve better mechanophore activation, relative to other non-specific and destructive bond scission events several approaches may be taken: develop architectures that direct force to the mechanophore, develop mechanophores more readily produce constructive outcomes in response to stress, and/or develop materials with extended stress and strain windows thus allowing the time and force necessary for sufficient mechanophore activation. Of these complementary approaches, chapter 4 addresses the ability to develop materials that better accumulate and store stress under load without catastrophic failure and provides an example of systems that make use of multiple molecular-level strategies to achieve efficient activation in bulk materials. Finally, the work described in chapter 5 may lead to an alternate approach to performing covalent chemistry in bulk materials. Significant changes in reactivity are observed when low forces (< 200 pN) are applied to these catalyst complexes, suggesting that constructive covalent polymer remodeling may be accessible through the activation of transition metal complexes as opposed through direct covalent bond activation, effectively amplifying the mechanical input.

Likely, however, is that the most valuable application of covalent mechanochemistry lies outside what we have proposed here, and perhaps beyond what anyone has speculated. I have been fortunate to work in this field during what I would characterize as its adolescence. When I arrived, the field had been established and the basic foundation had been laid. This left us in need of tools in the search for applications: synthetic methods, new mechanophores, material architectures, characterization techniques, etc… I was lucky to be involved with many of these efforts and hope that a sort of playful exploration of mechanochemistry comes through in this dissertation. Beyond that I hope that the concepts and tools described herein will influence others as the field reaches maturity and applications continue to emerge.

Appendix A. High Mechanophore Content Polyester-Acrylate ABA Block Copolymers: Synthesis and Sonochemical Activation*

A.1 Introduction

In the past five years, the covalent mechanochemistry of polymeric[17] and small molecule[45] systems has generated a great deal of interest, in terms of both material science and synthetic chemistry. Most studies to date have focused on systems with a single mechanophore per polymer chain;[28,30,33,39] an approach that has enabled the discovery of new mechanically induced chemistry and tools for stress monitoring. Single molecule architectures are likely to be limited, however, for applications in stress-responsive mechanical properties or scalable stoichiometric reactivity, due to low mechanophore concentration.[121] *gem*-Dihalocyclopropane mechanophores have demonstrated a rich array of mechanochemical activity,[18,96,105,107] and their post polymerization addition to polybutadiene based polymers has yielded the highest mechanophore content[84] and highest single-chain toughness[88] demonstrated in a synthetic polymer to date. While simple to synthesize, olefin containing polymers suffer from inherent instability due to ambient light, heat, and oxygen, often causing

---

* This chapter adapted from: Kean et al. (2012) *J. Polym. Sci., Part A: Polym. Chem., 50*, 3481-3484.

uncontrolled crosslinking. Furthermore, it is difficult to create complex architectures based on the post polymerization modification of polybutadiene.

In considering more robust and useful synthetic approaches, we start from the desire to engineer non-scissile mechanophores which typically means that ring systems must be embedded along the polymer backbone.[139] Backbone rings cannot easily be introduced by the traditional polymerization of vinyl monomers, and while ring-opening metathesis polymerization (ROMP) has been used,[107] the synthesis of complex fused ring monomers can be cumbersome. Furthermore, the ROMP methodology produces olefin-containing backbones whose stability is limited by the factors discussed above. While a rich array of functional groups can easily be incorporated into condensation polymers, mild and controllable polycondensation procedures typically generate polymers of low molecular weight (MW). This limits both bulk material utility and mechanochemical activation by pulsed ultrasound, where high molecular weights (> 40 kDa) are typically required to experience sufficient shear forces along the polymer backbone. Here, we report that the synthesis of an ABA triblock copolymer harvests the advantages of polycondensation and radical polymerization, giving access to stable, mechanophore-rich polymers of desirable molecular weight.

A.2 Results and Discussion

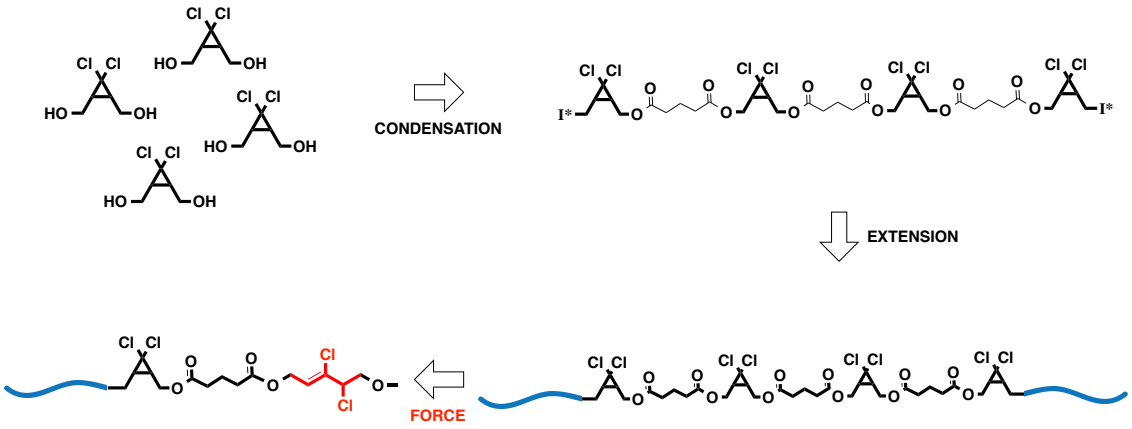

Scheme 8 Condensation-chain extension concept for the synthesis of high mechanophore content ABA triblock copolymers

Recently, Soucek[235] and Oh[236] have described the chain-extension of polyester based macroinitiators by controlled radical polymerization (CRP). From a design perspective, this approach appeared ripe for use in mechanochemical systems. Under ultrasound induced elongational flow, forces tend to accumulate about the center of a polymer chain,[79,80] while in the bulk either physical entanglements or thermoplastic domains are required for the accumulation of sufficient stress for activation. In an ABA triblock copolymer, the B block would then represent a potential "sweet spot" in terms of mechanochemical activation. The general strategy was to build a mechanophore rich block by polycondensation and utilize chain extension by CRP to yield a high MW, mechanically active material featuring the known mechanophore *gem*-dichlorocyclopropane (gDCC),[84] which undergoes a mechanically-accelerated transformation to a 2,3-dichloroalkene (Scheme 8). The synthesis (Scheme 9) began with

a polyesterification procedure based on that of Moore and Stupp.[141] A *g*DCC containing diol **(Diol 1**) was reacted with stoichiometric glutaric acid in the presence of diisopropylcarbodiimide (DIC) and dimethylaminopyridinium toluenesulfonate (DPTS) to suppress *N*-acylurea termination. After 24 hours, an excess of **Diol 1** was added to ensure the formation of a predominantly α,ω-hydroxy ditelechelic polymer (**Polymer 1**). Esterification of the endgroups in the presence of α-bromoisobutyryl bromide generated the difunctional, mechanophore-laden, macroinitiator (**Polymer 2**) with M_n = 26 kDa and PDI = 1.50 by GPC-MALS. **Polymer 2** was then chain extended (Scheme 9) under standard single-electron transfer living radical polymerization (SET-LRP) conditions[125] in DMSO with methyl acrylate (MA) to generate a 136 kDa, 1.17 PDI triblock copolymer (**Polymer 3,** Figure 81).

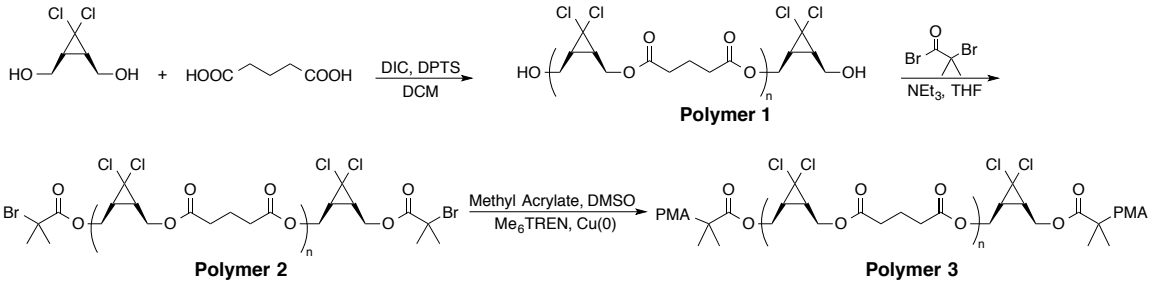

Scheme 9 Synthesis of high mechanophore content ABA triblock copolymers.

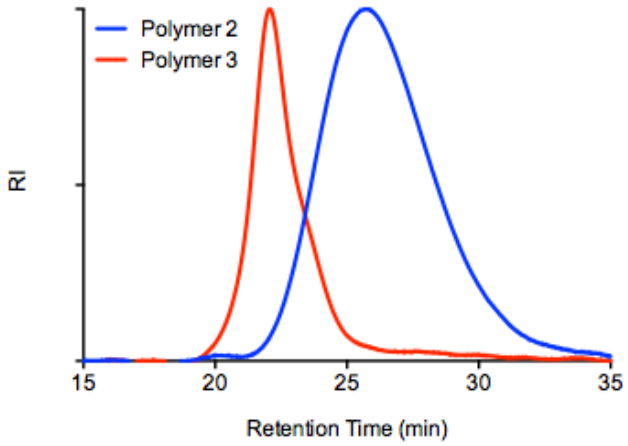

Figure 81 GPC-RI traces illustrating the molecular weight increase upon chain extension of **Polymer 2** (blue) by SET-LRP to generate **Polymer 3** (red).

The mechanochemical activity of **Polymer 3** was then tested by subjecting it to pulsed ultrasound in acetonitrile at 6-9 °C under N_2. These conditions mimic those previously employed by our group, and the expected conversion of gDCC units to 2,3-dichloroalkenes was indeed observed, with increased conversion as a function of sonication time (Figure 82). The percent ring opening was determined by ^{1}H NMR, and the MWs were determined by GPC-MALS for various sonication times. After 1 scission cycle, where the molecular weight has been halved, the percent ring opening was determined to be 55%. Estimating a degree of polymerization (DP_N) of 98 (see experimental section) for the mechanophore block, this corresponds to approximately 54 ring opening events per chain scission. This conversion, as a function of sonication time, is summarized in Figure 82 showing the gradual appearance of peaks at δ = 4.37, 4.70. 4.76, and 6.10 ppm corresponding to the 2,3-dichloroalkene products. For reference,

previous studies on polybutadiene-*g*DCC copolymers showed a 35% ring opening per scission cycle;[84] here we attribute the apparent increase in activity to the block architecture, where the *g*DCC functionalities are highly localized about the center of the chain, so that a higher fraction of them experience the force necessary for activation.

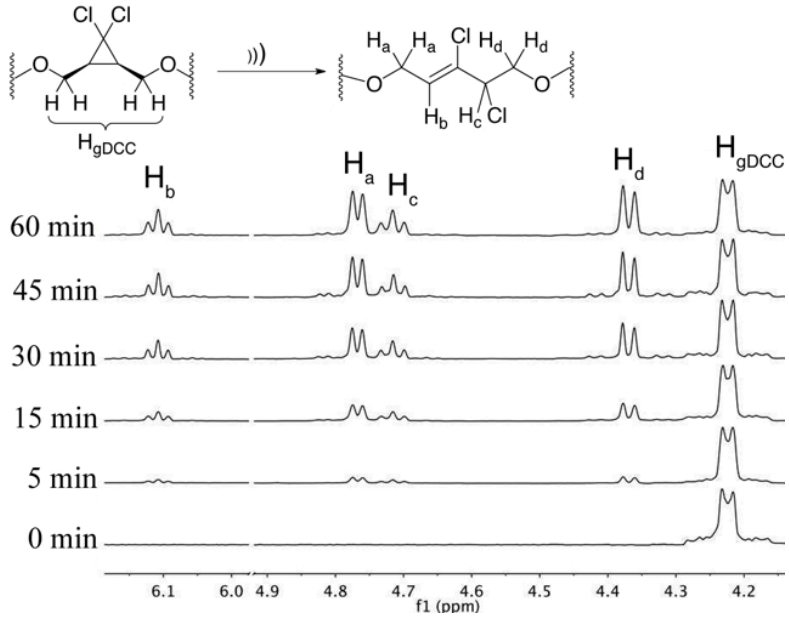

Figure 82 Mechanochemical activation of gDCC mechanophores by ^{1}H NMR with increasing sonication times.

During the course of these studies, we noted a dramatic increase in the stability of **Polymer 3** compared to analogous polybutadiene based systems. In our experience, casual handling of polybutadiene or ROMP derived *g*DHC polymers, tends to result in a loss of solubility over time, often in less than one week, but we were able to dissolve and characterize **Polymer 3** after one month at room temperature in the presence of light with no measurable change in MW or ^{1}H NMR spectrum. The lack of olefin functionality

can most likely be credited with this increase in stability, which in our experience is similar to that of simple acrylate polymers synthesized by copper catalyzed CRP.

A.3 Conclusion

In conclusion, we have developed a versatile method for the abundant incorporation of cyclic mechanophores into high MW block copolymers. The ABA architecture ensures a mechanophore rich region about the center of the chain, allowing for large amounts of sonochemical activation. The polymer system described here also exhibits excellent long-term stability, potentially enabling extended quantitative studies, a previously tedious task, with a wider variety of systems. Additionally, CRP approaches to block copolymer synthesis potentially allow for a wide variety of phase-segregated microstructures and bulk mechanical properties to be generated. The general nature of the carbodiimide polyesterification procedure as well as the near ubiquitous use of SET-LRP conditions in the synthesis of mechanophore linked polymers will provide the opportunity to apply this approach to a variety of mechanochemical systems and enable the generation of functional, stress-responsive materials. Most intriguing in this regard are non-scissile cyclic mechanophores, which are the basis for mechanochemical remodeling in polymeric systems.[121]

A.4 Experimental

A.4.1 Materials and Methods

Diol 1[237] and *4*-(Dimethylamino)pyridinium-*4*-toluenesulfonate (DPTS)[141] were synthesized as previously described. Methyl acrylate was purchased from Sigma Aldrich and passed through a short column of basic alumina to remove inhibitor. Dry solvents (THF and DCM) were obtained from a Pure Solv™ solvent purification system. All other reagents were purchased from Sigma Aldrich and used without further purification.

Gel Permeation Chromatography (GPC) was performed on an in-line two column system (Agilent Technology PL gel, 10^3 and 10^4 Å) using inhibitor-free tetrahydrofuran (THF) as mobile phase. Molecular weights were calculated using an inline Wyatt Dawn EOS multi-angle light scattering (MALS) detector and a Wyatt Optilab DSP Interferometric Refractometer (RI). The dn dc^{-1} values were determined by on-line calculation using injections of known concentration and mass. ^{1}H NMR was conducted on either a 400 MHz or 500 MHz Varian spectrophotometer and the residual solvent peak ($CDCl_3$, 7.26 ppm) was used as the chemical shift reference. Fourier transform infrared spectroscopy was performed on a Nicolet 6700 FT-IR spectrophotometer.

Ultrasound experiments were performed in acetonitrile on a Vibracell Model VCX500 operating at 20 kHz with a 13.1 mm replaceable titanium tip probe from Sonics

and Materials. Sonications were performed at polymer concentrations of 2.5 mg mL^{-1} in 16 mL of acetonitrile. Solutions were sparged with bubbling N_2 for the thirty minutes prior to sonication. Sonications were performed at 6-9 °C in an ice-water bath at 35% amplitude (~12.5 W cm^{-2}) with a pulse sequence of 1 s on/1 s off.

A.4.2 Synthesis and characterization

Synthesis of Polymer 1:

Using a modified procedure by Moore and Stupp:[141] Diol **1** (1.00 g, 5.85 mmol), glutaric acid (772 mg, 5.85 mmol), and DPTS (687 mg, 2.34 mmol) were added to a 25 mL 2-neck round bottom flask and flushed with argon. Dry CH_2Cl_2 (10 mL) was added by syringe and the solution was heated to 37 ^oC while stirring until solution became homogenous. After cooling to room temperature, DIC (2.73 mL, 17.6 mmol) was added dropwise by syringe and the solution was allowed to stir under argon for 24 hours. An additional portion of Diol **1** (200 mg, 1.16 mmol) and DIC (0.91 mL, 5.85 mmol) were added to ensure hydroxy end-functionalization. The solution was allowed to stir for an additional 24 hours then precipitated twice from CH_2Cl_2 into MeOH to yield 698 mg (44% based on initial monomer mass minus 11.7 mmol (187 mg) H_2O) of a white gummy polymer. **^{1}H NMR** (400 MHz, $CDCl_3$) δ = 4.20-4.30 (br d, 4H), 2.43-2.49 (br t, 4H), 2.10-2.17 (br t, 2H), 1.95-2.04 (br m, 2H); **^{13}C NMR** (101 MHz, $CDCl_3$) δ = 172.20, 61.46, 59.98, 32.72, 30.79, 19.75; **GPC-MALS**: M_n = 21,500, PDI = 1.70, dn dc^{-1} = 0.072.

Synthesis of Polymer 2:

Polymer 1 (626 mg, 0.029 mmol) was dissolved in 5 mL dry THF in a 10 mL round bottom flask with stirbar. After purging with argon, triethylamine (0.061 mL, 0.44 mmol) was added and the solution cooled to 0 ^{o}C. Bromoisobutyryl bromide (0.036 mL, 29 mmol) was added dropwise and the solution was allowed to warm to room temperature and stir overnight. The solution was precipitated into MeOH, redissolved in CH_2Cl_2 and reprecipitated into MeOH to yield 426 mg (68%) of a white gummy polymer. **^{1}H NMR** (500 MHz, $CDCl_3$) δ = 4.20-4.30 (br d, 4H), 2.43-2.49 (br t, 4H), 2.10-2.17 (br t, 2H), 1.95-2.04 (br m, 2H); **^{13}C NMR** (101 MHz, $CDCl_3$) δ = 172.39, 61.56, 60.17, 32.91, 30.97, 19.91; **GPC-MALS**: M_n = 26,200, PDI = 1.50, dn dc^{-1} = 0.072.

Synthesis of Polymer 3

Polymer 2 (100 mg, 0.0047 mmol) was dissolved in 2 mL DMSO in a 10 mL Schlenk flask with a stirbar wrapped in copper wire (~2 cm, 20 gauge). Methyl acrylate (0.980 mL, 10.8 mmol) was added and the solution was subjected to three freeze-pump-thaw cycles. After the final cycle, the flask was placed in a water bath thermostated at 25 ^{o}C and Me_6TREN (1.4 μL, 0.0094 mmol) was added by microsyringe and the solution was allowed to stir under argon for 1 hour. The polymerization was stopped by exposing to air and the solution was diluted with DCM and twice precipitated into cold MeOH to yield 401 mg (77% based on conversion) of a white gummy polymer. **^{1}H NMR**

(400 MHz, $CDCl_3$) δ = 4.20-4.30 (br d, 4H), 3.59-3.72 (br s, 41H, PMA) 2.43-2.49 (br t, 4H), 2.25-2.40 (br, 14H, PMA), 2.10-2.17 (br t, 2H), 1.95-2.04 (br m, 2H), 1.85-2.00 (br, 7 H, PMA), 1.60-1.75 (br, 14 H, PMA), 1.35-1.60 (br, 7 H, PMA); **^{13}C NMR** (101 MHz, $CDCl_3$) δ = 174.85, 172.44, 61.57, 60.22, 51.72, 41.25, 34.92, 32.95, 31.01, 19.95; **GPC-MALS**: M_n = 136,000, PDI = 1.17, dn dc^{-1} = 0.069.

A.4.3 Sonication of Polymer 3

Polymer 3 (40 mg) was dissolved in 16 mL of acetonitrile. The solution was sparged with bubbling N_2 for the thirty minutes prior to sonication. Sonications were performed at 6-9 ^oC in an ice-water bath at 35% amplitude (~12.5 $W*cm^{-2}$) with a pulse sequence of 1s on/1s off under N_2. After the appropriate time, sonication was stopped and the solutions were evaporated to a minimal volume and precipitated into cold MeOH. Samples were dried under high vacuum and subjected to analysis by GPC-MALS and NMR. Representative data shown for 1 hour sonication time (55% ring opening, 1 scission cycle). **^{1}H NMR** (400 MHz, $CDCl_3$) δ = 6.06-6.14 (br t, 0.55H), 4.75-4.82 (br, d, 1.1H), 4.68-4.75 (br t, 0.55 H), 4.30-4.40 (br d, 1.1H) 4.20-4.30 (br d, 1.8H), 3.59-3.72 (br s, 41H, PMA) 2.43-2.49 (br t, 4H), 2.25-2.40 (br, 14H, PMA), 2.10-2.17 (br t, 1H), 1.95-2.04 (br m, 2H), 1.85-2.00 (br, 7 H, PMA), 1.60-1.75 (br, 14 H, PMA), 1.35-1.60 (br, 7 H, PMA); **^{13}C NMR** (101 MHz, $CDCl_3$) δ = 174.94, 172.53, 172.08, 133.23, 126.63, 64.71, 61.63, 60.93, 60.30, 59.75, 51.80, 41.33, 41.17, 35.79, 35.00, 34.31, 32.90, 31.09, 19.91; **GPC-MALS**: M_n = 68,400, PDI = 1.18, dn dc^{-1} = 0.069.

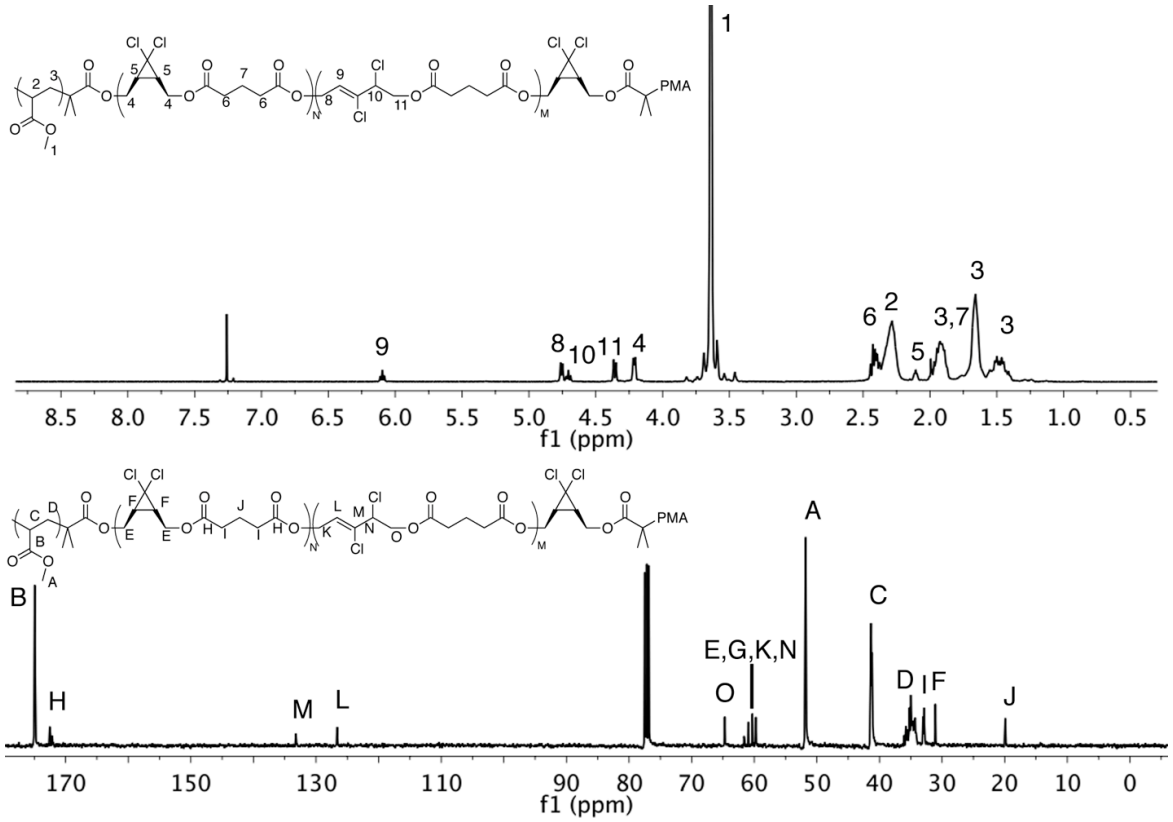

Figure 83 ^{1}H NMR spectrum before (top) and after (bottom) sonication of **Polymer 3.**

References

1. Fridlyand, K. Y., Zhizhenkov, V. V., Egorov, E. A. & Vettegren, V. I. Influence of molecular-interactions on mechanical stresses distribution along chemical bonds in polymers. *Vysokomol. Soedin., Ser. A* (1976) **18**, 1534-1539.

2. Friedland, K. J., Marikhin, V. A., Myasnikova, L. P. & Vettegren, V. I. Supermolecular structure and mechanical-stress distribution among chemical bonds in polymers. *J. Polym. Sci., Part C: Polym. Symp.* (1977), 185-194.

3. Vettegren, V. I., Vorobev, V. M. & Fridlyand, K. Length of overstressed sections of polymer-molecules. *Vysokomol. Soedin., Ser. B* (1977) **19**, 266-268.

4. Voroboyev, V. M., Razumovskaya, I. V. & Vettegren, V. I. Deformation of interatomic bonds in polymers. *Polymer* (1978) **19**, 1267-1272.

5. Flory, P. J. Network topology and the theory of rubber elasticity. *Br. Polym. J.* (1985) **17**, 96-102.

6. Flory, P. J. *Principles of polymer chemistry*. Cornell University Press (1953).

7. Shaw, M. T. & MacKnight, W. J. *Introduction to polymer viscoelasticity*. Wiley-Interscience (2005).

8. Kausch, H. H. & Plummer, C. J. G. The role of individual chains in polymer deformation. *Polymer* (1994) **35**, 3848-3857.

9. Porter, R. S. & Johnson, J. F. The Entanglement Concept in Polymer Systems. *Chem. Rev.* (1966) **66**, 1-27.

10. Wool, R. P. *Polymer interfaces: structure and strength*. Hanser Publishers (1995).

11. Isono, Y., Itoh, K., Komiyatani, T. & Fujimoto, T. Differential dynamic modulus of polyisobutylene with high molecular weight. 1. Single-step large shearing deformations. *Macromolecules* (1991) **24**, 4429-4432.

12. Offenbach, J. A. & Tobolsky, A. V. Chemical relaxation of stress in polyurethane elastomers. *J. Colloid Sci.* (1956) **11**, 39-47.

13. Porter, R. S. & Casale, A. Recent studies of polymer reactions caused by stress. *Polym. Eng. Sci.* (1985) **25**, 129-156.

14. Staudinger, H. & Heuer, W. High polymer compounds, 93. Announcement. Decomposition of thread molecules of polystyrene. *Ber. Dtsch. Chem. Ges.* (1934) **67**, 1159-1164.

15. Staudinger, H. & Leupold, E. O. On isoprene and caoutchuc, 18. Announcement: Viscosity-research on Balata. *Ber. Dtsch. Chem. Ges.* (1930) **63**, 730-733.

16. Staudinger, H. & Bondy, H. F. On isoprene and caoutchuc, 19. Announcement: On the molecular size of caoutchuc and Balata. *Ber. Dtsch. Chem. Ges.* (1930) **63**, 734-736.

17. Caruso, M. M. *et al.* Mechanically-Induced Chemical Changes in Polymeric Materials. *Chem. Rev.* (2009) **109**, 5755-5798.

18. Black, A. L., Lenhardt, J. M. & Craig, S. L. From molecular mechanochemistry to stress-responsive materials. *J. Mater. Chem.* (2011) **21**, 1655-1663.

19. Kauzmann, W. & Eyring, H. The Viscous Flow of Large Molecules. *J. Am. Chem. Soc.* (1940) **62**, 3113-3125.

20. Billmeyer, F. W. Polymer stress reactions. *J. Polym. Sci., Polym. Lett. Ed.* (1978) **16**, 616-617.

21. Junkichi, S. Mechanochemistry of polymers. *Prog. Polym. Sci.* (1989) **14**, 451-596.

22. Beyer, M. K. & Clausen-Schaumann, H. Mechanochemistry: The Mechanical Activation of Covalent Bonds. *Chem. Rev.* (2005) **105**, 2921-2948.

23. May, P. A. & Moore, J. S. Polymer mechanochemistry: techniques to generate molecular force via elongational flows. *Chem. Soc. Rev.* (2013) **42**, 7497-7506.

24. Paulusse, J. M. J. & Sijbesma, R. P. Selectivity of mechanochemical chain scission in mixed palladium(ii) and platinum(ii) coordination polymers. *Chem. Commun.* (2008), 4416-4418.

25. Paulusse, J. M. J., Huijbers, J. P. J. & Sijbesma, R. P. Quantification of Ultrasound-Induced Chain Scission in PdII–Phosphine Coordination Polymers. *Chem. Eur. J.* (2006) **12**, 4928-4934.

26. Kersey, F. R., Yount, W. C. & Craig, S. L. Single-molecule force spectroscopy of bimolecular reactions: System homology in the mechanical activation of ligand substitution reactions. *J. Am. Chem. Soc.* (2006) **128**, 3886-3887.

27. Encina, M. V., Lissi, E., Sarasúa, M., Gargallo, L. & Radic, D. Ultrasonic degradation of polyvinylpyrrolidone: Effect of peroxide linkages. *J. Polym. Sci., Polym. Lett. Ed.* (1980) **18**, 757-760.

28. Berkowski, K. L., Potisek, S. L., Hickenboth, C. R. & Moore, J. S. Ultrasound-induced site-specific cleavage of azo-functionalized poly(ethylene glycol). *Macromolecules* (2005) **38**, 8975-8978.

29. Hickenboth, C. R., Rule, J. D. & Moore, J. S. Preparation of enediyne-crosslinked networks and their reactivity under thermal and mechanical conditions. *Tetrahedron* (2008) **64**, 8435-8448.

30. Hickenboth, C. R. *et al.* Biasing reaction pathways with mechanical force. *Nature* (2007) **446**, 423-427.

31. Kingsbury, C. M. *et al.* Shear activation of mechanophore-crosslinked polymers. *J. Mater. Chem.* (2011) **21**, 8381-8388.

32. Lee, C. K. *et al.* Force-Induced Redistribution of a Chemical Equilibrium. *J. Am. Chem. Soc.* (2010) **132**, 16107-16111.

33. Potisek, S. L., Davis, D. A., Sottos, N. R., White, S. R. & Moore, J. S. Mechanophore-linked addition polymers. *J. Am. Chem. Soc.* (2007) **129**, 13808-13809.

34. Beiermann, B. A. *et al.* Environmental effects on mechanochemical activation of spiropyran in linear PMMA. *J. Mater. Chem.* (2011) **21**, 8443-8447.

35. Silberstein, M. N. *et al.* Modeling mechanophore activation within a crosslinked glassy matrix. *J. Appl. Phys.* (2013) **114**, 023504.

36. Karthikeyan, S., Potisek, S. L., Piermattei, A. & Sijbesma, R. P. Highly Efficient Mechanochemical Scission of Silver-Carbene Coordination Polymers. *J. Am. Chem. Soc.* (2008) **130**, 14968-14969.

37. Piermattei, A., Karthikeyan, S. & Sijbesma, R. P. Activating catalysts with mechanical force. *Nat. Chem.* (2009) **1**, 133-137.

38. Groote, R., Jakobs, R. T. M. & Sijbesma, R. P. Mechanocatalysis: forcing latent catalysts into action. *Polym. Chem.* (2013) **4**, 4846-4859.

39. Wiggins, K. M., Syrett, J. A., Haddleton, D. M. & Bielawski, C. W. Mechanically Facilitated Retro [4 + 2] Cycloadditions. *J. Am. Chem. Soc.* (2011) **133**, 7180-7189.

40. Church, D. C., Peterson, G. I. & Boydston, A. J. Comparison of Mechanochemical Chain Scission Rates for Linear versus Three-Arm Star Polymers in Strong Acoustic Fields. *ACS Macro Lett.* (2014) **3**, 648-651.

41. Chen, X., Wudl, F., Mal, A. K., Shen, H. & Nutt, S. R. New Thermally Remendable Highly Cross-Linked Polymeric Materials. *Macromolecules* (2003) **36**, 1802-1807.

42. Koti Ainavarapu, S. R., Wiita, A. P., Dougan, L., Uggerud, E. & Fernandez, J. M. Single-Molecule Force Spectroscopy Measurements of Bond Elongation during a Bimolecular Reaction. *J. Am. Chem. Soc.* (2008) **130**, 6479-6487.

43. Kucharski, T. J. & Boulatov, R. The physical chemistry of mechanoresponsive polymers. *J. Mater. Chem.* (2011) **21**, 8237-8255.

44. Kucharski, T. J. *et al.* Kinetics of Thiol/Disulfide Exchange Correlate Weakly with the Restoring Force in the Disulfide Moiety. *Angew. Chem. Int. Ed.* (2009) **48**, 7040-7043.

45. Yang, Q. Z. *et al.* A molecular force probe. *Nat. Nanotechnol.* (2009) **4**, 302-306.

46. Steenwinkel, P. *et al.* Intramolecularly Stabilized 1,4-Phenylene-Bridged Homo- and Heterodinuclear Palladium and Platinum Organometallic Complexes... *Organometallics* (1998) **17**, 5411-5426.

47. Rodriguez, G. *et al.* Bifunctional Pincer-type Organometallics as Substrates for Organic Transformations and as Novel Building Blocks for Polymetallic Materials. *J. Am. Chem. Soc.* (2002) **124**, 5127-5138.

48. Slagt, M. Q., Klein Gebbink, R. J. M., Lutz, M., Spek, A. L. & van Koten, G. Synthetic strategies towards new para-functionalised NCN-pincer palladium(ii) and platinum(ii) complexes. *J. Chem. Soc., Dalton Trans.* (2002), 2591-2592.

49. Serpe, M. J. & Craig, S. L. Physical organic chemistry of supramolecular polymers. *Langmuir* (2007) **23**, 1626-1634.

50. Loveless, D. M., Jeon, S. L. & Craig, S. L. Rational control of viscoelastic properties in multicomponent associative polymer networks. *Macromolecules* (2005) **38**, 10171-10177.

51. Loveless, D. M., Jeon, S. L. & Craig, S. L. Chemoresponsive viscosity switching of a metallo-supramolecular polymer network near the percolation threshold. *J. Mater. Chem.* (2007) **17**, 56-61.

52. Yount, W. C., Loveless, D. M. & Craig, S. L. Small-molecule dynamics and mechanisms underlying the macroscopic mechanical properties of coordinatively cross-linked polymer networks. *J. Am. Chem. Soc.* (2005) **127**, 14488-14496.

53. Yount, W. C., Loveless, D. M. & Craig, S. L. Strong means slow: Dynamic contributions to the bulk mechanical properties of supramolecular networks. *Angew. Chem., Int. Ed.* (2005) **44**, 2746-2748.

54. Kersey, F. R., Loveless, D. M. & Craig, S. L. A hybrid polymer gel with controlled rates of cross-link rupture and self-repair. *J. R. Soc., Interface* (2007) **4**, 373-380.

55. Xu, D. H. & Craig, S. L. Multiple Dynamic Processes Contribute to the Complex Steady Shear Behavior of Cross-Linked Supramolecular Networks of Semidilute Entangled Polymer Solutions. *J. Phys. Chem. Lett.* (2010) **1**, 1683-1686.

56. Xu, D. H., Hawk, L. L., Loveless, D. M., Jeon, S. L. & Craig, S. L. Mechanism of Shear Thickening in Reversibly Cross-Linked Supramolecular Polymer Networks. *Macromolecules* (2010) **43**, 3556-3565.

57. Xu, D. H., Liu, C. Y. & Craig, S. L. Divergent Shear Thinning and Shear Thickening Behavior of Supramolecular Polymer Networks in Semidilute Entangled Polymer Solutions. *Macromolecules* (2011) **44**, 2343-2353.

58. Tashiro, K., Wu, G. & Kobayashi, M. Morphological effect on the Raman frequency shift induced by tensile stress applied to crystalline polyoxymethylene and polyethylene: spectroscopic support for the idea of an inhomogeneous stress distribution in polymer material. *Polymer* (1988) **29**, 1768-1778.

59. Gamstedt, E. K. & Talreja, R. Fatigue damage mechanisms in unidirectional carbon-fibre-reinforced plastics. *J. Mater. Sci.* (1999) **34**, 2535-2546.

60. Ortiz, C. & Hadziioannou, G. Entropic Elasticity of Single Polymer Chains of Poly(methacrylic acid) Measured by Atomic Force Microscopy. *Macromolecules* (1999) **32**, 780-787.

61. Zhulina, E., Walker, G. C. & Balazs, A. C. Modeling the Interactions between Atomic Force Microscope Tips and Polymeric Substrates. *Langmuir* (1998) **14**, 4615-4622.

62. Florin, E., Moy, V. & Gaub, H. Adhesion forces between individual ligand-receptor pairs. *Science* (1994) **264**, 415-417.

63. Rief, M., Gautel, M., Oesterhelt, F., Fernandez, J. M. & Gaub, H. E. Reversible Unfolding of Individual Titin Immunoglobulin Domains by AFM. *Science* (1997) **276**, 1109-1112.

64. Grandbois, M., Beyer, M., Rief, M., Clausen-Schaumann, H. & Gaub, H. E. How Strong Is a Covalent Bond? *Science* (1999) **283**, 1727-1730.

65. Tennyson, A. G., Wiggins, K. M. & Bielawski, C. W. Mechanical Activation of Catalysts for C-C Bond Forming and Anionic Polymerization Reactions from a Single Macromolecular Reagent. *J. Am. Chem. Soc.* (2010) **132**, 16631-16636.

66. Wiggins, K. M., Hudnall, T. W., Tennyson, A. G. & Bielawski, C. W. Selective scission of pyridine-boronium complexes: mechanical generation of Bronsted bases and polymerization catalysts. *J. Mater. Chem.* (2011) **21**, 8355-8359.

67. Makosza, M. & Wawrzyniewicz, M. Reactions of organic anions. XXIV. Catalytic method for preparation of dichlorocyclopropane derivatives in aqueous medium. *Tetrahedron Lett.* (1969) **10**, 4659-4662.

68. Sonnenberg, J. & Winstein, S. Rearrangement of 6,6-Dibromobicyclo[3.1.0]hexane. *J. Org. Chem.* (1962) **27**, 748-751.

69. Selms, R. C. D. & Combs, C. M. Addition Products of Dichlorocarbene to Norbornylene and Norbornadiene and Their Rearrangements. *J. Org. Chem.* (1963) **28**, 2206-2210.

70. Ghosez, L., Slinckx, G., Glineur, M., Hoet, P. & Laroche, P. Stereochemistry of the cyclopropyl-allyl rearrangements. : II. Thermal ring opening of the chlorofluorocarbene-norbornene adducts. *Tetrahedron Lett.* (1967) **8**, 2773-2776.

71. Pinazzi, C. & Levesque, G. Addition De Dihalocarbenes Sur Les Cis-1.4 Polyisoprenes Et Sur Quelques Polyenes Analogues. *C. R. Hebd. Seances Acad. Sci.* (1965) **260**, 3393.

72. Pinazzi, M. C. P., Villette, J. P. & Pleurdea.A. Modification of Polydienes by Dihalocarbenes - Study of 3,4-Polyisoprene Molecular Model. *Eur. Polym. J.* (1973) **9**, 1121-1126.

73. Dewitt, W. G., Hurwitz, M. J. & Albright, F. Preparation and Properties of Polyisoprene-Dichlorocarbene Adduct. *J. Polym. Sci., Part A-1: Polym. Chem.* (1969) **7**, 2453-2455.

74. Bradbury, J. H. & Perera, M. C. S. Dichlorocarbene Modified Natural Rubber. *Br. Polym. J.* (1986) **18**, 127-134.

75. Sang, S. T. M. *J. Rubb. Res. Inst. Malaysia* (1978) **26**, 48.

76. Schmid, J. & Rommel, O. *Z. Physikal. Chem.* (1939) **185**, 97.

77. Price, G. J. & Smith, P. F. Ultrasonic Degradation of Polymer Solutions .1. Polystyrene Revisited. *Polym. Int.* (1991) **24**, 159-164.

78. Price, G. J. & Smith, P. F. Ultrasonic Degradation of Polymer Solutions .2. The Effect of Temperature, Ultrasound Intensity and Dissolved-Gases on Polystyrene in Toluene. *Polymer* (1993) **34**, 4111-4117.

79. Koda, S., Mori, H., Matsumoto, K. & Nomura, H. Ultrasonic degradation of water-soluble polymers. *Polymer* (1994) **35**, 30-33.

80. Frenkel, J. Orientation and rupture of linear macromolecules in dilute solutions under the influence of viscous flow. *Acta Physicochim. URSS* (1944) **19**, 51-76.

81. Price, G. J. & Smith, P. F. Ultrasonic Degradation of Polymer Solutions .3. The Effect of Changing Solvent and Solution Concentration. *Eur. Polym. J.* (1993) **29**, 419-424.

82. Doulah, M. S. A proposed mechanism for the degradation of addition polymers in cavitating ultrasonic fields. *J. Appl. Polym. Sci.* (1978) **22**, 1735-1743.

83. Komoroski, R. A., Horne, S. E. & Carman, C. J. Carbon-13 NMR microstructural characterization of dichlorocarbene adducts of polybutadiene. *J. Polym. Sci., Polym. Chem. Ed.* (1983) **21**, 89-96.

84. Lenhardt, J. M., Black, A. L. & Craig, S. L. gem-Dichlorocyclopropanes as Abundant and Efficient Mechanophores in Polybutadiene Copolymers under Mechanical Stress. *J. Am. Chem. Soc.* (2009) **131**, 10818-10819.

85. Suslick, K. S. *et al.* Acoustic cavitation and its chemical consequences. *Philos. Trans. R. Soc., A* (1999) **357**, 335-353.

86. Parham, W. E. & Yong, K. S. Steric and electronic effects in the solvolysis of cis- and trans- mono- and dihalocyclopropanes. *J. Org. Chem.* (1970) **35**, 683-685.

87. Ong, M. T., Leiding, J., Tao, H. L., Virshup, A. M. & Martinez, T. J. First Principles Dynamics and Minimum Energy Pathways for Mechanochemical Ring Opening of Cyclobutene. *J. Am. Chem. Soc.* (2009) **131**, 6377-6379.

88. Wu, D., Lenhardt, J. M., Black, A. L., Akhremitchev, B. B. & Craig, S. L. Molecular Stress Relief through a Force-Induced Irreversible Extension in Polymer Contour Length. *J. Am. Chem. Soc.* (2010) **132**, 15936-15938.

89. Bustamante, C., Smith, S. B., Liphardt, J. & Smith, D. Single-molecule studies of DNA mechanics. *Curr. Opin. Struct. Biol.* (2000) **10**, 279-285.

90. Lake, G. J. & Thomas, A. G. The Strength of Highly Elastic Materials. *Proc. R. Soc. London, Ser. A* (1967) **300**, 108-119.

91. Huang, Z. & Boulatov, R. Chemomechanics with molecular force probes. *Pure Appl. Chem.* (2010) **82**, 931-951.

92. Ribas-Arino, J., Shiga, M. & Marx, D. Understanding Covalent Mechanochemistry. *Angew. Chem. Int. Ed.* (2009) **48**, 4190-4193.

93. Ribas-Arino, J., Shiga, M. & Marx, D. Mechanochemical Transduction of Externally Applied Forces to Mechanophores. *J. Am. Chem. Soc.* (2010) **132**, 10609-10614.

94. Konda, S. S. M., Brantley, J. N., Bielawski, C. W. & Makarov, D. E. Chemical reactions modulated by mechanical stress: Extended Bell theory. *J. Chem. Phys.* (2011) **135**, 164103-164108.

95. Klukovich, H. M., Kouznetsova, T. B., Kean, Z. S., Lenhardt, J. M. & Craig, S. L. A backbone lever-arm effect enhances polymer mechanochemistry. *Nat. Chem.* (2013) **5**, 110-114.

96. Lenhardt, J. M. *et al.* Characterizing the mechanochemically active domains in gem-dihalocyclopropanated polybutadiene under compression and tension. *J. Mater. Chem.* (2011) **21**, 8454-8459.

97. Woodward, R. B. & Hoffmann, R. Stereochemistry of Electrocyclic Reactions. *J. Am. Chem. Soc.* (1965) **87**, 395-397.

98. Woodward, R. B. & Hoffmann, R. The Conservation of Orbital Symmetry. *Angew. Chem. Int. Ed.* (1969) **8**, 781-853.

99. DePuy, C. H. Cyclopropanols. *Acc. Chem. Res.* (1968) **1**, 33-41.

100. Duffey, D. C., Gueldner, R. C., Layton, B. R. & Minyard, J. P. Structure assignments and reactivities of bromochlorocarbene-olefin adducts. *J. Org. Chem.* (1977) **42**, 1082-1085.

101. Mark, J. E. *Physical properties of polymers handbook*. Springer (2007).

102. Black Ramirez, A. L. *et al.* Microstructure of Copolymers Formed by the Reagentless, Mechanochemical Remodeling of Homopolymers via Pulsed Ultrasound. *ACS Macro Lett.* (2011), 23-27.

103. Black, A. L., Orlicki, J. A. & Craig, S. L. Mechanochemically triggered bond formation in solid-state polymers. *J. Mater. Chem.* (2011) **21**, 8460-8465.

104. Dolbier, W. R. Thermal rearrangements of gem-difluorocyclopropanes. *Acc. Chem. Res.* (1981) **14**, 195-200.

105. Lenhardt, J. M. *et al.* Trapping a Diradical Transition State by Mechanochemical Polymer Extension. *Science* (2010) **329**, 1057-1060.

106. Sobek, J., Martschke, R. & Fischer, H. Entropy control of the cross-reaction between carbon-centered and nitroxide radicals. *J. Am. Chem. Soc.* (2001) **123**, 2849-2857.

107. Lenhardt, J. M. *et al.* Reactive Cross-Talk between Adjacent Tension-Trapped Transition States. *J. Am. Chem. Soc.* (2011) **133**, 3222-3225.

108. Klukovich, H. M., Kean, Z. S., Iacono, S. T. & Craig, S. L. Mechanically Induced Scission and Subsequent Thermal Remending of Perfluorocyclobutane Polymers. *J. Am. Chem. Soc.* (2011) **133**, 17882-17888.

109. Cordier, P., Tournilhac, F., Soulie-Ziakovic, C. & Leibler, L. Self-healing and thermoreversible rubber from supramolecular assembly. *Nature* (2008) **451**, 977-980.

110. Sheiko, S. S. *et al.* Adsorption-induced scission of carbon-carbon bonds. *Nature* (2006) **440**, 191-194.

111. Lebedeva, N. V., Sun, F. C., Lee, H. I., Matyjaszewski, K. & Sheiko, S. S. "Fatal Adsorption" of brushlike macromolecules: High sensitivity of C-C bond cleavage rates to substrate surface energy. *J. Am. Chem. Soc.* (2008) **130**, 4228-4229.

112. Ramirez, A. L. B. *et al.* Mechanochemical strengthening of a synthetic polymer in response to typically destructive shear forces. *Nat. Chem.* (2013) **5**, 757–761.

113. Kean, Z. S., Black Ramirez, A. L., Yan, Y. & Craig, S. L. Bicyclo[3.2.0]heptane Mechanophores for the Non-scissile and Photochemically Reversible Generation of Reactive Bis-enones. *J. Am. Chem. Soc.* (2012) **134**, 12939-12942.

114. Kean, Z. S., Niu, Z., Hewage, G. B., Rheingold, A. L. & Craig, S. L. Stress-Responsive Polymers Containing Cyclobutane Core Mechanophores: Reactivity and Mechanistic Insights. *J. Am. Chem. Soc.* (2013) **135**, 13598-13604.

115. Kean, Z. S. *et al.* Increasing the Maximum Achievable Strain of a Covalent Polymer Gel Through the Addition of Mechanically Invisible Cross-Links. *Adv. Mater.* (2014) **26**, 6013-6018.

116. Zhao, X. Multi-scale multi-mechanism design of tough hydrogels: building dissipation into stretchy networks. *Soft Matter* (2014) **10**, 672-687.

117. Lake, G. J. & Thomas, A. G. The Strength of Highly Elastic Materials. *Proc. R. Soc. London, Ser. A* (1967) **300**, 108-119.

118. Kean, Z. S. *et al.* Photomechanical Actuation of Ligand Geometry in Enantioselective Catalysis. *Angew. Chem., Int. Ed.* (2014), DOI: 10.1002/anie.201407494.

119. Gossweiler, G. R. *et al.* Mechanochemical Activation of Covalent Bonds in Polymers with Full and Repeatable Macroscopic Shape Recovery. *ACS Macro Lett.* (2014) **3**, 216-219.

120. Silberstein, M. N. *et al.* Modeling mechanophore activation within a crosslinked glassy matrix. *J. Appl. Phys.* (2013) **114**.

121. Kean, Z. S. & Craig, S. L. Mechanochemical remodeling of synthetic polymers. *Polymer* (2012) **53**, 1035-1048.

122. Klukovich, H. M. *et al.* Tension Trapping of Carbonyl Ylides Facilitated by a Change in Polymer Backbone. *J. Am. Chem. Soc.* (2012) **134**, 9577-9580.

123. Kryger, M. J., Munaretto, A. M. & Moore, J. S. Structure–Mechanochemical Activity Relationships for Cyclobutane Mechanophores. *J. Am. Chem. Soc.* (2011) **133**, 18992-18998.

124. Ischay, M. A., Anzovino, M. E., Du, J. & Yoon, T. P. Efficient Visible Light Photocatalysis of [2+2] Enone Cycloadditions. *J. Am. Chem. Soc.* (2008) **130**, 12886-12887.

125. Lligadas, G., Rosen, B. M., Monteiro, M. J. & Percec, V. Solvent Choice Differentiates SET-LRP and Cu-Mediated Radical Polymerization with Non-First-Order Kinetics. *Macromolecules* (2008) **41**, 8360-8364.

126. Kryger, M. J. *et al.* Masked Cyanoacrylates Unveiled by Mechanical Force. *J. Am. Chem. Soc.* (2010) **132**, 4558-4559.

127. Jung, M. E. in *Comprehensive Organic Synthesis*. Pergamon (1991).

128. Rosen, B. M., Lligadas, G., Hahn, C. & Percec, V. Synthesis of dendritic macromolecules through divergent iterative thio-bromo "Click" chemistry and SET-LRP. *J. Polym. Sci., Part A: Polym. Chem.* (2009) **47**, 3940-3948.

129. Beyer, M. K. The mechanical strength of a covalent bond calculated by density functional theory. *J. Chem. Phys.* (2000) **112**, 7307-7312.

130. Kean, Z. S., Ramirez, A. L. B. & Craig, S. L. High mechanophore content polyester-acrylate ABA block copolymers: Synthesis and sonochemical activation. *J. Polym. Sci., Part A: Polym. Chem.* (2012) **50**, 3481-3484.

131. Ciampolini, M. & Nardi, N. Five-Coordinated High-Spin Complexes of Bivalent Cobalt, Nickel, and Copper with Tris(2-dimethylaminoethyl)amine. *Inorg. Chem.* (1966) **5**, 41-44.

132. Podzimek, S. *Light Scattering, Size Exclusion Chromatography and Asymmetric Flow Field Flow Fractionation: Powerful Tools for the Characterization of Polymers, Proteins and Nanoparticles*. John Wiley & Sons (2011).

133. Beyer, M. K. The mechanical strength of a covalent bond calculated by density functional theory. *J. Chem. Phys.* (2000) **112**, 7307-7312.

134. Wiggins, K. M., Brantley, J. N. & Bielawski, C. W. Polymer Mechanochemistry: Force Enabled Transformations. *ACS Macro Lett.* (2012) **1**, 623-626.

135. Davis, D. A. *et al.* Force-induced activation of covalent bonds in mechanoresponsive polymeric materials. *Nature* (2009) **459**, 68-72.

136. Chen, Y. *et al.* Mechanically induced chemiluminescence from polymers incorporating a 1,2-dioxetane unit in the main chain. *Nat. Chem.* (2012) **4**, 559-562.

137. Akbulatov, S., Tian, Y. & Boulatov, R. Force–Reactivity Property of a Single Monomer Is Sufficient To Predict the Micromechanical Behavior of Its Polymer. *J. Am. Chem. Soc.* (2012) **134**, 7620-7623.

138. Akbulatov, S., Tian, Y., Kapustin, E. & Boulatov, R. Model Studies of the Kinetics of Ester Hydrolysis under Stretching Force. *Angew. Chem. Int. Ed.* (2013) **52**, 6992-6995.

139. Hermes, M. & Boulatov, R. The Entropic and Enthalpic Contributions to Force-Dependent Dissociation Kinetics of the Pyrophosphate Bond. *J. Am. Chem. Soc.* (2011) **133**, 20044-20047.

140. Larsen, M. B. & Boydston, A. J. “Flex-Activated” Mechanophores: Using Polymer Mechanochemistry To Direct Bond Bending Activation. *J. Am. Chem. Soc.* (2013) **135**, 8189-8192.

141. Moore, J. S. & Stupp, S. I. Room temperature polyesterification. *Macromolecules* (1990) **23**, 65-70.

142. Schenck, G. O., Kuhls, J. & Krauch, C. H. Photosensibilisierte Carbocycloadditionen von Philodienen an Konjugene zu Cyclobutan-Derivaten und exo-Diels-Alder-Addukten. *Justus Liebigs Ann. Chem.* (1966) **693**, 20-43.

143. Boulatov, R. Reaction dynamics in the formidable gap. *Pure Appl. Chem.* (2010) **83**, 25-41.

144. Segal, G. A. Organic transition states. III. Ab initio study of the pyrolysis of cyclobutane via the tetramethylene diradical. *J. Am. Chem. Soc.* (1974) **96**, 7892-7898.

145. Hoffmann, R., Swaminathan, S., Odell, B. G. & Gleiter, R. Potential surface for a nonconcerted reaction. Tetramethylene. *J. Am. Chem. Soc.* (1970) **92**, 7091-7097.

146. Doubleday, C. *et al.* Is tetramethylene an intermediate? *J. Am. Chem. Soc.* (1984) **106**, 447-448.

147. Pedersen, S., Herek, J. L. & Zewail, A. H. The Validity of the "Diradical" Hypothesis: Direct Femtosecond Studies of the Transition-State Structures. *Science* (1994) **266**, 1359-1364.

148. Baldwin, J. E. & Ford, P. W. Stereochemistry of the thermal cyclobutane to ethylene reaction. Pyrolysis of 7,8-cis,exo-dideuteriobicyclo[4.2.0]octane. *J. Am. Chem. Soc.* (1969) **91**, 7192-7192.

149. Doubleday, C. Tetramethylene. *J. Am. Chem. Soc.* (1993) **115**, 11968-11983.

150. Hoffmann, R. & Woodward, R. B. Orbital Symmetry Control of Chemical Reactions. *Science* (1970) **167**, 825-831.

151. Genaux, C. T., Kern, F. & Walters, W. D. The Thermal Decomposition of Cyclobutane1,2. *J. Am. Chem. Soc.* (1953) **75**, 6196-6199.

152. Schaumann, E. & Ketcham, R. [2 + 2]-Cycloreversions. *Angew. Chem. Int. Ed.* (1982) **21**, 225-247.

153. Robson, R., Grubb, P. W. & Barltrop, J. A. 402. Organic photochemistry. Part I. The irradiation of some charge-transfer complexes of cyclohexene. *J. Chem. Soc.* (1964), 2153-2164.

154. Barltrop, J. A. & Robson, R. The photochemistry of some charge-transfer complexes of cyclohexene. *Tetrahedron Lett.* (1963) **4**, 597-600.

155. Luo, Y. R. *Comprehensive Handbook of Chemical Bond Energies*. Taylor & Francis (2010).

156. Koltzenburg, G., Fuss, P. G. & Leitich, J. Die photsensibilisierte cycloaddition von maleinsäureanhydrid und einigen seiner derivate an acetylen und an 3-cyclobuten-1.2-dicarbonsäureannhydrid. Darstellung von derivaten des bicyclopropyls und des Bicyclo [2.2.0] hexans. *Tetrahedron Lett.* (1966) **7**, 3409-3414.

157. Nagao, Y. *et al.* Utilization of sulfur-containing leaving group. 7. Highly selective nonenzymic chiral induction into 3-methylglutaric acid and cis-4-cyclohexen-1,2-ylenebis(acetic acid) utilizing a functional five-membered heterocycle 4(R)-MCTT. *J. Org. Chem.* (1985) **50**, 4072-4080.

158. Könning, D., Hiller, W. & Christmann, M. One-Pot Oxidation/Isomerization of Z-Allylic Alcohols with Oxygen as Stoichiometric Oxidant. *Org. Lett.* (2012) **14**, 5258-5261.

159. Mukhopadhyay, C. & Datta, A. A Simple, Efficient and Green Procedure for the Knoevenagel Condensation of Aldehydes with N-Methylpiperazine at Room Temperature under Solvent-Free Conditions. *Synth. Commun.* (2008) **38**, 2103-2112.

160. Lipshutz, B. H., Bošković, Ž. V. & Aue, D. H. Synthesis of Activated Alkenylboronates from Acetylenic Esters by CuH-Catalyzed 1,2-Addition/Transmetalation. *Angew. Chem. Int. Ed.* (2008) **47**, 10183-10186.

161. Lee, K. Y. & Mooney, D. J. Hydrogels for Tissue Engineering. *Chem. Rev.* (2001) **101**, 1869-1880.

162. Calvert, P. Hydrogels for Soft Machines. *Adv. Mater.* (2009) **21**, 743-756.

163. Sun, J.-Y. *et al.* Highly stretchable and tough hydrogels. *Nature* (2012) **489**, 133-136.

164. Webber, R. E., Creton, C., Brown, H. R. & Gong, J. P. Large Strain Hysteresis and Mullins Effect of Tough Double-Network Hydrogels. *Macromolecules* (2007) **40**, 2919-2927.

165. Gong, J. P., Katsuyama, Y., Kurokawa, T. & Osada, Y. Double-Network Hydrogels with Extremely High Mechanical Strength. *Adv. Mater.* (2003) **15**, 1155-1158.

166. Okumura, Y. & Ito, K. The Polyrotaxane Gel: A Topological Gel by Figure-of-Eight Cross-links. *Adv. Mater.* (2001) **13**, 485-487.

167. Malkoch, M. *et al.* Synthesis of well-defined hydrogel networks using Click chemistry. *Chem. Commun.* (2006), 2774-2776.

168. Cok, A. M., Zhou, H. & Johnson, J. A. Synthesis of Model Network Hydrogels via Tetrazine-Olefin Inverse Electron Demand Diels-Alder Cycloaddition. *Macromol. Symp.* (2013) **329**, 108-112.

169. Cui, J. *et al.* Synthetically Simple, Highly Resilient Hydrogels. *Biomacromolecules* (2012) **13**, 584-588.

170. Sakai, T. *et al.* Highly Elastic and Deformable Hydrogel Formed from Tetra-arm Polymers. *Macromol. Rapid Commun.* (2010) **31**, 1954-1959.

171. Sakai, T. *et al.* Design and Fabrication of a High-Strength Hydrogel with Ideally Homogeneous Network Structure from Tetrahedron-like Macromonomers. *Macromolecules* (2008) **41**, 5379-5384.

172. Hawk, J. L. *Structure Activity Relationships in the Fracture of Hybrid Covalent/Metallosupramolecular Organogels* Ph.D. thesis, Duke University, (2014).

173. Xiao, Y., Friis, E. A., Gehrke, S. H. & Detamore, M. S. Mechanical testing of hydrogels in cartilage tissue engineering: beyond the compressive modulus. *Tissue Eng. Part. B. Rev.* (2013) **19**, 403-412.

174. Harrass, K., Kruger, R., Moller, M., Albrecht, K. & Groll, J. Mechanically strong hydrogels with reversible behaviour under cyclic compression with MPa loading. *Soft Matter* (2013) **9**, 2869-2877.

175. Albrecht, M. & van Koten, G. Platinum Group Organometallics Based on "Pincer" Complexes: Sensors, Switches, and Catalysts. *Angew. Chem. Int. Ed.* (2001) **40**, 3750-3781.

176. Xu, D. & Craig, S. L. Scaling Laws in Supramolecular Polymer Networks. *Macromolecules* (2011) **44**, 5465-5472.

177. Appel, E. A., del Barrio, J., Loh, X. J. & Scherman, O. A. Supramolecular polymeric hydrogels. *Chem. Soc. Rev.* (2012) **41**, 6195-6214.

178. Jeon, S. L., Loveless, D. M., Yount, W. C. & Craig, S. L. Thermodynamics of pyridine coordination in 1,4-phenylene bridged bimetallic (Pd, Pt) complexes containing two N,C,N' motifs, 1,4-M-2-C-6(CH2NR2)(4)-2,3,5,6. *Inorg. Chem.* (2006) **45**, 11060-11068.

179. Chen, Y. *et al.* Mechanically induced chemiluminescence from polymers incorporating a 1,2-dioxetane unit in the main chain. *Nat. Chem.* (2012) **4**, 559-562.

180. Ducrot, E., Chen, Y., Bulters, M., Sijbesma, R. P. & Creton, C. Toughening Elastomers with Sacrificial Bonds and Watching Them Break. *Science* (2014) **344**, 186-189.

181. Gong, J. P. Why are double network hydrogels so tough? *Soft Matter* (2010) **6**, 2583-2590.

182. Shull, K. R. Materials science: A hard concept in soft matter. *Nature* (2012) **489**, 36-37.

183. Henderson, K. J., Zhou, T. C., Otim, K. J. & Shull, K. R. Ionically Cross-Linked Triblock Copolymer Hydrogels with High Strength. *Macromolecules* (2010) **43**, 6193-6201.

184. Sijbesma, R. P. *et al.* Reversible Polymers Formed from Self-Complementary Monomers Using Quadruple Hydrogen Bonding. *Science* (1997) **278**, 1601-1604.

185. Appel, E. A. *et al.* Supramolecular Cross-Linked Networks via Host–Guest Complexation with Cucurbit[8]uril. *J. Am. Chem. Soc.* (2010) **132**, 14251-14260.

186. Chen, Y., Kushner, A. M., Williams, G. A. & Guan, Z. Multiphase design of autonomic self-healing thermoplastic elastomers. *Nat. Chem.* (2012) **4**, 467-472.

187. Tuncaboylu, D. C., Sari, M., Oppermann, W. & Okay, O. Tough and Self-Healing Hydrogels Formed via Hydrophobic Interactions. *Macromolecules* (2011) **44**, 4997-5005.

188. Griffith, A. A. The Phenomena of Rupture and Flow in Solids. *Philos. Trans. R. Soc. London, Ser. A* (1921) **221**, 163-198.

189. Bastide, J. & Leibler, L. Large-scale heterogeneities in randomly cross-linked networks. *Macromolecules* (1988) **21**, 2647-2649.

190. Cristiano, A., Marcellan, A., Keestra, B. J., Steeman, P. & Creton, C. Fracture of model polyurethane elastomeric networks. *J. Polym. Sci., Part B: Polym. Phys.* (2011) **49**, 355-367.

191. Gent, A. N. Adhesion and Strength of Viscoelastic Solids. Is There a Relationship between Adhesion and Bulk Properties? *Langmuir* (1996) **12**, 4492-4496.

192. Schindelin, J. *et al.* Fiji: an open-source platform for biological-image analysis. *Nat. Meth.* (2012) **9**, 676-682.

193. Neilson, B. M. & Bielawski, C. W. Illuminating Photoswitchable Catalysis. *ACS Catalysis* (2013) **3**, 1874-1885.

194. Stoll, R. S. & Hecht, S. Artificial Light-Gated Catalyst Systems. *Angew. Chem. Int. Ed.* (2010) **49**, 5054-5075.

195. Gostl, R., Senf, A. & Hecht, S. Remote-controlling chemical reactions by light: Towards chemistry with high spatio-temporal resolution. *Chem. Soc. Rev.* (2014) **43**, 1982-1996.

196. Fors, B. P. & Hawker, C. J. Control of a Living Radical Polymerization of Methacrylates by Light. *Angew. Chem. Int. Ed.* (2012) **51**, 8850-8853.

197. Neilson, B. M. & Bielawski, C. W. Photoswitchable NHC-promoted ring-opening polymerizations. *Chem. Commun.* (2013) **49**, 5453-5455.

198. Sud, D., Norsten, T. B. & Branda, N. R. Photoswitching of stereoselectivity in catalysis using a copper dithienylethene complex. *Angew. Chem. Int. Ed.* (2005) **44**, 2019-2021.

199. Sud, D., McDonald, R. & Branda, N. R. Synthesis and coordination chemistry of a photoswitchable bis(phosphine) ligand. *Inorg. Chem.* (2005) **44**, 5960-5962.

200. Huang, Z. & Boulatov, R. Chemomechanics: chemical kinetics for multiscale phenomena. *Chem. Soc. Rev.* (2011) **40**, 2359-2384.

201. Koumura, N., Zijlstra, R. W. J., van Delden, R. A., Harada, N. & Feringa, B. L. Light-driven monodirectional molecular rotor. *Nature* (1999) **401**, 152-155.

202. Wang, J. B. & Feringa, B. L. Dynamic Control of Chiral Space in a Catalytic Asymmetric Reaction Using a Molecular Motor. *Science* (2011) **331**, 1429-1432.

203. Akbulatov, S., Tian, Y. C. & Boulatov, R. Force-Reactivity Property of a Single Monomer Is Sufficient To Predict the Micromechanical Behavior of Its Polymer. *J. Am. Chem. Soc.* (2012) **134**, 7620-7623.

204. Kucharski, T. J. *et al.* Kinetics of Thiol/Disulfide Exchange Correlate Weakly with the Restoring Force in the Disulfide Moiety. *Angew. Chem. Int. Ed.* (2009) **48**, 7040-7043.

205. Tian, Y. C., Kucharski, T. J., Yang, Q. Z. & Boulatov, R. Model studies of force-dependent kinetics of multi-barrier reactions. *Nat. Commun.* (2013) **4**.

206. Kucharski, T. J., Yang, Q. Z., Tian, Y. C. & Boulatov, R. Strain-Dependent Acceleration of a Paradigmatic S(N)2 Reaction Accurately Predicted by the Force Formalism. *J. Phys. Chem. Lett.* (2010) **1**, 2820-2825.

207. Trost, B. M. & VanVranken, D. L. Asymmetric transition metal-catalyzed allylic alkylations. *Chem. Rev.* (1996) **96**, 395-422.

208. Trost, B. M., Vanvranken, D. L. & Bingel, C. A Modular Approach for Ligand Design for Asymmetric Allylic Alkylations via Enantioselective Palladium-Catalyzed Ionizations. *J. Am. Chem. Soc.* (1992) **114**, 9327-9343.

209. Trost, B. M., Zambrano, J. L. & Richter, W. On the source of transfer of stereochemical information in ligands for Pd-catalyzed AAA reactions. *Synlett* (2001), 907-909.

210. Tang, W. J. & Zhang, X. M. New chiral phosphorus ligands for enantioselective hydrogenation. *Chem. Rev.* (2003) **103**, 3029-3069.

211. Zhang, Z. G., Qian, H., Longmire, J. & Zhang, X. M. Synthesis of chiral bisphosphines with tunable bite angles and their applications in asymmetric hydrogenation of beta-ketoesters. *J. Org. Chem.* (2000) **65**, 6223-6226.

212. Raghunath, M. & Zhang, X. A correlation study of bisphosphine ligand bite angles with enantioselectivity in Pd-catalyzed asymmetric transformations. *Tetrahedron Lett.* (2005) **46**, 8213-8216.

213. Qiu, L. Q. *et al.* A new class of versatile chiral-bridged atropisomeric diphosphine ligands: Remarkably efficient ligand syntheses and their applications in highly enantioselective hydrogenation reactions. *J. Am. Chem. Soc.* (2006) **128**, 5955-5965.

214. Dierkes, P. & van Leeuwen, P. The bite angle makes the difference: a practical ligand parameter for diphosphine ligands. *J. Chem. Soc., Dalton Trans.* (1999), 1519-1529.

215. van Leeuwen, P. W. N. M., Kamer, P. C. J., Reek, J. N. H. & Dierkes, P. Ligand Bite Angle Effects in Metal-catalyzed C−C Bond Formation. *Chem. Rev.* (2000) **100**, 2741-2770.

216. Jeulin, S. *et al.* Chiral biphenyl diphosphines for asymmetric catalysis: Stereoelectronic design and industrial perspectives. *Proc. Natl. Acad. Sci. U. S. A.* (2004) **101**, 5799-5804.

217. Ozawa, F., Kubo, A. & Hayashi, T. Palladium-Catalyzed Asymmetric Arylatioun of 2,3-Dihydrofuran-1,8-Bis(Dimethylamino)Naphthalene as an Efficient Base. *Tetrahedron Lett.* (1992) **33**, 1485-1488.

218. Mc Cartney, D. & Guiry, P. J. The asymmetric Heck and related reactions. *Chem. Soc. Rev.* (2011) **40**, 5122-5150.

219. Loiseleur, O., Hayashi, M., Schmees, N. & Pfaltz, A. Enantioselective Heck reactions catalyzed by chiral phosphinooxazoline-palladium complexes. *Synthesis* (1997), 1338-1345.

220. Allen, D. W. & Taylor, B. F. The chemistry of heteroarylphosphorus compounds. Part 15. Phosphorus-31 nuclear magnetic resonance studies of the donor properties of heteroarylphosphines towards selenium and platinum(II). *J. Chem. Soc., Dalton Trans.* (1982), 51-54.

221. Andersen, N. G., Parvez, M. & Keay, B. A. Synthesis, Resolution, and Applications of 2,2′-Bis(diphenylphosphino)-3,3′-binaphtho[2,1-b]furan. *Org. Lett.* (2000) **2**, 2817-2820.

222. Suárez, A., Méndez-Rojas, M. A. & Pizzano, A. Electronic Differences between Coordinating Functionalities of Chiral Phosphine−Phosphites and Effects in Catalytic Enantioselective Hydrogenation. *Organometallics* (2002) **21**, 4611-4621.

223. Jeulin, S. *et al.* Difluorphos, an Electron-Poor Diphosphane: A Good Match Between Electronic and Steric Features. *Angew. Chem. Int. Ed.* (2004) **43**, 320-325.

224. Zhang, X. US 6,521,769 B1. US 6,521,769 B1 patent (2003).

225. Gorobets, E., Parvez, M., Wheatley, B. M. M. & Keay, B. A. Use of H-1 NMR chemical shifts to determine the absolute configuration and enantiomeric purity for enantiomers of 3,3 '-disubstituted-MeO-BIPHEP derivatives. *Can. J. Chem.* (2006) **84**, 93-98.

226. Yamaguchi, M., Shima, T., Yamagishi, T. & Hida, M. Palladium-catalyzed asymmetric alkylation via π-allyl intermediate: Acetamidomalonate ester as a nucleophile. *Tetrahedron Lett.* (1990) **31**, 5049-5052.

227. Larsen, M. B. & Boydston, A. J. Successive Mechanochemical Activation and Small Molecule Release in an Elastomeric Material. *J. Am. Chem. Soc.* (2014) **136**, 1276-1279.

228. Horacek, M. *et al.* Reduction of bis eta(5)-(omega-alkenyl)tetramethylcyclopentadienyl titanium dichlorides: An efficient synthesis of long-chain ansa-bridged titanocene dichlorides by acidolysis of cyclopentadienyl-ring-tethered titanacyclopentanes. *Chem. - Eur. J.* (2000) **6**, 2397-2408.

229. Harris, R. K., Becker, E. D., Cabral de Menezes, S. M., Goodfellow, R. & Granger, P. NMR nomenclature: nuclear spin properties and conventions for chemical shifts. IUPAC Recommendations 2001. International Union of Pure and Applied Chemistry. Physical Chemistry Division. Commission on Molecular Structure and Spectroscopy. *Magn. Reson. Chem.* (2002) **40**, 489-505.

230. Shank, R. & Shechter, H. Notes: Simplified Zinc-Copper Couple for Use in Preparing Cyclopropanes from Methylene Iodide and Olefins. *J. Org. Chem.* (1959) **24**, 1825-1826.

231. Jones, N. A., Liddle, S. T., Wilson, C. & Arnold, P. L. Titanium(III) Alkoxy-N-heterocyclic Carbenes and a Safe, Low-Cost Route to TiCl3(THF)3. *Organometallics* (2007) **26**, 755-757.

232. Schmid, R., Foricher, J., Cereghetti, M. & Schönholzer, P. Axially Dissymmetric Diphosphines in the Biphenyl Series: Synthesis of (6,6′-Dimethoxybiphenyl-2,2′-diyl)bis(diphenylphosphine)('MeO-BIPHEP') and Analogues via an ortho-Lithiation/Iodination Ullmann-Reaction Approach. *Helv. Chim. Acta* (1991) **74**, 370-389.

233. Allen, J. V. *et al.* Palladium-catalysed asymmetric allylic substitution: a ligand design incorporating steric and electronic effects. *J. Chem. Soc., Perkin Trans. 1* (1994), 2065-2072.

234. Tian, Y. C. & Boulatov, R. Comparison of the predictive performance of the Bell-Evans, Taylor-expansion and statistical-mechanics models of mechanochemistry. *Chem. Commun.* (2013) **49**, 4187-4189.

235. Chatterjee, U., Wang, X., Jewrajka, S. K. & Soucek, M. D. Polyester/Poly(meth)acrylate Block Copolymers by Combined Polycondensation/ATRP: Characterization and Properties. *Macromol. Chem. Phys.* (2011) **212**, 1879-1890.

236. Nelson-Mendez, A., Aleksanian, S., Oh, M., Lim, H.-S. & Oh, J. K. Reductively degradable polyester-based block copolymers prepared by facile polycondensation and ATRP: synthesis, degradation, and aqueous micellization. *Soft Matter* (2011) **7**, 7441-7452.

237. Pustovit, Y. M., Ogojko, P. I., Nazaretian, V. P. & Rozhenko, A. B. Reactions of cycloalkanecarboxylic acids with SF4. II. Fluorination of gem-dichlorocyclopropanecarboxylic acids with SF4. *J. Fluorine Chem.* (1994) **69**, 231-236.

Biography

Zachary Shane Kean

Born January 4th, 1985 in Cocoa Beach, FL.

Education

Duke University

Ph.D. Chemistry, Durham NC, 2010-2014

Advisor: Stephen L. Craig

University of California, Berkeley

M.S. Chemistry, Berkeley CA, 2008

University of Florida

B.S. Chemistry, Summa Cum Laude, Gainesville FL, 2007

Advisor: Kenneth B. Wagener

Awards

Graduate Student Travel Award, ACS Division of Polymer Chemistry, 2014

Hauser Fellowship, Duke University, 2013

CBTE Predoctoral Fellowship (NIH NIGMS), Duke University, 2011-2013

Marcus Hobbs Fellowship, Duke University, 2012

CLAS 4-Year Scholar, University of Florida, 2007

University Scholars Research Grant, University of Florida, 2006

Joseph P. LaFornara Chemistry Award, University of Florida, 2006

Publications

Kean, Z.S., Akbulatov, S., Tian, Y., Widenhoefer, R.A., Boulatov, R., Craig, S.L. (2014). Photomechanical Actuation of Ligand Geometry in Enantioselective Catalysis. *Angew. Chem., Int. Ed., DOI: 10.1002/anie.201407494.*

Wang, J., Kouznetsova, T.B., **Kean, Z.S**., Fan, L., Mar, B.D., Martínez, T.J., Craig, S.L. (2014). A Remote Stereochemical Lever Arm Effect in Polymer Mechanochemistry. *J. Am. Chem. Soc., 136*, (in press).

Kean Z.S., Hawk J.L., Lin S., Zhao X., Sijbesma R.P., Craig S.L. (2014). Increasing the maximum achievable strain of a covalent polymer gel through the addition of mechanically invisible cross-links. *Adv. Mater., 26*, 6013-6018.

Kean, Z.S., Niu, Z., Hewage, G.B., Rheingold, A.L., Craig, S.L. (2013). Stress-responsive polymers containing cyclobutane core mechanophores: Reactivity and mechanistic insights. *J. Am. Chem. Soc., 135,* 13598-13604.

Ramirez, A.L.B., **Kean, Z.S.**, Orlicki, J.A., Champhekar, M., Elsakr, S.M., Krause, W.E., Craig, S.L. (2013). Mechanochemical strengthening of a synthetic polymer in response to typically destructive shear forces. *Nature Chem., 5,* 757-761.

Klukovich, H.M., Kouznetsova, T.B., **Kean, Z.S.**, Lenhardt, J.M., Craig, S.L. (2013). A backbone lever-arm effect enhances polymer mechanochemistry. *Nature Chem., 5*, 110-14.

Klukovich, H.M., **Kean, Z.S.**, Ramirez, A.L.B., Lenhardt, J.M., Lin, J., Hu, X., Craig, S.L. (2012). Tension trapping of carbonyl ylides facilitated by a change in polymer backbone. *J. Am. Chem. Soc., 134*, 9577-80.

Kean, Z.S., Ramirez, A.L.B., Craig, S.L. (2012). High mechanophore content polyester-acrylate ABA block copolymers: Synthesis and sonochemical activation. *J. Polym. Sci., Part A: Polym. Chem., 50*, 3481-84.

Kean, Z.S., Craig, S.L. (2012). Mechanochemical remodeling of synthetic polymers. *Polymer*, *53*, 1035-48.

Kean, Z.S., Ramirez, A.L.B., Yan, Y., Craig, S.L. (2012). Bicyclo[3.2.0]heptane mechanophores for the non-scissile and photochemically reversible generation of reactive bis-enones. *J. Am. Chem. Soc., 134*, 12939-42.

Klukovich, H.M., **Kean, Z.S.**, Iacono, S.T., Craig, S.L. (2011). Mechanically induced scission and subsequent thermal remending of perfluorocyclobutane polymers. *J. Am. Chem. Soc., 133*, 17882-88.

Delgado, P.A., Liu, D.Y., **Kean, Z.S.**, Wagener, K.B. (2011). Synthesis of poly(3-dodecyl-2,5-thienylene vinylene) by solid-state metathesis polycondensation. *Macromolecules, 44*, 9529-32.

Matloka, P.P., **Kean, Z.S.**, Wagener, K.B. (2010). Chain internal/chain end latent crosslinking in thermoset polymer systems. *J. Polym. Sci., Part A: Polym. Chem., 48*, 1866-77.

Matloka, P.P., **Kean, Z.S.**, Greenfield, M., Wagener, K.B. (2008). Synthesis and characterization of oligo(oxyethylene)/carbosilane copolymers for thermoset elastomers via ADMET. *J. Polym. Sci., Part A: Polym. Chem., 46*, 3992-4011.